CHEMICAL REVIEWS

Review

Cite This: Chem. Rev. 2018, 118, 7804−7864

pubs.acs.org/CR

The Many "Facets" of Halide Ions in the Chemistry of Colloidal Inorganic Nanocrystals

Sandeep Ghosh*,‡ and Liberato Manna*,§,#

‡McKetta Department of Chemical Engineering, The University of Texas at Austin, Austin, Texas 78712-1589, United States

§Department of Nanochemistry, Istituto Italiano di Tecnologia (IIT), via Morego 30, I-16163 Genova, Italy

#Kavli Institute of Nanoscience and Department of Chemical Engineering, Delft University of Technology, Van der Maasweg 9, 2629 HZ Delft, The Netherlands

ABSTRACT: Over the years, scientists have identified various synthetic "handles" while developing wet chemical protocols for achieving a high level of shape and compositional complexity in colloidal nanomaterials. Halide ions have emerged as one such handle which serve as important surface active species that regulate nanocrystal (NC) growth and concomitant physicochemical properties. Halide ions affect the NC growth kinetics through several means, including selective binding on crystal facets, complexation with the precursors, and oxidative etching. On the other hand, their presence on the surfaces of semiconducting NCs stimulates interesting changes in the intrinsic electronic structure and interparticle communication in the NC solids eventually assembled from them. Then again, halide ions also induce optoelectronic tunability in NCs where they form part of the core, through sheer composition variation. In this review, we describe these roles of halide ions in the growth of nanostructures and the physical changes introduced by them and thereafter demonstrate the commonality of these effects across different classes of nanomaterials.

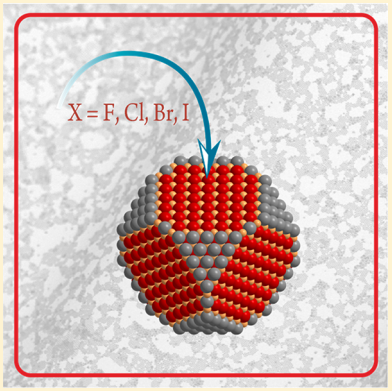

CONTENTS

Received: March 12, 2018
Published: July 31, 2018

DOI: 10.1021/acs.chemrev.8b00158
Chem. Rev. 2018, 118, 7804−7864

1. INTRODUCTION

Colloidal synthesis has been the mainstay of the wet chemical synthetic strategies used to create nanoscale materials of a broad range of inorganic compounds exhibiting remarkably narrow size distribution, rationally tunable morphology, stoichiometric composition variation, charge carrier doping, and tailored surface chemistries.[1] This surfactant-assisted precision synthesis protocol, first described during the mid-1990s,[2] provides the most versatile set of nanoscale materials which have been exploited in varied applications ranging from thin film devices (through photovoltaics, digital displays, optoelectronics) to nanomedicine (imaging and theranostics). The versatility of the colloidal synthesis stems from the fact that it routinely produces modular nanocrystals (NCs) in the essentially "free" colloidal disposition (stabilized by the surfactant layer on their surfaces). This enables solution processability and hence easy integration into various geometries like thin film device architectures and bulk polymer matrices. This specific set of features, however, is hardly attainable from physical methods like e-beam lithography or molecular beam epitaxy which are otherwise known to produce high-quality nanostructures but at a very high operational cost and restricted solution processability.

Over the past 25 years (and counting), the complexity of the NCs produced through colloidal synthesis has expanded by leaps and bounds, both compositionally and morphologically. Exotic shapes and heterostructuring such as $Cu_{1.94}S$-CuS nanodumbbells,[3] M−Pt−Fe_3O_4 (M = Au, Ag, Ni, Pd) heterotrimers,[4] octapod-shaped CdSe(core)/CdS(pods) NCs,[5] etc., all illustrate the morphological prowess of the colloidal technique. A number of synthetic methods for preparing colloidal NCs are available, major ones being coprecipitation in aqueous phase, reverse micelle templating technique, solvothermal synthesis, and surfactant-assisted growth in a hot organic solvent (or mixture of solvents).[6]

Considering that nanochemistry aims at developing synthetic protocols that are capable of producing large quantities of stable NCs with tunable size and shape, a rational design and optimization of the synthetic protocols and a rigorous understanding of the growth mechanism are of paramount importance. To this end, numerous research groups have made substantial efforts toward elucidating the nucleation and growth processes of colloidal NCs. Furthermore, the excellent control over the growth of NCs is generally accomplished by the use of surfactants possessing long alkyl chains which serve the dual role of complexation agents to the metal precursors and the eventual surface ligands to the NCs. Despite this level of control over the growth of NCs and their ease of use as printable inks for optoelectronic devices achieved through the surfactants, the very same molecules serve more as a hindrance toward charge hopping between NCs in a film leading to poor device performance.[7] A range of new ligand strategies had been explored recently just to address this specific challenge to minimize the interparticle spacing for enhanced carrier transport and achieve complete passivation of the NC surface for reducing defect state recombination losses. A favored pathway for displacing these surfactants has been through postsynthetic ligand exchange strategies whereby they are replaced by shorter molecules, even single atoms/ions. These considerations need an understanding of the processes taking place at the nanoscale surfaces, and it is only been until recently that researchers have come to fully appreciate the factors affecting them.

The growth of NCs occurs in a rather complex mixture of salts and surfactants, and hence, it is often not possible to separate the influences of different reactants. Nevertheless, over the course of several years, numerous reports have surfaced which have made an effort to unravel these complex intricacies. The role of foreign chemical moieties in such a scenario then becomes crucial even if they are present in minute quantities. For instance, designing the growth of a highly faceted NC involves understanding the surface energies of crystal facets a few nanometers across and their interactions with other chemical entities. Halide ions/atoms are one such chemical entity that are perfectly poised to interfere with the synthesis and processing of inorganic NCs, mostly due to their ubiquitous nature and high electronegativities. Ignoring or eliminating the influence of halide ions is difficult since they are often present, in trace amounts, as adsorbed species on the glassware and/or the magnetic stir bar as it is a general practice in many laboratories to wash them with the aid of hydrochloric acid (the quintessential "acid bath"). They are often present as counterions of the metal salt used in the synthesis, e.g., $CuCl_2$ is a common precursor for copper chalcogenide NCs, while Au NCs are almost always produced from chloroauric acid ($HAuCl_4$). Halide counterions in NC synthesis often show up on the NC surface as has been recently demonstrated for HfO_2[8] and InP NCs.[9] It is common knowledge in the case of NC synthesis that changing the counterion changes the final product in terms of phase, morphology, and even composition. Of all the common counteranions like acetate (OAc^-), nitrate (NO_3^-), etc., halide ions exhibit the most intriguing results since they show the highest reactivities of all the metal salts owing to their highly ionic nature. Also, halide ions can be contained, in trace amounts, in the surfactants used in the synthesis,[10] and even in the solvents used in the workup step.[11]

Exploring the influence of halide ions on the growth of inorganic NCs and the effect they exert on their surfaces then becomes an important research aspect in the case of colloidal NCs. This further leads to improved understanding of the resulting optoelectronic properties of the NCs and finally to better performing NC thin film devices. Factors like this have made halide ions come under intense scrutiny very recently, as can be judged by the breadth of the literature covered in this review. The inclination to exploit halide ions stems from the fact that they are single-atom ligands for a NC surface with a strong affinity toward metal cations which are known to populate the surface of a binary semiconductor or oxide NC. However, despite the fact that they are almost ubiquitous in synthesis protocols, it has been only recently that halide ions are being considered an important player in influencing the growth and surface functionalization of inorganic NCs (post-2005).

The above considerations merit a comprehensive treatment on this subject which so far has been lacking in the literature. Recent review articles, such as that by Juarez and Lohse, have attempted at giving an outlook on the influence of halide ions on the synthesis of semiconductor and metal NCs, respectively.[12,13] However, we aim to go beyond the conventional wisdom to paint a unifying picture that can be put to good use by a

DOI: 10.1021/acs.chemrev.8b00158
Chem. Rev. 2018, 118, 7804−7864

practicing nanochemist in designing more focused NC synthesis and functionalization strategies. The seemingly unconnected reports in the literature give rise to chemical trends having underlying principles common to all classes of nanomaterials, and we aim to demonstrate the same to the reader by furnishing an updated account of research in this area and by finally providing a thorough outlook.

In general, halide ions are important surface active species which influence colloidal NC growth and affect the resulting physical properties through their presence on the NC surface. They can undergo selective binding on the crystal facets, form strong complexes with the precursors, or participate in oxidative etching during synthesis. On the other hand, they can modify the intrinsic electronic structure of semiconducting NCs through their presence on the NC surfaces. Hence, the first section of the Introduction (section 1.1) will be devoted to the discussion of these mechanisms. We will treat this subject in two broad areas: those where halide ions influence (i) growth kinetics (section 1.1.2) as surface active species and/or complexing agents of the atoms/ions involved in the growth of colloidal inorganic NCs together with organic surfactants and (ii) the ligand shell (section 1.1.3) as short ligands in postsynthesis approaches to ensure electrical accessibility of NCs. The use of halide ions in postsynthesis processing of NCs comes from the consideration that such ions, if incorporated in the ligand shell, can be seen as the shortest X-type ligands which is bound to facilitate charge transport between the NCs.

In order to set the stage for the above discussions, the review starts by revisiting the general nature and chemical aspects of halide species and their interaction with bulk metallic and semiconductor surfaces (section 1.1.1). While there are numerous experimental data (from both experimental and computational works) on metal and group IV semiconductors surfaces, much fewer investigations have addressed the III−V semiconductors, and basically no experimental works exist on bulk II−VI and IV−VI semiconductors. This is likely related to the progressive difficulty in obtaining stable and clean surfaces for the latter materials. Overall, these studies of bulk surfaces reveal interesting insights on the way halide species can interact with surface atoms.

Thereafter, the concepts and factors related to the kinetics and thermodynamics of colloidal NC growth relevant to the influence of halide ions are presented in section 1.1.2. A brief overview of NC surface chemistry is also included in section 1.1.3 (halide ions in NC ligand shell) in order to give the reader an idea about the halide binding on NC surfaces. The contents of sections 1.1.2 and 1.1.3, which discuss the key halide influences on NCs, are presented in the light of the insights obtained from earlier bulk studies (section 1.1.1). These considerations are then followed into section 1.2, where the influence of halide ions as part of the crystal stoichiometry is dealt with, with major emphasis on spectral tunability through halide composition variation (section 1.2.1). Having provided these tools to the reader, the subsequent sections delve more specifically toward illustrating the applicability of these concepts to a wide range of nanomaterials classes. The further subdivision into metal (section 2), semiconductor (section 3), metal oxide (section 4), and metal halide NCs (section 5) was necessary since the surface chemistry of the NCs vary depending on the composition and hence the influence of halide ions on them. Also, the synthetic chemistry is very different in these classes of NCs, and halide ions show slightly different dynamics, albeit of the same fundamental origin. Finally, we wrap up with closing thoughts in the outlook (section 6), where we speculate future research directions and how the question of halide ions can be an important one in varied chemical environments involving materials.

1.1. Halide Ions as Surface Active Species

1.1.1. Interaction with Bulk Surfaces. Since the key manner by which halide ions influence NC growth and their physicochemical properties is through their binding to the NC surfaces, a prologue based on halide binding on bulk crystal surfaces will serve us to understand the microscopic origins of these effects. In fact, the focused attention toward the effect of halide ions on NC growth stems from the availability of a vast pool of prior research on bulk surfaces that largely formed the basis for understanding the interaction of halide ions with "nanoscale" surfaces in turn.

On Bulk Metal Surfaces. The halide−metal bonding is an important consideration in this scenario since, as we will see below, that defines most of the processes that govern the interaction between halide species and surfaces. Interaction between the bulk metal surface and the halide species is generally modeled in the realm of electrochemistry, and this viewpoint is especially useful to draw parallels with colloidal nanochemistry. This is so because, in the solution growth and manipulation of NCs, the interface between the NC surface and the solvent (containing a complex mixture of salts and surfactants) can be likened to that between a metal electrode and an electrolyte solution. The metal−electrolyte interface is characterized by the presence of an electric double layer where the electronic charge on the metal surface is counterbalanced by the opposite charges in the vicinal solution. Similarly, in colloidal nanochemistry, the surface active halide species act on the NC surfaces through their presence in the solution in close proximity to these surfaces.

The electronegativities of halides vary in the order F > Cl > Br > I, while the covalent or ionic radii follow the opposite sequence. An obvious extension of this fact is that most effects due to halide species also follow a similar progression. For instance, the anion of the most electronegative halide species, fluoride (F^-), has a strongly bound solvation shell and hence interacts with the electrode surface through a purely electrostatic interaction. On the contrary, the other halide species like chloride (Cl^-), bromide (Br^-), and iodide (I^-) exhibit weakly bound solvation shells, part of which can be stripped in order to form a direct chemical bond with the metal surface. The direct consequence of these factors is that in the case of tightly bound solvation shells like that for F^-, the excess ion concentration at a metal surface is independent of the chemical nature of the ionic species and solely depends on electrostatic considerations. The direct chemical bonding by Cl^-, Br^-, and I^-, on the other hand, results in ionic surface concentrations exceeding that given due to just the electrostatic interactions.[14,16,18] This is known as specific adsorption and was first observed in the case of Hg electrodes.[17]

Surface coverage due to specific adsorption of ions can be considerably larger than that for nonspecific adsorption. This leads to the formation of ordered and close-packed adlayer structures of specifically adsorbed ions on the metal surfaces. In connection to this, the most extensively studied class of specifically adsorbed anions is actually the halide ions due to their simple monatomic structure and ubiquitous nature.[17] The specific adsorption of an ion is heavily dependent on the solvation energy with greater specific adsorption exhibited by

DOI: 10.1021/acs.chemrev.8b00158
Chem. Rev. 2018, 118, 7804−7864

the ion with lesser ion−solvent interaction. For halide ions, the ion−solvent interaction decreases in the order $F^- > Cl^- > Br^- > I^-$.[14] At a constant ionic charge, the larger the size of the ion, the lesser is the ion−solvent interaction, which correlates well in this particular case (Figure 1a).[14] Consequently, the degree of specific adsorption increases in the order $F^- < Cl^- < Br^- < I^-$.[15] This means that F^- exhibits a weakly specific or nonspecific adsorption, and this manifests in the domain of colloidal NC chemistry as the scarcity of reports on the effect of F^- ions in metal NC growth and surface properties.

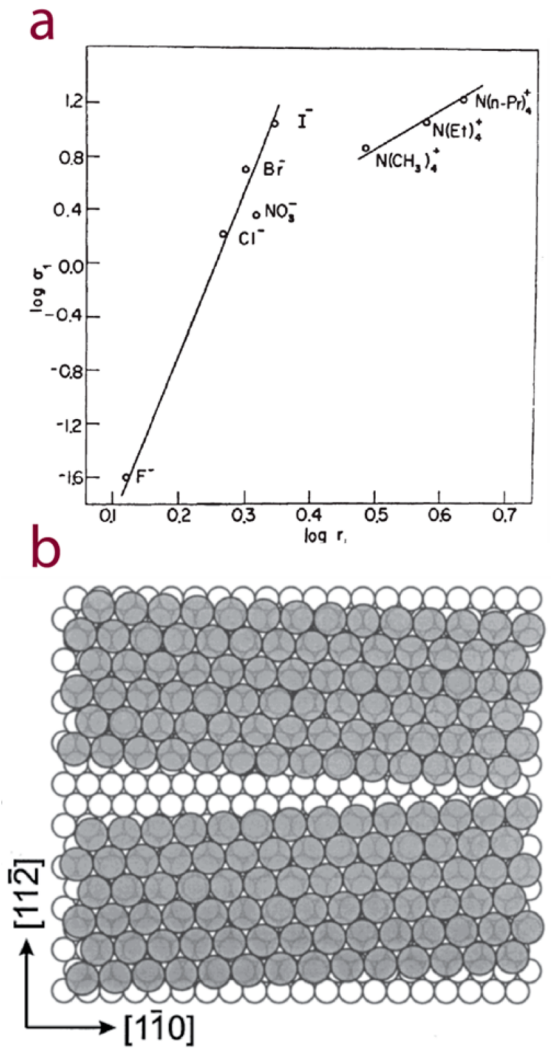

Figure 1. Specific adsorption and ordered halide adlayer formation. (a) Specific adsorbability (σ_1) as a function of the ionic radius (r_i) for selected ions at the "potential of zero charge".[14] Reprinted by permission from ref 15. Copyright 1980 Springer International Publishing AG. (b) Ordered Br adlayer structure on Au(111).[16] Reproduced from ref 17. Copyright 2002 American Chemical Society.

The study of the ordered halide adlayers on single-crystal metal surfaces is still a burgeoning area of research. Numerous research groups have reported their in situ studies on metals crystallizing in the face-centered cubic (fcc) structure such as noble metals like Au, Ag, Pt, Pd, Cu, Ni, Rh, etc.[17] Two competing interactions come into play in the observed halide adlayer structures: adsorbate−adsorbate and adsorbate−substrate interactions. The adsorbate−substrate interactions do not seem to stabilize the ordered halide adlayer structures since the disordered adlayer structure was never found in coexistence with the ordered phase. This indicates that the ordered phase is exclusively stabilized by the repulsive adsorbate−adsorbate interaction. However, the potential range of the ordered phases depends on the strength of the metal−halide interaction and the "potential of zero charge" of the metal surface. For instance, halides form predominantly close-packed hexagonal adlayer structures on the hexagonally packed (111) surfaces of fcc metals (Figure 1b), indicating the isotropic adsorbate−adsorbate interactions.[16]

These ordered adlayer structures have significant implications on the electrochemical reactivity of a metal surface, particularly in deposition and etching. The specifically adsorbing anions, especially those that form complexes with the metal ions, strongly influence the electrochemical deposition and dissolution kinetics through the formation of an adsorbed intermediate.[19] A preadsorbed monolayer of these anions on the electrode surface also significantly influences the continuous faradaic reactions, e.g., as has been demonstrated in the case of Pd dissolution by iodine in a halide-free electrolyte.[20] On the contrary, the opposite effect involving a reduced reaction rate due to blocking of reaction sites by these specifically adsorbed anions can occur as well. Examples include inhibition of oxygen reduction on Au, Ag and Pt surfaces.[21,22] Apart from these, the kinetics of electrochemical reactions is also altered due to the changes in the potential distribution in the double layer because of the presence of specifically adsorbed anions.[17]

On Bulk Semiconductor Surfaces. Although halide binding to bulk metal surfaces shows some remarkable characteristics, the same on bulk semiconductor surfaces has profound effects on the intrinsic electronic structure and the consequent physical properties. This happens due to the fundamental differences in the nature of the electronic states of the surface atoms in the two cases.[23] For metals, the surface electronic states are spatially extended and can be easily shared with the incoming adsorbate moieties while significantly affecting the structure of these species as they move toward the metal surface. On the contrary, surface electronic states in semiconductors tend to be spatially localized, and bonding with incoming adsorbate moieties is essentially covalent. In general, many technologically relevant processes proceed through reactions on semiconductor surfaces, e.g., dopant incorporation, epitaxial layer growth, etc. Consequently, a fundamental topic of interest in the surface science of semiconductors comprises of elucidating the chemistry of the adsorbate binding event and its implications on the electronic structure and physical properties of the semiconductor.[24] This, in turn, affects the performance of semiconductor devices, especially for those fabricated from nanostructures since they necessitate high local control over surface properties.

Halogens form strong monovalent and directional bonds to semiconductor surfaces and hence are ideal for structural studies.[25] Moreover, the high electronegativities exhibited by them leads to appreciable levels of charge transfer during bonding/adsorption which facilitates their study by surface-sensitive techniques. Usually the first step toward studying semiconductor surface chemistry involves preparing stable surfaces with tailored properties. The initial preparation comprises of etching in order to obtain a fresh surface, and halogens play a crucial role in this matter.[24,25] They have been used extensively by the microelectronics industry as etchants for semiconductors, which prompted fundamental studies aimed at addressing the interaction of bulk semiconductor surfaces with halogen species. However, due to issues of surface degradation

DOI: 10.1021/acs.chemrev.8b00158
Chem. Rev. 2018, 118, 7804−7864

under ambient circumstances (oxygen and moisture) over time, most of these studies were performed under pristine conditions, i.e., ultrahigh vacuum (UHV) environment while employing ion beams and plasma so that the interactions can be studied on a reproducibly clean surface.

Nevertheless, halide binding to semiconductor surfaces under solution conditions, which are of much less stringent nature than the UHV environment, have also been reported. For instance, treatment with an alcoholic solution of bromine is a common method for preparing fresh surfaces of II−VI (e.g., CdE; E = S, Se, Te) and III−V (GaAs) semiconductors.[24] In early comparative studies on wet etching of III−V and II−VI semiconductor surfaces involving Br_2/methanol as etchant, marked differences were found in the etching rates of polar surfaces of II−VI semiconductors (with anion faces being etched faster) as opposed to the III−V semiconductor faces.[26] These differences were easily rationalized with the more ionic bonding character of the II−VI lattice compared to a III−V lattice, with the etchant being more reactive toward the electron-rich anions. However, later studies reported conflicting results on differences in etch rates among the (0001), $(10\bar{1}0)$, and $(11\bar{2}0)$ faces of hexagonal CdSe[27,28] or between the (0001) and the $(000\bar{1})$ faces of the same material.[29]

It is noteworthy in this context that "clean" semiconductor surfaces are characterized by a plethora of reconstructions.[31] Upon creation of a surface, dangling bonds are generated which contain *less* than two spin-paired electrons as opposed to former "bulk bonding" with *exactly* two spin-paired electrons. These dangling bonds often contribute to surface electronic states with energies within the band gap that greatly impact semiconductor processes through acting as electron or hole traps. This lends instability to the dangling bonds which need to be "passivated" in order to lower the free energy of the system. Depending upon the context, the term passivation can assume different meanings.[24,32] One description is the surface treatment which does not necessarily affect the electronic structure but merely provides a protective layer by blocking the chemically active sites, a definition more pertaining to the case of metals (previous subsection). The other description refers to the surface treatment that chemically alters the surface state density through formation of strong covalent bonds between the surface atom and the adsorbate which essentially satisfy the dangling bonds.[24,33] A few bulk studies have addressed the preferential binding of halide ions on specific sites driven by the necessity of passivating the surface dangling bonds, as described below.

The rich coordination chemistry of a semiconductor surface provides diverse binding sites for small moieties like halide ions. However, the spatially localized electronic states on semiconductor surfaces reduce the surface diffusion of the adsorbed species, as compared to metals.[23,34] This leads to site-specific adsorption of incoming moieties.[24] A relevant demonstration was made by Liu et al. wherein the authors reported the site selectivity of the adsorption/reaction of bromine (Br_2) on GaAs(001) surfaces.[30] The bromine molecules were found to only react with the second-layer Ga atoms posited in the trenches and defects on the As-rich GaAs(001) in the initial adsorption stage (Figure 2a). The net attraction between the Ga atom and the bromine molecule was driven by the interaction between the highest occupied molecular orbital (HOMO) of the bromine molecule and the empty dangling bond of Ga. On the contrary, the filled dangling bond of As and the HOMO of the bromine molecule engaged into a repulsive interaction, as schematically shown in Figure 2b. This acted as a barrier toward

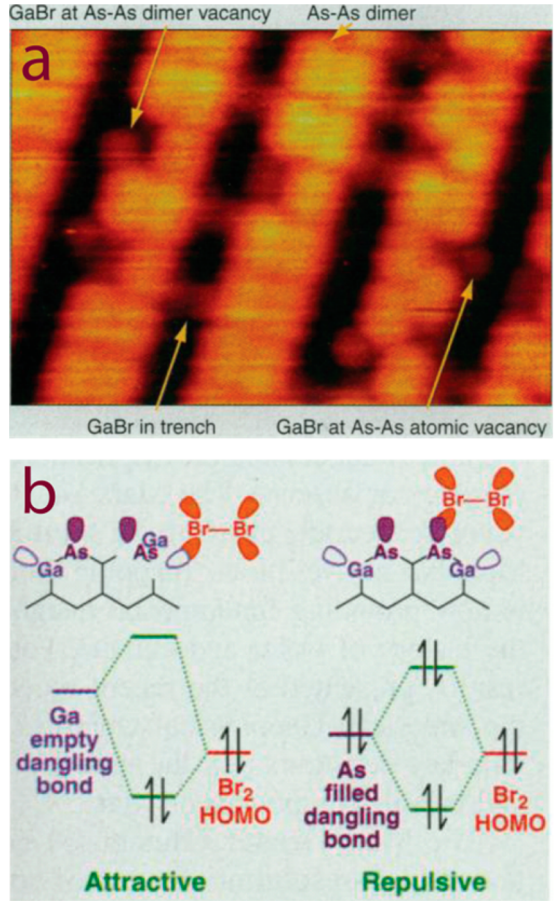

Figure 2. Site-specific adsorption of halide ions on semiconductor surfaces. (a) Scanning tunneling microscopy (STM) image of a reconstructed GaAs(001) surface after adsorption/reaction with bromine, showing selective reaction with Ga sites. (b) Molecular orbital schematic of the bonding between the frontier orbitals of bromine and the unfilled dangling bonds of Ga (left) and the filled dangling bonds of As (right).[30] Reproduced with permission from ref 23. Copyright 1999 AAAS.

the interaction of bromine with the As−As and As−Ga back bonds. Similar arguments were also employed to explain the higher reactivity of the less filled center Si dangling bond toward F_2, Cl_2, and Br_2 than the more filled corner Si dangling bonds on Si(111)[35] and for iodine(I_2) adsorption on InAs(001) surfaces.[36] These results directly allude to nanoscale systems where halide ions (or other negatively charged ligands, for that matter) are found to specifically bind to the metal cations in a semiconductor NC, as discussed in subsequent sections.

Other General Considerations. A qualitative approach that has been widely used in rationalizing the relative affinities between metal cations and halide anions is the principle of Pearson's hard and soft acid−base (HSAB) theory, whereby hard or soft cations preferentially bind to hard or soft anions, respectively.[37,38] The hardness of an ion is loosely determined by the ratio of its ionic charge to size, which means that harder species are highly charged ions with relatively small size and softer species exhibit the opposite characteristics. By this definition, the hardness of halide ions follows the sequence F^- > Cl^- > Br^- > I^- and can be applied to understand the ion−solvent interaction described previously in the case of specific adsorption on metal surfaces. The HSAB theory is invoked in various reports in order to validate the interaction of halide ions

DOI: 10.1021/acs.chemrev.8b00158
Chem. Rev. 2018, 118, 7804−7864

with crystal facets and complexation strength with metal precursors affecting growth kinetics of NCs and their colloidal stabilization.

All the influences discussed in the above subsections are pertinent to colloidal nanochemistry save for the exception that we are often dealing with a complex solution containing various ions and molecules instead of a comparatively simple interface between a metal electrode and the electrolyte solution. This contributes to an added layer of complexity in studying nanoscale colloidal systems. In studying the effects of halide ions in colloidal nanochemistry, one must consider the presence of other adsorbates, namely, the surfactant molecules possessing long alkyl chains and largely different solvent dynamics than simple aqueous electrolytes considered in bulk studies. For instance, Br^- adsorption on Au (111) surfaces was studied using an acidic solution of sodium bromide (NaBr) on single crystals of Au oriented along the (111) direction.[16] Analysis of the nanoscale systems by drawing heavily on the bulk then becomes complicated, although the detailed bulk studies can always be used as a first approximation in designing experimental work on colloidal NCs.

In the ensuing sections we will demonstrate the applicability of these principles, which had been developed for bulk surfaces, in forming a basis for understanding the processes that happen at the nanoscale. The specific examples are covered in the materials sections (section 2 onward) where the correlation with the bulk studies is referred to intermittently.

1.1.2. Influencing NC Growth and Stability. *General Considerations.* Colloidal synthesis techniques have gradually evolved into a largely separate branch of synthetic chemistry in its own merit with its distinct set of thermodynamic and kinetic considerations. A chemist has to invoke the principles of inorganic chemistry to design the core of a NC: those of organometallic and coordination chemistry to address the NC surface−ligand interaction[39] and those of organic chemistry to appreciate the ligand−solvent interaction.[40] Hence, a brief overview of the major experimental steps involved in the formation of colloidal NCs in solutions, as depicted schematically in Figure 3a, is a natural starting point for appreciating the role of halide ions in this research area.

The colloidal route of NC formation can be essentially divided into two steps: (a) nucleation of "seeds", when a critical concentration of the active monomer species is achieved, followed by a burst of nucleation of NCs, and (b) growth of these seeds into NCs, by assimilating the additional monomers from the reaction medium. The starting point of designing such a chemical synthesis is to identify suitable molecular precursors which are generally inorganic salts or organometallic compounds. These moieties release the reactive chemical species, referred to as the monomers above, through various chemical reactions. The choice of the chemical reaction is generally dependent on the nature of the inorganic core and broadly includes pyrolysis of organometallic precursors (for compound semiconductor NCs), hydrolysis of metal salts, accompanied by subsequent oxidation (for metal oxide NCs) or reduction of metal ions (for noble metal NCs).

LaMer and Dinegar's pioneering work in the 1950s on the growth description of sulfur colloids can be invoked in most cases to account for the formation of monodispersed colloidal NCs[41] under certain approximations. The so-called LaMer diagram is depicted in Figure 3b, showing the three NC growth regimes on the temporal evolution of the monomer concentration curve. Regime I corresponds to the "formation of monomers", which steadily rises with time as the reaction proceeds. At a critical monomer concentration (point of supersaturation) in regime II, "nucleation" occurs. A fast growth of these nuclei ensues, leading to a sudden drop in monomer concentration (corresponding to the curve maximum). No additional nucleation events occur if the monomer concentration drops below the supersaturation level, at which point purely the "growth" regime (regime III) commences. Other processes such as aggregation and Ostwald ripening can also occur during NC growth, as are depicted in Figure 3b. Aggregation of nuclei during growth can cause hindrance in obtaining colloidal stability and is generally prevented by the presence of surfactant molecules in the growth mixture. Ostwald ripening, on the other hand, entails dissolution of smaller NCs while the larger NCs are further enlarged in size. It is a thermodynamically driven process which occurs due to the

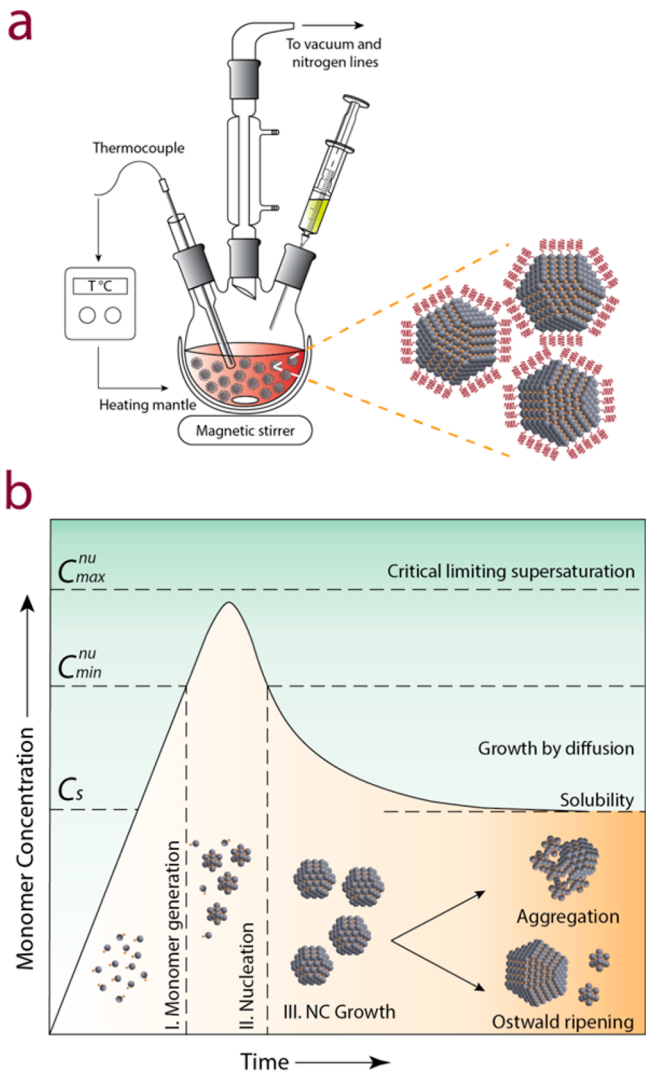

Figure 3. Aspects of the colloidal technique for solution growth of NCs. (a) Schematic of a glassware setup widely used for colloidal synthesis of NCs, generating surfactant-capped NCs soluble in a variety of solvents. (b) LaMer—Dinegar growth curve depicting the various stages of monomer generation (I), nucleation (II), and growth (III) involved in the solution synthesis. Other processes like aggregation and Ostwald ripening have also been included, which can occur during synthesis. Reimagined from ref 41. Copyright 1950 American Chemical Society.

DOI: 10.1021/acs.chemrev.8b00158
Chem. Rev. 2018, 118, 7804−7864

instability of smaller NCs when the concentration of monomers in solution drops below a critical threshold.[42]

Thermodynamic and Kinetic Control. Several intricately entangled thermodynamic (surface capping, reduction potential, etc.) and kinetic (monomer concentration, temperature etc.) factors play a crucial role in the colloidal growth. Much of the outcome of a colloidal synthesis, especially the shape and size of the resultant NCs, is dependent upon whether the reaction has been performed under thermodynamic or kinetic control.[43,44]

Discerning the differences between thermodynamic and kinetic regimes of NC growth control can be best appreciated by considering the competition between the rates of monomer *deposition* on the growing nuclei and that of surface monomer *diffusion*. The morphology of the final NC is determined by the relative magnitude of these two processes. When the diffusion occurs at a higher rate than deposition, the system is under thermodynamic control and the initially deposited monomers diffuse to lower energy sites to attain equilibrium. On the LaMer−Dinegar curve (Figure 3b) it means that the reaction is much further ahead in regime III, where the monomer concentration is not high enough to cause further deposition and hence the already deposited monomers cause NC surface reconstruction. However, when the deposition occurs at a much higher rate than diffusion, the system is under kinetic control and the NC will attain a thermodynamically less favorable shape (kinetic product). Generally, this is the very initial portion of regime III (or around the crossover region between regimes II and III) in Figure 3b.

There are several ways in which a NC growth can be tuned to obtain thermodynamic or kinetic product. In principle, a thermodynamically controlled product is obtained when a system gets a sufficient amount of time to let all of the atoms arrive at their final positions in order to attain the minimum Gibbs free energy for the entire system. The shape of the NC under such circumstances is considered as the *equilibrium shape*, which can be achieved by raising the temperature of the system or by giving the reaction sufficiently long time to complete. The total Gibbs free energy of an individual NC is largely the sum of that for the bulk and the excess caused by the surface, as expressed by the following equation

$$\Delta G = \Delta G_{\text{bulk}} + \gamma \Delta A$$

Here, γ represents the surface energy per unit area while A denotes the total surface area of the NC. Hence, at a fixed volume, a minimum Gibbs free energy for such a system will be achieved under the condition of a minimized total surface free energy. The surface free energies of the different crystallographic planes constituting the NC generally differ from each other. The cause of this includes differences in atomic arrangement and varied interactions with the surfaces species (surfactant molecules, in general). In this regard, it is important to note that the oft-assumed spherical shape for a NC is difficult nay almost impossible to achieve since several high-index facets (with Miller indices > 1) with high surface energies would be required to attain such a shape.

Surface free energy modification under the influence of various chemical moieties has often been used to explain NC growth under thermodynamic control.[44−46] Capping agents play an important role in this regard, which can be ionic or molecular species (such as surfactants) that exhibit selective binding to different crystal facets of a NC. This lowers the surface free energies of those facets leading to an altered NC shape as the expression of the stabilized facet is maximized. From a kinetic perspective, this also entails the alteration of relative growth rates of different crystallographic planes. The chemisorbed capping agent will hinder the further deposition of atoms on that particular facet, leading to slower growth and greater NC surface share of that facet. Furthermore, the surface passivation will increase the energy barrier to surface diffusion, and hence, the final NC shape is generally a result of the interplay of these various processes. The importance of the role played by capping agents/surfactant in NC growth is perhaps best demonstrated by the fact that in many cases the impurities found in the commercially supplied batches were proven to be the actual morphology descriptors. This has led to reproducibility issues in the past, e.g., the case of tri-*n*-octylphosphine oxide in the growth of cadmium selenide NCs[47−49] and that of in situ formed acetate ions for lead selenide NCs.[50,51]

Another factor in controlling growth is the reactivity of different precursors since that would determine the rate of monomer formation and hence the eventual rate of deposition. Hence, depending on the availability of monomers, the growth can be pushed to thermodynamic or kinetic regimes. A simple yet effective demonstration of this is through the controlled rate of continuous precursor injection in order to keep a constant supply of monomers and hence keep the reaction in the kinetic growth regime.[52] On the other hand, precursor reactivity plays a significant role in deciding phase purity during NC growth. A good example of this is balancing the reactivity of the metal precursors in forming NCs of ternary and quaternary chalcogenides.[53−55] For instance, this was achieved in the synthesis of $CuFeS_2$ NCs through using CuI as the precursor because that ensured a slower release of the Cu^+ ions which matched that of the Fe precursor.[56] Other copper halides (CuCl, CuBr) led to the formation of Cu−S phases as impurity instead due to faster Cu^+ release.

Halide Ions' Influence on NC Growth. As mentioned above, there are multiple ways in which the halide ions influence the thermodynamic and kinetic factors of NC growth. However, the three most fundamental means of halide influence that emerge from studying different classes of NCs are depicted in Figure 4. The basic processes depicted here remain the same for most syntheses, although the actual course of the reaction might vary depending on the specific chemistry of a material system, where one or all of these influences work in conjunction with other chemical factors. In fact, almost always, more than one of these principles were cited to explain the halide effect on a NC synthesis in the literature, and it is generally impossible to rule out one mechanism in favor of the other. These three processes, namely, selective binding on crystal facets, complexation with the precursors, and oxidative etching, are the subject of the ensuing text.

Facet-Specific Capping. The oft-cited capping action of halide ions/atoms and its subsequent effect is depicted in Figure 4a. As described in the previous section, facet-specific capping by the halide ions leads to changes in the relative surface free energies of the NC facets and eventually to changes in the final morphology of the product. NC morphologies that are not generally accessible otherwise, i.e., in halide-free conditions, could be produced under the action of halide capping. Owing to their highly electronegative character, halide ions strongly adsorb on the crystal facets, which generally have a sizable fraction of metal atoms, even if semiconductor NCs are considered. The relative binding on the different crystal facets then is dependent on the density of metal atoms which defines the halide packing on the surface and eventually the surface free

DOI: 10.1021/acs.chemrev.8b00158
Chem. Rev. 2018, 118, 7804−7864

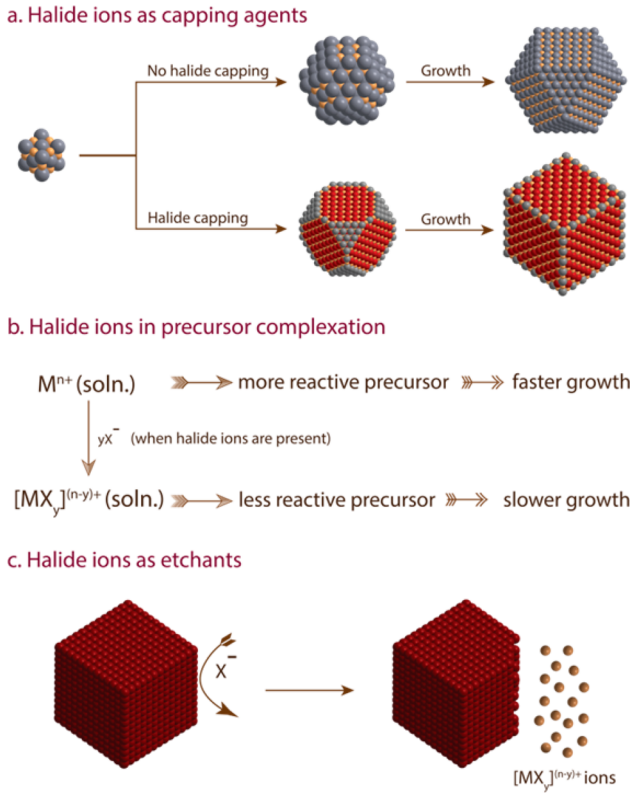

Figure 4. Schematic depiction of the various influences of halide ions on NC growth processes. (a) Halide ions, as surface/facet capping agents, can direct the morphology of NCs in ways that are not generally accessible otherwise. (b) Complexation with the precursors hinders the availability of monomers leading to slower growth kinetics due to the higher stability of the complex. (c) Halide ions can act as etchants on NC surfaces and edges under conditions that are oxidative or otherwise, leading to reshaping of the NCs and sometimes to their complete dissolution.

energy.[46] The modified thermodynamic stability and the kinetic growth rate of the crystal facets then dictate the fate of the final products.[44] Then again, in a surfactant-assisted solution synthesis of NCs, halide capping rarely acts alone and generally shows up acting in concert with other molecules. For instance, in the case of gold NCs, halide ions form soft templates (micelles or lamellar structures) with surfactant molecules that lead to anisotropic growth (see section 2.1 below).

All other factors notwithstanding, some simple considerations can be employed while designing halide-assisted shape control in colloidal NCs. The electronegativity of the halogen, the composition of the NC core material, and the strength of the bonding between the metal atom and the adsorbing atom are some of these aspects. A grasp of the interplay of these influences can be used to estimate the extent of facet stabilization. This can be exemplified in the case of NCs of binary compounds viz. metal oxides and metal chalcogenides. For metal chalcogenide NCs (i.e., where the anion is either S, Se, or Te) any of the halogens (F, Cl, Br, I) can form stronger bonds with the surface metal atoms owing to their higher electronegativity. On the contrary, in the case of metal oxide NCs, it is only fluorine which has a higher electronegativity than oxygen (the anion in the lattice) and hence in a situation to form stronger bonds with the surface metal atoms and alter the surface energies. Indeed, this fact can be appreciated from the numerous reports on F capping in metal oxide NCs (section 4) and a paucity of work involving other halides. This means, to a first approximation, introducing fluorine in the growth mixture of a metal oxide NC is in a favorable situation to yield shape control than other halide candidates. However, factors such as hardness and size compatibility of the incoming surface-coordinating atom to the receiving NC lattice can also complicate this simple notion.

Precursor Complexation. The other process by which halide ions largely affect the NC growth is that by forming strong complexes with the precursor atoms/ions involved in the nucleation and growth of NCs, as shown in Figure 4b. This factor is also influenced by the enhanced affinity of halide species toward metal atoms/ions and hence contributes toward regulating their availability and eventual monomer formation in the growth solution.[11] The formation of a strong complex reduces the rate of monomer generation, thereby slowing down the NC growth. This is often used by the synthetic nanochemist as a handle to slow down the reaction kinetics and access products (NC shapes) that are otherwise formed transiently in a faster halide-free growth (kinetic product).[57] Furthermore, the rate of nucleation can also be drastically reduced through the formation of halide complexes which can be a useful ploy in the growth of heterostructured NCs as in that case homogeneous nucleation has to be minimized. For instance, this strategy has been used to suppress homogeneous nucleation in the synthesis of rod-shaped and branched NCs starting from preformed NC seeds.[11,58,59]

An additional aspect that needs to be considered is that the electrochemical potential of metal ions (for example, Au ions) participating either in the growth or in the dissolution of NCs can be modified considerably when they are complexed with various molecules in solution. An example is provided by Rodríguez-Fernández et al.,[60] who studied the dissolution of gold nanorods (NRs) operated by $AuCl_4^-$ according to the following reaction scheme

$$AuCl_4^- + 2Au^0 + 2Cl^- = 3AuCl_2^-$$

The dissolution was found to occur only when CTAB is present, as the strong binding of $AuCl_2^-$ to CTAB modifies the reduction potential of $AuCl_4^-$. In a broader context then, halide ions too can strongly modify the electrochemical potential of redox species involved in the synthesis/dissolution of NCs, and therefore, the formation of these complexes needs to be taken into account.

Etching. Apart from these two growth-controlling mechanisms, a third process has also been identified in various cases: that where the halide ions act as etchants. It is a well-known fact that halide ions are good etchants to NC surfaces, a process that can be likened to the corrosion of a piece of metal. As schematically depicted in Figure 4c, the presence of halide ions in a NC solution can lead to dissolution of the surface atoms through their reaction with the halide ions. The etching process leads to the formation of similar strong complexes as mentioned in the previous paragraph. This phenomenon pertains to major yet varied implications in colloidal NC chemistry, both during and post synthesis. For instance, halide etching has been used for reshaping NCs through facet-specific etching, which is generally defined by the differential reactivity of the different crystal facets toward the halide ions. More aggressive etching pertains to destabilization of the NC surface to the extent that aggregation or fusion gets initiated and sometimes even leading to complete dissolution. This aspect can be turned into a powerful synthesis tool such as when NCs undergo oriented attachment, e.g., in the synthesis of PbS nanosheets starting from PbS NCs upon their

DOI: 10.1021/acs.chemrev.8b00158
Chem. Rev. 2018, 118, 7804−7864

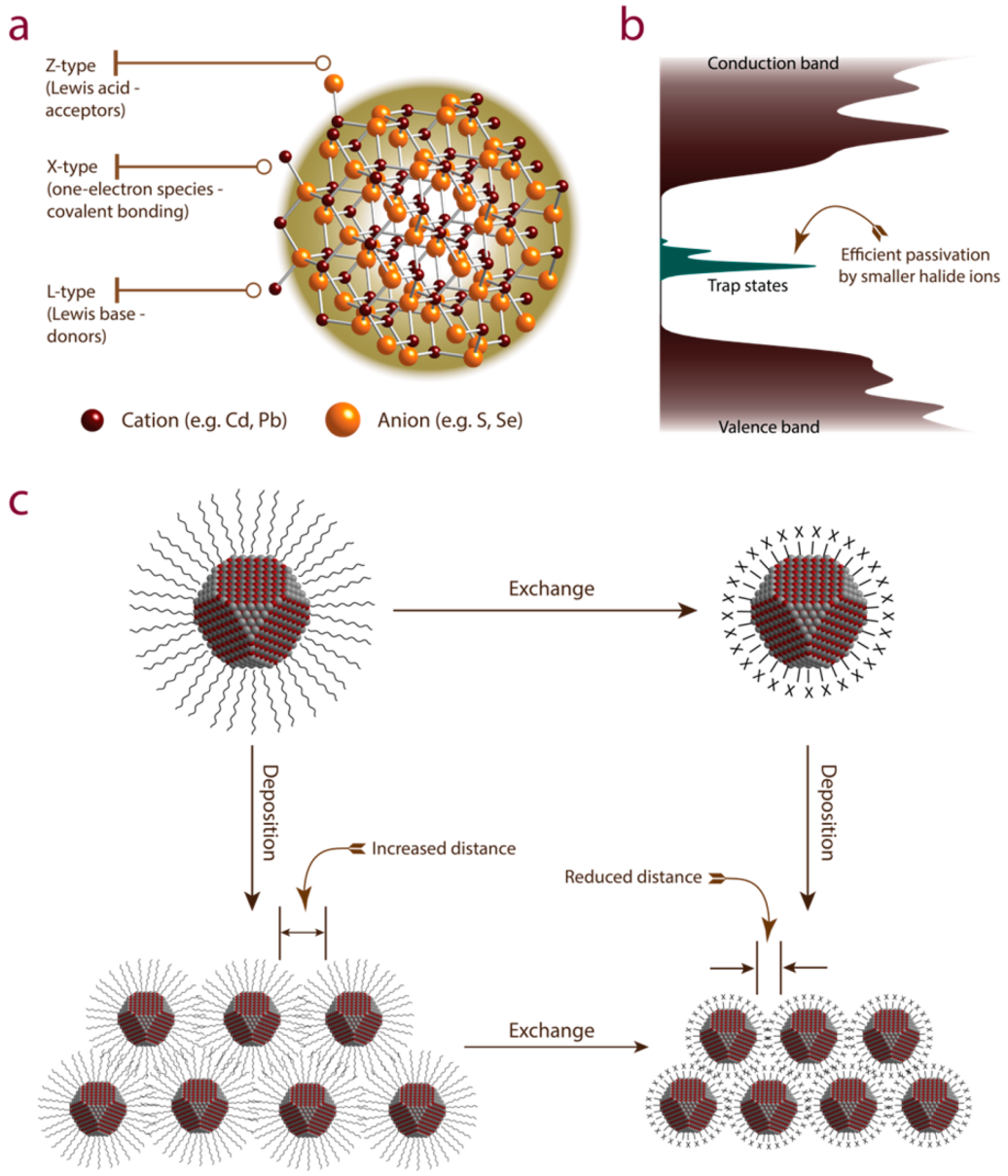

Figure 5. Surface chemistry of NCs and the effect of halide moieties on the NC surface depicted in the schematics. (a) Categorization of the ligands on a binary semiconductor NC surface according to the covalent bond classification scheme. (b) More efficient passivation of mid-band-gap trap states by halide ligands leading to improved optoelectronics in semiconductor NCs—one of the many mechanisms by which halide ligands influence the intrinsic electronic properties of the NCs. (c) Surface ligand shell modification by exchanging with halide (X) ions and eventual deposition of NCs into a thin film architecture. Reduced inter-NC distance can be achieved through this procedure resulting in better electrical performance. The sequence of the two fabrication steps of "exchange" and "deposition" steps can be interchanged according to the chemistry involved.

reaction with chlorine-containing solvents.[61] In the initial stages of a NC synthesis, etching can also be used to tune the seed population in such a way that it affects the final product morphology. This is particularly relevant for those synthesis protocols where the initially formed seed population exhibits two distinct distributions, e.g., crystalline and twinned seeds formed primarily due to tiny thermal fluctuations. Halide etching, in these situations, can be employed to remove the more reactive seeds (i.e., seeds with higher Gibbs free energy, twinned seeds in this particular example) in the early stages of growth so that a more size- and shape-focused NC synthesis is achieved. For instance, this is often observed in the polyol synthesis of some noble metal (silver, palladium) NCs, where shape focusing is routinely achieved through oxidative etching of multiple twinned seeds in favor of single-crystalline ones.[62,63]

Hence, the various means by which halide ions largely affect NC growth has been delineated in this subsection. However, it might be somehow obvious to the reader by now as to how complex and multivariate the role of halides can be. The synergistic actions of surface adsorption, ability of adsorbed species to engage in forming complexes with other ions and surfactants in the solution and in locally influencing the rate of redox reactions, are all factors that can contribute to a specific growth pattern and that can rarely be disentangled. More often than not, it is hard to bundle all of the different mechanisms of action in a grand unifying and predictive scheme: each case is somehow unique and pertinent to the set of conditions under which a given type of NC is synthesized. Nevertheless, many reports have shed light on several relevant cases, and these are discussed in detail in the major sections that follow, dedicated to

DOI: 10.1021/acs.chemrev.8b00158
Chem. Rev. 2018, 118, 7804−7864

the various materials systems. More on the role of surface attachment of halide ions and its implications is included in the next subsection, which should provide the reader a holistic viewpoint to look at the various roles that halide ions play.

1.1.3. Participating in NC Ligand Shell. It was mentioned before, in passing, that halide counterions of metal precursors used in the NC synthesis often end up on the NC surface. Also, the discussion in the previous subsection points toward the fact that halide ions are surface active species which have important implications on the NC growth. In this subsection, we will elaborate on how the presence of halide ions on the NC surface leads to interesting and useful changes on the physicochemical properties of the resulting NCs. This is particularly relevant for semiconductor NCs where halides induce changes in the electronic structure and also on inter-NC communication.

Before we delve into the discussion of the role of halide ions as surface ligands, it is imperative to take a brief overview of the nature of the surface−ligand interactions. The covalent bond classification scheme is particularly useful in this regard, although it was first proposed by Green et al. for describing the metal−ligand bonding in organometallic complexes.[64,65] This classification approach is based on the number of electrons that each neutral ligand contributes to the surface atom−ligand bond and also on the identity of the electron donors and acceptor groups,[33] as schematically depicted in Figure 5a. Hence, a ligand can contribute either 2 (L-type), 1 (X-type), or 0 (Z-type) electrons to the bonding orbital of surface atom−ligand interaction and are labeled accordingly. L-type ligands are neutral molecules acting as Lewis bases (electron pair donors, e.g., amines and phosphines) that datively coordinate to the surface metal atoms. The one-electron contributors, or the X-type ligands, possess an odd number of valence electrons and form an equal electronic contribution (i.e., one electron each) covalent bond with the surface atoms. Examples include negatively charged moieties such as carboxylates, phosphonates, and even ions like $CdCl_3^-$ and $InCl_4^-$, etc. Halide ions (X^-) can be considered to fall in this category, although depending on the identity they can also be considered Z-type. The Z-type ligands are generally the neutral electron pair acceptors (Lewis acids) such as metal carboxylates or metal chlorides. The identity of the ligand moiety or the description of it then becomes important as, for instance, in the case of Cl^- ligand on a CdSe NC surface can be both considered as Cl^- (X-type) as well as $CdCl_2$ (Z-type).[66] This is mostly because X-type ligands (Cl^-, in this particular case) bind to the excess surface cations (Cd) on a NC surface lending charge balance to the NC, effectively "passivating" the surface trap states (Cd dangling bonds). If these excess surface cations are considered as part of the ligand shell instead of the NC, this ligand ($CdCl_2$) can then be considered Z-type instead, binding to a charge-neutral NC. In this regard, it is important to recognize that electron-rich L- and X-type ligands, being nucleophilic in nature, generally bind to the surface sites that are electron deficient (Lewis-acidic character; typically, the surface metal cations that are undercoordinated). On the other hand, Z-type ligands show an affinity toward undercoordinated surface sites that are electron rich (Lewis-basic character; undercoordinated surface anions) instead (Figure 5a). However, an example of positively charged electrophilic X-type ligand also exists in the form of the archetypal proton (H^+) that binds to the oxide NC surfaces.[8]

In the case of halide ligation on semiconductor NC surfaces, the negatively charged X-type definition has been the most useful in explaining the changes in the physicochemical properties. Halide ions have been demonstrated to affect the intrinsic electronic properties of semiconductor NCs by various means.[33] One of the obvious ones is halide ions acting cooperatively with the bulkier ligand molecules already bound at the surface of the NCs in ensuring that a greater number of surface atoms is actually passivated (Figure 5b) and thus contributing to reduce the number of surface trap states. The more efficient passivation of surface trap states is made possible due to the smaller size of the halide ions, which lets them access the interatom trenches that bulkier organic ligands with long alkyl chains find hard to access.[67] For semiconductor NCs, this is especially important as it reduces the defect states recombination losses that are directly correlated to the number of uncoordinated atoms on the surface.

However, more careful investigations have also been reported in the literature which unraveled more about halide ligation on semiconductor NC surfaces than meets the eye in the first attempt. For instance, depending on the ligand makeup of the NCs, halide ions can also introduce hole traps, which can be either shallow or deep depending on the specific nature of the halide ligand, e.g., whether this is $CdCl_2$ (shallow) or CdI_2 (deep) in the case of cadmium chalcogenide NCs.[68] Similarly, according to another theoretical analysis, halide ligation leads to the generation of a rather large net dipole moment which can rigidly downshift both the valence band minimum and the conduction band maximum.[69,70] Interestingly, most of these influences of halide ions can be directly correlated to their highly electronegative character.

Surface chemistry, in general, has important implications for the tunability of the NC electronic properties, and the above considerations point to the fact that it is especially more so relevant when halide ligands are on the surface. While the optoelectronic properties of the semiconductor NCs are influenced by their presence on the NC surface, there is one other way in which halide ligands influence the dynamics of semiconductor NCs, that by affecting the properties of solids fabricated from these NCs. The halide-passivated NCs, when assembled into a thin film device, exhibit improved charge conduction compared to NCs passivated by bulky organic ligands which generally form an insulating layer between the NCs. Solid-state NC devices comprising of a NC thin film, such as solution-processed solar cells, thin film field effect transistors, light-emitting diodes, etc., all require efficient charge transport through the film. Bulky organic ligands, although important for solution processability, are hence detrimental for electronic devices, and a strategy that can be used for improved conduction can be achieved through the halide ions. This is generally done through exchanging the native surfactant ligands by halide ions, unless halide ions are already present on the surface by virtue of the synthesis protocol. However, the exchange with halide ions and deposition thereafter is the general approach that is considered most of the time (Figure 5c). The success of this strategy is based on the fact that the bulkier organic molecules are replaced by smaller halide ions which reduce the inter-NC distance and hence improve the charge carrier transport. In this regard, it is important to note that this strategy is not just unique to halide ions but also applicable to other small molecules which can reduce the distance between adjacent NCs.[33]

Figure 5c further schematically demonstrates that the sequence of the two steps of "exchange" and "deposition" can be interchanged in order to get to the same end structure. In the solid-state protocol, where deposition precedes exchange, the bulky organic ligands are displaced by halide ions on the

DOI: 10.1021/acs.chemrev.8b00158
Chem. Rev. 2018, 118, 7804−7864

deposited film. However, this postdeposition ligand exchange is known to create cracks in the film due to contraction of the film resulted by the NCs coming close together. This is detrimental for the overall film performance in addition to issues of inefficient ligand exchange and the presence of residual organic moieties on the device. The reverse method, that is one where deposition follows exchange, has been gaining popularity recently. In this case, a polar solvent of high dielectric constant, such as *N*-methylformamide, is required to confer colloidal stability to the halide-capped NCs which are then used to deposit NC films exhibiting high electron mobility.[71] This approach has the advantage that no postdeposition ligand stripping is required.

Apart from these factors, passivation with halide ions can also improve the overall stability of the NCs, as has been demonstrated for PbSe NCs, which became more resistant to oxidation in air owing to $CdCl_x$ treatment, with Pb sites passivated by Cl and Se sites by Cd. The improved stability was then translated into a higher power conversion efficiency in solar cells made from these NCs.[72] Along similar lines, Cl termination of Si NCs provides higher colloidal stability to the NCs and in addition provides surface Si−Cl bonds characterized by the lowest unoccupied molecular orbital (LUMO) energy that is close to that of the highest occupied molecular orbital (HOMO) of donor molecules. This facilitates binding of donor molecules to the surface of the NCs, further improving their stability.[73]

1.2. Halide Ions in the NC Core

The discussion in the preceding sections was mostly centered around the influence of halide ions on the NC surfaces and when present as precursors in the synthesis mixture (which sometimes end up on the NC surface anyway). This section discusses halide ions in the context of being part of the bulk instead. Halide ions when present as part of the crystal stoichiometry bring forth a different level of complexity to the realm of colloidal NCs. By virtue of their high electronegativity values, halide atoms usually yield a significant level of polarity to the bonds they form with other atoms. Now, in the colloidal NC paradigm the synthetic difficulty increases as the bonding among the crystal constituents becomes progressively more covalent. This means that NCs of a group IV semiconductor like Si require more elevated temperatures for crystallization than those of a less covalently bonded II−VI semiconductor like CdSe.[74] Conversely, halide ions when constituting a part of the crystal stoichiometry bestow a much more ionic character to the bonding which affects the synthesis and processing of such NCs in unprecedented ways. Consequently, these NCs may require lesser energy for crystallization and hence lower synthesis temperatures.[75] Furthermore, the fairly ionic character renders some halide-constituting NCs (like those of lead halide perovskites, for instance) somewhat soluble in most polar solvents, making it difficult to isolate and purify them by standard colloidal methods. Nevertheless, in the context of this review, the major influence that halide ions exert is the progressive tuning of the optoelectronic characteristics of these NCs through anion exchange, as discussed below.

1.2.1. Inducing Optical Tunability. Binary or ternary semiconductor NCs comprising of halide anions exhibit their characteristic optoelectronic properties at the nanoscale. However, the presence of halide ions in the NC lattices confers a new type of functionality to such NCs, that of systematic spectral tunability through changing the nature and concentration of the constituent halide ions. The recent surge in interest in halide perovskite NCs plays witness, with this phenomenon being demonstrated in almost all halide-containing NCs.

The halide-induced tunability comes forth due to the direct modulation of the band structure since in most of these compounds the frontier orbitals comprise of a significant contribution from halide orbitals.[76−79] Consequently, the nature of the band edges, i.e., the valence band maximum (VBM) and the conduction band minimum (CBM), is influenced by the halide composition. This fact has been elucidated in calculated band structures for methylammonium lead halide perovskites (Figure 6a) and in electrochemical measurements on cesium lead halide perovskite NC solutions (Figure 6b). In line with the halide electronegativities, Cl inclusion increases the band gap, while Br and I lead to a progressive decrease, which is reflected in the spectral response of these NCs.

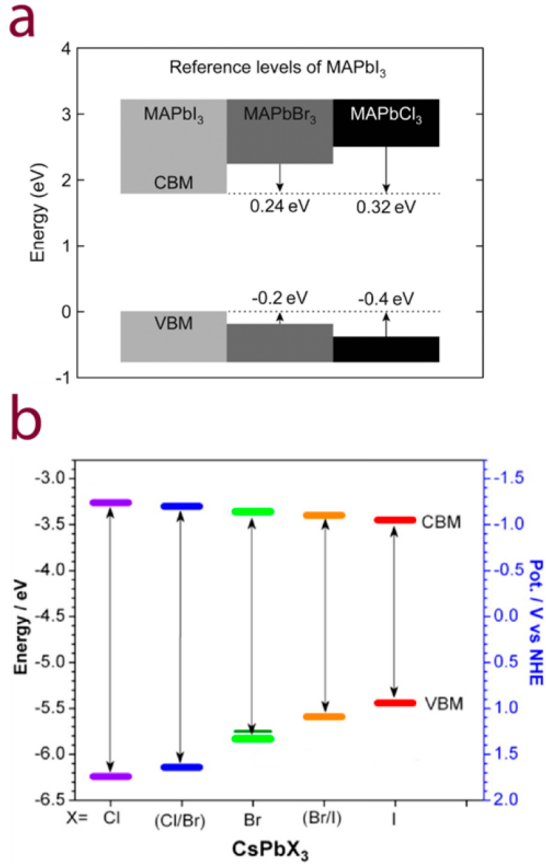

Figure 6. Dependence of the band edge positions on the halide composition of the stoichiometry. (a) Band alignment between methylammonium lead halide perovskites constituting I, Br, and Cl (right to left). Reproduced from ref 76. Copyright 2015 American Chemical Society. (b) Progressive changes in the band edge energies of cesium lead halides, tuned by the halide composition. Adapted from ref 77. Copyright 2016 American Chemical Society.

Here again, one can appreciate that the role of halide species can be multifaceted and specific for each type of NC and the combination of the inorganic core material and the nature of the pre-existing ligand shell. In the sections that follow, we will analyze the most relevant case studies in which halide ions have been exploited in the various steps of NC synthesis and processing. This comprehensive survey will take a journey through various materials systems, starting from metals and

DOI: 10.1021/acs.chemrev.8b00158
Chem. Rev. 2018, 118, 7804−7864

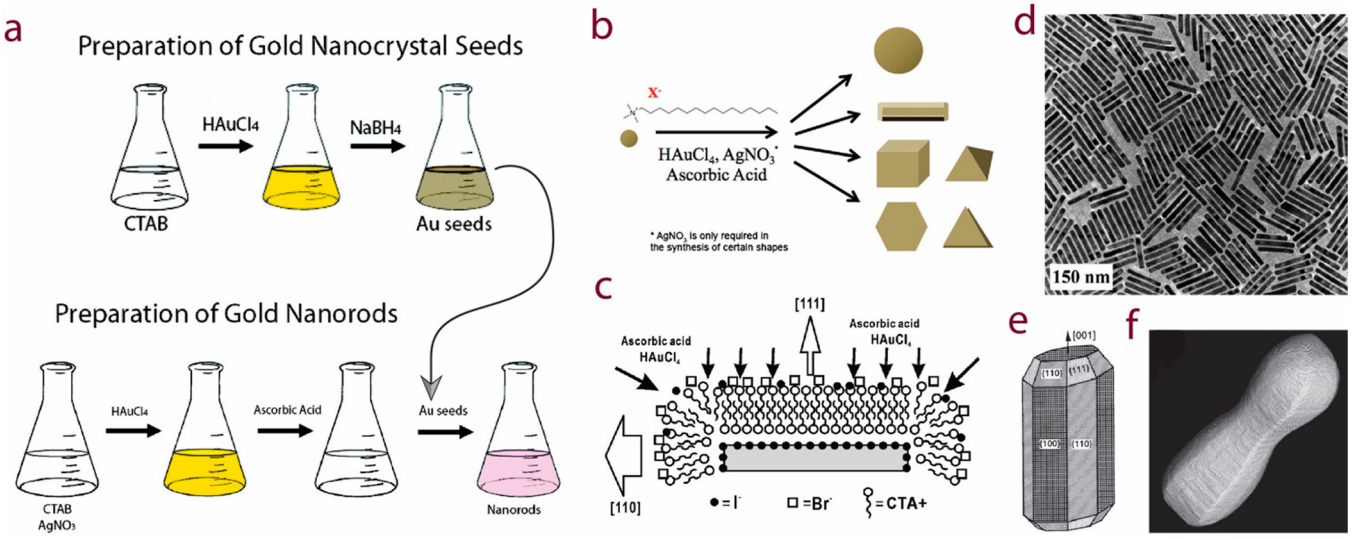

Figure 7. Seeded growth approach for preparing anisotropic gold NCs and the effect of halide ions on the growth. (a) Schematic showing the two steps involved in the seed-mediated growth of Au NRs. Adapted from ref 95. Copyright 2008 American Chemical Society. (b) General seed-mediated synthetic conditions to yield a wide variety of anisotropic Au NCs. Reproduced from ref 13. Copyright 2013 American Chemical Society. (c) Cartoon depicting the influence of CTAB bilayer template on the NC growth in the presence of iodide ions, which acted as a barrier to crystal growth during nanoprism formation. The thickness of the arrows signifies the rate of facet growth, i.e., the growth along the [111] facet was repressed compared to [110] when iodide ions were introduced. Reproduced from ref 96. Copyright 2007 American Chemical Society. (d) Representative TEM image of Au NRs prepared by the seed-mediated method using hydroquinone as the reducing agent. Adapted from ref 94. Copyright 2013 American Chemical Society. (e) Structural model of the Au NR. Reproduced with permission from ref 97. Copyright 1999 Elsevier Science B.V. (f) Electron tomography 3D reconstruction of a dumbbell-like Au NC formed due to the preferential growth at the tips of a NR in the presence of iodide ions. Reproduced with permission from ref 98. Copyright 2008 John Wiley and Sons.

going through the most common semiconductors, followed by oxides and finally to some selected cases involving halide-containing NCs showing spectral tunability associated with anion exchange.

2. METAL NANOCRYSTALS

The primary influences that the halide ions have displayed in the case of metal NCs are those in the growth of these NCs. In fact, the effect of halide moieties on the growth of noble metal NCs is very well catalogued, and numerous research groups have devoted attention to this specific field. This is probably due to the fact that faceted NCs of noble metals are highly effective catalysts and halide ions are a common descriptor of facet-directed growth.

The effect of halide ions in the case of metal NCs has manifested in the growth of anisotropic nanostructures which display distinctive optical and electronic properties. Halide ions play an important role in directing the anisotropy in metal NCs through controlling the growth kinetics by their facet-specific capping, selective binding with the precursors, and participation in etching the NCs, both pre- and postsynthesis.[13] Noteworthy in this regard is the fact that shape control synthesis of metal NCs can be achieved by the modulation of the surface energies through adsorption of other small molecules as well.[80] However, halide ions show the most diverse set of effects on the synthesis of metal NCs as detailed in the following.

2.1. Gold (Au) NCs

2.1.1. Faceting and Growth Control. Among metal NCs, gold has been the most extensively studied, primarily due to the ease of synthesis and the morphology-dependent wide color gamut that colloidal Au solutions exhibit.[81,82] In addition, anisotropy in these NCs leads to shape-dependent physical and chemical properties which has garnered extensive attention in the past few years mostly due to the potential of developing application in the areas of spectral detection, catalysis, energy, and nanomedicine.[83−86] This has led to numerous researchers exploring the rational control of shape through wet chemical protocols in order to tailor the properties of gold NCs since shape tuning led to a wider array of accessible properties in these NCs. Among the various synthesis parameters available for shape control, halide ions have only been recently found to be an important influencing factor. One of the first reports in this regard came from Sastry's group in 2005, wherein Shankar et al. elucidated the role of halide ions in the formation of (111) facet-bound triangular citrate-stabilized Au NCs through the well-known Turkevich method.[87] They reported that the Cl^- ions from the precursor chloroaurate ions promote the formation of these NCs while Br^- and I^- ions (introduced as potassium salts), which can replace surface-bound Cl^- ions, inhibit the growth. In another report in the following year from the same group, Rai et al. described the effect of halide ions on the formation of biogenically prepared flat Au nanotriangles.[88] In this synthesis, involving the use of lemongrass leaf extract as a natural reducing agent, they demonstrated that the presence of Cl^- and Br^- ions in the reaction mixture promoted the growth of Au nanotriangles. I^- ions, on the other hand, completely suppressed the nanotriangle growth and led to the formation of aggregated spherical and hollow NCs. The single-crystalline nature of the nanotriangles was confirmed by their electron diffraction pattern, which could be indexed to the fcc structure of gold. It was further ascertained that the major facets of the nanoprisms were constituted by the [111] crystal planes which were primarily exposed to the incoming electron beam. Furthermore, iodide ions transformed the as-synthesized flat Au nanotriangles to circular disk-like structures with greater propensity than other halide ions in a postsynthetic treatment. These observations were rationalized on the basis of the affinity of halide ions for

DOI: 10.1021/acs.chemrev.8b00158
Chem. Rev. 2018, 118, 7804−7864

metal surfaces which increases in the order $F^- < Cl^- < Br^- < I^-$.[17] This means that iodide ions have a stronger affinity to chemisorb on the gold surfaces and thus induce surface reconstruction and inhibit nanotriangle growth from the oriented attachment of the small NCs that form in the earlier stages of the reaction.[89]

An innovative development in the anisotropic Au NC growth came from the advent of the seeded growth method, described by several groups in the early 2000s.[90−93] In this method a mild reducing agent (ascorbic acid) is used to selectively reduce Au^{3+} to Au^+ in an aqueous CTAB solution of chloroauric acid ($HAuCl_4$) to which small gold seeds are added that catalyze the reduction of Au^+ on their surface. This way a temporal as well as physical separation of nucleation and growth was achieved wherein seed particles were first prepared separately and employed later as both nucleation points and catalysts for growing gold NCs. This process provides very precise control over the final NC shape which in turn can be regulated by a range of aspects such as size/shape of the seed particles, concentration of the surfactants, and metal/reductant ratio in the reaction mixture. A generic seeded growth approach employed to form anisotropic gold NCs is schematically shown in Figure 7a, which typically starts with the formation of gold seeds through the reduction of gold salt by sodium borohydride in the presence of citrate or cetyltrimethylammonium bromide (CTAB).[90,91] A separate growth solution, composed of a gold salt, CTAB, silver nitrate (essential for gold NR growth, not so much for other morphologies, Figure 7b)[92] and a weak reducing agent such as hydroquinone or ascorbic acid,[94] is prepared, and the preformed seed solution is added to it. The synergistic interaction of the various reagents present in the growth solution can then be regulated to achieve shape control in the final NCs. Among the various factors, halide ions used as the counterion in the CTA−X (CTA = cetyltrimethylammonium cation) molecule were recently found to have an important influence on the resulting NC morphology formed through the seed-mediated process.

The role of CTAB, which contained the bromide ion, was originally thought to be that of providing a soft template through the formation of cylindrical micelles that directed the anisotropic growth of gold NRs.[90] However, one of the first reports that indicated that there is more to the influence of CTAB than just a template was due to Ha et al. in 2007.[96] They observed that the addition of small amounts of iodide ions (as potassium iodide) in the growth solution led to the formation of triangular nanoprisms instead of the NRs, which are usually formed in the absence of I^- ions. The changes in the NC morphology were largely attributed to the adsorption of iodide ions on low-indexed gold surfaces which significantly alters the growth rate on different crystal facets. The formation of the (111) faceted triangular nanoprisms was hence a result of repression of crystal growth along the (111) direction due to iodide adsorption, as schematically depicted in Figure 7c. Although these findings were seemingly in contrast to those by Sastry's group (wherein I^- ions strongly suppress the formation of nanoprisms itself),[87,88] Ha et al. observed suppression of nanoprism growth as well, above a critical I^- concentration in the reaction mixture. It is imperative to note in this regard that Ha et al. studied the effect of iodide ions in the presence of a large bromide ion contribution (due to CTAB) unlike Sastry's studies. Furthermore, the authors reported that replacing the counterion in CTA−X from the usual Br^- (in CTAB) to Cl^- led to the formation of nanorice structures. These observations were rationalized on the basis of NC growth from a seed crystal being governed by halide adlayers, since counterions of cationic surfactants are known to affect the micellar adsorption and/or surface morphology of these surfactant molecules on solid surfaces.[99,100] This report has since then prompted other researchers to explore the specific adsorption of halide ions as an important factor in the seed-mediated Au NC synthesis.

Further insights into the adsorption behavior of CTA−X salts onto gold surfaces upon changing the halide counterion came from Kawasaki et al. at about the same time.[101] They examined the surfactant adsorption by using quartz crystal microbalance and atomic force microscopy and found that a high-affinity adsorption on the gold surfaces (by Br^- and Cl^- counterions of CTA−X) led to the formation of anisotropic NCs while a low-affinity adsorption (by F^-, for instance) only produced spherical NCs. These studies, however, were not performed in the realm of the seed-mediated growth but yielded important foundations to call upon, nevertheless.

Drawing on the work of Ha et al.,[96] in 2008 the group of Liz-Marzán reported further findings on the influence of iodide ions on the seed-mediated growth of Au NRs (representative TEM image of a set of Au NRs shown in Figure 7d).[98] In this study, Grzelczak et al. demonstrated that the gold salt reduction preferentially takes place at the growing NR tips in the presence of small amounts of I^- ions in the growth solution, yielding a dumbbell-like nanostructure. To understand the role played by iodine in this case, it is important to take the crystalline structure and the surface chemistry of the Au NRs into account. The initial rods, i.e., before I^- treatment, are enclosed by eight {110} and {100} alternating side facets with the tip terminated by {100}, {110}, and {111} facets, as depicted in the structural model in Figure 7e.[97] It was suggested that a small amount of I^- could exchange the surface Br^- ions from CTAB, specifically at the tips where the {111} facets were present, leading to dumbbell-like shapes as shown in Figure 7f. This preferential absorption of iodide ions on the {111} facets is similar to that reported by Ha et al.[96] and Rai et al.[88] However, unlike Ha et al., Grzelczak et al. observed enhanced growth at the {111} facets which was attributed to the presence of silver, a component whose role in the Au NR growth in conjunction with halide ions is discussed below. In a later study, Fan et al. demonstrated that the edge length of gold nanoplates grown by the seed-mediated method could be adjusted by varying the I^- content of the reaction.[102]

Silver nitrate has been an essential component for high-yield synthesis of Au NRs,[92] but the specific role played by Ag(I) ions is a matter of controversy. In their original report, Jana et al. hypothesized that Ag(I) ions react with CTAB forming an AgBr-type compound that preferentially adsorbs on some Au facets and restricts growth in that direction.[90] Later, Liu et al. proposed the underpotential deposition of Ag(I) ions on the longitudinal facets which permitted faster reduction at the rod tips leading to anisotropic growth, with CTAB playing a more passive role.[103] The deposition of a metal submonolayer or monolayer on a different metal surface at a potential that is significantly less negative than for bulk deposition is called underpotential deposition (UPD), and the UPD shifts for silver on gold surfaces vary in the order of (110) > (100) > (111).[19,103] However, hints of synergistic interaction between the bromide and silver ions in the growth of gold NRs became apparent from the report by Hubert et al., wherein they proposed that the facet-specific capping agent was some form of $CTA^+−Br^−−Ag^+$ complex, which they synthesized ex situ from CTAB and AgBr and successfully employed in the seedless variation of Au NR synthesis, along with CTAB.[104] The $CTA^+−Br^−−Ag^+$ was shown to have a higher affinity toward gold surfaces than CTAB

DOI: 10.1021/acs.chemrev.8b00158
Chem. Rev. 2018, 118, 7804−7864

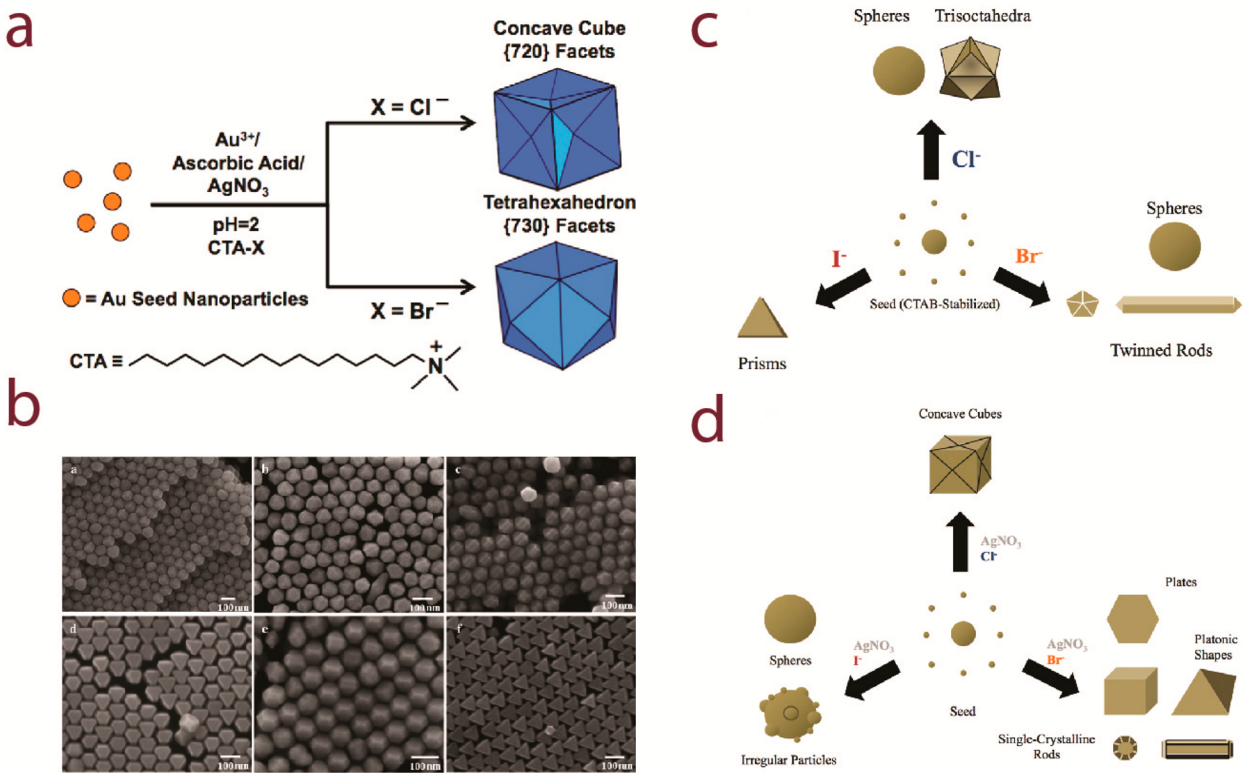

Figure 8. Effect of halide ions on the growth of highly faceted anisotropic Au NCs by the seed-mediated process. (a) Schematic showing the morphological effects of changing the counterion in the CTA−X surfactant—chloride led to {720}-faceted concave cubes, while bromide led to {730}-faceted tetrahexahedra. Reproduced from ref 107. Copyright 2010 American Chemical Society. (b) SEM images of various highly faceted Au NCs obtained by simply varying the iodide content in a growth process employing a CTAC and KI combination. Reproduced with permission from ref 109. Copyright 2011 John Wiley and Sons. Schematic shapes representing Au NCs of various morphologies obtained while using different halide ions: (c) in the absence of silver ions and (d) in the presence of the silver ions. Some shapes can also be prepared in the presence of more than one halide ion by slightly tweaking the other growth conditions. Reproduced from ref 13. Copyright 2013 American Chemical Society.

and hence thought to be the anisotropy promoter that forms in situ in the seed-mediated growth of Au NRs.

Further complications regarding the role of halide ions in the anisotropic Au NC growth arose when a report from Korgel's group showed that the yield of Au NRs depended strongly on the CTAB used.[95] In this report, Smith et al. obtained varying results from CTAB procured from ten different suppliers, which prompted the authors to conclude that an impurity in CTAB was very important in the NR formation. Later, multiple groups concluded that iodide is the impurity which is present in CTAB in significant but varying levels depending upon the supplier and is responsible for observed morphological variations.[10,105,106] Smith et al. (Korgel's group) concluded that iodide adsorption on Au {111} surfaces inhibits NR growth,[10] whereas Mirkin's group concluded otherwise.[105]

These studies generated further interest in studying the effect of changing the halide counterion in CTA−X surfactants, which Ha et al. briefly mentioned in their study in 2007 (described above).[96] A report from Mirkin's group in 2010 is worth mentioning in this regard, which demonstrated the formation of concave Au nanocubes, enclosed by 24 high-index {720} facets produced from a modified seed-mediated method where Br^- was replaced by Cl^- in the CTAB surfactant (i.e., CTA−Cl was used).[107] Interestingly, given the rest of the conditions identical, Ming et al. reported in the previous year the formation of convex nanocubes enclosed by 24 high-index {730} facets when CTAB was used instead.[108] The concave nanocubes from Mirkin's group can be envisaged as cubes with the centers of the six square faces "pushed in", generating square-pyramid-shaped depressions. Likewise, the convex or tetrahexahedral NCs by Ming et al. could be generated by "pulling out" the center of the six square faces. Intriguingly, this morphology tuning could be achieved through a simple change of the halide counterion in the surfactant as schematically shown in Figure 8a, although a low-growth solution pH was also maintained by using hydrochloric acid in both cases.

In the wake of all of these studies, the role of CTAB in seed-mediated growth of Au NRs was re-examined by Garg et al.[110] Although the cylindrical micellar template formation by the CTAB molecules was considered as one of the driving forces toward anisotropic NR growth, the authors found that bromide ions added as sodium bromide (NaBr) could lead to NR formation even when the concentration of the CTA^+ ions (contributed from CTAB) was well below the critical micelle concentration (cmc). They concluded that the bromide ions actually induce the NR formation which is the primary reason behind using such a high amount of CTAB for NR growth in the first place, although micelle formation as a necessary prerequisite for NR formation was not completely ruled out. The authors further reported that they were not able to achieve anisotropic growth when CTAC was used as the surfactant though. At about the same time (2010), Huang's group reported a systematic shape evolution of anisotropic gold NCs into various highly faceted structures when they used CTAC and NaBr, where controlling the bromide concentration was critical for cube formation.[111] However, 1 year later Bullen et al. reported an

DOI: 10.1021/acs.chemrev.8b00158
Chem. Rev. 2018, 118, 7804−7864

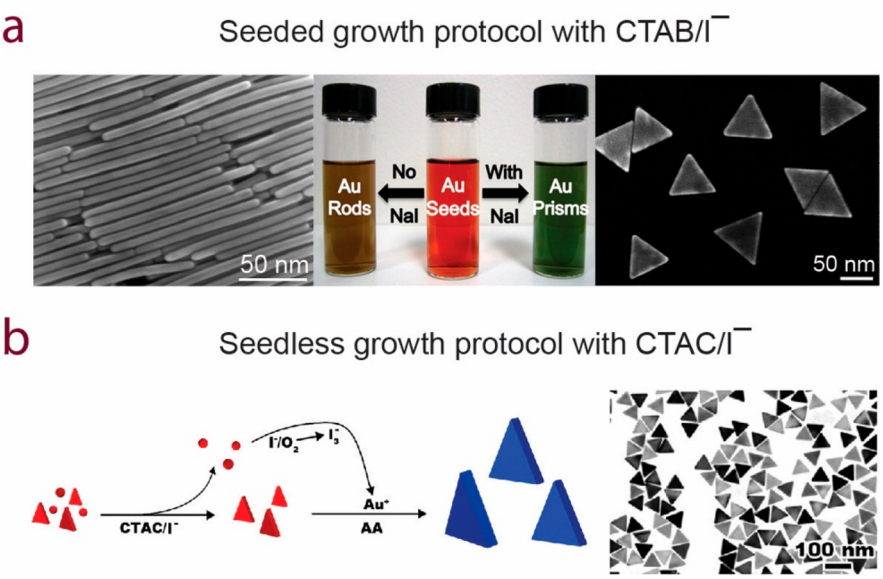

Figure 9. Role of iodide ions in the growth of Au nanoprisms enclosed by {111} facets. (a) Presence of iodide ions led to the formation of Au nanoprisms through a seeded-growth protocol, while its absence yielded the more generally known NRs when high-quality CTAB is used as a surfactant. Reproduced from ref 116. Copyright 2013 American Chemical Society. (b) Scheme showing the oxidative etching of less stable shapes by iodide ions (actually, tri-iodide ions, I_3^-, formed in situ) leading to uniform nanoplates (shown in the TEM image) through a faster seedless synthesis employing CTAC and KI). Reproduced from ref 117. Copyright 2013 American Chemical Society.

inverse relation between the concentration of bromide ions in the growth solution (introduced as CTAB and potassium bromide, KBr) and the NR growth rate,[112] in contrast to Garg et al. More recently, a report by Si et al. described that a critical $[Br^-]/[Au^{3+}]$ ratio of ~200 is necessary for obtaining maximum aspect ratio in the as-grown Au NRs.[113] The NR growth seemed to be poisoned beyond this critical value, thereby yielding shorter lengths, which was explained on the basis of complete blockage of all of the growing facets by the excess bromide ions preventing nanorod formation.

Further investigations on this topic came again from Huang's group, where they demonstrated systematic shape evolution in the growth of highly faceted Au NCs (Figure 8b) by simply varying the I^- content while using a CTAC and KI combination.[109] They noted a preferential growth of {111} facets accompanied by a suppression of the growth of {110} facets due to an increased amount of iodide, i.e., reduction of gold ions along different crystallographic directions was modulated by the I^- ions, which contributed to the understanding developed by the Korgel and Mirkin groups earlier.[10,105] Jiao et al. examined the synergistic interaction between iodide and silver ions as a factor that influences growth evolution of Au NCs ranging from thick NRs, cuboidal NRs, dogbone-like NRs to dumbbell NRs.[114]

Mirkin's group offered a systematic study as a follow up of their earlier work on the highly faceted concave Au nanocubes[107] that aimed to introduce some method in the various (and at times conflicting) interpretations obtained from the previous reports that used several combinations of halide ions in the seeded growth of Au NCs.[115] In this 2012 report, Langille et al. demonstrated that the ratio of silver and halide ions and the nature of the halide counterion could be exploited for a rational synthesis design of a range of anisotropic Au NCs. They described three major roles of halide ions:

(a) Modulating the reduction potential of Au^+–halide complexes prior to seed addition—the reduction potential and solubility decreased in the order $[AuCl_2]^-$ > $[AuBr_2]^-$ > $[AuI_2]^-$, which led to slow particle growth upon addition of a larger halide ion.

(b) Passivating Au NC surfaces—the binding affinity of the halide ions also increases with the size of the halides (Cl^- < Br^- < I^-) and contributed to the formation of thermodynamically favorable products with increasing concentrations of Br^- and I^-, effects of I^- being stronger.

(c) Modulating the extent of silver UPD in the silver-assisted synthesis—the extent of modulation depended upon the concentration of the halide ions in solution and followed the interaction trend of Au and Ag with different halides viz. Ag UPD–Cl > Ag UPD–Br > Ag UPD–I and Au–I > Au–Br > Au–Cl. Furthermore, trace amounts of larger halide ions decreased the stability of the Ag UPD layer, leading to shapes with higher energy facets. On the other hand, larger amounts of Br^- or I^- prevented silver deposition altogether, thereby limiting the number of accessible shapes.

These synthesis design considerations, which demarcated the role of halide ions from that of silver ions, were schematically summarized by Lohse et al. and have been reproduced in Figure 8c and 8d.[13]

Another systematic study on the question of halide ions was recently due to DuChene et al., where they used high-purity CTAB and CTAC to ascertain the individual roles of chloride, bromide, and iodide ions on the anisotropic growth of Au nanostructures from citrate-stabilized seeds.[116] This study aimed to address the conflicting reports regarding the role of iodide ions present as impurities in CTAB, with Mirkin's group concluding that the presence of iodide is a requisite for anisotropic growth (formation of NRs and nanoprisms),[105] while Korgel's group offering the opposite viewpoint.[10] The use of high-purity CTAB in the study conducted by DuChene et al. helped them to earmark the role of each halide ion (in the presence of CTAB) without interference from impurities:

DOI: 10.1021/acs.chemrev.8b00158
Chem. Rev. 2018, 118, 7804–7864

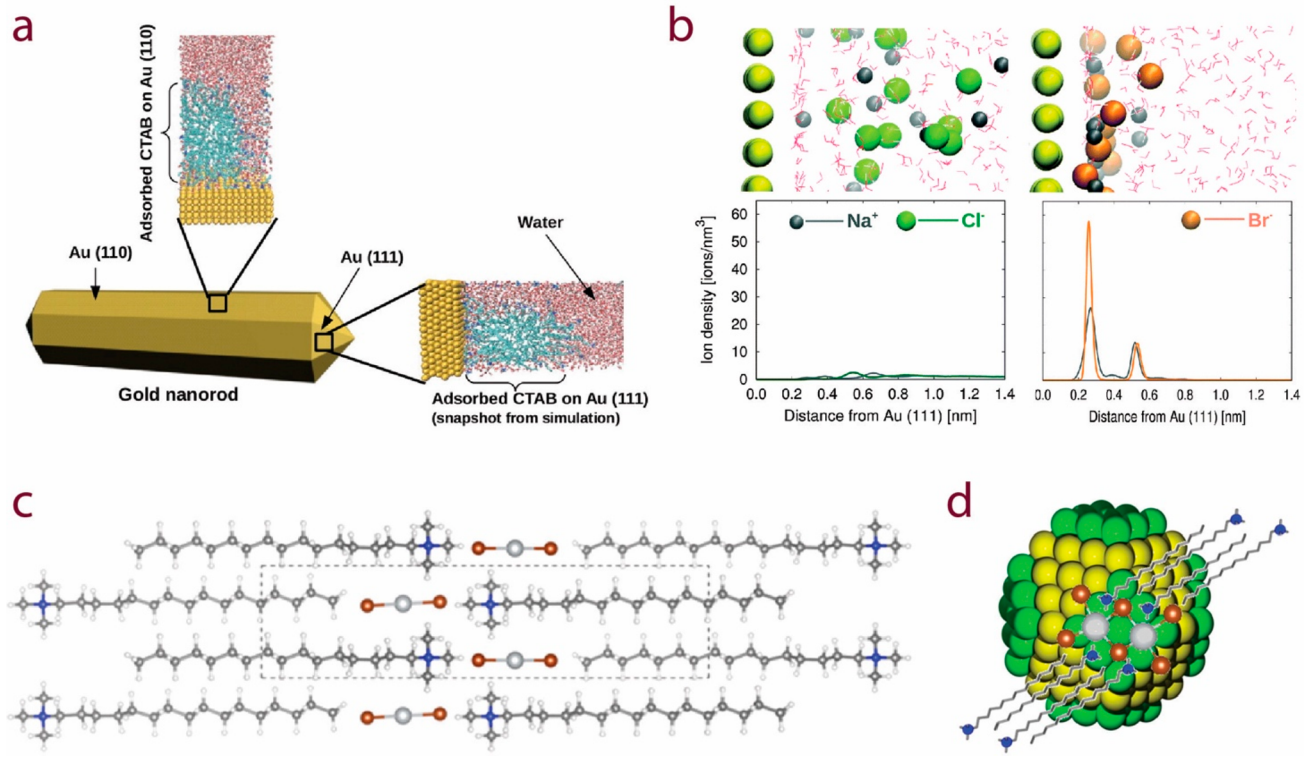

Figure 10. Theoretical descriptors of halide ion influence on the anisotropic growth of Au NRs. (a) Snapshots from molecular dynamics simulations of interaction of CTAB molecules (in aqueous solutions) with different facets of a gold NR. Reproduced from ref 119. Copyright 2013 American Chemical Society. (b) Snapshots from molecular dynamics simulations of interaction of NaCl (left) and NaBr (right) with Au(111) surface with the respective ion density as a function of distance plotted below the snapshots. Water molecules represented as sticks. Adapted with permission from ref 120. Copyright 2016 Royal Society of Chemistry. (c) Ball-and-stick model of the crystal lattice of the CTAB−AgBr complex (Br, brown; Ag, large gray spheres; C, gray; H, white; N, blue). (d) Wulff construction of a gold nanoparticle seed showing the preferential adsorption of CTAB−AgBr complex on the {100} planes, which leads to the symmetry breaking event. (Yellow atoms constitute the {111} planes, while green ones represent the {100} plane.) Adapted from ref 121. Copyright 2014 American Chemical Society.

(a) Br^-, essential for the formation of Au NRs;
(b) Br^- and I^- (controlled combination), essential for the formation of high-quality Au nanoprisms;
(c) Cl^-, ineffective at promoting anisotropy and detrimental at high concentrations.

These studies, which did not employ silver(I) ions, were a useful addition to Langille's conclusions on similar systems (Figure 8c).[115] The results obtained are schematically summarized along with representative TEM images in Figure 9a. As mentioned earlier, the degree of specific adsorption of halide ions on low-index Au surfaces scale as $I^- > Br^- > Cl^- \gg F^-$,[17] and chloride ions were in addition shown to yield poorly ordered adlayers on low-index Au facets in comparison to bromide and iodide ions.[18] This directly translates into a hindrance toward the formation of facet-selective halide adlayer in the presence of chloride ions, thereby yielding disordered NC growth with a roughly isotropic morphology. Likewise, I^- ions exhibit a substantial hindrance toward NR formation due to a strong affinity toward Au{111} facets and hence displace bromide adatoms from these surfaces, leading to the growth of nanoprisms. The necessity of bromide ions for the formation of Au NRs was attributed to strong selective binding on Au{100} facets, which facilitated the elongation in the [110] direction.

From the discussion so far in this section it might seem that the presence of bromide ions is of utmost importance for the formation of Au NRs. However, a recent study from Murray's group shows that bromide ions are not an absolutely necessity for Au NR formation.[118] In this report, Ye et al. demonstrate the synthesis of Au NRs with a high degree of dimensional tunability by using a bromide-free surfactant mixture comprising of alkyltrimethylammonium chloride (such as CTAC) and sodium oleate. Yet, it is imperative to note that this "bromide-free" protocol was not truly free of bromide since the seed NCs were still produced by a standard CTAB-assisted method. They also found that this surfactant mixture is much less sensitive to trace impurities like iodide ions, in contrast to that reported for CTAB by the Mirkin and Korgel groups.[10,105] Further insights in this regard came from Chen et al. in their 2014 paper where they explored the role of iodide ions in the synthesis of triangular Au nanoplates, albeit in a seedless variation of the growth process involving CTAC and potassium iodide.[117] They demonstrated that iodide serves a dual function: that of selective removal of other less stable shapes by oxidative etching through the formation of the tri-iodide ions (I_3^-) in addition to the selective binding to the Au {111} facets, which cumulatively facilitates the uniform formation of the nanoplates. This seedless method, schematically shown in Figure 9b along with a representative TEM image, has an added advantage of being much faster (completed within 10 min) than the traditional seeded growth process that takes several hours and produced monodisperse nanoplates with high yield.

An understanding of the influence of halide ions on the anisotropic growth of Au NCs will not be complete without a microscopic view of the process, which has been lacking until very recently. In the first among a couple of reports by Meena and Sulpizi, molecular dynamics simulations were used to

DOI: 10.1021/acs.chemrev.8b00158
Chem. Rev. 2018, 118, 7804−7864

explicitly model the interaction of CTAB with gold (111), (110), and (100) surfaces (Figure 10a), where CTAB molecules were found to be forming a layer of distorted cylindrical micelles.[119] The channels among these micelles provided direct ion access to the surface and allowed ions like $AuCl_2^-$, found in the growth solution, to freely diffuse to the gold surface from the bulk solution. The anisotropic growth was clearly shown to be favored due to a lower CTAB on (111) surfaces which also exhibited higher electrostatic potential—a combination that favors higher growth rate at the tip (111) facets. This study was followed by another one from the same group, wherein they simulated the adsorption of CTAB/CTAC mixtures (at different ratios) on gold surfaces.[120] They reported that replacing Br^- with Cl^- (or CTAB with CTAC to be more accurate) led to less compact surfactant layers, and also a lowering in selectivity in packing density among different facets was observed as the Cl^- content went up, so much so that upon full replacement the CTAC micelles prefer to diffuse into the electrolyte solution, leaving the gold surfaces unprotected, which leads to isotropic growth as has been reported by several experimental groups and discussed above. As a demonstration, Figure 10b shows the snapshots of simulations performed on the adsorption of aqueous NaCl and NaBr solutions on Au(111) surfaces and shows a higher likelihood of finding Br^- ions closer to the surfaces than Cl^- ions.

A similar conclusion was also drawn by Almora-Barrios et al. in their density functional theory simulations which modeled the synergistic role of silver and bromide ions in the growth of NRs.[121] The computed adsorption energies of just the halide ions on different gold surfaces show that Cl^- ions adsorb endothermically, Br^- being almost thermoneutral and I^- exothermically bonded. This directly translates into Cl^- ions being unable to block surface growth while I^- ions are too strongly bound, thereby blocking the growth process or the self-healing of labile structures. The binding of Br^- ions was deemed ideal since it is strong enough to direct anisotropy but then again weak enough to let self-healing (adsorption/readsorption) during the growth. However, since the NRs grow from spherical seeds, the anisotropic growth should involve a symmetry breaking event in order to induce growth in a particular direction, which is generally brought about by the Ag^+ ions. A 100% yield of NRs can indeed be ensured by the inclusion of Ag^+ in the growth solution,[122] but adsorption of silver on different gold facets alone cannot account for the anisotropy. The authors found that it is the formation of a $[Br{-}Ag{-}Br]^-$ complex, entrapped by CTA^+ cations forming the crystal shown in Figure 10c, that induces the symmetry breaking event. The resulting CTAB−AgBr complex, as also reported by Hubert et al. earlier,[104] exhibited preferential adsorption on the lateral {100} facets which prompts epitaxial growth of AgBr crystal patches on these facets, thereby blocking growth in this specific direction (Figure 10d).

2.1.2. Surface Etching. From the discussion in the previous section it is apparent that halide ions have a propensity to adhere to gold surfaces with the degree of specific adsorption on low-index Au surfaces scaling as $I^- > Br^- > Cl^- \gg F^-$.[17] Numerous researchers have exploited this spontaneous chemisorption of halide ions (especially iodide ions which exhibit the strongest attachment) to instigate interesting changes in the morphology and concomitant properties of Au NCs. In fact, Pal et al. showed that gold dissolution can already be initiated at room temperature in suitable aqueous iodide-containing systems almost 20 years back.[123] One of the earliest demonstrations on NCs, however, was due to Cheng et al. in 2003, wherein they studied the effect of iodide chemisorption on citrate-stabilized Au NCs.[124] The resulting electron injection into the NCs led to particle fusion and fragmentation in solution. The iodide adsorption displaced the surface citrate ions which lowered the surface potential. This led to increased van der Waals attractive forces between the Au NCs. NC aggregation was observed as a result both in solution and on a solid support. Similar aggregation of octadecylamine-capped Au NCs upon using iodide and bromide species was also reported by Singh et al. in 2007.[125] Kanehara et al. showed controllable size tuning of Au NCs through a bromide-induced coalescence pathway.[126] On the other hand, bromide-induced etching has been exploited to reshape Au NCs as well.[60,127,128] Tsung et al. shortened Au NRs through an oxidative dissolution which took place selectively at the rod tips in the presence of bromide ions (as CTAB; scheme shown in Figure 11a).[127]

Iodine has been shown to fuse gold NRs through dissolution by Wang et al. in 2008.[129] This iodide-induced gold dissolution approach was used to weld gold domains grown on the tips of shape-controlled cadmium chalcogenide NCs by Figuerola et al. in 2009 in order to obtain end-to-end assemblies of various geometries.[130] They exploited the shape anisotropy of these NCs to selectively grow Au islands at specific locations on their surfaces. Small amounts of molecular iodine were then used to destabilize and induce coalescence of the gold domains belonging to different NCs, thereby forming larger Au particles bridging two or more NCs through their tips. This "nano-welding" approach led to linear and cross-linked chainlike assemblies of NRs, propeller, and flowerlike structures from bullet-shaped NCs and networks of tetrapods (schematically shown in Figure 11b). This strategy can be envisaged as a robust alternative to organic and biomolecule-mediated assembly as it introduces an inorganic junction between the NCs.

In an alternative protocol, halide ions have been shown to be effective agents in concurrent growth and etching processes aimed at obtaining NCs with more complex shapes. Guo et al. described the formation of irregularly layered assemblies of gold nanoplates in the presence of Cl^- moieties in 2008, where a slower rate of reduction was attributed to the oxidative etching of the gold atoms by Cl^- ions.[131] The following year Soejima et al. presented a room-temperature "nanocarving" strategy for obtaining complex gold nanoplates having corolla- and propeller-like architectures using bromide ions in a one-pot method.[132] In this simultaneous growth and etching of gold nanoplates in aqueous solution in the presence of poly(vinylpyrrolidone) and molecular oxygen, bromide ions serve the dual role of inhibiting growth along the {111} direction by forming stable adlayers (while promoting growth along the lateral {110} direction) and promoting oxidative dissolution of gold NCs by converting the oxidized Au(I) species to soluble $AuBr_2^-$ ions that led to the formation of ultrathin nanocrevasses (Figure 11c).

Other examples of halide-based dissolution protocols include oxidation and subsequent dissolution of Au NCs in the presence of Br^- (as tetraoctylammonium bromide) and air.[133] Also, the iodide dissolution method was put in use for more complex cases such as that for leaching out gold from Au(core)/iron oxide (shell) heteronanostructures to obtain iron oxide nano-containers and nanoparticles with reactive concave surfaces (Figure 11d), as demonstrated by George et al. in 2011.[134] Liu et al. used the influence of Br^- additive (NaBr) that fused the glutamic acid-stabilized gold nanoparticles together to fabricate

DOI: 10.1021/acs.chemrev.8b00158
Chem. Rev. 2018, 118, 7804−7864

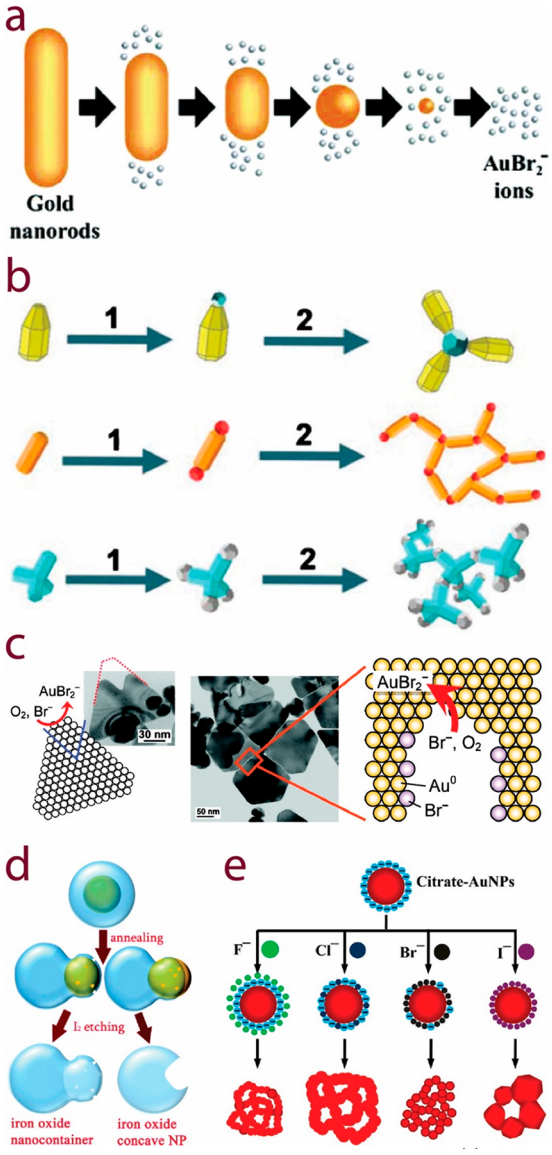

Figure 11. Halide ions acting as etchants on Au NCs. (a) Scheme showing the shortening of Au NRs through oxidative dissolution in the presence of bromide ions. Reproduced from ref 127. Copyright 2006 American Chemical Society. (b) Schematic end-to-end assembly formation of shape-controlled cadmium chalcogenide NCs of various geometries, mediated by the coalescence of tip-Au domains induced by molecular iodine. Reproduced with permission from ref 130. Copyright 2009 John Wiley and Sons. (c) Schematic illustration of vertex erosion and crevasse formation in Au nanoplates through oxidative dissolution in the presence of Br^- ions in a simultaneous growth and etching process. Adapted from ref 132. Copyright 2009 American Chemical Society. (d) Sketch showing the formation of iron oxide nanocontainers and concave nanoparticles formed through iodine-induced leaching out of gold domains from the starting Au(core)/iron oxide (shell) heteronanostructures. Adapted from ref 134. Copyright 2011 American Chemical Society. (e) Formation of spongelike gold nanostructures under the influence of postsynthetic halide treatment on citrate-stabilized Au NCs. Adapted from ref 136. Copyright 2014 American Chemical Society.

sponge-like gold nanostructures.[135] Other sodium halide salts resulted in the formation of irregular aggregates instead, with NaI leading to the formation of larger nanoparticles as well. The reactivity of the different halides was in line with their degree of affinity to gold surfaces ($I^- > Br^- > Cl^- \gg F^-$, as per Magnussen et al.[17]). In particular, NaF and NaCl were unable to replace glutamic acid from the gold surfaces and induced aggregation through a screening effect of the salt addition. Br^- and I^-, on the other hand, were able to replace the ligands where I^- was reactive enough to augment the van de Waals interaction among the NCs leading to faster aggregate formation and particle enlargement. The primary factor behind the sponge formation was believed to be the subtle balance between the van der Waals attractive forces and the electrostatic repulsion among gold surfaces which was found to be optimum for Br^- in this case. Later, Zhang et al. extended this study to citrate-stabilized gold NCs to yield similar spongelike structures.[136] The morphology of the sponges was dependent on the nature of the halide ions (Figure 11e), as also described by Liu et al. More recently, Stein et al. studied the kinetics of these processes on polyethylene glycol-stabilized Au NCs in highly concentrated halide solutions.[137] Oxidative etching of Au NRs by hydrogen peroxide and assisted by halide ions was also found to follow a similar trend.[138]

More recently, there have been reports in the literature where halide-induced etching/dissolution was put to interesting uses. Korgel et al. reported that halide-containing surfactants play an important role in ordered structural transitions in dodecanethiol-capped NC superlattices when heated.[139] They showed that in the absence of any halide-containing surfactants the superlattices do not undergo any transitions until about 190–205 °C when the gold cores coalesce. On the other hand, in the presence of halide-containing surfactants (and oxygen), the same phenomenon occurs at a much lower temperature since the thermal stability of the NCs was reduced through the destabilization of the Au–thiol bond. Zhang et al. demonstrated that the iodine-mediated etching of Au NRs can be employed for the quantitative detection of dissolved oxygen through monitoring the spectrophotometric signatures of nanorod shortening, i.e., blue shift of the longitudinal surface plasmon resonance band.[140] Desmonda et al. demonstrated the influence of halide additives to generate Au nanostructures attached to paper for surface-enhanced Raman scattering substrates.[141] Another example of the influence of halide ions in the etching of gold nanoparticle was reported by Saa et al.,[142] who identified the enzyme horseradish peroxidase as a suitable agent capable of inducing a gradual oxidation of gold NRs, with only trace concentrations of hydrogen peroxide. Halide ions were found to be essential for this reaction to take place. The fact that low amounts of hydrogen peroxide were required to trigger this reaction enabled the authors to exploit the process to design a sensor for detecting physiological glucose concentrations in the human serum.

2.1.3. Alloyed NC Growth. Halide moieties have proved to be important factors in devising successful growth strategies for NCs of alloyed or bimetallic compositions with Au. For instance, Tsuji et al. described a two-step microwave-assisted polyol synthesis of Au@Ag core–shell NCs where the presence of Cl^- moieties was essential for obtaining the desired geometry.[143] The core–shell geometry was achieved through growing an Ag shell on a preformed Au core which was not feasible in the absence of Cl^- ions. The amount of Cl^- ions was calculated by taking into account the contribution from $HAuCl_4$, the gold precursor. The presence of Cl^- ions contributed to oxidative etching of homogeneously nucleated Ag clusters and favored the heterogeneous nucleation on Au seeds. Furthermore, the formation of AgCl reduced the reaction kinetics through

DOI: 10.1021/acs.chemrev.8b00158
Chem. Rev. 2018, 118, 7804–7864

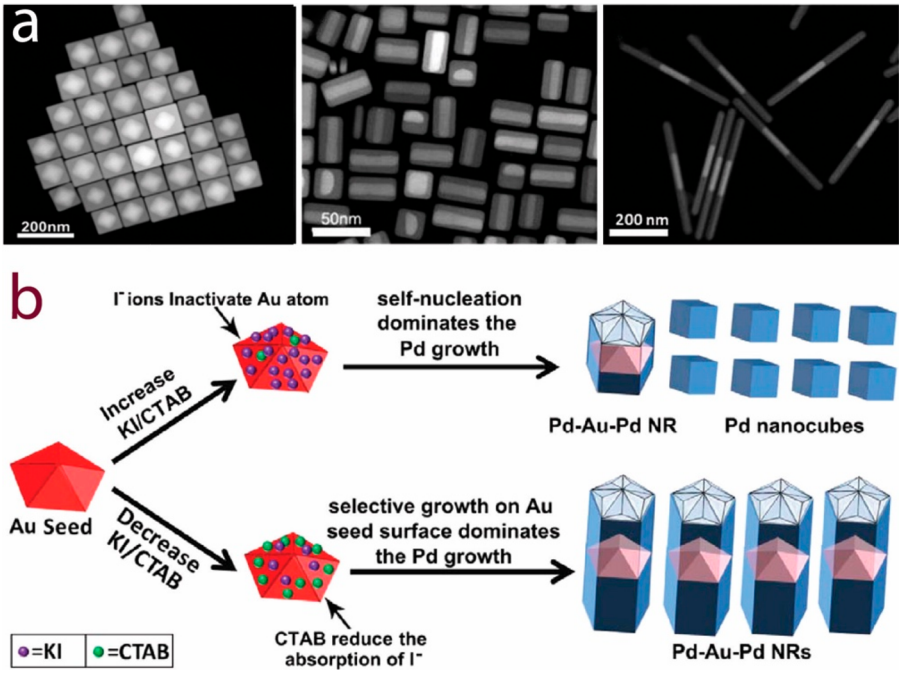

Figure 12. Halide-assisted nanoheterostructuring with Au. (a) Representative HAADF-STEM images of Au@Ag core−shell NCs of various geometries obtained by seeded growth in the presence of Cl^- ions. Adapted from ref 145. Copyright 2013 American Chemical Society. (b) Scheme showing the effect of competition between Br^- and I^- ions on the morphology of Pd−Au−Pd segmental NRs. Reproduced from ref 151. Copyright 2013 American Chemical Society.

reduced availability and nucleation from the Ag precursor, leading to slow facet-selective crystal growth.

Further studies on a similar system were performed by Hong et al., where they demonstrated an Ag shell growth on Au nanodisks as seeds in the presence of I^- ions in aqueous solution.[144] The I^- additives were useful in tuning the direction of the shell growth, i.e., the shell was formed homogeneously over the entire nanodisk surface in their absence, while their presence dictated the growth in the direction perpendicular to the basal plane of the nanodisks. This difference was attributed to slow reaction kinetics (due to formation of more stable AgI) along with the selective heterogeneous nucleation and growth of Ag on the basal {111} facets where I^- ions preferentially adhere and draw the Ag^+ ions to the surface for eventual reduction.

Overgrowth of Ag shell on preformed Au seeds and the effect on halide additives on the growth process was further explored by Gómez-Graña et al.[145] The authors performed the growth process on Au seeds of various morphologies in aqueous solution and concluded that Ag{100} facets are preferentially formed on the shell regardless of the starting morphology and are stabilized by Cl^- ions. The representative HAADF-STEM images of various nanostructures obtained by the authors are shown in Figure 12a. This study was built upon the one from Park et al. describing the Ag shell growth in aqueous solution assisted by slow growth kinetics due to the interaction between Br^- ions (from CTAB) and the Ag precursor.[146] More exotic shapes like Ag@Au−Ag concave NCs have recently been synthesized in the presence of CTAC-derived Cl^- ions by Ahn et al.[147] The authors suggest that halide-assisted oxidative etching and selective facet deposition are responsible for obtaining this specific morphology.

Au−Pd is another combination that has been explored at the nanoscale extensively due to its various catalytic applications. Lee et al. demonstrated a CTAC-assisted one-pot synthesis of Au@Pd core−shell NCs, a geometry not accessible in the presence of a stronger reductant like ascorbic acid (and hence faster reduction kinetics).[148] It was not clear whether oxidative etching by the Cl^- ions was responsible for shape focusing however. Similar influence of Cl^- ions was also demonstrated by Lu et al. in their seed-mediated aqueous synthesis of tetrahexahedral Au@Pd core−shell heteronanostructures.[149] This unique morphology was obtained only when CTAC was used; CTAB led to the formation of cubic core−shell morphology, while the absence of any halide additive resulted in irregular shapes accompanied by smaller Pd NCs. The oxidative etching of the homogeneously nucleated Pd by the added halide ions was clearly at play here in the exclusive formation of the heteronanostructures.

The influence of I^- ions was explored by Annan et al. on the seed-mediated synthesis of rod-shaped Au@Pd core−shell NCs as well.[150] The final morphology was dependent on the presence (or absence) of I^- ions since their selective adsorption on the Pd{110} facets led to changes in the relative growth rate of the three low-index facets [{111}, {110}, and {100}]. Hence, the presence of I^- ions led to the exposure of both {110} and {111} facets in the shell morphology, while in their absence, only {100} facets were dominant. Other exotic structures can also be accessed with the presence of I^- ions in the growth mixture such as the recently reported Pd−Au−Pd segmental nanorods synthesized through Pd overgrowth on Au decahedral NCs through a seed-mediated process.[151] The growth was said to have been mediated by the competition between Br^- (from added CTAB) and I^- ions toward complexing with the Pd precursor and adsorbing on the Au decahedra, modifying the kinetics in the process. $PdBr_4^{2-}$ being more reactive that PdI_4^{2-} led to faster growth, while a higher concentration of Br^- reduced the adsorption of I^- on the Au decahedra, facilitating the formation of the segmental nanorod geometry. Lower Br^- concentration, on the other hand, enabled homogeneous nucleation through increased adsorption of I^- on the surfaces

DOI: 10.1021/acs.chemrev.8b00158
Chem. Rev. 2018, 118, 7804−7864

of Au decahedra which reduced their surface activity (scheme shown in Figure 12b). Similar growth strategies for obtaining Au@Pd NCs involving halide additives as directional overgrowth agents were also reported by other authors.[152,153] In fact, I^- ions were shown to assist the formation of exotic heteostructures like Au−Pd−Au core−shell−frame nanobricks through limiting the growth of the Pd seeds along the {100} surfaces at the corners and edges, facilitating the Au depositions at those sites in the process.[154]

A recent report on the hydrothermal synthesis of Au−Pd heteronanostructure exploits the differential reduction rates of Au and Pd precursors when varying Br^-/Cl^- ratios were used to separately obtain core−shell and alloyed geometries.[155] In this study, Hsu et al. tuned the CTAB/CTAC ratio to modulate the reduction rates of $HAuCl_4$ and H_2PdCl_4 in a coreduction process. In the presence of excess Br^- (or CTAB), the reduction rates of resulting precursor complexes $AuBr_4^-$ and $PdBr_4^{2-}$ are well balanced leading to the formation of alloyed NCs. On the contrary, at higher Cl^- concentrations, the core−shell geometry with a higher local gold content in the core was observed, and this was attributed to the much faster reduction rates for $AuCl_4^-$ than $PdCl_4^{2-}$ complexes.

2.2. Silver NCs

2.2.1. Altered NC Growth Kinetics. Unlike Au NCs where the effect of halide ions can almost never be neglected due to chloroauric acid ($HAuCl_4$) being the choice gold precursor, the influence of halide ions on the growth and transformation of silver (Ag) NCs can be properly delineated since the primary precursor is generally the halide-free silver nitrate ($AgNO_3$). Major contributions in this regard came from Xia's group, where they studied the effect of halide handles on the so-called polyol synthesis of Ag NCs over the years.[62,156−160] The polyol synthesis involves the reduction of silver precursor (silver nitrate) by ethylene glycol at elevated temperatures in the presence of poly(vinylpyrrolidone). In the first such report in 2004, Wiley et al. studied the consequences of adding minute amounts of NaCl to the standard polyol synthesis of Ag nanostructures.[62] They observed dramatic changes on the synthetic pathways and the morphologies of both the nuclei and the products. The addition of Cl^- species led to the formation of monodisperse batches of single-crystalline Ag nanoparticles of the shape of cubes and tetrahedrons with truncated corners and/or edges. The influence of halide ions is remarkable in this scenario since it is generally difficult to obtain high yields of single-crystal Ag nanoparticles due to twinning at small sizes. At small particle sizes thermal instabilities can provide sufficient energy to induce fluctuations between single-crystal and twinned morphologies, the rates of which decrease with increasing particle size.[161] Hence, a mixture of single-crystalline, single-twinned, and multiply twinned structures is generally produced in a Boltzmann-like distribution of crystal structures with the lowest energy multiply twinned dodecahedron being the most abundant one.[162] In the presence of Cl^- ions, the higher reactivity of twinned particles can lead to oxidative dissolution of these nanoseeds early on during the reaction, leading to a slow nucleation and growth of nanoparticles where reduction of silver ions would compete with the oxidative dissolution of the twinned nuclei. In the course of the reaction, the single-crystal seeds continued their slow growth whereas the twinned seeds were eventually consumed, as depicted in Figure 13a.

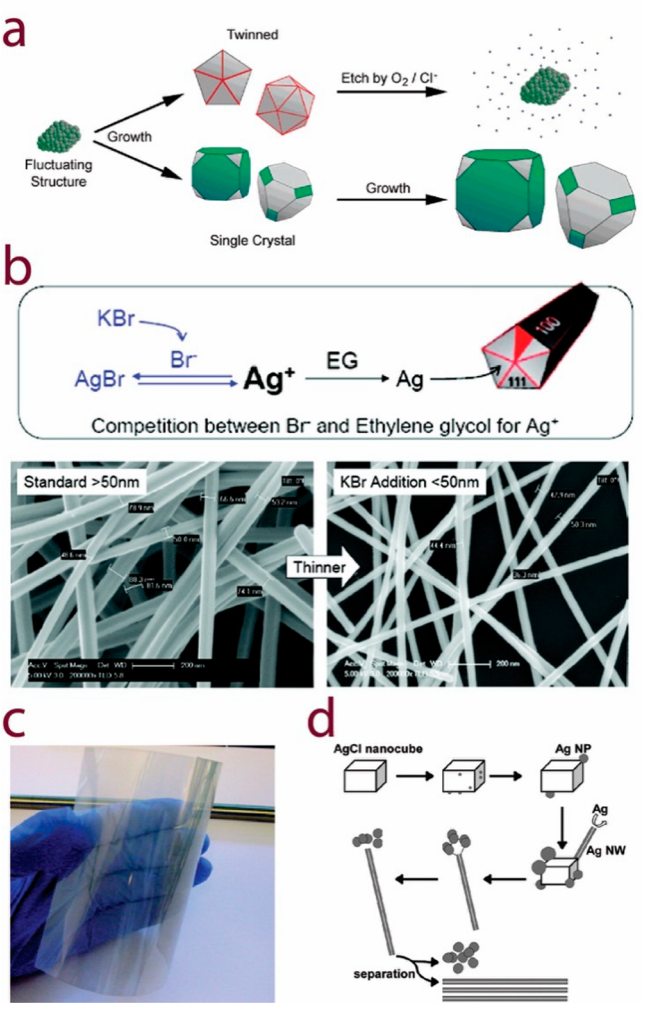

Figure 13. Effect of halide ions on the growth of Ag NCs. (a) Cl^--assisted synthesis of single-crystal Ag NCs where oxidative dissolution of twinned seeds led to high monodispersity in the final cubes and tetrahedrons with truncated corners and/or edges. Reproduced from ref 62. Copyright 2004 American Chemical Society. (b) Reduction of the diameters of Ag NWs synthesized by the polyol method in the presence of Br^- ions, which slowed reduction kinetics through forming stable complexes with the Ag^+ ions. (c) Transparent conducting film fabricated from the same Ag NWs. Adapted from ref 58. Copyright 2010 American Chemical Society. (d) Mechanism governing the heterogeneous nucleation and growth of Ag NWs from AgCl precursors. Reproduced from ref 163. Copyright 2013 American Chemical Society.

This study was followed by reports on using hydrochloric acid by Im et al.[156] and iron(III) chloride by Zhou et al.[164] for the synthesis of single-crystal nanocubes. Apart from being a more robust etching procedure, silver chloride (AgCl) was found to form at the initial stages which might have served as seeds in this case, similar to that for Ag NWs (vide infra). Indeed, Chang et al. showed later that they could produce Ag NWs through the same pathway by simply aging the freshly prepared $AgNO_3$ precursor solution for 5 min.[165] In this case, the aging process merely increased the density of seeds and also changed the population of single and twinned crystal seeds. Later, HCl was also used to demonstrate size tuning in Ag NCs making use of its oxidative etching ability.[166] Then in 2006 Wiley et al. reported the selective nucleation of silver nanoparticles with a single (111) twin which could be grown into right bipyramids by a polyol

DOI: 10.1021/acs.chemrev.8b00158
Chem. Rev. 2018, 118, 7804−7864

method in the presence of NaBr.[157] These single-twinned seeds were not produced when Cl^- ions were present, possibly due to the more corrosive nature of these ions which preferentially etched the twinned particles away. The relatively less corrosive Br^- ions etched away those seeds with multiple twin defects but left the seeds with a single twin defect to grow. Subsequent modification of this synthesis protocol, wherein the concentration of Br^- was doubled, led to the formation of Ag nanobars.[158] Later, Zhang et al. examined this protocol in more detail to conclude that ionic bromide salts were more effective for the nanobar formation than covalent molecules.[159] Chloride and iodide ions were ineffective toward nanobar formation; Cl^- yielded nanocubes, whereas I^- led to the formation of cuboctahedra.

In 2012, Br^- addition in the polyol synthesis was exploited to produce Ag nanowires with diameters smaller than 30 nm which can be used as conductive elements in transparent electrodes commonly employed in touch screen panels and flat and flexible displays.[167] For instance, Hu et al. successfully reduced the diameters of pentatwinned Ag NWs to less than 50 nm from about 100 nm through the addition of KBr in polyol synthesis (Figure 13b) and fabricated transparent conductive films from them (Figure 13c).[58] Then in 2013 Lee et al. reduced the diameters further to the range of 15−30 nm through a high-pressure polyol synthesis in the presence of a mixture of Br^- and Cl^- ions.[168] In 2015, further control on the diameter and concomitant optoelectronic performance of Ag NWs through adjusting the concentration of Br^- (in the added Br^- and Cl^- mixture) was demonstrated by Li et al.[169] It is important to note that the halide ions serve to bind with Ag^+ ions generating more stable complexes which slow down the reduction kinetics,[58,170] in addition to NC surface capping which reduces the rate of atomic addition to the growing NWs as well.[171] However, the decrease in diameter observed by Li et al. upon Br^- addition was believed to be caused by an increase in the number of nucleation events, with a smaller contribution from slower reduction kinetics. This increase in nucleation events was attributed to the formation of a silver halide nanoparticle precipitate, which has been demonstrated to be an effective agent for heterogeneous nucleation of Ag NWs (Figure 13d).[163,172]

This complex interplay of the various factors dictating the growth kinetics was put to good use by da Silva et al. in 2016 to further refine the synthesis and obtain Ag NWs with a pentatwinned structure of even higher aspect ratios (~1000, with diameters < 20 nm) through restraining their lateral growth by both Br^- and poly(vinylpyrrolidone) which capped the {100} side facets.[160] They slowed down the reduction kinetics by introducing the $AgNO_3$ precursor through a syringe pump and by using Br^- at an appropriate concentration at the same time, so that the precursor gets converted into a more stable silver bromide (AgBr). Using Cl^- additive (NaCl) instead of Br^- resulted in larger diameter NWs, which means that Cl^- ions were less effective in slowing down the reaction kinetics and hence confining the lateral growth. On the other hand, the formation of the sparingly soluble AgI upon adding NaI slowed the reaction kinetics to such an extent that it led to the formation of large and irregular structures.

Indeed, it was the presence of Cl^- ions in polyol synthesis that was previously exploited to produce Ag NWs. For instance, in one of the first such reports, Gou et al. presented a microwave-assisted polyol synthesis of Ag NWs in the presence of NaCl in 2007.[170] The rapid microwave heating was believed to have created more nucleation sites, but oxidative dissolution of many of these sites resulted in a dynamic equilibrium which favored a 1D growth. Oxidative etching of smaller particles by Cl^- ions was also demonstrated to play an important part in yielding Ag NWs by Tsuji et al.[175,176] Slowed down reduction kinetics due to the formation of AgCl was indicated to be responsible for the NW growth later.[177] However, unlike Br^- (as described in the previous paragraph), the amount of added NaCl exhibited hardly any remarkable effect on the diameter and the length of the NWs,[178] although a recent report claims diameter and aspect ratio tunability with Cl^- ions when used in conjunction with the added oxidative ability of Fe^{3+} ions.[179]

Apart from the oxidative role played by halide ions, chemists have also separately explored the anisotropic growth of Ag NCs promoted by halide ions selectively capping specific crystal facets. Kim et al. described selective vertical growth in Ag nanoplates in the presence of I^- ions, wherein they were able to control the lateral and vertical dimensions of the nanoplates by varying the time at which the I^- ions were added to the growth mixture (Figure 14a).[173] The nanoplates were composed of basal {111} facets and alternate {111} and {100} facets on the edges. As is apparent from the scheme depicted in Figure 14a, halide ions promoted the growth in the {100} direction in the order of $Cl^- < Br^- < I^-$. Along similar lines, Zhang et al. reported

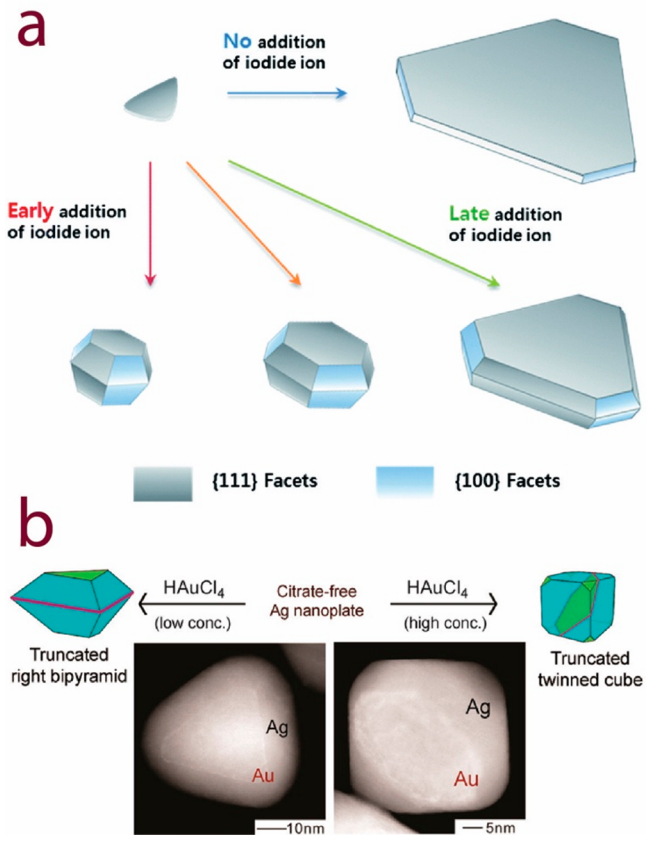

Figure 14. Selective facet capping by halide ions as a Ag NC growth promoter. (a) Growth promotion in the {100} direction of Ag nanoplates leading to selective vertical growth in the presence of I^- ions, with the resulting morphology dependent upon the time of addition of the I^- species. Reproduced with permission from ref 173. Copyright 2014 Royal Society of Chemistry. (b) Vertical growth in Ag nanoplates in the presence of Cl^- ions introduced as $HAuCl_4$; morphology dependent on the Cl^- concentration. Reproduced from ref 174. Copyright 2014 American Chemical Society.

DOI: 10.1021/acs.chemrev.8b00158
Chem. Rev. 2018, 118, 7804−7864

the formation of Ag nanoplates with a triangular or hexagonal shape in the presence of Cl^- ions, which exhibited further vertical growth into truncated right bipyramids or twinned cubes on addition of $AgNO_3$ depending upon the Cl^- concentration (Figure 14b).[174] They used $HAuCl_4$ as the Cl^- source and that for Au to be used as a marker in electron microscopy analysis. The {111} facets were believed to have grown in preference to the {100} facets when Cl^- ions were present.

2.2.2. Sculpting NCs through Etching. The corrosive nature of halide ions toward metal surfaces had been utilized in sculpting different morphologies for Ag NCs by various researchers. An et al. used Cl^- ions to etch out the corners and side facets of photochemically prepared citrate-stabilized Ag nanoprisms to obtain disk-like NCs.[180] The silver atoms at the side {110} and corner facets possess higher surface energy (owing to a lower Ag coordination number) than those at the basal {111} planes[181] and hence were etched away with relative ease. Moreover, the vertex areas of the nanoprisms were capped with a lesser amount of citrate ions than the basal facets and were more susceptible to the Cl^- attack. The sculpting process produced small Ag clusters which were believed to have formed from the etched-out Ag atoms, and might have contributed to the increase in thickness of the resulting nanodisks through deposition on the basal planes. This two-stage sculpting process is depicted in Figure 15a. The same group then went on to study

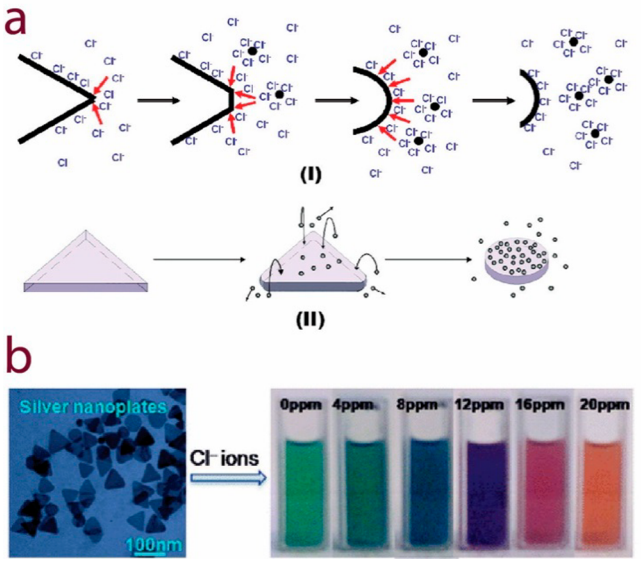

Figure 15. Halide ions acting as etchants on Ag NCs. (a) Mechanism of the two-stage sculpting process of Ag nanoprisms in the presence of Cl^- ions: (I) Ag atoms getting etched off from the vertex areas and (II) the small Ag clusters formed from the etched-out Ag atoms deposit on the basal planes increasing the thickness of the resulting nanodisks. Reproduced from ref 180. Copyright 2008 American Chemical Society. (b) Colorimetric sensing of Cl^- ions at different concentrations by silver nanoplates. Reproduced from ref 183. Copyright 2008 American Chemical Society.

the effect of the nature of halide ions on the sculpting process and suggested that the etching ability followed the order of $Cl^- < I^- < Br^-$.[182]

These reports were followed by a consecutive growth-and-etch process described by Cathcart et al. in 2009.[184] They obtained Ag NCs of various planar twinned morphologies ranging from the starting triangular nanoprisms to hexagonal and rounded platelets and to smaller cubic and bipyramidal particles by this method, accompanied by the concomitant plasmon resonance tuning. The nanoprism edges were rounded when the synthesis was performed in the presence of Br^- ions, while introducing Cl^- ions during the synthesis led to the formation of larger and well-defined nanoprisms. The NC transformations by the postsynthetic halide treatment were affected by the nature of the halide ions, with Cl^- bringing about a slower change than Br^- and I^- at the same concentration, in line with the degree of halide adsorption ($I^- > Br^- > Cl^-$) and resulting covalency in the metal–halide bond. The sensitivity of the plasmon resonance optical response of the Ag NCs in the presence of halide ions was demonstrated by Linner et al. back in 1993[185] and has been exploited for colorimetric detection of halide ions by Jiang et al. in recent times (2008), as shown for the detection of Cl^- ions at ppm level concentration in Figure 15b.[183]

2.3. Palladium NCs

2.3.1. NC Growth Modulation. Similar to the other noble metals crystallizing in the face-centered cubic crystal structure discussed so far (Au and Ag), halide ions show particular propensity to bind strongly to high-index crystal facets (those having at least one index larger than 1) of Pd surfaces as well.[80] Naturally, this tendency has also been exploited in the growth and transformation of Pd NCs. The effect of halide ions on the polyol process (as had been used extensively in the case of Ag NCs; see section 2.2.1) as a suitable synthetic handle for synthesizing Pd NCs had been demonstrated early on by numerous reports from Xia's group.[186−191] However, unlike Ag NCs, the polyol synthesis of Pd NCs involves the reduction of $PdCl_4^{2-}$ precursor, which already contains Cl^- species, by ethylene glycol at elevated temperatures in the presence of poly(vinylpyrrolidone). In the first of these reports in 2005 Xiong et al. showed that the oxidative dissolution by added Cl^-species led to the removal of twinned particles leaving behind the single-crystal cuboctahedra, similar to that in the silver system.[186] Almost immediately followed another report from Xiong et al., which described the selective synthesis of triangular or hexagonal nanoplates through a substantially slowed down growth kinetics by introducing a couple of oxidative etchants in the growth mixture: Fe(III) and Cl^- species.[187] The dual oxidative dissolution of the multiply twinned particles (from their admixture with single-crystal particles) was necessary to achieve a tighter control over the nucleation and reduction kinetics and obtain anisotropic thin platelets. Both of these processes were extremely slow and led to the continuous growth of the Pd seeds as more Pd atoms were added to their surfaces, although the small number of seeds and high Pd precursor concentration led to additional nucleation events forming Pd atoms. However, the formation of thermodynamically favored single-crystal cuboctahedra could not be completely prevented, and the final product exhibited a relatively broad distribution in shape and size.

These reports were followed by another one from Xiong et al. where they demonstrated the growth of highly anisotropic Pd nanostructures viz. nanobars bounded by {100} facets and single-crystal NRs with {100} and {110} lateral facets in kinetically controlled conditions achieved through the chemisorption of Br^- ions on the seeds which promoted the formation of these facets.[188] The one-dimensional growth was induced through the breaking of the cubic symmetry of the Pd fcc structure that was accomplished through an interplay of various

DOI: 10.1021/acs.chemrev.8b00158
Chem. Rev. 2018, 118, 7804−7864

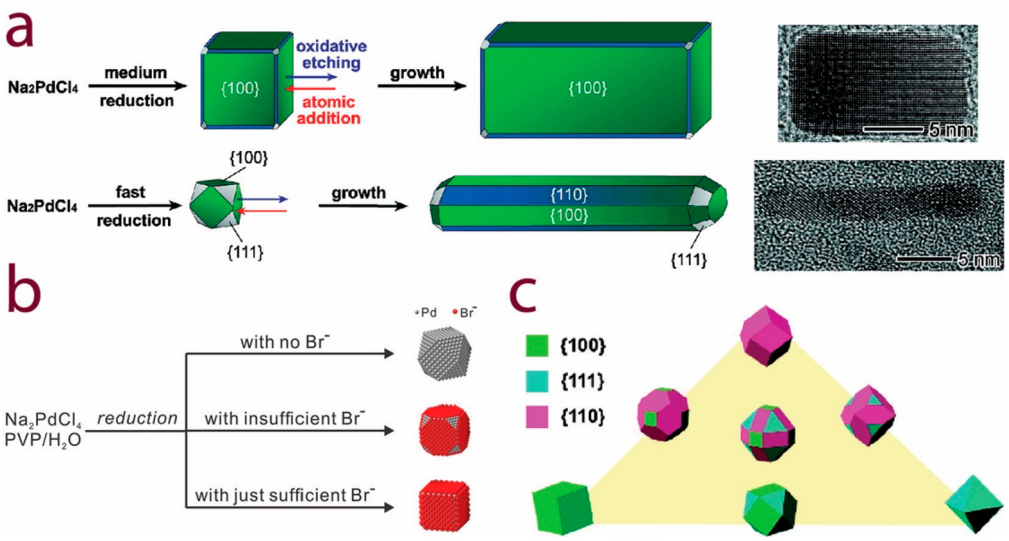

Figure 16. Influence of halide ions as the growth of Pd NCs. (a) Mechanistic pathways responsible for the formation of Pd NRs and nanobars in the presence of Br^- ions, with representative TEM images of the respective nanostructure. Kinetically controlled growth accomplished through the chemisorption of Br^- ions that promoted the {100} and {110} facets. Oxidative etching was realized by the Cl^- ions from the $PdCl_4^{2-}$ precursor. Adapted from ref 188. Copyright 2007 American Chemical Society. (b) Shape modulation through controlling the Br^- content in the growth mixture, which selectively adsorbed on the Pd{100} facets and slowed the growth rate along the [100] direction. Adapted from ref 189. Copyright 2013 American Chemical Society. (c) Geometrical models of the single-crystal Pd nanostructures with various polyhedral shapes that can be achieved through exploiting the interplay between I^- content and the reaction temperature which favored the formation of different facets at different combinations. Reproduced from ref 192. Copyright 2010 American Chemical Society.

processes which also include the oxidative etching by the Cl^- ions (from $PdCl_4^{2-}$ precursor) of one specific facet, apart from the Br^- chemisorption. This localized oxidative etching creates an active site for atomic addition, which leads to the formation of an elongated nanostructure with a square cross-section when done quickly and when done at medium rate leads to the formation of nanobars (Figure 16a). The NRs obtained were thinner than the nanobars, since more seeds were formed at a faster reduction rate.

It is important to note here that corrosion occurs from only one side of Pd nanocubes, even though all of the sides are equivalent {100} facets.[193] This was an important factor in the synthesis of these kinetic products, which could be aged to obtain the more thermodynamically favored cuboctahedrons. Interestingly, Br^- ions did not participate in oxidative etching, being less corrosive than Cl^-. This difference was apparent from the lower aspect ratios of the nanostructures obtained when Na_2PdBr_4 was used as the Pd precursor instead of Na_2PdCl_4. The influence of the chemisorption was also defined by the halide ions employed. In fact, going by the trend in chemisorption of the halide ions on Pd surfaces ($Cl^- < Br^- < I^-$, as per Carrasquillo et al.[194]), the surface protection and promotion of {100} and {110} surfaces were not remarkable when KCl was used instead of KBr and led to the formation of the cuboctahedrons. On the other hand, I^- chemisorption was so strong that larger particles with well-defined shapes were difficult to grow. The authors also extended this anisotropic shape control to Au and Pt nanostructures.

It is however imperative to remember that in all of these studies by Xia et al. Na_2PdCl_4 was used as a precursor which contributed to the halide content of the reaction mixture in ethylene glycol. The role of halides in the formation of the nanocubes, hence, is difficult to delineate without considering the precursor contribution. Huang et al. addressed this issue by using the intrinsically halide-free palladium acetylacetonate as the Pd precursor and demonstrated the formation of Pd nanocubes in dimethylformamide in the presence of I^-[195] instead of Br^- for polyol synthesis as described above.[188] The different reaction media and precursors should then be taken into account while discussing the growth processes.

Later in 2013 Peng et al. demonstrated further implications of the selective chemisorption of Br^- ions on Pd surfaces.[189] The selective adsorption to Pd{100} facets slowed the growth rate along the [100] direction forming cubes enclosed by {100} facets. Ab initio studies on the adsorption behavior of Br on Pd surfaces support such a scenario.[196] Peng et al. further determined a critical concentration of the Br^- additive that was able to produce Pd nanocubes. Hence, the morphology of the final product was controlled by the Br^- content in the reaction mixture (Figure 16b) with the formation of the thermodynamically favored cuboctahedrons in the absence of any Br^-. Truncated nanocubes with some {111} facets were produced when the amount of Br^- was below the critical value, since the Pd{100} surfaces could not be fully stabilized. Liu et al. further demonstrated that these nanocubes could be transformed into octahedra simply through oxidative etching by HCl.[190]

Another report from Xia's group investigated the use of iodide ions in manipulating the strength of the oxidative etching and selective capping of the {100} facets.[191] They synthesized Pd right bipyramids (RBPs) that have a singly twinned structure, covered by six right-isosceles triangular {100} facets and bisected by a very thin twin plane along the ⟨111⟩ direction. Similar to Peng et al. (described above),[189] the I^- content was crucial in the formation of this unique structure since an increase led to the formation of nanocubes and a decrease resulted in multiple-twinned NRs. Control experiments suggested that Cl^- ions have no capping effect on Pd(100) surfaces, unlike Br^- and I^-.[189,191] Recent (2017) investigations from Xia's group indicate the increased propensity of etching by I^- ions at the vertices of

DOI: 10.1021/acs.chemrev.8b00158
Chem. Rev. 2018, 118, 7804−7864

the NRs.[197] Also, Peng et al. did not observe the formation of RBPs due to the stronger etching power of the Br^- ions which led to dissolution of the twinned seeds blocking the formation of RBPs.[189]

Similar conclusions were drawn in reactions performed in an aqueous medium as well. The preferential binding of I^- ions to the Pd{100} facets had been used previously to induce anisotropy, albeit in the realm of hydrothermal synthesis of Pd nanostructures.[198,199] Similarly, Niu et al. demonstrated the synthesis of single-crystal Pd nanostructures with various polyhedral shapes through a seed-mediated protocol where I^- was used as an additive.[192] The various shapes (rhombic dodecahedral, cubic, octahedral, and their derivatives) were made accessible through exploiting the interplay between I^- content and the reaction temperature which favored the formation of different facets at different combinations (Figure 16c). A similar systematic shape evolution was demonstrated by Liu et al., wherein Pd NCs were directly grown in an aqueous mixture of H_2PdCl_4, CTAC, KBr, KI, and ascorbic acid.[200] The particle shape control was achieved by adjusting the amount of KBr added. Then in 2014 Lu et al. described a hydrothermal synthesis of 5-fold twinned nanowires and single-twinned RBPs by adjusting the oxidative etching ability of the halide ions through their electrostatic interactions with small organic molecules.[201] Further modulation of the oxidative etching was brought about by using hydrochloric acid (HCl) which led to the shape evolution of Pd NCs from nanocubes bounded by {100} facets to octahedrons bounded by {111} facets.[202] Contrary to the observations by Xiong et al.,[188] the surface protection and promotion of {100} facets leading to the formation of nanocubes was possible even in the absence of Br^- additive in this case, probably because the synthesis involved the reduction of H_2PdCl_4 precursor in the presence of cetylpyridinium chloride surfactant—a very different chemical environment. Previously, oxidative etching by HCl was utilized in controlling the size of the Pd NCs.[166] Shape control using Cl^- ions was also demonstrated by Nalajala et al. in an aqueous medium.[203] They show that the weakly adsorbing Cl^- ions can protect the {100} surfaces dictating anisotropic growth when used above a threshold value and the presence of atmospheric oxygen was minimized slowing down the oxidative etching. The amount of dissolved oxygen in the reaction medium was not found to be an important factor when Br^- was used instead. In a slightly different approach, Pd NCs were obtained by a Br^--mediated laser ablation protocol in water, where the selective adsorption on {100} facets was shown to play a part in forming the resultant morphology.[204]

A substantial contribution toward understanding the influence of halide ions on the growth of Pd NCs in aqueous media was also made by Xia's group.[63,205−210] In the first such report in 2007 Xiong et al. presented the synthesis of 5-fold-twinned NRs and RBPs of Pd in aqueous solution containing Br^- ions.[205] Later in 2009 Lim et al. reported the growth of Pd nanobars in an aqueous solution through the reduction of Na_2PdCl_4 with ascorbic acid in the presence of Br^- ions as the capping agent which promotes the formation of {100} facets.[63] The aspect ratio of the obtained nanostructures was controlled simply by adjusting the temperature. Similar to the observations made in the case of polyol synthesis,[186] the population of differently structured seeds (single crystal and twinned) in this case could also be controlled by taking advantage of oxidative etching by Cl^- ions contributed from the Na_2PdCl_4 precursor when the reaction is performed in air. The coupling of this etching process with the fast reduction by ascorbic acid ensured the formation of the thermodynamically favored single-crystal cuboctahedrons and selective etching of the twinned particles (Figure 17a). When Br^- ions were added to this reaction

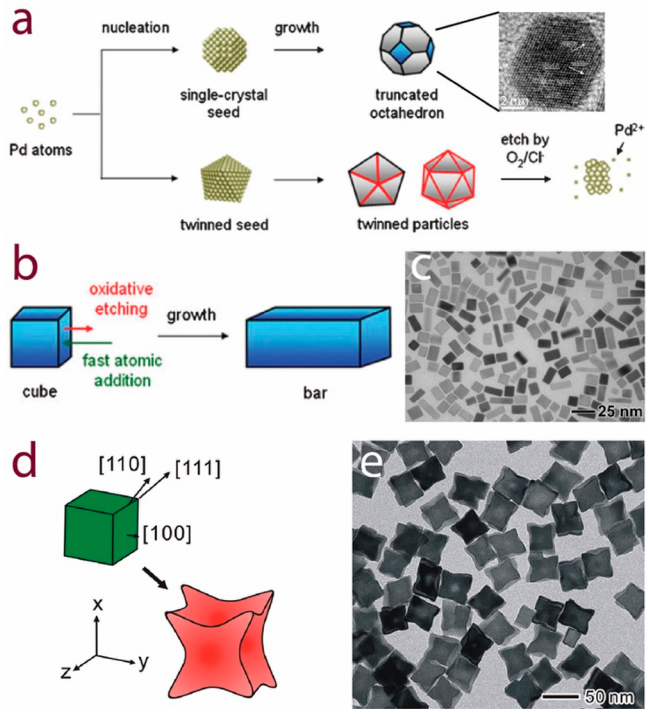

Figure 17. Exploiting the interplay of the etching and capping prowess of halide ions on the growth of Pd NCs. (a) Mechanism showing the formation of thermodynamically favored single-crystal octahedrons and selective etching of the less stable twinned particles by Cl^- ions (from the Na_2PdCl_4 precursor) in the presence of air and coupled with fast reduction by ascorbic acid. (b) Preferential adsorption of Br^- ions to the Pd{100} facets then led to the formation of Pd nanobars when combined with localized oxidative etching by Cl^- ions, described in a. (c) TEM image of the nanobars formed by halide mediation. Adapted with permission from ref 63. Copyright 2009 John Wiley and Sons. (d) Schematic depiction of the formation of concave nanocubes of Pd through preferential overgrowth of the corners and edges at lower Br^- concentrations which favored growth along the ⟨111⟩ and ⟨110⟩ directions. Adapted from ref 209. Copyright 2013 American Chemical Society.

mixture, they preferentially chemisorbed onto the {100} facets and favored their formation. This led to Pd NCs enclosed by these very facets, such as nanobars and NRs, similar to the observations by Xiong et al. in the case of polyol synthesis.[188] The localized oxidative etching that took place on only one of the six {100} faces was instrumental in the preferential growth of this particular face.[193] This could break the symmetry of the nanocube eventually leading to anisotropic growth into a nanobar (mechanistically shown in Figure 17b, representative TEM image in Figure 17c).

Further mechanistic insights into this growth process were offered in a subsequent report by Lim et al. in 2010, where they demonstrated that the Br^--assisted growth at early stages was dominated by particle coalescence, followed by shape focusing through recrystallization[206] In 2011 Jin et al. showed that the rate of reduction of Na_2PdCl_4 could be controlled by adjusting the concentrations of the added Br^- and Cl^- ions.[207] Apart from binding to the {100} facets, the halide species can also modulate

DOI: 10.1021/acs.chemrev.8b00158
Chem. Rev. 2018, 118, 7804−7864

the reaction kinetics through forming stable complexes with Pd^{2+} ions in aqueous solutions. Also, upon increasing the amount of ascorbic acid relative to that of Na_2PdCl_4 and KBr, concave nanocubes of Pd enclosed by 24 high-index {730} facets could be obtained by a seeded growth protocol where Pd nanocubes were used as seeds.[208] This was possible due to the preferential overgrowth at the corners and edges of a cubic seed along the ⟨111⟩ and ⟨110⟩ directions, which grew faster during fast reduction by increased amount of ascorbic acid, as schematically depicted in Figure 17d. A representative TEM image of the concave nanocubes is shown in Figure 17e.

The critical role of the Br^- capping in the growth of these concave nanocubes has been recently examined by Peng et al. through the application of the collision model.[210] During seed-mediated growth, the incoming Pd atom upon collision can desorb, deposit, or migrate on the surface of the receiving Pd nanocube seed. The presence of a capping agent that passivates selective regions of the seed will then retard the deposition, only letting desorption and migration occur. This means that the incoming Pd atoms can only nucleate and grow on the bare surfaces of the seed. Building on this hypothesis, they demonstrated experimentally that the heterogeneous nucleation of Pd atoms occurred only at the corner and edge sites when the {100} side faces were passivated with chemisorbed Br^- ions. On the other hand, upon advanced removal of the Br^- ions prior to the seeded growth, the incoming Pd atoms were found to randomly nucleate on the entire nanocube surface.

2.3.2. Forming Alloyed NCs. The halide "factor" that has been exploited in developing growth strategies for Pd NCs, as illustrated in the previous section, has also been put to use while developing synthesis protocols for growing alloyed and bimetallic nanostructures with other metals. Combining Pt with Pd has received considerable attention in this matter, mostly due to Pt being a fundamental catalyst in many processes and also as a way to reduce consumption of the expensive Pt metal in catalysis. In one of these earliest reports in 2009, Huang et al. demonstrated the synthesis of hollow single-crystalline Pd/Pt alloy nanocubes by a solvothermal protocol with dimethylformamide (DMF) as the solvent and I^- ions as morphology controllers.[195] They used the halide-free palladium acetylacetonate precursor unlike the more commonly used Na_2PdCl_4 as described for numerous reports in the previous section. This provided the authors a unique opportunity to examine the role of halides in these growth processes without having to take the chloride contribution from the precursor into account. The same reaction yielded multiple-twinned NCs in the absence of I^- ions and in the presence of other halide ions (F^-, Cl^-, and Br^-). The I^- ions preferentially coordinate with the Pd^{2+} ions forming the PdI_4^{2-} precursor when introduced in a mixture of $Pd(acac)_2/Pt(acac)_2$ in DMF. Although according to reduction potential considerations, Pt(II) should be reduced before Pd(II) upon coordination by the same ligands; the authors showed that Pd nanocubes were formed first followed by their galvanic replacement by Pt(II) species in the presence of I^-. This variation was attributed to the different reduction kinetics due to more favorable reduction of PdI_4^{2-} over $Pt(acac)_2$. The nanocubes were mainly enclosed by {100} facets.

A hydrothermal synthesis of Pd–Pt nanocubes exhibiting similar faceting was also reported by Yin et al. later in 2011.[211] They used a mixture of Br^- and I^- ions as {100} facet-selective agents and used K_2PdCl_4 as the precursor. In the same year, Zhang et al. described a Br^--mediated galvanic replacement by $PtCl_6^{2-}$ ions from the {100} facets of Pd NCs.[212] Pd–Pt bimetallic NCs with a concave structure were formed due to this site-selective galvanic replacement which led to simultaneous dissolution of Pd atoms from the {100} facets and deposition of the Pt atoms on the {111} facets, as schematically shown in Figure 18a. This selective replacement was proposed to be

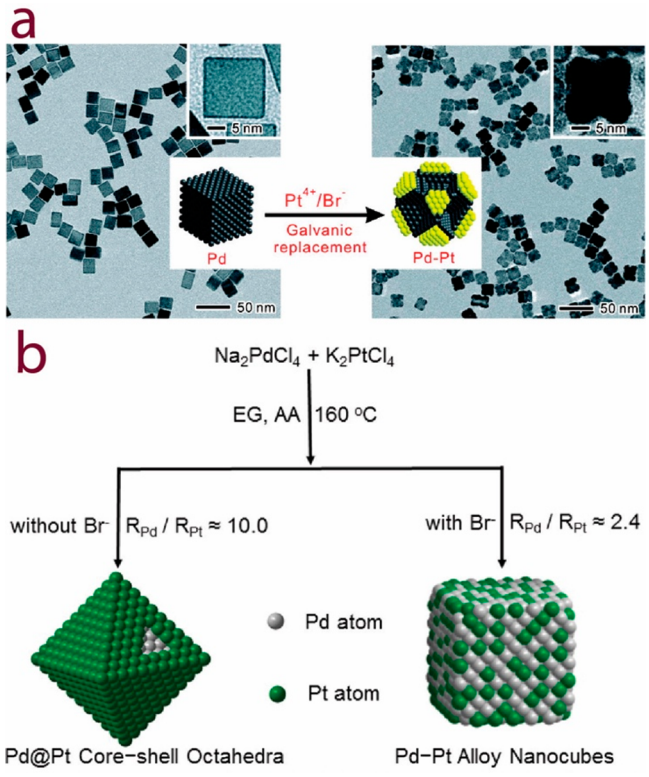

Figure 18. Alloying Pd with Pt under the influence of bromide ions. (a) Formation of Pd–Pt bimetallic NCs with a concave structure through galvanic replacement mediated by Br^- ions—simultaneous dissolution of Pd atoms from the side facets and deposition of Pt on the edges and corners. Reproduced from ref 212. Copyright 2011 American Chemical Society. (b) Scheme describing the different rates of reduction in the absence and presence of Br^- ions leading to two distinctive structures of Pd–Pt NCs. Adapted from ref 217. Copyright 2016 American Chemical Society.

induced and facilitated by the Br^- species through their preferential adsorption on the Pd{100} facets and strong complexation with the Pt^{4+} ions. No replacement occurred in the absence of Br^- ions. A similar strategy was also used in the synthesis of Pd–Rh core-frame concave nanocubes by the same group, except that the NCs were created by Rh overgrowth on the edges and corners of the Pd nanocubes and not by replacement.[213]

In 2012 Huang et al. demonstrated the synthesis of single-crystalline Pd–Pt alloy NCs with controllable shapes using halide ions as shape-directing agents.[214] More specifically, in a synthesis performed in DMF with K_2PdCl_4 and K_2PtCl_4 as respective metal precursors, alloy nanocubes enclosed by {100} facets were formed in the presence of I^- ions and octahedra/tetrahedra terminated by {111} facets were obtained when Cl^- ions were employed. Intriguingly, a mixture of these nanostructures was obtained when Br^- ions were used as an additive. In 2015, a Br-mediated synthesis of Pd@Pt core–shell nanowires through a galvanic replacement pathway was described by Li et al.[215] Zhang et al. obtained morphologies

DOI: 10.1021/acs.chemrev.8b00158
Chem. Rev. 2018, 118, 7804–7864

ranging from dendritic core−shell, layered core−shell, to mesoporous core−shell for Pd−Pt nanoparticles by changing the halide ions added to the growth mixture.[216]

For these bimetallic and alloy NCs the principal means by which the halide ions influence the reduction kinetics is largely through them influencing the redox potentials of the metal precursors by way of ligand exchange. The recent contribution from Xia's group is noteworthy, where they elucidated the mechanisms responsible for the formation of Pd−Pt bimetallic NCs with two distinctive structures, which form due to differential relative rates of reduction between Pd and Pt precursors in the presence and absence of bromide ions (Figure 18b).[217] In the absence of Br^- ions, the initial reduction rate for $PdCl_4^{2-}$ precursor was 10 times as fast as that for $PtCl_4^{2-}$ precursor, resulting in the formation of core−shell Pd@Pt octahedra. Cube-shaped alloy NCs were formed instead when Br^- ions were present, since the ratio of reduction rates dropped from 10 to 2.4 in this case owing to the ligand exchange forming $PdBr_4^{2-}$ and $PtBr_4^{2-}$. Also, the selective capping of the {100} facets by Br^- ions played a vital role in defining the cubic morphology.

Xia's group also extended these growth strategies in synthesizing Pd−Cu bimetallic tripod NCs by a seeded growth method, where triangular plate-like Pd seeds were used for preferential deposition of Cu on the three corners as the strong binding of Br^- ions on the {100} side facets hinders further atomic attachment in those sites.[218] In 2015, Cabot's group demonstrated the synthesis of Pd_2Sn NRs through a coreduction process in the presence of Cl^- ions.[219] The aspect ratio of the NRs was dependent on the Cl^- content since the growth at the nanorod tips was aided by the selective desorption of surfactant TOP molecules by Cl^- ions.

2.4. Copper NCs

Although halide ions have been demonstrated to play an important role in the growth of Cu NCs by a few research groups, there are not many comprehensive studies on this matter. Nevertheless, the principles behind the effect of halide ions on the growth and transformation of Cu NCs are the same ones as illustrated above. One of the first reports was due to Filankembo et al. in 2003.[220] They demonstrated the growth of Cu NRs in $Cu(AOT)_2$−isooctane−water solution enabled by the chloride ions where the aspect ratio was varied by adjusting the chloride concentration in the growth mixture. Br^- ions, on the other hand, had an almost negligible effect on the aspect ratio increment. Similar to the case of other fcc metals as seen above, the nanorod formation was attributed to the selective adsorption of Cl^- ions on the side {100} facets, thus hindering their growth, while the tip {111} facets grew preferentially. Further studies on this microemulsion-based system were performed by Kitchens et al., where propane was used as a solvent and HCl as the source of Cl^- ions.[221] They reported a faster growth rate at a higher concentration of Cl^- ions in the growth mixture. The corrosive nature of halide ions was also used by Huang et al. in preparing CuO nanoshells from Cu nanoparticles.[222] In 2013, Venkatasubramanian et al. demonstrated an electrochemical approach for the synthesis of anisotropic copper nanoplates in the presence of Br^- ions.[223] The Br^- ions were said to bind selectively to the higher energy {111} crystal facets constituting the faces of the nanoplates, thereby altering the relative surface energies of the various facets and influencing the growth kinetics, which favored lateral growth.

2.5. Rhodium NCs

Similar to Pd, Rh NCs are also important for many catalytic applications, and hence, an understanding of the effect of their faceting on the catalytic performance is important. However, such manipulation of morphology and even more so the effect of halide on that, as has been discussed in the case of other noble metals, has otherwise been challenging for Rh NCs which is reflected in the far fewer number of reports in this case. The first such demonstration was by Somorjai's group in 2008, where trimethyl(tetradecyl)ammonium bromide was used as Br^- source in a polyol synthesis, which stabilized the {100} facets of Rh nanocubes and facilitated their formation in the process.[224] However, $RhCl_3$ was used as the Rh precursor, and hence, the Cl^- ion contribution on the growth cannot be completely ruled out, although no chlorine was detected in the subsequent elemental analysis of the nanocubes. Br^- ions induced the shape selectivity as is evident from the primary products being cubes and truncated cubes, while in its absence faceted yet polydisperse NCs were produced (Figure 19a). The authors further extended this growth strategy to obtain Pt and Pd nanocubes.

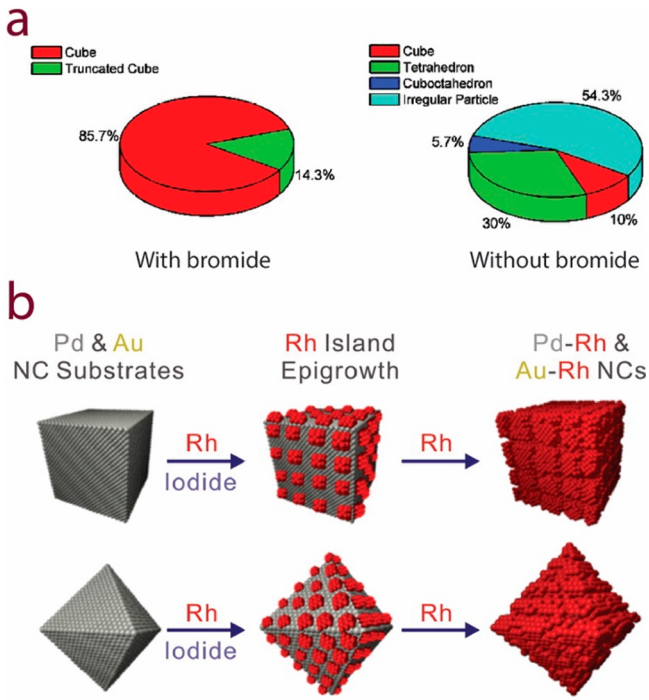

Figure 19. Halide ions influencing Rh NC growth. (a) Distribution of shapes produced in the presence and absence of Br^- ions, with the former showing higher shape selectivity. Adapted from ref 224. Copyright 2008 American Chemical Society. (b) Schematic showing the epigrowth of Rh on Pd (and Au) NCs in the presence of I^- ions. Adapted from ref 227. Copyright 2012 American Chemical Society.

The effect of various halide ions on Rh NC growth in the aqueous media was investigated by Yuan et al.[225] They obtained varying morphologies such as cubes, horned particles, dendrites, and network-shaped wires upon changing the halide additive. Previous to that, Bi et al. synthesized hollow Rh nanotubes through galvanic replacement between Ag nanowires and $RhCl_3$ in the presence of I^- ions, which reduced the redox potential of Ag species and hence made the replacement possible.[226] Regarding exotic nanostructures of Rh, Sneed et al. made an

DOI: 10.1021/acs.chemrev.8b00158
Chem. Rev. 2018, 118, 7804−7864

important contribution through their report on Rh epigrowth on Au and Pd NCs mediated by I^- ions.[227] The surfaces of the well-defined Au and Pd NCs were used as substrates for epitaxial overgrowth of Rh in an aqueous medium with ascorbic acid being used as a reducing agent in the presence of CTAB. The Rh islands formed on the Pd (or Au) surfaces in a grid-like arrangement, as shown schematically in Figure 19b. This overgrowth was not possible to achieve in the absence of I^- ions, however. The authors allude to different roles played by the I^- ions to explain their findings, which include inhibition of nucleation events through complexation with Rh ions in solution, drawing the Rh ions to the seed surfaces and promoting the reduction of Rh on Pd surfaces. The authors did not account for the influence of Br^- (from CTAB) and Cl^- (from metal precursors) ions present in the growth mixture, however.

2.6. Platinum NCs

With nanocrystalline platinum being an important fundamental catalyst, a plethora of efforts has been devoted toward studying their solution synthesis. In one of the first reports, the preferential binding of I^- ions on {100} rather than on {111} facets, which leads to different growth rates of the said facets, was exploited by Yamada et al. to generate Pt nanocubes enclosed by six {100} facets.[228] However, K_2PtCl_4 was used as a precursor, and the role of Cl^- was not accounted for. Furthermore, high-index planes that are associated with large number of atomic steps, edges etc offer enhanced catalytic performance in terms of activity and/or selectivity. To this end, bromide ions were shown to be particularly useful. Yu et al. described the synthesis of Pt concave nanocubes that were enclosed by high-index facets of the likes of {510}, {720}, and {830} in the presence of Br^- ions in aqueous solution.[229] As observed for other cases involving noble metals, Br^- ions served as capping agents that blocked the growth in the [100] direction. The concave structure formed as the reaction progressed from the initially formed {100}-bounded Pt nanocubes that underwent preferential overgrowth at the corners and edges, as has been shown in the case of Pd as well by the same group.[208] The slowed reduction kinetics due to complexation of Br^- ions with the Pt precursor was also invoked to explain the results. Br^--induced etching has also been used in smoothening NC surfaces.[230] Later in 2012 Yin et al. reported the synthesis of Pt nanoflowers mediated by I^- ions in a polyol process, which was also attributed to reduced kinetics due to complexation and capping roles assumed by the halide ions.[231] The shape-directing ability of I^- ions in the case of Pt NCs was used in 2015 by Michel et al. to produce tetrahedral particles through reduction of Pt(IV) salts by hydrogen.[232] On the other hand, Martínez-Rodríguez et al. showed that HCl in the aqueous phase can be used to obtain Pt nanocubes through a water-in-oil microemulsion method.[233]

The selective etching by halide ions is another aspect that was put to use in generating cage- and ring-like nanostructures of Pt. Fan et al. used Au polyhedron NCs as templates for selectively growing Pt layers at specific regions which generated these exotic structures upon further etching to remove the gold template.[234] The edge facets were selectively etched by iodine, which created highly active sites where Pt atoms reduce and deposit, generating bimetallic nanostructures.

Similar synthetic manipulations were also demonstrated in the case of heteronanostructures containing Pt. Hwang et al. described in 2015 a synthesis of Pt−Ni alloy core−shell NCs through a thermal decomposition method in the presence of CTAC.[235] Other uses of halides have also been realized in the case of alloyed nanostructures containing Pt. For instance, Choi et al. showed in 2016 that octahedral PtNi NCs upon postsynthetic halide treatment exhibit significantly enhanced durability against leaching out of surface atoms during the oxygen reduction reaction.[236] They found that halides bind to the surface Ni more strongly and hence retard their loss during catalytic cycles; in particular, bromide was the most effective. In 2017, uniform PtPb concave nanocubes enclosed by {520} facets have been synthesized where the synergistic effect of CTAB, oleylamine, and I^- ions was employed to exercise shape control.[237]

2.7. Iron (and Iron-Based) NCs

The magnetic characteristics of iron nanostructures make them a sought-after class of nanomaterials for electronic and biomedical applications. However, the synthesis of monodisperse Fe NCs which are also stable in the ambient and biological conditions has been a major challenge for nanochemists. Halide-ions mediation was an important factor for the successful synthesis, as demonstrated by Lacroix et al. in their synthesis of body-centered cubic (bcc) Fe NCs through thermal decomposition of iron pentacarbonyl in the presence of hexadecylammonium chloride.[238] The obtained NCs exhibited much improved stability and magnetic characteristics even in physiological conditions owing to higher crystallinity. The formation of a crystalline structure was attributed to the presence of the Cl^--containing surfactant (hexadecylammonium chloride) which slowed down the decomposition of the Fe precursor facilitating improved crystallinity. In its absence the decomposition was found to be swift and led to the formation of amorphous nanoparticles. The same group studied the kinetics of this growth protocol, later in 2014, by adding different small molecular salts containing Cl^- and Br^- ions instead of a halide-containing surfactant.[239] The growth kinetics was supposed to have slowed down due to the strong binding between Fe and halide ions, and the preferential adsorption of halide ions on particular crystal facets was not invoked in the explanation.

The motivation for exploring the role of Br^- in these mechanistic studies also came from a prior report by Yang et al. in 2012.[240] They demonstrated the synthesis of iron carbide (Fe_5C_2) nanoparticles where Br^- ions were found to be essential in the conversion of iron pentacarbonyl into Fe_5C_2. Similar to Lacroix et al.,[238] amorphous nanoparticles were produced in the absence of Br^- ions, while its presence led to the formation of well-crystallized Fe_5C_2 NCs and was attributed to the slower kinetics as well. The NC growth was proposed to have proceeded through the formation of Fe NCs which serve as the Fe source for the eventual iron carbide phase. The presence of Br^- was also crucial in rendering the NCs resistant to oxidation. A similar role of Br^- ions was demonstrated by Gao et al. in their synthesis of Fe_3C/Fe nanocomposites.[241]

In 2017, Yang et al. reported the modulation of iron carbide phases assisted by halide ions.[242] The adsorption of Cl^- ions on the Fe sites was essential in achieving kinetic control on these transformations.

3. SEMICONDUCTOR NANOCRYSTALS

In the case of semiconductor NCs, the influence of halide ions has been studied from various angles. Compared to metal NCs where the literature is extensive on their effect on NC growth, the influences of halide ions on the growth of semiconductor NCs remains much less explored and has only been catching up in recent times. The larger focus has been on the effects that

DOI: 10.1021/acs.chemrev.8b00158
Chem. Rev. 2018, 118, 7804−7864

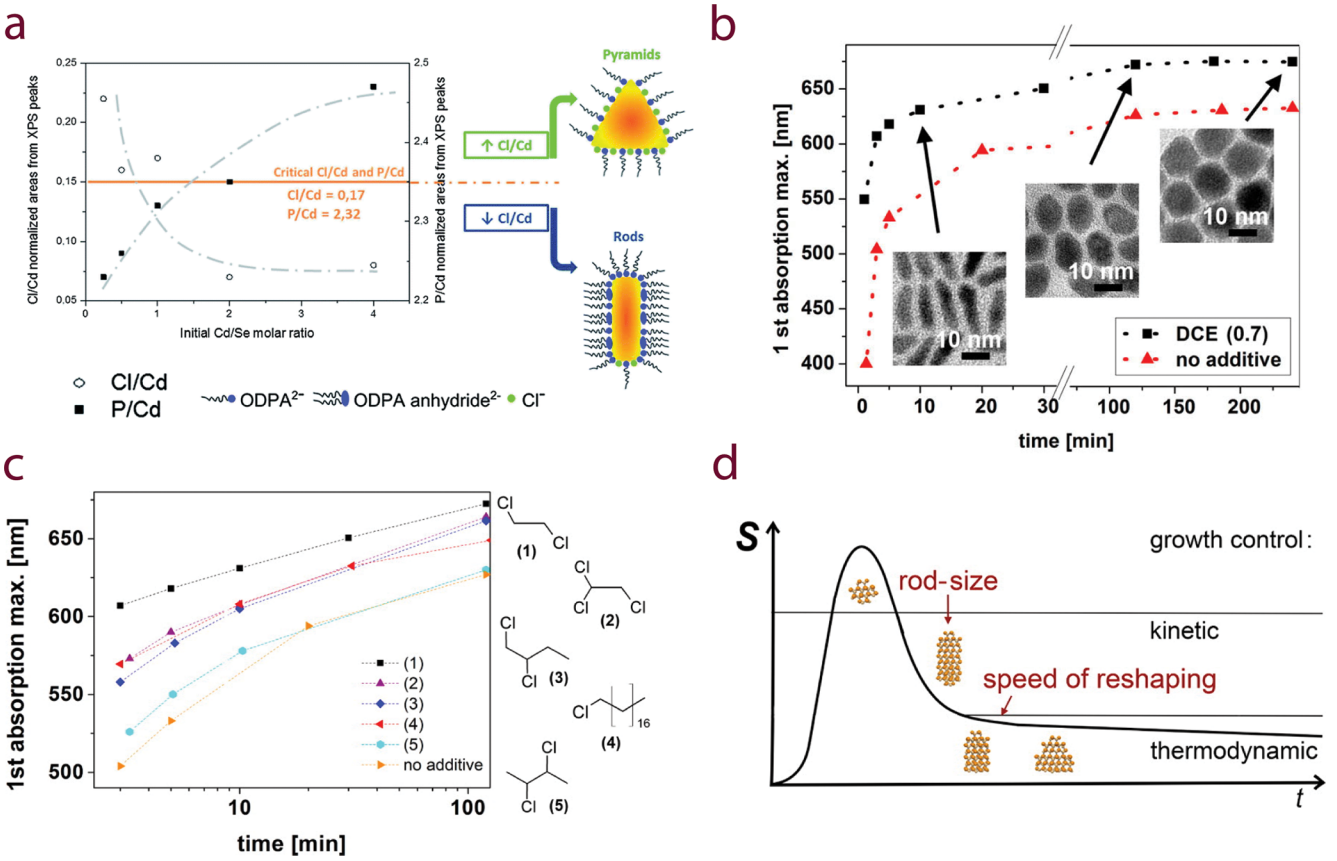

Figure 20. Halide-assisted ripening transformation of rod-like CdSe NCs into pyramidal shape. (a) Correlated XPS data showing the critical amount of chloride ions required to induce the transformation of rods into pyramids (horizontal line indicates the critical values). Reproduced with permission from ref 243. Copyright 2014 Royal Society of Chemistry. (b) Evolution of the ripening with and without DCE monitored through the first absorption maximum and TEM imaging. (c) Evolution of ripening under the influence of different chloroalkanes. (d) LaMer plot showing the evolution of pyramid formation. Adapted from ref 244. Copyright 2014 American Chemical Society.

halides exert by being present on the surface of these NCs, as can be assessed from the examples detailed below, which deal with the changes in intrinsic optoelectronic properties and the electrical properties of the ensembles fabricated from them. In addition, the surface ligation of halide ions leads to other changes in the semiconductor NC systems, e.g., improved stability in lead chalcogenide NCs, as described below.

3.1. Cadmium Chalcogenide (CdE, E = S, Se, Te) NCs

3.1.1. Surface Binding and Growth Control. Cadmium chalcogenides have been the poster boy of nanoscale research, and it is no wonder that a considerable amount of attention will be devoted to these semiconductor nanomaterials when it comes to halide-assisted growth/transformation. Recent efforts follow the trend in the same direction wherein the influence of halide ions (especially chloride) was studied on the growth of CdE NCs. For instance, Juarez and co-workers demonstrated the reshaping of initial rod-like NCs into pyramids under the influence of halide ions recently in back-to-back papers.[243,244] They used the reaction between tri-*n*-octylphosphine (TOP) and covalent organic halide-bearing molecules to release the halide ions in situ. Palencia et al. demonstrated that the reaction between TOP (or TOP:Se) and 1,2-dichloroethane (DCE) was responsible for the inclusion of Cl in the ligand shell of the pyramids.[243] Furthermore, they studied the effect of chloride ions under different Cd/Se precursor molar ratios and found that an excess of Cd precursor does not favor the incorporation of Cl in the ligand shell but an excess of Se precursor does. Hence, the influence of chloride ions was dictated by the relative contents of cadmium or selenium in the reaction mixture. This is in parallel to the fact that in Cd-excess conditions DCE reacted with the Cd complex to form a nonactive chlorinated species that did not trigger the reshaping, in contrast to Se-excess conditions. The reshaping and the inclusion of chloride ions in the ligand shell were simultaneous effects and hence were linked to the presence of active chloride in the reaction mixture at Se-excess conditions. In fact, an elegant demonstration of the inclusion of chloride in the ligand shell was achieved using XPS, where the relative content of chloride and phosphorus (constituent of the phosphonate moieties that were used as the organic passivants) were measured with respect to the cadmium and selenium content of the NCs, as shown in Figure 20a. The Cl/Cd and P/Cd ratios followed opposite trends as a function of the Cd/Se ratio, as expected since the phosphonate moieties should reduce in number to make space for the chloride moieties for passivating the NC surface. A 2014 report from the same group also explored the effect of chloride ions on the oxidation of these NCs through cyclic voltammetry and X-ray photoelectron spectroscopy.[245]

In a more generalized approach from Juarez's group, Meyns et al. studied the effect of various other halogenated additives like organic chlorine-, bromine-, and iodine-bearing compounds on the reshaping of CdSe NRs to hexagonal pyramids in a hot-injection process.[244] The course of ripening was monitored using optical extinction spectroscopy, first absorption maximum

DOI: 10.1021/acs.chemrev.8b00158
Chem. Rev. 2018, 118, 7804−7864

in particular, and TEM imaging of the aliquots at different growth stages as shown in Figure 20b. The rods maintained an elongated morphology even after 4 h of growth when DCE was not present. However, the presence of DCE led to the thermodynamically controlled ripening of the NRs into hemimorphic hexagonal dipyramids of wurtzite CdSe. As in the previous case above, the shape evolution was accompanied by a modification of the ligand shell as well. It was also noted that the structure of the halogenated molecule dictated the degree of the influence on the ripening process (Figure 20c). Although pyramidal NCs were obtained in all cases, the temporal evolution and homogeneity varied.

Meyns et al. explained the shape evolution from NRs to hexagonal pyramids as a result of X-type ligand coordination to flat and sloped Cd-rich facets with a strong influence of halides on the equilibrium shape. They calculated the adsorption energies for both X-type (phosphonate and halide moieties) and L-type (neutral molecules which were possibly present in the reaction mixture) ligands on the different wurtzite CdSe facets and established the possible degree of passivation. Halide ions followed the usual trend as dictated by their electronegativity (i.e., $Cl^- > Br^- > I^-$). The NC synthesis was described using the standard LaMer model where the NCs were found to grow along the wurtzite *c* axis leading to rod-shaped NCs in the kinetic regime. Once the monomer concentration was depleted over the course of the reaction, the NCs grew in all directions before thermodynamically controlled ripening resulted in equilibrium shapes as shown in Figure 20d. In the presence of halide ions, the equilibrium shape tended toward a polyhedral morphology owing to the surface energy of the crystal facets which were different from a halide-free growth.

In another ripening protocol, Saruyama et al. reported a drastic structural transformation of small colloidal CdE NCs into large pencil-shaped ones through an Ostwald ripening process that was induced by chloride ions.[246] The morphological transformation was accompanied by a crystal-structure transformation from zinc blende to wurtzite, and [0001] was found to be the preferential growth direction. It was also established that the countercation of the chloride ions does not influence the ripening process. Zou et al. reported a similar phenomenon in their noninjection synthesis of CdS NCs wherein they used cationic surfactants, cetyltrimethylammonium chloride (and bromide), as the halide source.[247] The phase transformation was associated with an increase in NC size with an increase in halide content, and the morphology varied from spherical to multiarmed. The ineffective countercation might seem contrary to what Meyns et al. reported, but actually in their case they studied the effect of organohalide compounds.[244]

Saruyama et al. also demonstrated that these transformation reactions could be readily extended to obtain various functional materials owing to their uniform morphology and highly faceted structure. They obtained a semiconductor−metal heterostructure through deposition of gold islands on the CdS nanopencils. A similar approach was recently developed by Hinrichs et al. where chloride ions were employed to produce monodisperse metal−CdE heterostructures.[248] They added small amounts of $CdCl_2$ to the more generally used Cd precursor CdO for the deposition of CdE on gold seeds and found that the mole fraction of $CdCl_2$ was important for shape tuning and yielding monodisperse heterostructures. They further showed the versatility of this approach by extending it to different metal−semiconductor combinations.

Following these reports, a recent work (2015) on direct synthesis of CdSe NCs by Ghosh et al. demonstrated the reversal of crystal polarity and concomitant morphological changes on the growth of wurtzite CdSe NCs that was a result of the deliberate addition of chloride moieties in the reaction mixture.[59] The resulting pyramid-shaped NCs (or nanopyramids, NPYs) comprised of an equilateral basal $(000\bar{1})$ facet which is polar in nature and three $(40\bar{4}5)$ nonpolar lateral facets giving them the shape of a slightly flattened tetrahedra, as schematically shown in Figure 21a. The apex opposite to the

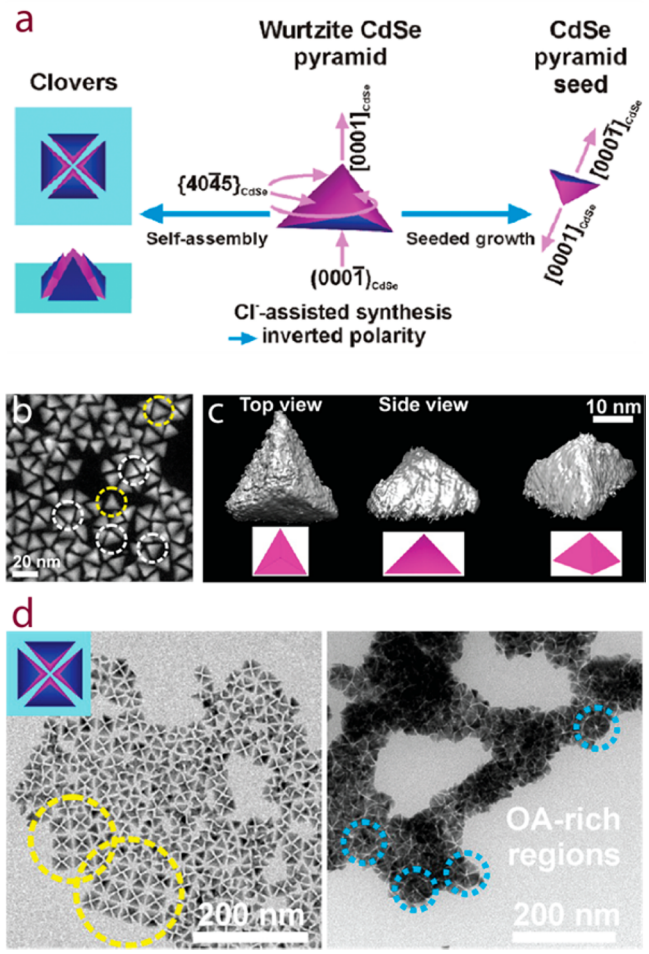

Figure 21. Reversed polarity in CdSe NCs as an influence of chloride ions. (a) Schematic showing the growth direction of CdSe NPYS and its effect on the self-assembly upon chloride passivation. (b) HAADF-STEM image of a group of NPYs; thickness contrast facilitating observation of the flattened pyramidal shape (yellow circles, equilateral triangle; white circles, isosceles triangle). (c) Isosurface view along different orientations of the reconstructed volume of an NPY (through HAADF-STEM tomography). (d) Clovers formed through self-assembly of the NPYs where the nonpolar lateral facets congregate inward with the polar basal facets pointing outward. Reproduced from ref 59. Copyright 2015 American Chemical Society.

basal facet points toward the (0001) direction as was confirmed by HRTEM analysis. This preferential growth of the $(000\bar{1})$ facet over the (0001) was in contrast to the chloride-free case wherein the (0001) was the favored growth direction, as reported earlier on wurtzite CdSe(core)/CdS(shell) NRs.[249] The polarity of the NCs was essentially reversed in the presence of chloride ions. The growth direction and other crystallographic

DOI: 10.1021/acs.chemrev.8b00158
Chem. Rev. 2018, 118, 7804−7864

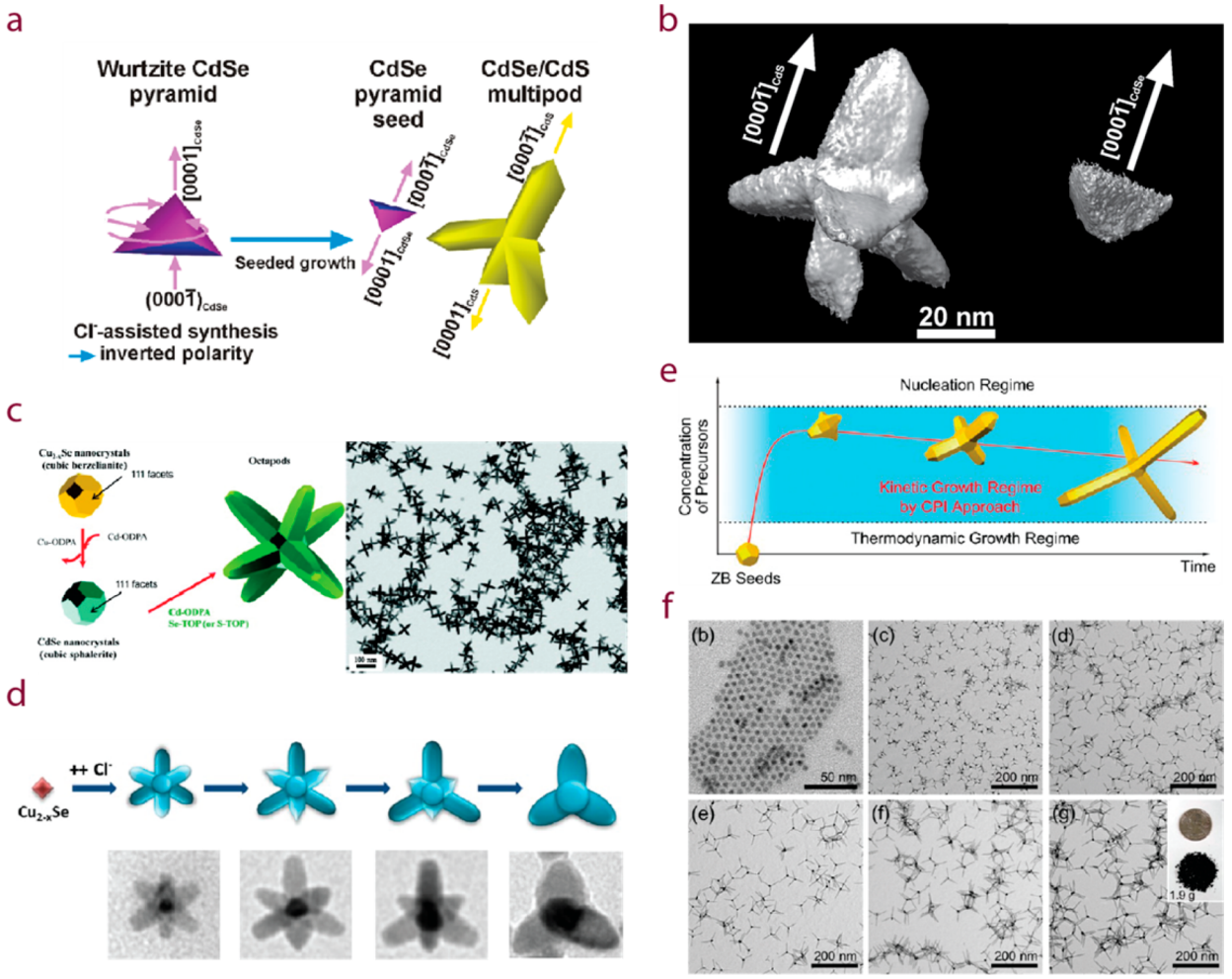

Figure 22. Halide-assisted seeded growth of branched CdE NCs. (a) Schematic showing the epitaxial growth of CdS pods on the wurtzite CdSe facets of the NPYS. (b) Isosurface view of a branched CdSe(core)/CdS(pods) NC and the corresponding CdSe NPY seed, oriented according to the direction of the pod growth on the seed (through HAADF-STEM tomography). Reproduced from ref 59. Copyright 2015 American Chemical Society. (c) Schematic depiction of the CdSe(core)/CdS(shell) octapod NC formation, and overview TEM image of these NCs. Reproduced from ref 5. Copyright 2010 American Chemical Society. (d) Schematic structures (and the corresponding TEM images) showing the evolution of the CdSe(core)/CdS(shell) multipod nanostructures on increasing the mole fraction of $CdCl_2$ introduced in the reaction mixture, starting from $Cu_{2-x}Se$ seeds. Reproduced from ref 11. Copyright 2012 American Chemical Society. (e) Schematic illustration of the continuous precursor injection approach to achieve the growth of CdSe tetrapod NCs in the kinetic regime. (f) TEM images showing the different stages of the tetrapod NC growth. Reproduced from ref 57. Copyright 2013 American Chemical Society.

aspects of these NPYs were derived with the assistance of exit wave (complex wave function of the electrons after they have passed through the sample) reconstruction. The unique shape of the NPYs can be envisaged from the HAADF-STEM imaging (Figure 21b) and tomography (Figure 21c), wherein the NPYs can be viewed along both the equilateral projection (yellow circles) and the isosceles projection (white circles) in Figure 21b.

In this case it was assumed that the polar crystal facets are terminated preferentially by the positively charged cadmium ions (polar facets expose either the cation or the anion) since negatively charged phosphonate moieties were employed as surface passivants. This means that the chloride ions essentially reside on the surface of the NPYs (as a part of the ligand shell, along with phosphonate moieties) as was verified through ligand exchange experiments. Also, the crystallographic differences meant that the two facets might exhibit a differential ligand makeup which manifested itself in the self-assembly induced by the presence of oleic acid forming "clover-like" tetrameric units in the presence of oleic acid, as shown in Figure 21d. The oleic acid molecules probably dimerized and served as glue by interdigitizing the alkyl chains of the phosphonate moieties on the lateral facets involved in the clover formation. This was less efficient for the polar basal planes that either had a lesser coverage by alkyl phosphonates or residual charges which prevented attractive interaction and led them to mildly be involved in a short-range superstructure.

This reversal of crystal polarity was explained using the differential binding of the chloride ions on the polar crystal facets, thereby imparting differential thermodynamic stability. Density functional theory (DFT) calculations modeled on the binding of chloride ions on the surface Cd atoms support such a notion. In general, the (0001) facet exhibits one dangling bond per Cd atom compared to three by the $(000\bar{1})$ facet and hence is more easily passivated by ligand moieties yielding higher stability. This is generally the case with chloride-free growth where $[0001]$ is the preferential growth direction and the less stable $[000\bar{1}]$ ending into a tip.[249] However, in the case of the

DOI: 10.1021/acs.chemrev.8b00158
Chem. Rev. 2018, 118, 7804−7864

CdSe NPYs, the chloride ions bridging two surface Cd atoms nicely mimic the presence of the Se atoms with minimal bond distortion, conferring higher thermodynamic stability to the $(000\bar{1})$ facet—a situation not feasible on the (0001) facet without serious bond distortion. Furthermore, the surface binding of the chloride leaves room for other molecules (phosphonate moieties) for binding and electronically satisfy the remaining Cd dangling bonds

A comparison between the works of Juarez et al. and Ghosh et al.,[59,243,244] as described above, brings out important distinctions. The bipyramids obtained by Juarez et al. were a result of a ripening protocol using covalent halide-bearing molecules unlike the ionic cadmium chloride as chloride source in the direct synthesis of CdSe NPYs. Moreover, unlike the NPYs,[59] the $(000\bar{1})$ facets of Juarez's NCs were unstable and etched away during the course of ripening owing to weak passivation, collapsing into a tip. Recently, de la Cueva et al., from the same group, deposited gold dots or shells on these pyramids wherein the nature of the overgrowth of gold was influenced by the presence of chloride on the NC surface,[250] which is similar to the mechanism governing the adsorption of these CdSe pyramids on carbon sp^2 surfaces.[251]

Chloride etching as a means to tailor the size and shape of CdE NCs through a postsynthetic pathway has also been demonstrated in detail by Lim et al.[252,253] They studied the chemical and photochemical etching of CdSe NRs, CdSe tetrapods, CdS nanowires, and CdSe nanoplatelets where the chloride ions were generated either by chemical activation of chloroalkane solvents with tributylphosphine or by photo-induced electron transfer from the NCs to the chloroalkane molecules adsorbed on the surface of the NCs. The etching process could be combined with colloidal synthesis to achieve selective anisotropic reshaping of the NCs. An elegant demonstration of this effect was made by Kim et al. in the end-to-end assembly of CdSe NRs assisted by tip etching by the chloride ions.[254]

Indeed, the influence of halide ions on the NC growth can be harnessed to produce various heterostructures and branched morphologies. The availability of highly faceted NCs with crystal facets which are obtainable only due to halide ions made it possible to produce unusual morphologies that are otherwise not so easily accessible. The CdSe NPYs with reversed polarity, when exploited to grow CdS pods, led to such a peculiar structure.[59] The seeded growth method was carried out in the presence of chloride ions introduced as $CdCl_2$ and is schematically represented in Figure 22a. The as-prepared branched NCs exhibited an unusual rocket-like shape with a dominant central asymmetric pod and three shorter pods emanating from its base. The larger axial pod growth in the $[000\bar{1}]$ CdS direction further lends support to the stability of this particular crystal facet under the presence of halide ions. As shown in Figure 22b, the differential pod growth on the two types of crystal facets of the CdSe NPYs can be appreciated from the isosurface view of the branched NCs in comparison with the seed NPYs obtained through HAADF-STEM imaging. This epitaxial growth of CdS pods over the CdSe NPY seeds was not observed in the absence of $CdCl_2$. Instead, CdS particulates nucleated separately in the absence of chloride ions. This means halide etching was at play in the heterostructure growth that suppressed the homogeneous nucleation.

In a related but earlier report on branched NCs, Kim et al. described the shape evolution of octapod-shaped CdSe(core)/CdS(pods) NCs in the presence of chloride ions.[11] These NCs were obtained through a sequential cation-exchange and seeded growth process wherein spherical $Cu_{2-x}Se$ NCs were used as seeds.[5] The $Cu_{2-x}Se$ seeds first undergo a rapid cation exchange with Cd^{2+} to form sphalerite CdSe NCs. The wurtzite CdS pods then grow on top of these NCs forming the octapod morphology in the same reaction mixture, as depicted schematically in Figure 22c. Kim et al. found that the presence of chloride ions was essential for growing these nanostructures. Similar to the situation with CdSe NPYs described in the previous paragraph, CdS nucleated separately in the absence of chloride ions, accompanied by low reproducibility of the growth of multipod structures. These observations were rationalized on the basis of chloride ions forming strong complexes with cadmium, thereby reducing its availability and preventing the homogeneous nucleation of CdS NCs. The scenario is similar to that reported by Palencia et al. for their nanorod-to-pyramid reshaping as described above, wherein an excess of cadmium precursor led to the formation of "nonactive" chlorinated species which did not participate in the transformation.[243] Hence, the presence of chloride ions provided enhanced ability to play with nucleation and growth kinetics, leading to heterogeneous nucleation of CdS pods on CdSe seeds. However, the mole fraction of $CdCl_2$ was critical in getting the desired amount of branching since at larger mole fractions most of the initially formed octapods tended to reshape into tetrapods. Figure 22d schematically depicts the evolution of the octapod reshaping in excess $CdCl_2$ conditions, accompanied by TEM images of the actual growth stages. As described later for CdSe NPYs,[59] this was explained on the basis of an additional role played by the chloride ions, that of influencing the relative stabilities of various crystal facets by selective adhesion and/or selective etching.

In another report on the seeded growth process of producing branched NCs, Lim et al. demonstrated the synthesis of CdSe tetrapod NCs using a continuous precursor injection approach in the presence of halide ligands.[57] This approach is slightly different than the usual NC growth in the thermodynamic regime; they maintained the reaction condition in the kinetic growth regime through successive injections of precursors to achieve anisotropic growth, as depicted schematically in Figure 22e. Zinc-blende CdSe NCs were employed as seeds which underwent phase transformation to wurtzite, accompanied by the growth of wurtzite arms on the crystal facets of the seeds, yielding the tetrapod morphology. Controlled amounts of halide ligands, in the form of various alkylammonium halide molecules, were required to trigger the pod growth on the seed facets, since halide-mediated displacement of the oleate ligands was necessary to enable the phase transformation and subsequent growth. Similar to the observation by Saruyama et al.,[246] the nature of the countercation of the halide ions did not influence the tetrapod growth. Also, as in the case of our CdSe NPYs,[59] the authors report here that the wurtzite arms of the tetrapods grew along the $[000\bar{1}]$ direction. Figure 22f shows the representative TEM images of the various stages of the tetrapod NC growth. The authors could scale up the synthesis of these tetrapod NCs with high morphological uniformity, up to 1.9 g as shown in an inset in Figure 22f.

A recent work by Gerdes et al. demonstrates the formation of CdSe nanosheets upon using halogenated alkanes as additives in the reaction mixture.[255] Both halide complexation to modify growth kinetics and selective halide capping of crystal facets were invoked in order to explain the formation of these highly anisotropic structures.

DOI: 10.1021/acs.chemrev.8b00158
Chem. Rev. 2018, 118, 7804−7864

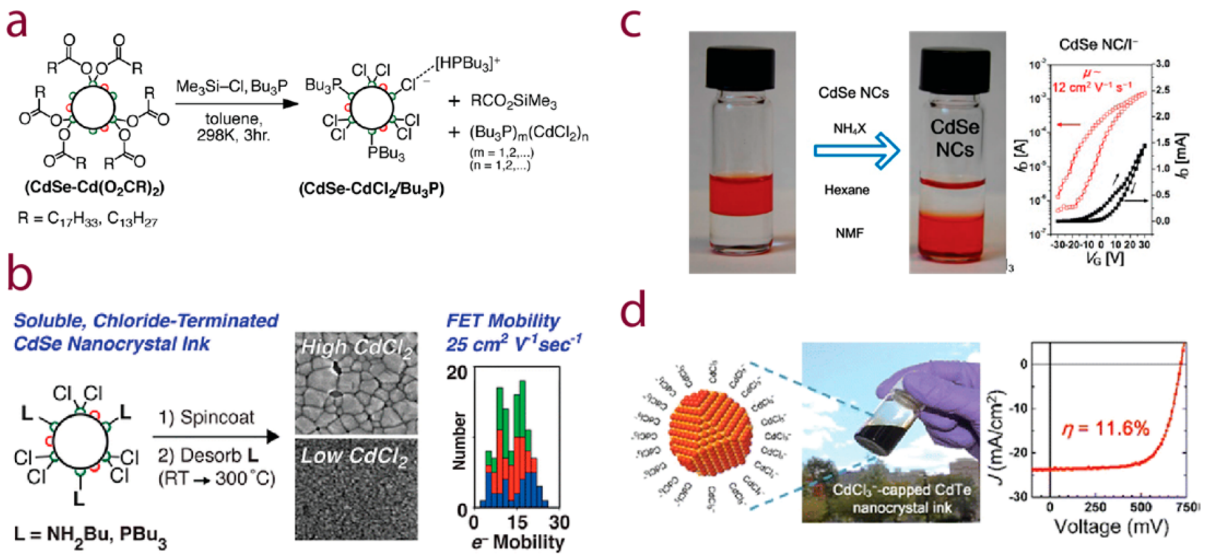

Figure 23. Halide insertion on CdE NC surfaces through postsynthetic ligand exchange procedures. (a) Representative scheme showing the replacement of the native ligands of carboxylate-terminated CdSe NCs with chloride ions in the presence of TBP L-type ligands. Reproduced from ref 266. Copyright 2013 American Chemical Society. (b) Effect of $CdCl_2$ content on the thin films deposited from amine- and phosphine-bound, chloride-terminated CdSe NCs, which showed electron mobilities as high as 25 $cm^2/(V\ s)$. Reproduced from ref 66. Copyright 2014 American Chemical Society. (c) Biphasic ligand exchange protocol where organic-capped CdSe NCs in hexane transfer to the NMF layer containing the halide source (NH_4X); subsequent films deposited from I^--capped CdSe NCs exhibit electron mobilities of 12 $cm^2/(V\ s)$. Reproduced from ref 71. Copyright 2014 American Chemical Society. (d) $CdCl_3^-$-capped CdTe NCs obtained through the biphasic ligand exchange protocol, thin film solar cells of which showed power conversion efficiencies exceeding 10%. Reproduced from ref 270. Copyright 2016 American Chemical Society.

Although chloride (halide) ions produce interesting and unforeseen changes in the growth of CdE NCs, efforts to synthesize nanostructures with $CdCl_2$ as the sole Cd precursor generally are rare. As described by Peng's group, this is primarily due to the high stability of the cadmium salt/complexes which fail to properly initiate a nucleation leading to bulky structures.[256] However, Lazell et al. reported the synthesis of CdS NCs using $CdCl_2$,[257] and Pawar et al. synthesized CdS NCs through the thermolysis of a single-source precursor obtained from CdX_2−thiosemicarbazone (X = Cl and I) complexes.[258]

3.1.2. Affecting NC Properties through Surface Ligation. There have been numerous literature reports on introducing halide ions as ligands through postsynthetic ligand exchange pathways on cadmium chalcogenide NCs. One of the main motivations for introducing chloride (halide) ions on the CdE NC surfaces comes from the fact that apart from being a choice chloride source for CdE NCs, $CdCl_2$ is more commonly used in the semiconductor industry as an etchant which promotes grain growth, recrystallization, and interdiffusion between the semiconductor layers. This has been particularly more relevant in the case of physical vapor-deposited CdS/CdTe thin film solar cells, where $CdCl_2$ is routinely used to improve cell performance.[259,260] Several mechanisms have been conjectured to be the cause of such improvements, which include elimination of deep defect levels which act as fast recombination centers in the CdTe film, decrease in the recombination centers in the CdS−CdTe junction, and the suppression of nanograins at the grain boundaries.[261] In fact, the $CdCl_2$ treatment has also been employed in improving the performance of solution-processed CdTe NC solar cells.[262−264] Jasieniak et al. showed that $CdCl_2$ was instrumental in stripping the organic ligands from the NC surfaces, which reduced the energy barrier to crystal growth and prevented film contamination.[264] Hence, replacing the native ligands on CdE NCs with halide ions is an attractive option since the active material (CdE) and the grain growth promoter (halide) can be included simultaneously for subsequent device fabrication.

One of the first reports on halide ligation came from Owen et al. in 2008, where the authors used NMR spectroscopy to monitor the displacement of native phosphonate ligands on CdSe NC surfaces with chlorotrimethylsilane and tridecyltrimethylammonium chloride as the incoming chloride ion source.[265] This study provided useful insights on the surface chemistry of CdSe NCs and more importantly pointed toward the fact that a ligand exchange can only proceed with the aim of balancing charges between the surface Cd^{2+} and the incoming ligand. This report was followed by two recent reports from Owen's group where they studied these chloride-exchanged CdSe NCs in action.[66,266] In the first report Anderson et al. replaced the native ligands of carboxylate-terminated CdSe NCs with chloride (chlorotrimethylsilane as the chloride source) ions in the presence of tri-*n*-butylphosphine (TBP) L-type ligands, as schematically shown in Figure 23a.[266] The role of the TBP ligands was to bind to the surface of the CdSe NCs (along with chloride termination) in order to stabilize them in organic solvents for further characterization and processing. Just chloride termination of the NC surface would otherwise render these NCs insoluble in common nonpolar solvents. The effect of ligand coverage on the NC optical properties was then demonstrated through adsorption/desorption of other L-type ligands like small primary amines. They concluded that as long as the coverage of L-type ligands is high the surface-bound chloride ligands can support a nonstoichiometric NC without introducing surface trap states. In the subsequent paper, Norman et al. explored the electrical transport properties of these soluble phosphine- and amine-bound, chloride-terminated CdSe NCs and the effect of annealing them.[66] The sintering process was made of the three distinct steps of desorption of organic ligands, particle fusion, and subsequent grain ripening. The evolution of electrical transport and grain growth was

DOI: 10.1021/acs.chemrev.8b00158
Chem. Rev. 2018, 118, 7804−7864

distinctly dependent on the chloride content of the film, with higher content facilitating grain growth at lower temperature (Figure 23b). This study clearly showed how small changes in the NC composition can influence the resulting mesostructure and transport characteristics. It was also concluded that fusion of the NC solid was required to achieve charge mobilities greater than 0.1 $cm^2/(V\ s)$, which was not possible upon ligand desorption alone. This helps to explain the high temperatures routinely employed in fabricating high-mobility devices from colloidal CdSe NCs. The devices fabricated by the authors demonstrated electron mobilities as high as 25 $cm^2/(V\ s)$ and on/off ratios of 10^5 with less than 0.5 V hysteresis.

In a related work, Zanella et al. used propyltrichlorosilane as the chloride ion source that displaced the organic surfactants covering the NC surfaces of different materials.[267] When applied to NC films of CdE, this treatment led to the reduction of the distance between neighboring NCs, which is otherwise defined by the organic ligand chain length and is generally a deterrent toward electronic communication between the NCs. Strong enhancement in both dark and photocurrent was observed as a result. A strong quenching of the photoluminescence was observed, however, similar to Owen's observations.[265,266] In a 2018 report, Li et al. used an alternative chlorinating agent, thionyl chloride ($SOCl_2$), that is widely employed in synthetic organic chemistry, as a suitable alternative.[268] They showed that when used for replacing alkylcarboxylate ligands on CdSeZnS−ZnS core−shell−shell NCs, this milder chlorinating agent maintained the PLQY, which translated into improved device performance.

In this regard, it is imperative to understand that the steps involved in ligand exchange of NCs and subsequent thin film deposition from NC solution (for electrical transport studies) are highly interrelated and can cause complications. For instance, prior to film deposition, a complete ligand exchange with the short and negatively charged chloride ions would render the NCs insoluble in the common organic solvents, thereby hindering the film deposition from solution. This issue was addressed by Norman et al. through exchanging the native ligands with chloride ions in the presence of other L-type ligands in solution.[66] The L-type ligands, like amines and phosphines, were the agents that maintained the solubility of these NCs. These phosphine- or amine-bound, chloride-terminated CdSe NCs were then spin coated on silicon dioxide substrates and subsequently annealed to desorb the organic ligands prior to electrical measurements. However, the variation in composition caused by the desorption that can introduce surface defects in the NCs cannot be completely ruled out. On the other hand, Zanella et al. performed the ligand exchange *after* the NC film deposition through dipping the drop-cast film in a solution containing the incoming ligand (propyltrichlorosilane).[267] This procedure, although simpler and involving fewer steps, is generally plagued by the formation of cracks in the NC film (due to eventual reduced inter-NC separation) accompanied by the problems of inefficient exchange and the presence of residual organic moieties.

A simpler, one-step procedure to obtain halide-capped NCs with good colloidal stability and solution processability should then be a more attractive alternative. This involves the choice of a suitable solvent which can provide electrostatic stabilization of the NCs. A polar solvent with an extraordinarily high dielectric constant ($\varepsilon \approx 182$) like *N*-methylformamide should be a natural choice for stabilizing the NCs with charged halide ligands. Other more commonly used polar solvents with lower dielectric constants, such as formamide ($\varepsilon \approx 106$), dimethylformamide ($\varepsilon \approx 36$), hydrazine ($\varepsilon \approx 55$), and dimethyl sulfoxide ($\varepsilon \approx 47$), are incapable of stabilizing NCs capped with charged inorganic moieties. Zhang et al. developed a methodology of ligand exchange and subsequent solution stabilization of the CdSe NCs following this very logic.[71] They demonstrated a solution-phase ligand exchange employing ammonium halide and/or sodium (potassium) halide molecules as incoming sources of halide ions. The ligand exchange was carried out in an immiscible biphasic mixture where the halide precursors were dissolved in the polar phase (NMF, bottom layer) and the organic ligand stabilized NCs in the nonpolar hexane phase (top layer). The ligand exchange would result in the transfer of the NCs from the hexane to the bottom NMF layer, resulting in a colorless top phase in a matter of minutes to hours, as shown in Figure 23c. However, the authors did not observe any changes in the optical properties of the halide-stabilized NCs, unlike Anderson et al.[266] The presence of the compact halide ions on the NC surfaces greatly facilitated the inter-NC electronic communication, as demonstrated by the high electron mobilities ($\mu \approx 12\ cm^2/(V\ s)$) measured from a spin-coated thin film of I^--capped CdSe NCs (Figure 23c). Niu et al. demonstrated a similar protocol of ligand exchange by using alternative halide sources, namely, methylammonium halides (CH_3NH_3X).[269]

As independent entities, Cl^- and $CdCl_2$ appear to, respectively, belong to the donor X-type and the acceptor Z-type ligand categories according to Greens' covalent bond classification scheme.[65] Z-type ligands are neutral acceptor molecules that bind to the surface chalcogenide ions of a NC through a Lewis-acidic interaction. However, in the case of CdSe NCs, the distinction between Cl^- and $CdCl_2$ is a semantic one, since the surface layer of excess metal ions may or may not be considered as part of the ligand shell.[66] A similar argument also holds for $CdCl_3^-$, which was recently used by Talapin's group to fabricate thin film solar cells of CdTe NCs.[270] In this report, Zhang et al. employed $CdCl_3^-$ as surface ligands and dopants and also as sintering promotors for the eventual solution-processed CdTe NC thin film. The main advantage of fabricating a solar cell through this approach was the ability to obtain very thin yet continuous layers of high-quality CdTe that is otherwise a difficulty for the more common vapor-phase depositions. Moreover, this procedure eliminated the additional $CdCl_2$ treatment and demonstrated thin-film solar cells with power conversion efficiencies exceeding 10%, which is a record for a sub-400 nm CdTe absorber layer (Figure 23d).

Although the reduced inter-NC separation was assumed to be the origin of improved electronic transport, it is quite possible that the halide ions influence the electronic structure of the NCs as well. It is not completely clear if the observed mobility changes are a combined consequence of spatial and electronic changes effected by the halide ligands. Greaney et al. provided important insights in this regard when they studied the case of CdSe NCs capped with cadmium halide ligands (CdX_2, X = Cl, Br, I).[68] They used the L-type ligand butylamine to retain the solubility of these NCs, apart from the CdX_2 moieties like Anderson et al.[266] They examined the trap states landscape of these NCs by ultrafast transient absorption, time-resolved photoluminescence, and surface photovoltage spectroscopies. The photocurrent response from the films of these NCs was found to be strongly dependent on the surface halide ions and ascribed to the changes in the electronic structure of the NCs. A simple electronic picture was proposed on the basis of their findings, which is presented in Figure 24a. The CdX_2 ligands

DOI: 10.1021/acs.chemrev.8b00158
Chem. Rev. 2018, 118, 7804−7864

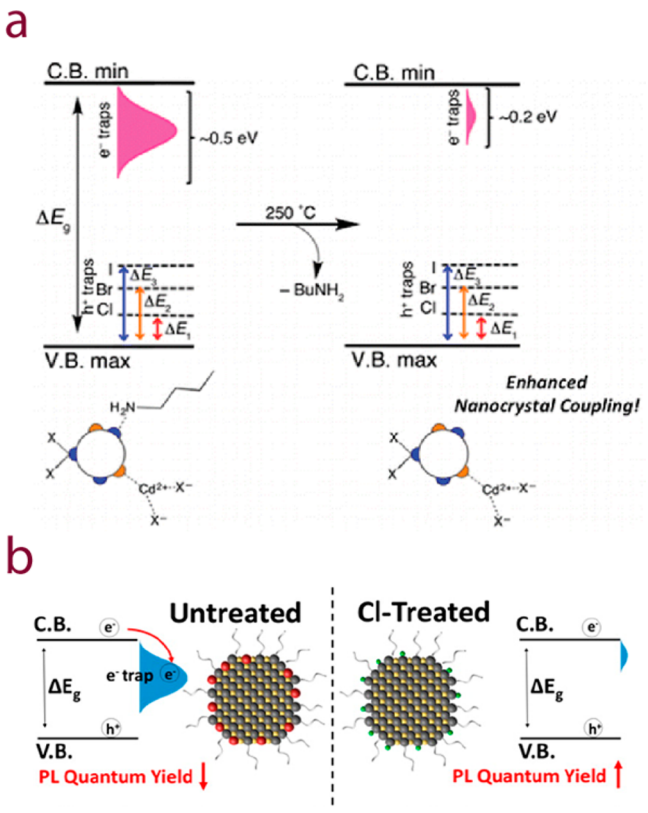

Figure 24. Changes in the electronic structure of CdSe NCs upon halide passivation. (a) Energy landscape of CdX_2-treated CdSe NCs as a function of annealing (associated with desorption of the L-type butylamine ligand). Reproduced from ref 68. Copyright 2015 American Chemical Society. (b) PLQY upon Cl-passivation, due to removal of electron traps upon saturation of Cd dangling bonds. Reproduced from ref 271. Copyright 2016 American Chemical Society.

introduce surface hole traps whose energy varies according to the nature of the halide ion, with the shallowest traps created by $CdCl_2$ and the deepest ones by CdI_2. The butylamine ligands utilized during ligand exchange, on the other hand, create surface electron trap states which can be reduced upon annealing, signifying removal of butylamine and/or surface reconstruction. Theoretical perspective in this area has also been provided by Wang et al. through their first-principles study of chloride and iodide passivation effects on the electronic structure of $Cd_{33}Se_{33}$ quantum dots.[272] They found that the influence of the chloride passivants on the electronic structure of the NCs depends on the coordination number of the chloride moiety.

Contrary to the picture assumed by Greaney et al., Kim et al. proposed the removal of electron trap states upon Cl passivation of CdSe NC surfaces, as reflected by the improvement (from 9% to 22%; Figure 24b) in the photoluminescence quantum yield (PLQY).[271] They resorted to the usual replacement of native organic ligands with Cl moieties through postsynthetic ligand exchange by a methanol solution of ammonium chloride. The improvement in the PLQY was ascribed to the effective passivation of the unsaturated surface Cd atoms, as the sterically hindered and thereby incomplete organic ligand passivation gives rise to nonradiative recombination sites. The authors went on to show that the Cl-passivated NCs exhibit almost an order of magnitude improvement in their photocatalytic hydrogen generation activity compared to the organic ligand-passivated ones. Similar suppression of nonradiative decay pathways upon Cl passivation, resulting in PLQY of almost unity, has also been reported for CdTe NCs.[273]

3.2. Lead Chalcogenide (PbE, E = S, Se, Te) NCs

3.2.1. Growth and Transformation. Synthetic efforts which exploited the influence of halide ions on the growth of PbE NCs date back to 2006, when Cademartiri et al. from Ozin's group reported a diffusion-controlled heterogeneous synthetic route for producing PbS NCs.[274] The heterogeneous system was composed of a suspension of $PbCl_2$ in oleylamine to which the sulfur precursor was hot injected. Although the final NCs were capped with surface-adsorbed Cl^- ions, it was not clear whether organic moieties were totally absent from the ligand shell since the NCs were soluble in nonpolar solvents. The heterogeneity actually acts as a boon here since that limits the diffusion in the system, leading to high monodispersity and longer photoluminescent lifetimes. Moreover, the chloride capping led to better stability of the PbS NCs compared to those prepared by conventional methods using PbO as a precursor.

Recently, Beard and his colleagues built upon this protocol to synthesize PbS and PbSe NCs exhibiting halide passivation.[275] In their protocol shown in Figure 25a, Zhang et al. used a more reactive sulfur precursor, bis(trimethylsilyl) sulfide,[275] instead of the sulfur–oleylamine solution used by Cademartiri et al.[274] This enabled them to lower the injection temperature of the sulfur precursor and also obtain smaller PbS NCs (~2.2 nm) exhibiting larger band gaps (~1.7 eV) that constituted better performing solar cells (PCE of about 6.5%, Figure 25a). They also demonstrate the fabrication of Br^-- and I^--capped PbS NCs by employing $PbBr_2$ and PbI_2 as the lead precursors. The chloride passivation imparted higher photostability to both the PbS and the PbSe NCs when stored under air.

In a similar work in 2015, Zhang et al. described the synthesis of photostable PbSe NCs using $SnCl_2$ as the nucleation-promoting agent and $PbCl_2$ as the in situ halide passivation agent.[276] They could tune the sizes of PbSe NCs between 3 and 8 nm simply by controlling the $PbCl_2/SnCl_2$ ratio and the reaction time. The size of the NCs in this case was also decreased simply by using a fast nucleation agent ($SnCl_2$), while the halide passivation imparted greater stability. Further reduction in size through the assistance of chlorinated species was reported by Reilly et al. wherein red light-emitting NCs of diameter 1.6 nm were synthesized in the presence of 1,2-dichloroethane.[277] In the same vein, Kandel et al. demonstrated anisotropic growth of PbSe NCs in the presence of chloroalkanes.[278]

A more striking demonstration of the influence of chloride species on the growth of PbE NCs came from Weller's group back in 2010. In this work, Schliehe et al. reported the oriented attachment of PbS NCs into ultrathin two-dimensional single-crystal sheets, measuring in micrometers laterally.[61] The attachment process was initiated by chlorine-containing cosolvents like 1,2-dichloroethane (or similar linear chloroalkanes like 1,2-dichloropropane and 1,1,2-trichloroethane) which yielded small NCs of ~3 nm diameter with a highly reactive {110} facet triggering the oriented attachment process. The formation of the small NCs of ~3 nm diameter was of paramount importance for the oriented attachment and was not observed in the absence of chlorinated species (which yield bigger NCs of ~5 nm diameter), as shown schematically in Figure 25b. The exposure of the {110} facet is key to the oriented attachment here, which are present in small NCs but are preferentially consumed during the NC growth. The 3 nm

DOI: 10.1021/acs.chemrev.8b00158
Chem. Rev. 2018, 118, 7804–7864

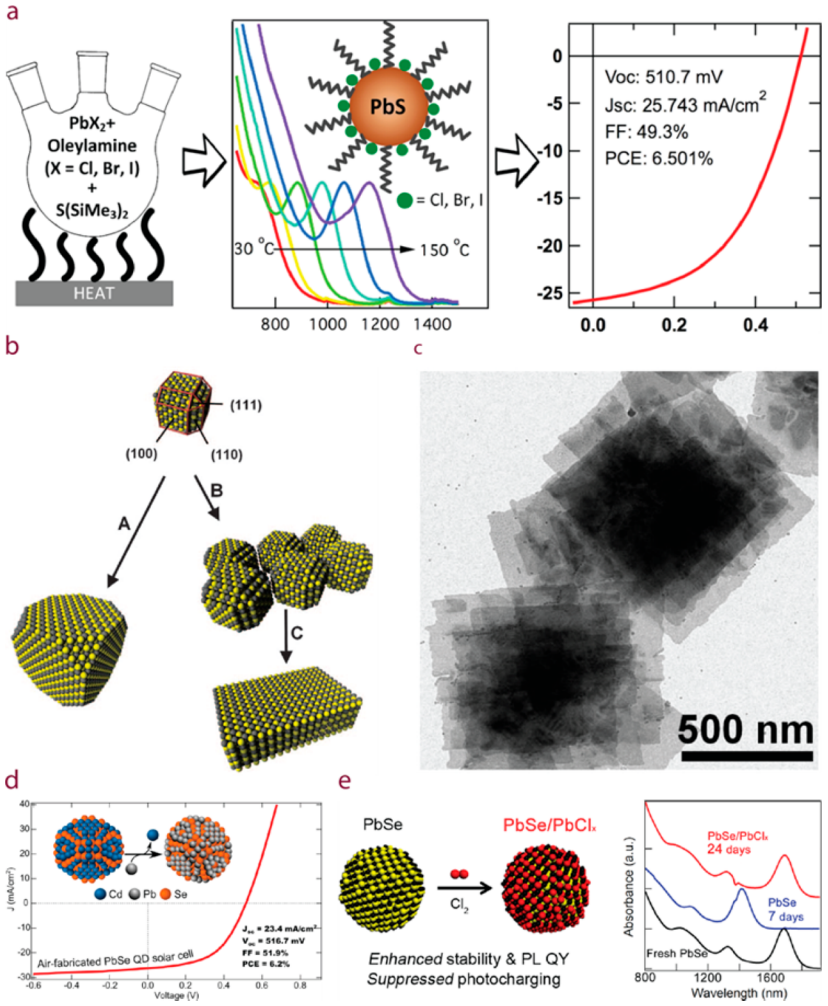

Figure 25. Effect of surface halide ions on the growth and optoelectronic properties of PbE NCs. (a) Diffusion-controlled synthesis of PbS NCs with in situ halide passivation. Halide passivation imparted higher photostability and led to high PCE of 6.5%. Reproduced from ref 275. Copyright 2014 American Chemical Society. (b) Scheme showing the formation of 2D PbS nanosheets by the oriented attachment of small PbS NCs in the presence of chloride ions and the formation of larger NCs in the absence of chloride ions. (c) TEM image of PbS nanosheet stacks. Reproduced with permission from ref 61. Copyright 2010 AAAS. (d) Schematic showing the cation exchange of CdSe NCs to PbSe NCs capped with a $CdCl_x$ layer, which rendered greater stability in air and PCE exceeding 6%. Reproduced from ref 72. Copyright 2014 American Chemical Society. (e) Formation of a protective $PbCl_x$ layer on the PbSe NC surface through postsynthetic molecular chlorine treatment, which prevented oxidation during long-term air exposure, as evidenced by the absorption spectra of PbSe NCs with (red) and without (blue) the protective $PbCl_x$ layer, and passivated trap states leading to improved PL efficiency. Reproduced from ref 280. Copyright 2012 American Chemical Society.

PbS NCs exhibit a truncated cuboctahedron shape with 6 {100}, 8 {111}, and 12 {110} facets (Figure 25b). When the NCs grow in the absence of the chlorinated species, the energetically unfavorable facets are minimized, resulting in truncated cubes bound with mainly {100} facets. However, in the presence of chloride compounds that act as lead complexing agents, the altered kinetics of nucleation and growth lead to ~3 nm particles exhibiting {110} facets. These small crystals then eventually stabilize through oriented attachment via the {110} facet, forming 2D sheets shown in Figure 25c. Later in 2014 Bhandari et al. explored this process further to demonstrate thickness tuning of the PbS sheets by using a series of chloroalkanes and reaction temperatures that enabled them to modify growth kinetics.[279]

More insights regarding the halide-assisted oriented attachment process were provided by a recent study by Koh et al.[281] In their synthesis of 2D PbSe nanoplatelets the authors observed that $PbCl_2$ moieties attached to the (111) and (110) facets form inter-NC bridges which favorably align the NCs for the attachment to proceed. Their DFT calculations indicate that the 2D bridging network was found to be more energetically favorable than 3D, which drives the nanoplatelet formation. Further, the authors suggest that PbI_2 does not lead to bridging, but it destabilizes the large (100) facets and hence provides a means for thickness variation of the nanoplatelets.

Apart from the direct synthetic protocols, halide ions also play a significant role in the chemical transformation of PbE NCs. In addition to their heterogeneous nucleation scheme,[275] Beard and his co-workers developed a cation-exchange pathway to obtain PbSe NCs with tunable sizes and in situ chloride and cadmium passivation.[72] As-synthesized CdSe NCs were injected into a hot $PbCl_2$/oleylamine mixture, which resulted in the formation of PbSe NCs passivated with Cd and Cl moieties, as schematically shown in Figure 25d. Owing to the $CdCl_x$ passivation, the as-synthesized NCs have excellent stability toward exposure to ambient air and can maintain their photoluminescence quantum yield for more than 30 days in air. This is a remarkable achievement considering the fact that

DOI: 10.1021/acs.chemrev.8b00158
Chem. Rev. 2018, 118, 7804−7864

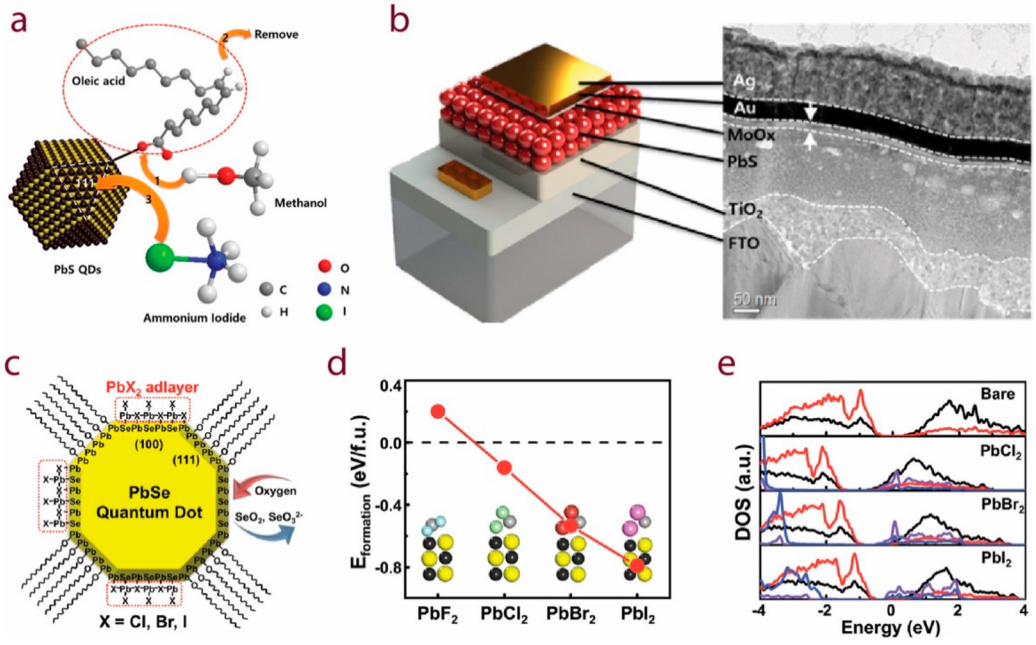

Figure 26. Using ammonium halides (NH_4X) to exchange native ligands on PbE NCs. (a) Schematic showing the replacement of native organic oleate ligands on PbS NC surfaces with iodide ions (using a solution of NH_4I in methanol). (b) Schematic and the respective cross-sectional TEM image of the heterojunction solar cell fabricated from the iodide-terminated PbS NCS. Adapted from ref 286. Copyright 2014 American Chemical Society. (c) Schematic showing the formation of atomically thin PbX_2 adlayer on the undercoordinated PbSe(100) facet formed by treating PbSe NCs with ammonium halides (NH_4X). (d) Formation energies of the different PbX_2 adlayers on the PbSe(100) surfaces, calculated using DFT. (e) Site-projected electronic density of states (DOS) for PbX_2/PbSe(100) showing the individual contributions from surface Pb (purple), bulk Pb (black), Se (red), and X (blue). Midband gap of the bare PbSe(100) after vacuum alignment is represented by the zero energy. Adapted from ref 69. Copyright 2014 American Chemical Society.

PbSe NC solution in hexane (in the absence of halide moieties) undergoes rapid oxidation upon exposure to air so that 50% of the NC converts into oxidation products within a span of a couple of hours.[282] The general strategies targeted at improving the resistance of PbSe NC surfaces toward oxidation involve passivating the undercoordinated Pb and Se sites. In the present case, the authors achieved this by a combination of Cl (for Pb sites) and Cd (for Se sites) passivations. The improved passivation led to high PCE (>6%, Figure 25d) from the solar cells fabricated from these NCs in ambient conditions and was attributed to the reduced recombination losses.

Prior to Beard's $CdCl_x$ passivation,[72] Bae et al. described a simpler $PbCl_x$ passivation on PbSe NCs as a means to prevent oxidation during long-term air exposure.[280] As schematically shown in Figure 25e, through postsynthetic treatment of the PbSe NCs using molecular chlorine (or more precisely a solution of chlorine in carbon tetrachloride), the Se atoms were preferentially etched out by the chlorine molecules which then reacted with the Pb ions to form the thin (1−2 monolayers) $PbCl_x$ passivation layer. The motivation behind exploring the molecular chlorine treatment was the authors' observation that the PbSe NCs exhibit higher PL intensity and spectral stability against oxidation when dispersed in chlorinated organic solvents like cholorform as compared to those dispersed in, say, hexane or toluene. The thin $PbCl_x$ layer was effective toward preventing oxidation during long-term air exposure and also ensured the passivation of trap states, thereby increasing the PL efficiency. The stability was evident from the optical absorption spectra, shown in Figure 25e, of the NCs with (red curve) and without (blue curve) the protective $PbCl_x$ layer. The surface passivation ensured that the NCs retained their optical signatures even after 24 days of air exposure.

3.2.2. Surface Binding Affects NC Properties. Compared to the postsynthetic ligand exchange protocols for introducing halide ligands on CdE NCs (as described in section 3.1.2 above), the efforts on PbE NCs are far more numerous and have contributed to a better understanding of the NC surface. The main motivation behind such detailed study stems from the fact that PbE NCs are important optoelectronic materials. However, despite their potential, susceptibility to oxidation has hampered their implementation.[69,280,283] This tendency leads to uncontrollable changes in their optical and electronic properties and sudden failure in solar cell performance.[72,275] Halide ions were found to be one of the important surface species for this situation, since they imparted protection against oxidation while facilitating inter-NC communication for improved thin film device performance. For instance, a 2016 report from Brutchey's group describes a solution-phase ligand exchange process for PbS NCs. In this work, Lu et al. employed the Z-type PbI_2 or the X-type NH_4I as incoming surface ligands along with *n*-butylamine (for solubility in organic solvents,[284] using the same logic as demonstrated by Owen in the case of CdSe NCs.[266] The ligand exchange was shown to be near-quantitative, and the PbI_2 passivation led to better colloidal stability and superior photovoltaic performance in polymer:NC hybrid solar cells.

Indeed, ammonium halides are one of the favored reagents for performing ligand exchange on PbE NCs, as demonstrated by several literature reports on this matter. For instance, in 2015 Sayevich et al. used ammonium iodide to perform postsynthetic ligand exchange on PbSe NCs to yield iodide capping that preserved the electronic structure and photophysical properties of these NCs at ambient conditions and also improved their transport characteristics.[285] Prior to that in 2014 Kim et al.

DOI: 10.1021/acs.chemrev.8b00158
Chem. Rev. 2018, 118, 7804−7864

employed ammonium iodide to replace the native oleate ligands on the PbS NC surfaces to obtain iodide-terminated NCs that were soluble in polar solvents like *N*,*N*-dimethylformamide without significant particle aggregation (as schematically shown in Figure 26a).[286] However, the solubility was compromised in the case of fluoride (F^-) or chloride (Cl^-) termination. This was rationalized on the basis of hard and soft acid base (HSAB) theory whereby the surface Pb^{2+} being a soft acid would like to bond strongly with a softer base for a halide ion, the iodide (I^-). The smaller and hence harder bases, fluoride and chloride ions, did not coordinate to the PbS NC-surfaces properly, leading to aggregation. The stable iodide-terminated NC solution was then used to fabricate solar cells (schematic device structure and cross-sectional TEM image shown in Figure 26b) which exhibited a PCE of 2.36% under ambient conditions.

This study came in close at the heels of another report from the same (Jeong) group, wherein they described a postsynthetic halide salt treatment of the PbSe NCs that led to their unprecedented air stability without significant alteration in optoelctronic characteristics.[69] In this work, Woo et al. achieved the halide passivation simply by incubating the NC growth solution with ammonium chloride. However, the native oleate ligands were not completely replaced by the chloride ions in this case and merely reduced by 3.5%. The NCs, both in solution and when deposited into a film, remained stable for days. The size-independent stability was explained by the passivation of undercoordinated PbSe(100) facet by atomically thin PbX_2 (X = Cl, Br, I) adlayers, as depicted in Figure 26c. As proposed earlier by the same group, the PbE NCs show size-dependent air stability depending on the occurrence of an oleate-capped Pb-rich (111) facet and the undercoordinated stoichiometric (100) facet.[283] Hence, the (100) facets are more prone to oxidation and a successful passivation of the same yields stability. The feasibility of the model of the atomically thin adlayer was further demonstrated by the calculated formation energies for different halides (Figure 26d), which showed that a PbF_2 layer was unlikely to form due to a discrepancy between the Pb−F and the Pb−Se bond lengths. The electronic structure analyses for the various halide adlayers also show a rigid downshift of the electronic bands by 0.4−1.1 eV, as in Figure 26e.

Sargent's group, on the other hand, used another variant of NH_4I, tetrabutylammonium iodide (TBAI), for their ligand exchange protocols on PbS NCs, among others.[7] They developed a solution ligand exchange protocol, as described by Ning et al.,[287] as well as a solid-phase procedure where PbS NC films were treated with a TBAI:methanol solution (Zhitomirsky et al.).[288] Ning et al. observed that the iodide ions partially displaced the native organic ligands (oleate; Figure 27a) and led to an increase in the PLQY of the solution-phase halide-treated NCs to 20% from that of 12% for untreated ones.[287] This was attributed to the reduced trap density upon halide treatment which translated into improved electron transport between NCs. They measured a PCE of 6.6% from solar cells fabricated from these NCs. Zhitomirsky et al. subsequently extended the idea of halide capping to achieve n-type doping in PbS NC films in 2014.[288] However, the halide capping in this case did not afford great protection against oxidation since the films turned p-type within 10 min of exposure to oxygen. The authors also found that the average carrier density and the mobility strongly depended on the nature of the halide ion.[289] The iodide passivation yielded the lowest doping density and highest carrier mobility, while chloride passivation exhibited the exact opposite characteristics. Hence,

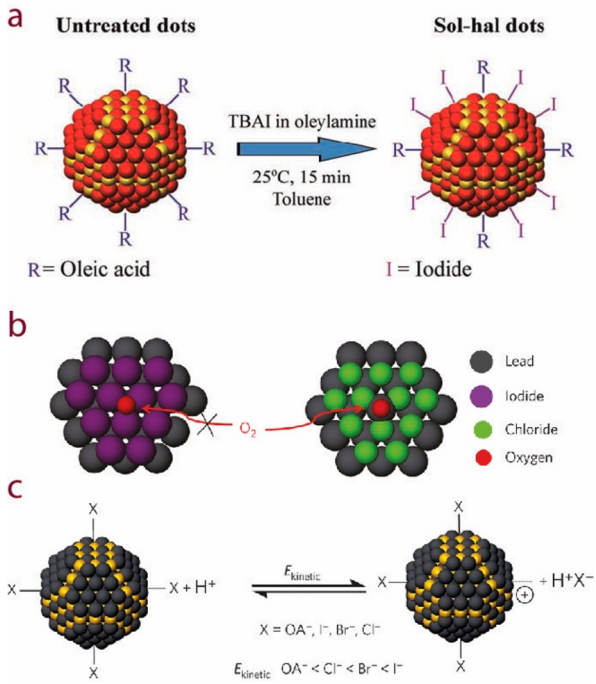

Figure 27. Iodide capping on PbE NCs brought about by ligand exchange using tetrabutylammonium iodide. (a) Solution-phase ligand exchange scheme for partially replacing native oleate ligands on PbS NCs with iodide ions. Reproduced with permission from ref 287. Copyright 2012 John Wiley and Sons. (b) Iodide capping on the NC surface affords greater protection from oxidation than the smaller chloride ions due to its sheer size which blocks the oxygen access of the NC surface. (c) Schematic representation of the desorption kinetics of different ligands under the attack of protons. Iodide was found to have the highest desorption energy. Adapted with permission from ref 291. Copyright 2014 Macmillan Publishers Limited.

the level of doping could be controlled in the range from 10^{16} to 10^{18} cm^{-3} by simply changing the halide ion. In 2015, Zhang et al. made similar conclusions from their experiments with methanol solutions of TBA−X salts on PbSe NC thin films.[290] Additionally, they found that the hot carrier thermalization time for the iodide-treated films can be three times as long as that for chloride treatment.

In a 2014 report from Sargent's group, Ning et al. resolved the issue of stability against oxidation for n-type PbS NC solids through solution halide treatment to obtain high-performance, air-stable films.[291] Their choice of halide ions for improved passivation was based on the small steric hindrance offered by them for complete coverage of the NC surface. Since protic solvents are typically used in desorbing the original ligands on a NC surface and prepare sites for the incoming ligands, an idea of the binding strength of the final ligand yields insights into its protective ability. The authors modeled the desorption of various ligand moieties on PbS NC surfaces under the attack of protic solvents using DFT calculations and found that iodide ions exhibit higher surface desorption energy than the others. This observation was also supported by the fact that iodide ions with their larger size could help protect the NC surface against oxidation, better than the other smaller halide ions (Figure 27b). The higher desorption energy of iodide ions was explained on the basis of HSAB theory whereby the H^+ being the hardest acid would show more affinity toward the harder base like Cl^- instead of the softer I^-, for the reaction scheme shown in Figure 27c. Experimentally, chloride and bromide termination revealed

DOI: 10.1021/acs.chemrev.8b00158
Chem. Rev. 2018, 118, 7804−7864

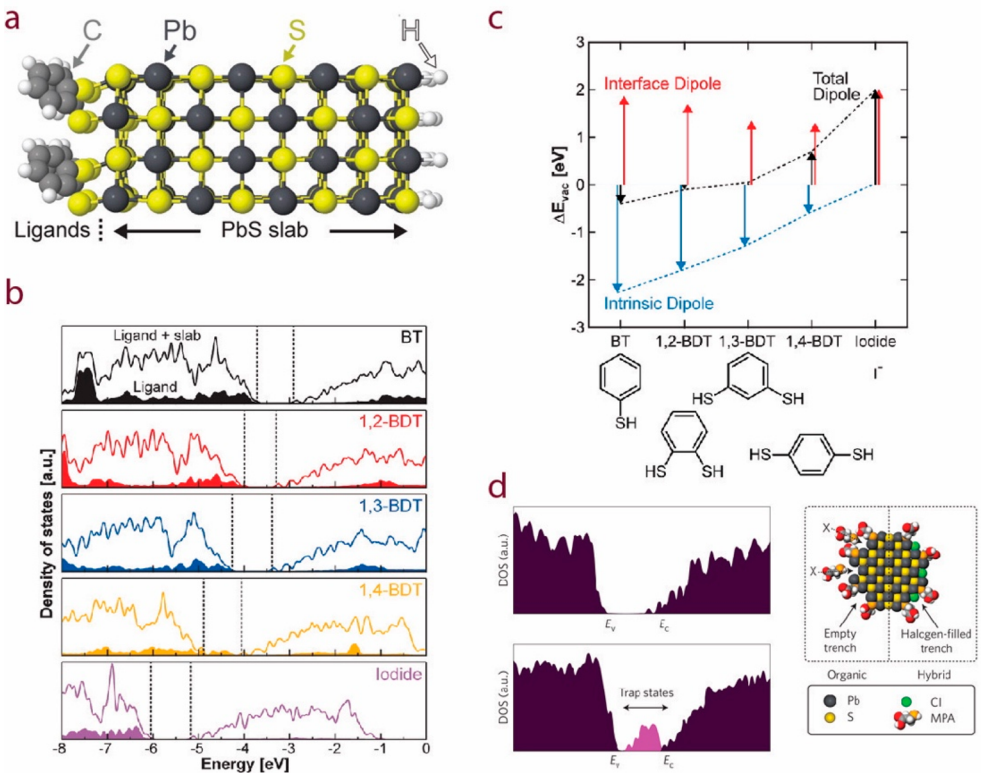

Figure 28. DFT calculations for energy shifts for PbS slabs induced by ligands. (a) PbS slab used for modeling: left side passivated with adsorbed ligands and right side with pseudohydrogen atoms for charge balance. (b) Electronic DOS for the five ligands considered: shaded curves represent the ligand, while the unshaded curves denote the ligand−slab system. (c) Energy shifts for the five ligands denoted by black arrows, with individual components denoted by red (ligand-surface−Pb-atom interface dipole moments) and blue (intrinsic dipole of the ligand) arrows. Adapted from ref 70. Copyright 2014 American Chemical Society. (d) Electronic DOS for a charge-balanced NC (upper) and that with trap states depicted in pink for noncharge-balanced NCs (lower panel); cartoon on the side depicting the ability of the halogens to fill up the interatom trenches which are otherwise inaccessible to bulky organic ligands and hence effectively passivate the NC surface. Reproduced with permission from ref 67. Copyright 2012 Macmillan Publishers Limited.

higher defect density than the iodide case, which also exhibited greater retention in the NC films compared to the chloride and bromide cases. The n-type character of the films was also retained upon air exposure for only the iodide termination. The devices fabricated from bromide- and chloride-treated NCs rapidly lost performance upon air exposure.

Zhang et al. slightly varied the ligand exchanging reagent to a combined ammonium sulfide and iodine treatment.[292] A surface PbI_2 layer was produced from the redox reaction between molecular iodine and PbS NC which effectively passivated the NC surface trap states.

The electronic properties of semiconductor NCs are dependent on both the NC size and the surface chemistry. The same is true for PbE NCs and requires detailed study since they are ideal materials for various optoelectronic applications. Brown et al. used ultraviolet photoelectron spectroscopy to elucidate the energy level shifts due to halide passivation along with that by different other ligands.[70] They found that these energy shifts scale with the ligand dipole moment and were also consistent with the performance of the photovoltaic devices. The ligand binding on the NC surface was modeled by approximating the NC as a semi-infinite PbS(100) slab, since (100) and (111) are the dominant facets in PbS NCs, as mentioned above (Figures 25b and 26c). One side of the slab was passivated with ligands and the other side with pseudohydrogen atoms for charge balance as depicted in Figure 28a, although the authors obtained similar results upon passivating both sides with ligands. The authors simulated the binding of five ligands, as depicted in Figure 28b and 28c, using first-principles DFT calculations. The electronic DOS for the ligands (shaded curves) and ligand−slab system (unshaded curves) for the five ligands reveal that the band gap remained relatively unchanged upon ligand adsorption, while the valence band maximum (VBM) and the conduction band minimum (CBM) shift in accordance to the electrostatic potential generated due to these ligands (Figure 28b). The energy level shifts upon ligand adsorption were then conceptualized as the sum of two dipole contributions: one from the dipole formed between the surface atom of the NC and the binding group of the ligand and the other from the intrinsic dipole moment of the ligand itself. These two competing electrostatic contributions then define the net shift in the energy levels upon ligand adsorption, which was found to scale as the total dipole moment generated, as shown in Figure 28c. Halide ions lack an intrinsic dipole moment, as opposed to the other ligands studied here, generating a large net dipole moment leading to the observed high band energy shifts.

This set of studies by Brown et al. provides important insights into the tunability of the NC electronic properties using their surface chemistry.[70] The energy level shifts can be used to predict changes in the PV device performance and can be used as a guide for the choice of ligand and device architecture for NC PV applications. Bawendi's group exploited these results to design a room-temperature solution-processed PV device from iodide-stabilized PbS NCs using a cascaded energy level

DOI: 10.1021/acs.chemrev.8b00158
Chem. Rev. 2018, 118, 7804−7864

architecture.[293] A very recent (2018) study by Yazdani et al. sheds further light on this matter through ab initio molecular dynamics simulations on halide-passivated PbS NCs.[294] They show that significant electron−phonon interactions can explain the large thermal broadening, and fast carrier cooling rates in PbE NCs and halide termination can suppress these effects.

Other sources of halide ligands include methylammonium halides (CH_3NH_3X), which have been used for solution ligand exchange on PbS NCs.[269] Propyltrichlorosilane is another chloride ion source which was used to replace the native ligands on PbSe NCs by Zanella et al.[267] Zhitomirsky et al. employed a solution treatment using chlorinated thiols on PbS NCs which resulted in a reduction in trap states and a PCE of 8.5% from the NC films.[295] Ibáñez et al. used HCl to displace the native oleate ligands on PbE NCs, which upon consolidation into dense pellets led to diffusion of the halide ions into the crystal structure, thereby doping the anion sublattice and achieved n-type electrical doping.[296] The authors further demonstrate the effectiveness of this doping strategy in controlling the charge transport properties through thermoelectric measurements on these pellets assembled from NC building blocks. Balazs et al. investigated the effect of counterions (ammonium, methylammonium, and tetrabutylammonium) in the iodide salt used for treating PbS NC thin films.[297] They found that a bulkier counterion like tetrabutylammonium hinder complete ligand exchange. More effective trap state passivation with 1-propyl-2,3-dimethylimidazolium iodide was recently demonstrated by Azmi et al. wherein the PbS NC thin films exhibited a PCE of 10.89% that was maintained at 90% after 210 days of air storage.[298]

As mentioned above, poorly passivated NC surfaces introduce mid-band-gap trap states which lead to poorly performing optoelectronic devices. Sargent's group demonstrated through DFT calculations that even a small imbalance between the number of ligands and the surface Pb atoms results in trap states that severely impede device performance in comparison to the trap-free case (DOS for the two cases shown in Figure 28d).[67] In this report, Ip et al. further explored if a complete passivation of the surface trap states is feasible using organic ligands alone and found that steric hindrance prevents the bulky organic molecules from accessing the intercation trenches leading to unpassivated trap states (Figure 28d). However, owing to their small size, halide atoms were conjectured to effectively passivate these sites. The authors then went on to demonstrate the effectiveness of the halide passivation through treating PbS NCs with $CdCl_2$ dissolved in a mixture of tetradecylphosphonic acid and oleylamine immediately after the nucleation and growth stages of the NCs. They compared the results with $PbCl_2$ as the chloride source and found that although the chloride ions effectively passivated the midgap states, the choice of cation was important since $CdCl_2$ treatment yielded higher hole mobilities in the NC films. In a 2014 report from Sargent group, Katsiev et al. provided further insights into the role of cations using photoelectron spectroscopies and found a reduction in the conduction band tail states when $CdCl_2$ was used in comparison to $PbCl_2$.[299] Marshall et al. extended the study further in a more recent paper, wherein they explored the effect of metal chloride salts with metals of varying oxidation states (from +1 to +3; Na^+, K^+, Zn^{2+}, Cd^{2+}, Sn^{2+}, Cu^{2+}, and In^{3+}) on PbSe NC solar cells.[300] $CdCl_2$ was found to be the most beneficial in terms of both device performance and resistance against oxidation. The solar cell fabricated with $CdCl_2$ treatment was stable in air for 270 days. However, in another study from the same group, PbI_2 treatment was found to be the most beneficial, although most of the organic ligands were removed in that exchange in addition to the chloride ions that resided on the surface as an end result of the synthesis protocol which involved cation exchange from CdE to PbE NCs by using $PbCl_2$ as the incoming cation source.[301]

Böhm et al. reported another variation of the $CdCl_2$ treatment where they employed a hybrid ligand solution containing $CdCl_2$ and 3-mercaptopropionic acid that are in equilibrium with a metal−ligand complex in solution.[302] Treating the NC films with this ligand solution helped passivate the sub-band-gap tail states in PbSe NCs.

3.3. Copper Chalcogenide (Cu_xE_y, E = S, Se, Te) NCs

3.3.1. Influencing NC Growth. It has only been very recently that researchers turned their attention toward the effect of halide ions on the formation of copper chalcogenide NCs. The first such study on the growth of copper chalcogenide NCs came from the group of Yinthai Chan in 2014.[303] In this work, Wu et al. described two-dimensional growth of Cu_2S NCs when halide ions were present in the reaction mixture, instead of the formation of spherical NCs in their absence. The 2D growth was rationalized on the premise of reduced availability of the copper(I) thiolate precursor due to the interference from the halide ion which inhibited its rate of formation from copper(I) acetate and dodecanethiol in situ. This inhibited the nucleation event and drove the NC growth into the thermodynamic regime which favored the formation of triangular nanoplates comprising of {002} lateral facets and {100} edge facets. Although chloride was introduced as hydrochloric acid (HCl), other halide sources such as copper(I) halides (CuX, X = Cl, Br, I) also resulted in nanoplate formation, albeit at a higher temperature. The authors also observed that the thickness of the nanoplates decreased with a concomitant increase in the lateral dimension upon increasing the chloride content in the reaction, as shown in Figure 29a.

A few months later, van der Stam et al. reported a similar observation wherein they obtained ultrathin $Cu_{2-x}S$ nanosheets through a synergistic interaction between halide ions (more specifically Br and Cl) and copper−thiolate precursor.[304] The formation and growth of colloidal $Cu_{2-x}S$ NCs proceeds through the thermolysis of Cu−dodecanethiol complex in solution, which involves the limiting C−S bond cleavage step.[305] van der Stam et al. showed that the halide ions, introduced as $SnBr_4$ and/or $SnCl_4$, stabilize the Cu−thiolate framework that preserves its 2D structural integrity even at temperatures high enough for C−S thermolysis to occur.[306] The liquid crystal phase of the Cu−dodecanethiol complex consists of a hexagonal columnar mesophase where each column comprises of a stack of tetranuclear $[Cu_4(\text{dodecanethiol})_4]$ discs which are held together by the weaker interdisc Cu−S interactions.[307] These interdisc and intercolumn interactions diminish at high temperatures and lead to a Cu-catalyzed C−S thermolysis that leads to the formation of Cu−S NCs. Halide ions interact with this copper-thiolate precursor to create a template that imposes 2D constraints on this very C−S thermolysis, leading to the formation of colloidal 2D $Cu_{2-x}S$ NCs.

Interestingly, bromide ions induce the formation of hexagonal sheets while chloride ions changed that shape to triangular, similar to the observations by Wu et al. as mentioned above and depicted in Figure 29b.[303] Iodide failed to generate nanosheets, on the other hand, and this phenomenon was explained on the basis of stronger interaction between the soft acid Cu(I) and the

DOI: 10.1021/acs.chemrev.8b00158
Chem. Rev. 2018, 118, 7804−7864

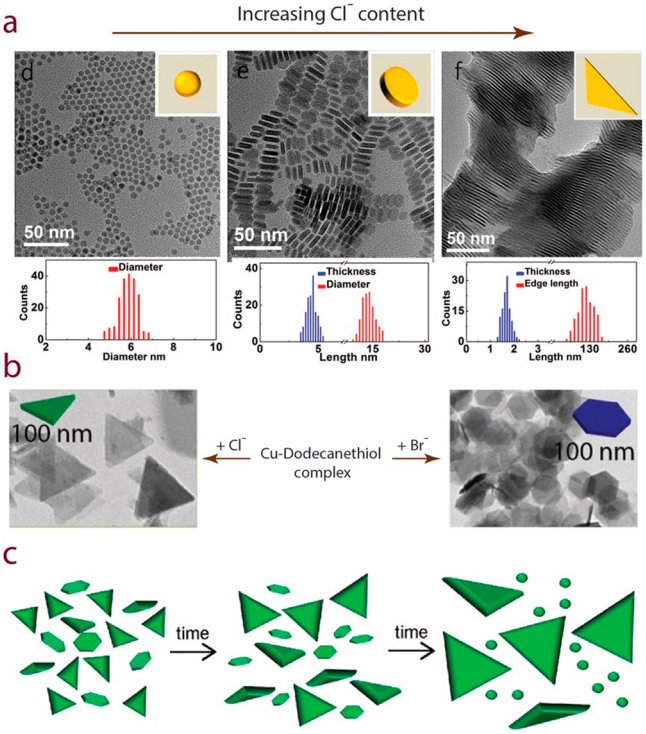

Figure 29. Influence of halide ions on the growth and transformation of Cu_xE_y NCs. (a) Increasing lateral dimension of Cu_2S nanosheets associated with a decrease in the thickness, as the chloride ion content of the growth reaction mixture increased. Adapted from ref 303. Copyright 2014 American Chemical Society. (b) Synergistic interaction between copper−thiolate complex and halide ions leading to the formation of $Cu_{2-x}S$ nanosheets. Br^- ions give rise to hexagonal shapes, while Cl^- ions lead to triangular sheets. Adapted from ref 304. Copyright 2015 American Chemical Society. (c) Schematic showing halide-assisted ripening of triangular CuS nanoprisms at the expense of unfaceted nanodiscs leading to bimodal size distribution. Adapted from ref 309. Copyright 2015 American Chemical Society.

softer base iodide ions (softer than chloride and bromide), which led to a 3D geometry of the halide−Cu−thiolate precursor. Later (2016), Bryks et al. demonstrated a similar Cl-assisted synthetic strategy for ultrathin Cu_9S_5 nanosheets.[308]

Hsu et al., on the other hand, explored the influence of halide ions on the growth of oleylamine-capped CuS NCs.[309] They found that the halide ions, when present in the reaction mixture as sodium or potassium halide, led to NC morphological transformation from nanodiscs to faceted triangular nanoprisms through a process akin to Ostwald ripening. They further demonstrated that this process likely occurred due to the competition between oleylamine and halide ions for surface binding sites and was strongest for the softer Lewis base I^- ions (compared to the harder bases Br^- or Cl^- ions) which had higher affinity for the surface Cu(I) ions (soft Lewis acids). A combination of halide-assisted and seed-mediated synthesis protocols was used where CuS triangular nanoprisms were formed as a result of ripening of the CuS nanodisc intermediates. A simultaneous shape-focusing and size-defocusing was described, i.e., the nanoprisms grew larger at the expense of smaller nanodiscs producing a bimodal size distribution, as schematically shown in Figure 29c. The authors also reported salient differences in growth patterns depending on the nature of the halide ion used in the synthesis. As mentioned above, by virtue of possessing higher affinity toward the Cu(I) ions, I^- slowed the ripening process by stabilizing the CuS surface which produced nanoprisms with more homogeneous size and shape distribution that resembled nanodiscs formed without the addition of halide ions. On the other hand, Cl^- and Br^- facilitated faster ripening leading to the formation and enlargement of faceted nanoprisms, at the expense of unfaceted nanodiscs that produced bimodal size distribution. Recent studies on the influence of Cl^- ions also include transformations of $Cu_{2-x}S$ NCs to anisotropic nanostructures[310] and promotion of 2D growth.[311]

3.3.2. Halide Ions as Ligand Moieties. Thus far there has been only one report of exploiting halide ions for a postsynthetic ligand exchange protocol on copper chalogenide NCs. Lee et al. effectively stripped the surface oleylamine ligands of $Cu_{2-x}Se$ NCs without passivating the NCs with chloride ions, through treatment of the NC films with a solution of ammonium chloride in methanol.[312] This improved the electronic coupling between the NCs which was demonstrated by the red shift in the direct and indirect band gaps, accompanied by a dampening in the surface plasmon resonance. The electrical conduction in the NC film also improved after ligand stripping, which led to improved thermoelectric performance of the NC thin films (Seebeck coefficient of 13 μV/K).

3.4. Silicon NCs

Achieving colloidal stability and device integration is a bit trickier for group IV NCs like that of Si, Ge, etc., than in the case of say metal chalcogenide NCs. The success in the latter case stems from the fact that the ligands on their surfaces are relatively labile and hence freely exchanged. In contrast, the surface ligands in the case of Si are covalently bound and are kinetically inert to exchange reactions. Consequently, this causes a hindrance toward exploiting the optoelectronic properties of thin film architectures where inter-NC communication becomes important at the device level (using short ligands) while colloidal stability is important for solution processing (effected typically by long alkyl chain ligands).

Wheeler et al. offered a solution to these issues together through their synthesis of Cl-terminated Si NCs which engaged in hypervalent interactions with donor molecules:,[73] Si is rendered a Lewis-acidic character upon bonding with Cl moieties which polarize the electron density away from the Si atomic centers. This makes them capable of engaging in pentavalent or even hexavalent bonding rather than their usual tetravalent coordination.[313] The hypervalent interactions by the surface Si−Cl groups with hard donor molecules (Lewis bases) provided colloidal stability in addition to doping of the Si NCs. They achieved the Cl-terminated surface through a nonthermal plasma synthesis which involved decomposition of $SiCl_4$ in the presence of hydrogen. In contrast to standard colloidal methods, nonthermal plasma synthesis is particularly useful for group IV NCs primarily due to the high crystallization energies required.[314] Adding appropriate hard donor solvents such as ketones, aldehydes, and nitriles could then achieve a stable colloidal solution. The merits of the Cl termination were demonstrated through the colloidal stability since a control experiment with H termination did not yield a solution. A pictorial representation through molecular ball-and-stick models of the interaction between the Si−Cl surface groups of Si NCs and the donor carbonyl group of 2-butanone is shown in Figure 30a.

The hypervalent interactions were further explained from a molecular orbital point of view, as schematically depicted in

DOI: 10.1021/acs.chemrev.8b00158
Chem. Rev. 2018, 118, 7804−7864

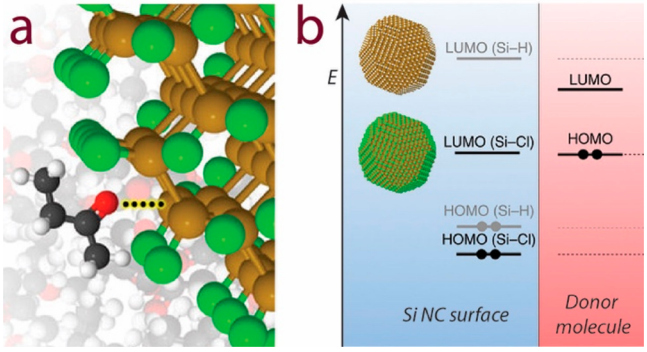

Figure 30. Exploiting halide handle in the synthesis and processing of Si NCs. (a) Ball-and-stick depiction of hypervalent interaction between the surface Si–Cl group (green and brown balls) of Cl-terminated Si NC surface and a hard donor molecule, 2-butanone (black, white and red balls). (b) Molecular orbital picture depicting the energetics of LUMO (Si–Cl)–HOMO (donor molecule) interaction. Adapted with permission from ref 73. Copyright 2013 Macmillan Publishers Limited.

Figure 30b. The lowest unoccupied molecular orbital (LUMO) of Si–H groups, being too high up in energy, does not favorably interact with donor molecules. On the other hand, the LUMO of the Si–Cl has a much lower energy due to polarization of electron density away from the Si surface atoms by Cl termination.[315] Hence, the highest occupied molecular orbital (HOMO) of the donor molecules that are much deeper in energy are more favorably posited to interact with the LUMO of Si–Cl. Similar hypervalent interaction-induced stabilization also operates in the case of Ge NCs terminated by Cl atoms, as reported by the same group earlier, although electrostatic stabilization was thought to be the dominant mechanism of stabilization at that time.[316]

Although the first report on Cl termination on Si NCs came from Baldwin et al. way back in 2002,[317] it was only recently that the potential of such surface manipulation was explored. Substantial contribution in obtaining halide-terminated Si NCs also came from Veinot's group.[318−320] In one of their first reports, Dasog et al. obtained Cl-terminated Si NCs through postsynthetic chlorination of H-terminated Si NCs.[318] Later, Islam et al. used Cl-terminated Si NCs produced by the same protocol in catalyzing the synthesis of poly-3-hexylthiophene.[319] The Lewis-acidic nature of the NC surface was utilized in this polymerization reaction. In a subsequent report, Dasog et al. presented postsynthetic halide insertion on the surface of Si NCs and studied its influence on their optical properties.[320] The halide termination quenched the fluorescence of the NCs however.

4. METAL OXIDE NANOCRYSTALS

Compared to the previously discussed classes of materials, the influence of halide ions on metal oxide NCs takes a slightly different course since it is only fluorine which has a lower electronegativity than oxygen and hence is in a situation to effectively perturb the surface energetics during NC growth. Indeed, as will be clear in the subsequent sections, the sheer number of literature reports on F adsorption on metal oxide NCs is larger than those concerning Cl, Br, or I. Interestingly, metal oxide NCs have been extensively synthesized starting from metal halide salts as either the most obvious precursors or as the most convenient ones.[321,322] A clear effect of halides in the overall growth and final properties of this class of NCs has been documented by numerous research groups.

4.1. TiO_2 NCs: Shape Control Meets Optical Modulation

Due to its numerous applications, the development of shape control in solution synthesis of nanostructured titanium dioxide (TiO_2) is an important research avenue aimed at realizing the full potential of the material. It is an industrially important wide-band-gap semiconductor, and nanostructuring enables its use as an active material in various geometries in electrochromics, photovoltaics, lithium-ion batteries, photocatalysis, etc.[323,324] TiO_2 crystallizes in three naturally existing polymorphs: rutile, anatase, and brookite,[324,325] out of which rutile is the most thermodynamically stable phase while anatase has been shown to be more photocatalytically active.[326] Anatase is also often found to be dominant in nanocrystalline TiO_2 owing to its lower surface energy than rutile.[323] On the other hand, brookite is usually formed as a mixture with other polymorphs and is a stable phase at low temperatures.[327]

The technological relevance of TiO_2 has prompted many bulk studies aimed at examining the surface adsorption of various atomic and molecular species.[325,326] Halide ions/atoms have also received their fair share of attention with several reports discussing the adsorption of Cl at TiO_2(110) surfaces.[328,329] The chlorine, dosed from an electrochemical source in the form of Cl_2, was shown to dissociate at room temperature and adsorb at the 5-fold O-coordinated surface Ti atoms in an on-top configuration, as shown schematically in Figure 31a.[328] Instead of the usual 6-fold O-coordinated Ti atoms in the crystal bulk, rows of 5-fold O-coordinated Ti atoms characterize the TiO_2 (110) surface, which are separated by 3-fold-coordinated and bridge-bonded O atoms (Figure 31a). The negatively charged Cl adatoms interact very differently with the surface Ti^{4+} and O^{2-} ions.

The various modes of interaction between the adsorbate (Cl_2) and the TiO_2 (110) surface are best understood by following the labels in Figure 31a, the first one being the approach of Cl_2 molecule to the surface (A).[328] The dissociation of the Cl_2 molecule on Ti atoms is an exothermic process which means that part of the excess energy liberated can be transferred into the kinetic energy of the resulting Cl atoms. If this dissociation happens in a trough (B), the Cl atoms remain confined to the Ti rows and possibly move a significant distance before their energies are compensated. These correlated Cl–Cl pairs can be observed in the STM image in Figure 31b, as denoted by circles. However, the distribution of these pairs in Figure 31b indicates a correlation across bridging oxygen rows as well, the pairs being widely spaced in this case. The authors invoke a so-called "cannon-ball mechanism" to explain this, according to which the Cl_2 molecule adsorbs in an upright orientation with respect to the surface (E). An abstractive adsorption process follows, and one Cl atom shoots out in the vacuum and lands in the neighboring trough or even further away. The single Cl adatom denoted by squares in STM image in Figure 31b was taken as an indicator of this canon-ball process. The scenarios labeled by D and C represent the unlikely situations of Cl_2 oriented perpendicular to Ti rows and the van der Waals radius of a Cl^- ion, respectively.

The adsorption mechanism described above was solely based on STM imaging. However, later photoemission experiments demonstrated that Cl adsorption also occurred in O vacancies, which is signified by the rapid quenching of the defect-related gap state upon Cl dosing to a slightly defective surface at room

DOI: 10.1021/acs.chemrev.8b00158
Chem. Rev. 2018, 118, 7804−7864

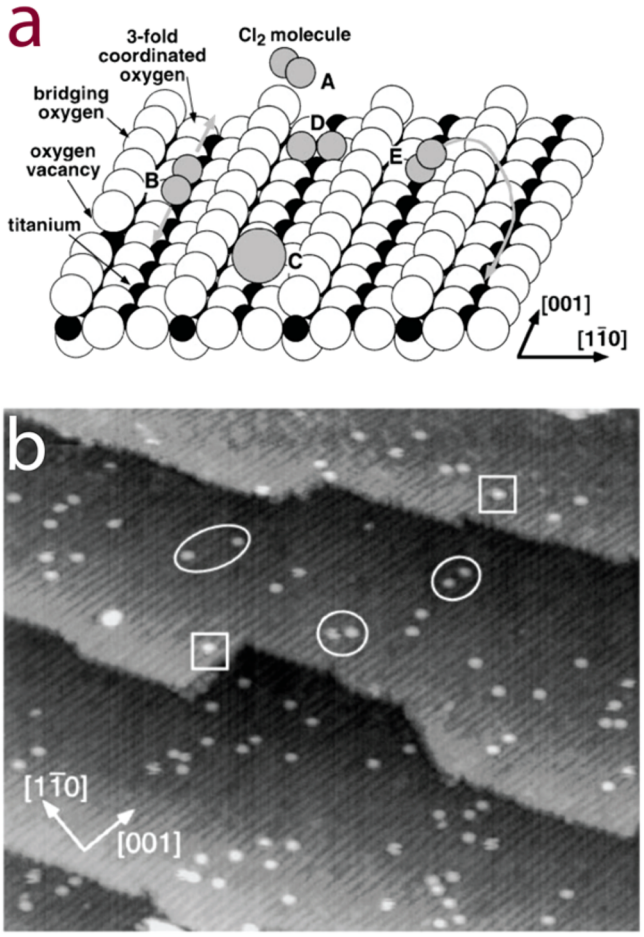

Figure 31. Adsorption and dissociation of Cl_2 on the TiO_2 (110) surface. (a) Model depicting the different adsorption modes of Cl atoms on the surface. (b) STM image of TiO_2 (110)-surface exposed to Cl_2 at room temperature, bright round spots being the adsorbed Cl atoms. Some Cl−Cl pairs and single chlorine adatoms are demarcated by circles and squares, respectively. Adapted with permission from ref 328. Copyright 1998 American Physical Society.

temperature.[329,330] The Cl atoms adsorbed in O vacancies are expected to have an image contrast similar to bridging oxygen atoms and hence were not observable during STM imaging. This means that the "single" Cl atoms shown in Figure 31b can very well be the leftover partners from a dissociated Cl−Cl pair, the other of which went on to fill a vacancy in the bridging oxygen rows. In addition, the calculations performed by these authors also demonstrated that Cl adsorption in an O vacancy is more favorable than at 5-fold-coordinated Ti atoms and corroborated further by Cl dosing at higher temperatures (~150 °C).[330]

No long-range halide ordering was observed in these bulk studies, and the localized and disordered adsorption of the Cl atoms was generally reported. The implications of these halogen-adsorption processes on TiO_2 surfaces have a more pronounced impact in nano- and microscale systems simply due to the larger surface area under investigation offered by these systems. For instance, Yang et al. reported a hydrothermal synthesis of anatase TiO_2 in 2008, where the introduction of hydrofluoric acid (HF) in the growth solution led to the formation of truncated bipyramical microcrystals.[331] This unique morphology is the result of the reversal of relative surface energies of the {001} and {101} facets, {001} being more stabilized by F termination and expressed at a high percentage in the microcrystals (47%). In general, {101} facets are thermodynamically more stable in F-free reaction conditions and can constitute about 94% of the surface (as per Wulff construction).[332] This work showed that F adatoms were especially well suited for this kind of relative free energy modulation of anatase TiO_2 surfaces.

On the basis of first-principles calculations, Yang et al. investigated the effect of 12 different types of nonmetallic adatoms (namely, H, B, C, N, O, F, Si, P, S, Cl, Br, or I) on the surface energy of {001} and {101} facets, as illustrated in Figure 32a and 32b.[331] The models used for the clean and adatom (X)-terminated surfaces are shown in Figure 32a, while Figure 32b shows the influence of these adsorbates on the free energy of these surfaces and the resulting surface area contributions in the anatase TiO_2 microcrystals and hence the resulting morphology (defined by the length parameter ratio, B/A). It is easy to see from Figure 32b that F termination yields the lowest values of surface energies for the two facets and also imparts more stability to the {001} facets. This directly translates into the dominance of {001} facets in the resulting TiO_2 microcrystals, shown in Figure 32c. The authors subsequently followed this work with another report on the solvothermal synthesis of anatase TiO_2 single-crystal microstructures where the synergistic influence of F^- ions and isopropanol was used to increase the percentage of {001} facets even further, resulting in rather flat microcrystals.[333] The stabilizing influence of F^- on the {001} facets has since been demonstrated in other aqueous syntheses of anatase TiO_2 nano/microsructures as well, where varied F sources were employed (apart from the commonly used HF). Notable examples include ammonium fluoride,[334] 1-butyl-3-methylimidazolium tetrafluoroborate,[335,336] 1-methylimidazolium tetrafluoroborate,[337] ammonium bifluoride,[338] etc.

The stabilizing influence of F termination on an otherwise high-energy reactive {001} facet created a surge of interest in studying this aspect, especially since TiO_2 is a very important photocatalyst and this activity is crystal facet specific in nature. Nanostructured TiO_2 is a particularly attractive platform for these studies as large surface areas can be accessed, which is beneficial for catalysis in general as more surface sites of the catalyst are available for the reaction under investigation. For instance, Chen et al. reported a microemulsion-based synthesis of truncated tetragonal nanobipyramids of TiO_2 by using sodium fluoride as the source of F^- ions.[339] They made a comparative investigation of the effect of different halide ions by using sodium halides (for F^-, Cl^-, and Br^- ions) in the reaction mixture and found that the presence of halide ions promoted the formation of larger NCs with F^- ions yielding the largest ones. Trentler et al. made a similar observation in their nonhydrolytic synthetic route involving an alkyl halide elimination reaction between titanium halide and titanium isopropoxide—smaller NCs formed upon increasing the size of the halide ion in the synthesis of TiO_2 NCs.[340] Ichimura et al. used metal fluoride salts (which include sodium, lithium, cesium fluorides) in their hydrothermal synthesis of anatase films on gold substrates that expose the {001} facets.[341] However, F^- has been found to act in synergy with other molecules/adsorbates as well, as has been demonstrated by a various research groups. Menzel et al. showed the cooperation between water, HF, and TiF_4 in the formation of TiO_2 nanoplatelets,[342] while the combined influence of HF and hydrogen peroxide has been reported in the formation of hollow microspheres of TiO_2 with exposed {001} facets[343] and truncated bipyramid-shaped NCs.[344] An interesting precursor TiO_xF_y was also shown to be useful for modulating the

DOI: 10.1021/acs.chemrev.8b00158
Chem. Rev. 2018, 118, 7804−7864

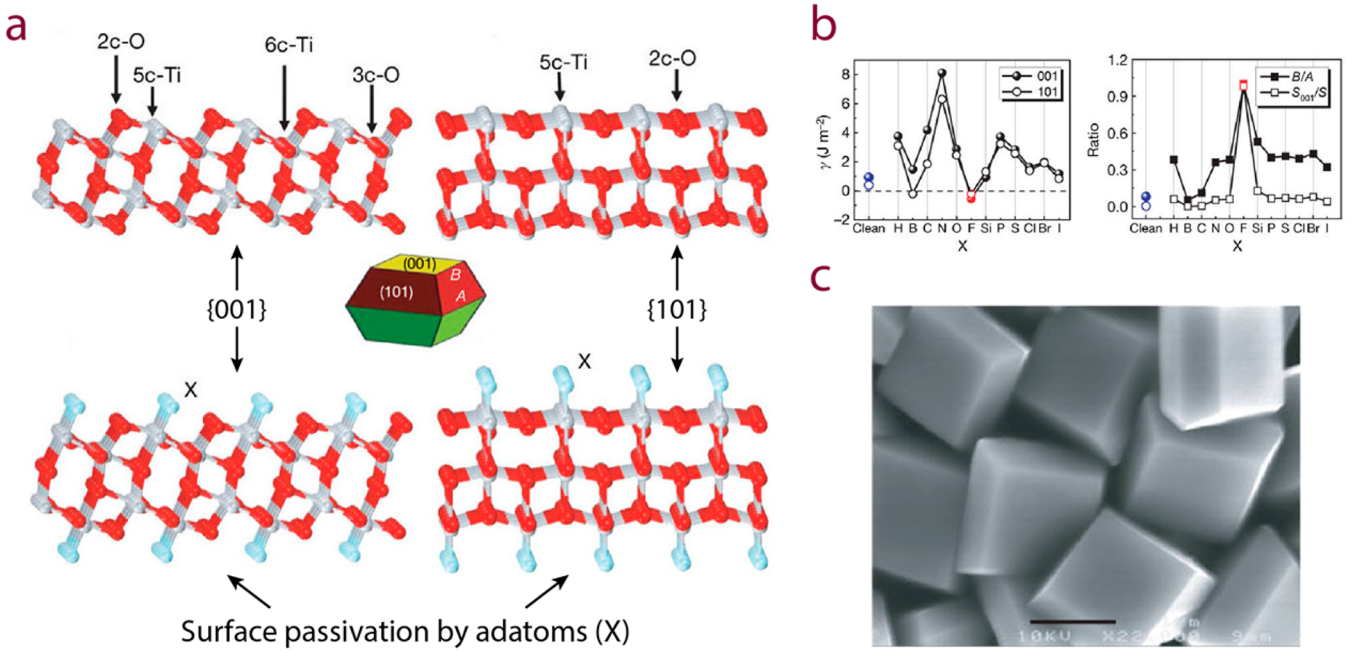

Figure 32. Adsorbate-induced surface energy alteration of {001} and {101} facets of anatase TiO_2 and its implication in microcrystal growth. (a) Ball-and-stick diagrams depicting unrelaxed TiO_2 facets without (top row) and with (bottom row) adatom (X) passivation. Ti and O atoms are represented by gray and red balls, respectively, with the prefix denoting the coordination, i.e., 6c-Ti implies a 6-fold-coordinated Ti atom. (b) Calculated surface energies of the facets (left plot) and surface area fraction contributed by the {001} facet (along with the ratio of length parameters, B/A) (right plot) upon adatom passivation. (c) TiO_2 microcrystals synthesized in the presence of F^- ions. Adapted with permission from ref 331. Copyright 2008 Macmillan Publishers Limited.

percentage of {001} facets in the resulting microcrystals simply by modifying the fluoride content.[345]

The surface energies of anatase TiO_2 decrease in the order {001} > {100} > {101}, which results in the equilibrium shape of its crystals being truncated octahedral bipyramid with {101} surfaces on the sides and {001} surfaces on the top and bottom truncation facets (Figure 33a, leftmost shape).[332,346] Both natural and synthetic anatase crystals exhibit this shape, and the degree of truncation can be defined by the ratio of the length parameters, B and A, as demarcated on the schematic (leftmost shape) in Figure 33a. This equilibrium shape exposes hardly about 10% of the {001} facets, and Yang's work on the use of F^- capping which reverses the facet stability order ({101} > {100}) was an important breakthrough,[331,333] as can be gauged from the plethora of research that followed (discussed above). Increasing the percentage of {001} facets, which leads to an increase in B/A ratio, and elucidating the mechanism responsible for it became one of the prime objectives of all these studies.[347] One of the most striking demonstrations of the influence of F^- capping was made by Han et al. in 2009 when they produced anatase TiO_2 nanosheets exhibiting a very high percentage of the {001} facets through a hydrothermal approach.[348] They showed that the {001} percentage increased with an increase in the added HF in the reaction mixture, and the lateral size of the sheets also increased. The average lateral size of the nanosheets could reach the order of 130 nm with 8 nm thickness, amounting to an average percentage of 89% of {001} facets. Figure 33b shows representative TEM images of some of the nanosheets prepared by this method. In comparison, Yang et al. reported the {001} content being up to about 64% in their microcrystals.[333] Later in 2011 Wen et al. extended the {001} proportion in their solvothermal synthesis of TiO_2 nanosheets to 98.7% which spanned few micrometers in lateral dimension.[349]

The {001} facet stabilization by F termination had been attributed to the strong bonding between the unsaturated Ti atoms and the incoming F atoms.[331] The strength of the Ti−F bonding is such that water dissociation on the {001} anatase surface, which otherwise occurs spontaneously on a clean surface, becomes highly unlikely upon F capping.[350] The chemistry of the F adsorption on the anatase crystal facets had been explored in a few literature reports. For instance, Zhang et al. used DFT calculations to show that the surface fluorination on the {001} facets can occur only through the dissociative adsorption of molecular HF under acidic conditions, while the dissociative adsorption of NaF is thermodynamically unfavorable.[351] This work rationalized the apparent dependence on pH reported by earlier works, e.g., Yang et al. used hydrochloric acid (HCl) for pH adjustment in addition to using HF as the morphology director.[331,333,348] Other reports discussing the role of in situ formed HCl in the growth of TiO_2 NCs also include an earlier one from 2003.[352] The authors demonstrated that increasing the Cl^- concentration led to the increased acidity of the solution which hinders nuclei formation and hence modifies growth rate. The hydrolytic equation of $TiCl_4$ ($nTiCl_4 + 2nH_2O \leftrightharpoons nTi(OH)_4 + 4nHCl$) mandates enhanced production of H^+ ions at higher concentrations of $TiCl_4$ in the highly acidic solution. Fewer NRs were formed in such scenarios, which means that a fine balance of Cl^- ions and resulting acidity needs to be achieved for optimized shape control.

A comprehensive shape control of anatase TiO_2 NCs in the nonaqueous surfactant-assisted synthesis regime through the influence of F^- ions was reported by Gordon et al. in 2012.[353] They employed a seeded growth method to produce highly uniform NCs with tailorable morphology through engineering the percentage of {001} and {101} facets by careful modulation of the cosurfactant and titanium precursor concentrations. The

DOI: 10.1021/acs.chemrev.8b00158
Chem. Rev. 2018, 118, 7804−7864

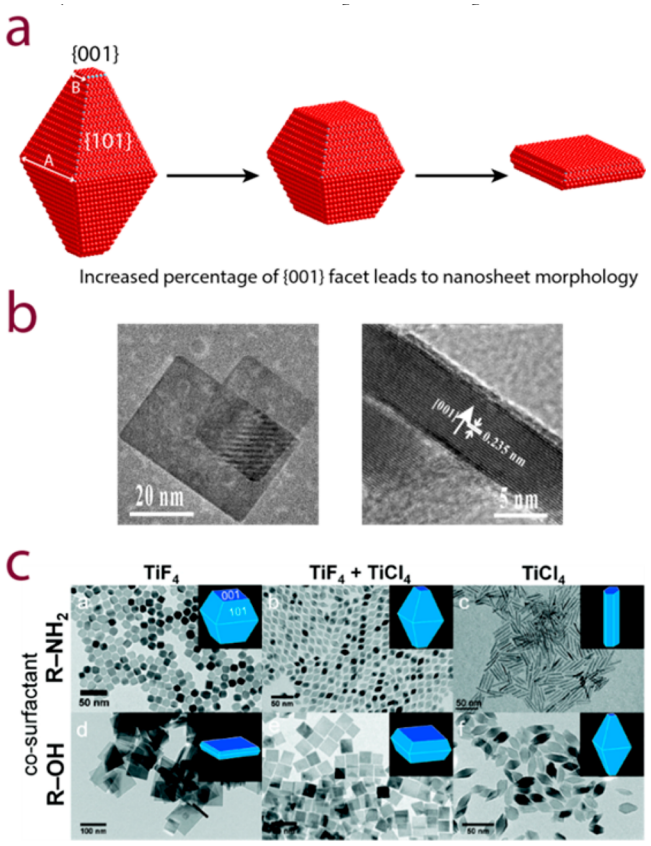

Figure 33. Implications of F^--facet capping on the morphology of solution-grown anatase TiO_2 NCs. (a) Schematic showing the changes in morphology of anatase TiO_2 NCs as the order of surface energy reverses for {001} and {101} facets upon F-capping. Percentage of {001} facets increases upon carefully modulated F capping, resulting in different NC shapes. (b) TiO_2 nanosheets exhibiting 89% of exposed {001} facets. Adapted from ref 348. Copyright 2009 American Chemical Society. (c) TiO_2 NCs of different shapes synthesized by careful modulation of the cosurfactant and titanium halide precursor concentrations. Reproduced from ref 353. Copyright 2012 American Chemical Society.

morphology descriptor was HF as well, which was released in situ from the reaction between the cosurfactant (oleylamine/octadecanol) and the titanium(IV) fluoride (TiF_4) precursor used in their synthesis. The percentage of {001} facets increased when F species were present in the growth mixture, as can be envisaged from Figure 33c, left column. Cl species, on the other hand, exhibited little deviation from the equilibrium shape of the NCs (Figure 33c, right column), save from reducing the amount of HF released and hence the reduced percentage of {001} facets when mixed (1:1 F/Cl) precursors are used (middle column, Figure 33c). This is line with the predictions made by Yang et al. (see Figure 32b).[331] The choice of the surfactants also bore a significant contribution to shape modulation. The {001} facets were expressed less when oleylamine was used since the in situ generated HF was sequestered by the excess amine in solution, reducing the amount available for surface capping.

Apart from modifying the surface energies and growth kinetics leading to NC shape modulation, the optical characteristics of nanostructured TiO_2 exhibit a significant influence from the halide adsorption. This phenomenon has already been shown in the bulk through photoemission,[329,330] electrochemical,[354] and photocatalytic activity measurements.[355−357] Halide doping in TiO_2 was initially thought to be causing a red shift in its absorption edge which enables visible-light-driven photocatalysis.[357,358] A later report, however, demonstrated that F doping has much less effect on the optical absorption of bulk TiO_2 and instead is involved in the creation of oxygen vacancies which leads to the visible-light-driven photocatalysis.[359] This is in line with the calculated band structure of F-doped TiO_2 by Yamaki et al., where it was shown that the localized F 2p levels due to F doping are posited deep within the valence band maximum of TiO_2.[360] A similar explanation was offered for the blue color of the NCs prepared by Gordon et al., which also exhibit a broad visible/NIR absorbance that peaks in the infrared and is ascribed to the localized surface plasmon resonance arising from the significant electron density.[353]

More recent reports on the question of F doping in TiO_2 offer further in-depth explanations. For instance, in 2008 Czoska et al. expanded on the picture offered by Yamaki et al. to demonstrate that F doping in TiO_2 forms two different F species in the crystal—one that substitutes oxide lattice sites yielding a bridging Ti−F−Ti bond in the bulk and the other being those on the surface yielding a terminal Ti−F bond.[361] The substitutional doping (of O^{2-} by F^-) induces the formation of Ti^{3+} species in an octahedral environment that introduces localized states just below the conduction band and leads to n-type doping. Jun et al. corroborated this picture experimentally through a suite of X-ray spectroscopies.[362] Seo et al. demonstrated that F insertion in TiO_2 passivates defect states and F acts as an n-type donor in their 2011 report.[363] The passivation of surface defect states on microcrystals of anatase TiO_2 was experimentally demonstrated by Rex et al. recently (2015).[364]

A pivotal work in this regard is that by Ma et al. where they took both adsorption by F^- and doping in anatase TiO_2 into account and conclusively explained the experimental knowledge amassed in this field so far.[365] The local geometric structures and local potential strengthen the Ti−O bonding in (101) and render it the most stable surface in vacuo. Another way of looking at the relative stability order is also the higher number of undercoordinated atoms in (001) (than (101), see Figure 34a), which makes it less stable. However, the authors explained that F-capping strengthens the Ti−O bonding in (001) while weakening them in (101) based on their DFT calculations. This leads to the lower surface energy of (001) over (101) under F adsorption. Note that this is in contrast to the prediction made by Yang et al.,[331] where the strong Ti−F bonding was deemed responsible for the changes in surface energy. Ma et al. found that the contribution of the Ti−F bond strength in surface stabilization per se was quite small.[365] Instead, it was the higher electronegativity of F which withdraws electron density from the Ti−O bond to the Ti−F bond, changing the Ti−O bond strength in the process. F adsorption changes the local structure of the surfaces (see Figure 34a, lower row), which particularly makes the orbital overlap between the Ti and the O atoms favorable for the (001) surface, especially the Ti5c and O2 in Figure 34a. These observations rationalize the apparent dearth of literature reports on the influence of other halides (Cl, Br, and I) on TiO_2 NCs since they exhibit little to no influence on TiO_2 surfaces due to smaller electronegativity than the O atoms.

This study further demonstrates that upon n-type doping in TiO_2 the surface energy order switches back to (101) being more stable despite F adsorption.[365] The n-type doping partly offsets the change in the Ti−O bond strength induced by F adsorption, leading to the switch. The electron withdrawal by

DOI: 10.1021/acs.chemrev.8b00158
Chem. Rev. 2018, 118, 7804−7864

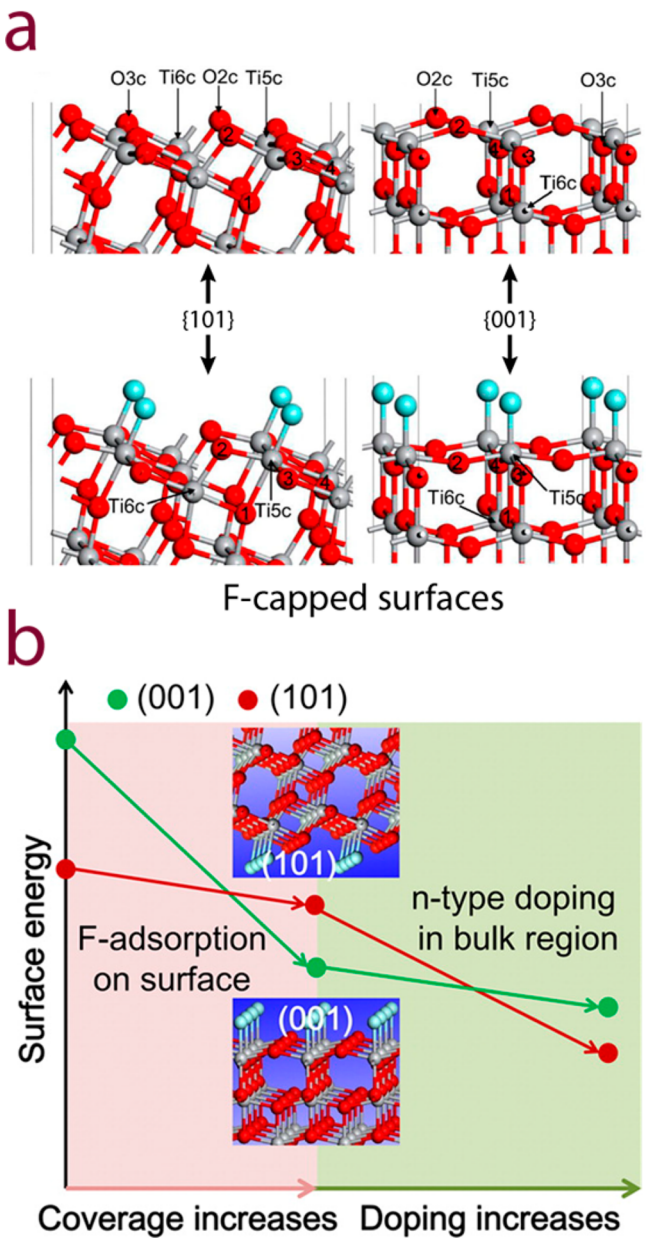

Figure 34. Adsorption vs doping of F^- in anatase TiO_2. (a) Ball-and-stick illustrations of optimized structures of {001} and {101} without (upper row) and with (lower row) F adsorption. (b) Schematic curve showing the changes in surface energies of {001} and {101} facets upon F adsorption and F doping. Surface energy order reverses upon adsorption and switches back upon n-type doping by F atoms. Reproduced from ref 365. Copyright 2015 American Chemical Society.

the F adsorption can come from the n-doped bulk lattice sites instead of the Ti−O bonds and hence counter the stabilizing influence of F capping. A schematic of this scenario presented by the authors is shown in Figure 34b. This explains the apparent discrepancy in the literature when it comes to increasing the percentage of {001} facets simply by increasing the F content of the growth solution, since different reaction conditions lead to varying levels of intrinsic and extrinsic n-type defects. A possible way of achieving a high percentage of {001} facets in the anatase TiO_2 NCs will then be by eliminating n-type defects or counteracting them by intentionally introducing shallow p-type defects coupled with F-assisted synthesis.

4.2. ZnO NCs: F Doping of Nanostructures

The effects of F doping/adsorption have been explored in the case of zinc oxide (ZnO) NCs as well but not described as rigorously as has been done in the case of TiO_2 NCs above. An important contribution in this regard was in 2017 from Papari et al., where they describe the implications of F inclusion in hydrothermally grown ZnO mesostructures.[366] Their electron paramagnetic resonance (EPR) measurements clearly indicate that the F atoms tend to occupy oxygen vacancies in the lattice, which induces the onset of luminescence centers. Similar quenching of oxygen vacancies has also been demonstrated for Cl doping of ZnO nanostructures.[367−370] F atoms are unique with regard to occupying O sites owing to their similar ionic radii (ionic radius of F^- is about 1.36 Å, while that for O^{2-} being 1.4 Å). This resultant doping led to the increment of localized charge, but the authors found that the F doping does not amount to any substantial change of plasma frequency and only results in enhancing the scattering rate as a consequence of increased grain boundary density. From their systematic growth experiments, the authors also conclude that the proportion of smaller particles decreases as the concentration of F^- increased in the reaction mixture, an observation attributed to the etching effect of the halide ions during the microcrystal growth. The authors allude to the F adsorption on specific crystal facets during growth but have not shown much experimental evidence toward the same.

The above results from Papari et al. are in good agreement with the theoretical perspective provided by Liu et al. where it was argued that F doping is not an effective means of providing free carriers at room temperature. Their DFT calculations show that F substitution for oxygen is energetically favorable for ZnO and can effectively decrease oxygen vacancies. However, interstitial doping by F can also appear at high F concentrations. The authors reason that the high transition energies for these F substituents and interstitials can lead to them acting, respectively, as deep donor and acceptor levels and cannot provide free carriers at room temperature. The authors further conjecture that the concomitant increase in carrier concentration and mobility upon F doping observed by other authors in nanocrystalline thin films[371] might then be a result of surface passivation effect of F atoms.

Apart from doping by F atoms and its effects on the electronic structure of ZnO, several authors have discussed the influence of the presence of F species in the growth solution of the nano/microcrystals. For instance, Gao et al. reported that the presence of F additives in the solvothermal synthesis of ZnO microcrystals significantly affected the resultant morphology with shapes varying from spheres to hexapods and hexagonal disks.[372] Similar observations have also been made in the case of hydrothermal synthesis by Zhang et al.[373] and Lee et al.[374]

4.3. Other Metal Oxide NCs

Besides the technologically relevant wide-band-gap metal oxides like TiO_2 and ZnO, the influence of halide ions has received moderate attention in the case of other metal oxide NCs. For instance, the halide effect has been explored in some detail for the NCs of tin(IV) oxide (SnO_2), another important wide-band-gap metal oxide.[375] In 2009, Han et al. reported a solvothermal synthesis of octahedron-shaped SnO_2 NCs exhibiting high-energy {221} facets.[376] The octahedral morphology of the NCs was attributed to the coordinative effect of both the H^+ and the Cl^- ions since the acidity of the growth solution played a major role in determining the shape of the resultant NCs. The presence of HCl affected the NC growth kinetics as it slowed down the

DOI: 10.1021/acs.chemrev.8b00158
Chem. Rev. 2018, 118, 7804−7864

hydrolysis of Sn^{4+} ions. Later in 2013 Wang et al. used sodium fluoride (NaF) as the morphology descriptor in a hydrothermal synthesis of SnO_2 nanoflowers.[375] The hierarchical nanoflowers were assembled from 2D nanosheets that expose high-energy facets, and modulation of surface energy of different facets by F adsorption was cited as the reason, as also confirmed by DFT calculations by the authors. In an earlier report, the same authors also considered the effect of F ions on the growth kinetics of these nanostructures.[377]

In an organic-phase synthesis of iron oxide NCs, Xu et al. showed that the presence of Cl^- or Br^- ions led to a cubic shape by stabilization of the {100} facets.[378] However, the role of halide ions was not properly delineated as the source of halide ions was the iron precursor itself ($FeCl_3$). Ma et al. found that different halide ions (F^-, Cl^-, Br^-, and I^-) show varying effects on the morphology of α-Fe_2O_3 hollow nanostructures grown by solvothermal synthesis.[379] The authors suggested that oriented attachment and self-assembly of initially formed particles, leading to these morphologies, are dependent on the way the specific halide ions are adsorbed on the surface of the particles. A recent (2017) synthesis of gold−iron oxide NC heterodimers indicates that the presence of chloride ions enabled the nucleation and growth of iron oxide domains on top of the preformed Au nanoparticles at temperatures much lower than those in their absence.[380]

In a study on copper-assisted size and shape control of In_2O_3 NCs, Selishcheva et al. found that when chloride ions were present in large concentrations (for example, when using both $CuCl_2$ and $InCl_3$) elongated In_2O_3 NCs were formed. Cu^+ ions were considered the main species adsorbing to the surface of the particles.[381] However, Cl^- ions were found to affect the reactivity of In^{3+} and Cu^+ ions in solution and therefore played an important role in regulating the final morphology of the particles. Prior to that, in 2011, Wang et al. found that the presence of Cl^- ions in the growth mixture of colloidal tin-doped indium oxide (ITO) NCs was responsible for the coalescence of growing NCs into nanoflower clusters.[382] It was hypothesized that the Cl^- ions being present on the surface of the NCs led to the dissolution and subsequent fusion of the nanocrystalline domains that are formed in the early stages of growth. Recently (2017), the incorporation of F^- doping in Sn:In_2O_3 NCs has been shown to yield highly faceted cubic morphology.[383]

From the discussion in the above sections it is apparent that halide ions for metal oxide NCs have been mostly exploited as size- and shape-directing agents and not in postsynthesis surface functionalization as such. Some examples in Cu_2O NCs also fit that description.[384,385] However, the role of halide ions in metal oxide NCs is not always easy to delineate since most syntheses of these NCs start with a metal halide precursor or employ a hydrohalic acid for pH adjustment. For a more robust exploration of the influence of halide ions in the case of metal oxide NCs, halide-free synthesis techniques should be a useful alternative, as have been developed for many metal oxide systems.[386,387]

Iodide ions can have a strong influence on the reactivity of metal oxide surfaces when absorbed on such surfaces as they can act as hole scavengers. A typical material that is intensively studied is titanium dioxide.[388−390] Another example is provided by Kim et al. on layered oxide semiconductors,[391] for which surface-bound iodide ions again can act as hole acceptors under band-gap excitation. There are also reports on metal oxide nanoparticles in conjunction with iodide ions as hole scavengers, see for example refs 392−394.

5. METAL HALIDE NANOCRYSTALS

Metal halide NCs require a different approach since the impact that halide ions induce in these NCs go way beyond their general surface activity as exemplified in other NC core compositions discussed so far. Being part of the NC core offers another level of tunability: that of optoelectronic characteristics simply through the changes in the halide composition of these NCs. The significant contribution of halide orbitals to the frontier orbitals in such compounds gives rise to this spectral tunability, and the following sections will exemplify this phenomenon in various classes of metal halide NCs.

5.1. Silver Halide NCs: From Photography to NC Growth

Silver halides have been extensively studied, especially in connection to their use in photographic emulsions,[395,396] due to their tendency to darken under light, following the formation of Ag domains upon photoreduction of Ag^+ ions. More recently, silver halides have found applications in various other fields, for example, as antimicrobial agents,[397] as photocatalysts,[398] and as fibers for mid-infrared spectrometric analysis.[399] Control over the size, shape, and composition of AgX microparticles has been an intensively explored area of research in the past, driven mainly by the photographic industry, since these parameters affect strongly the quality and sensitivity of the photographic films.[400] For example, the sensitivity of the film is proportional to the volume of the AgX grain: the larger the grain, the higher the sensitivity, although this holds up to a given grain size. Also, grain sizes around 0.3 μm scatter light strongly, and this in an unwanted effect as it decreases the sharpness of the image. The sensitivity is also dependent on the halide composition, with highest sensitivity reached using AgBr−AgI mixed crystals having a content of iodine in the 2−15% range,[400] but at the same time the iodide ions must be located inside the bulk of the crystals and not on the surface; otherwise, the sensitivity is again lowered. A wide range of synthesis methods and of formulations have been developed to prepare emulsions containing silver halides to be used as photographic materials. Such an extensive work has contributed greatly to understanding the parameters affecting the solubility of silver halides in various environments and the mechanisms of growth of AgX particles (for instance, how this is dependent on temperature, pH, and the presence of various complexing agents). With the advent of color photography, methods to control the shape of silver halide particles emerged. Since the color effect arises from the presence of sensitizing dyes adsorbed to the surface of the AgX crystals, particles with large surface-to-volume ratios were preferred in order to maximize the number of dyes adsorbed. Tabular grains became therefore widespread, and the mechanism of their growth (due to the formation of stacking faults on {111} facets) was studied in detail, together with the identification of the most suitable aspect ratios that needed to be attained to achieve optimal sensitization, considering also limits in the diffusion range of the photoelectrons and the overall mechanical instability of large tabular crystals.[400] The overall importance of these studies for colloidal nanoscience is that they have helped to shed light on the factors affecting the growth of colloidal particles and to strengthen the connection between theoretical models of nucleation and growth on one side and experimental results on the other.

Various approaches have been published in the past for the synthesis of AgX nanoparticles, a popular one being the use of microemulsions, especially if a good control over the size and size distribution of the particles is desired.[79,401−405] In the case

DOI: 10.1021/acs.chemrev.8b00158
Chem. Rev. 2018, 118, 7804−7864

of silver iodide, it was noticed that one-dimensional nanostructures (rods, wires) were formed at $[I^-]/[Ag+]$ precursor ratios significantly higher than 1:1.[401] This result was explained as due to competition between the nucleation of AgX particles and the formation of various complexes involving Ag^+ and I^- ions in solution. High $[I^-]/[Ag+]$ precursor ratios favor the formation of these stable complexes and tend to suppress the nucleation of AgI particles. The few nuclei formed are more constrained to grow following the tubular micellar template; hence, they evolve into rod or wire morphologies.[401] Another interesting way to control the size and composition of silver halide NCs, especially if ternary silver alloy NCs (for example, $AgCl_xBr_{1-x}$) are desired, is by carrying out the synthesis in solvents with high viscosity, such as ethylene glycol.[79] In fact, the halide composition of the ternary silver halide NCs was found to determine their shape.[406] The iodide-rich NCs were found to exhibit more twin defects, and the morphology evolved from cubic, bound by {100} facets, to hexagonal with {111} being the top and the bottom facets. The I^- ions were concluded to have higher affinity for the latter facets and hence stabilized them when present in larger quantities.

5.2. Halide Perovskite NCs: Tunable Emission through Fast Anion Exchange

Halide perovskites have recently come in the spotlight for record high efficiencies in solar cells.[78,407,408] These are compounds with AMX_3 composition (A and M are cations, X is Cl, Br, or I) and crystallize in the cubic-type perovskite lattice or in a lower symmetry lattice, isostructural to oxide perovskites. These structures are characterized by a 3-dimensional (3D) interconnection of their $[MX_6]^{4-}$ octahedra, with the A-site cation residing in the large voids in between. Many other structural and compositional variations to these archetypal materials have been the subject of intense investigation, including structures in which the octahedra are connected in 1D or 2D networks. However, the most intriguing characteristic of halide perovskites is tunability of their optoelectronic properties by varying their halide composition. Correspondingly, the other atomic constituents can also be chosen from a wide range of chemical elements. Consequently, the overall structural and compositional variety of perovskite (or perovskite-related) compounds that can be obtained is enormous (and so are their chemical and physical properties) and is not yet entirely explored. For example, research has been extended even to structures represented by arrays of disconnected units made of individual $[MX_6]^{4-}$ octahedra or $[M_2X_9]^{3-}$ dimers of octahedra[409] as well as to oxyhalides[410] and chalcohalides.[411]

Fueled by the surging interest in these materials, hybrid organic–inorganic and all-inorganic metal halide perovskite NCs have been developed and proposed as new contenders for optoelectronic applications,[75,412,413] due to their high efficiency in light emission, low energy threshold for lasing when the particles are organized in films, and ease of processability. Unlike other colloidal NCs that are relevant to optoelectronic applications (CdE, PbE NCs discussed above), all-inorganic $CsPbX_3$ NCs are defect-tolerant nanomaterials which exhibit highly efficient optical properties even in the presence of surface defects, a characteristic attributed to their unique electronic band structure.

It is beyond the scope of this review to cover such a vast topic on halide perovskite NCs and related materials. Instead, the reader can refer to the many reviews and perspective articles that have been published on the topic so far.[75,78,412,414] Here, we will only outline the most important roles played by halide ions in these materials and again direct the reader to more in-depth studies in each case.

5.2.1. Halide-Dependent Optical Properties and Fast Anion Exchange in Halide Perovskite NCs. A first important aspect is related to the modulation in the optical properties based on halide composition. Both organic–inorganic and all-inorganic halide perovskites can be prepared with different halide stoichiometries, with the consequence that their band gap is easily tunable through a broad spectral range,[415] starting from the high-band-gap chloride perovskites to the low-band-gap iodide ones. The documented evidence that halide ions are mobile in these materials[416] together with the presence of a high density of halide vacancies explains the ease by which halide perovskites can undergo partial or complete anion exchange (Figure 35a), even by mere exposure to hydrohalic acids.[417−420] A recent study by Koscher et al. has shed some light on anion-exchange transformations in perovskite NCs (Figure 35b).[421] For example, starting from $CsPbBr_3$ NCs, the exchange of Br^- with I^- ions is fast, most likely because I^- ions form weaker bonds than Br^- ions with Pb^{2+}, and the NCs form intermediate alloy structures. On the other hand, the

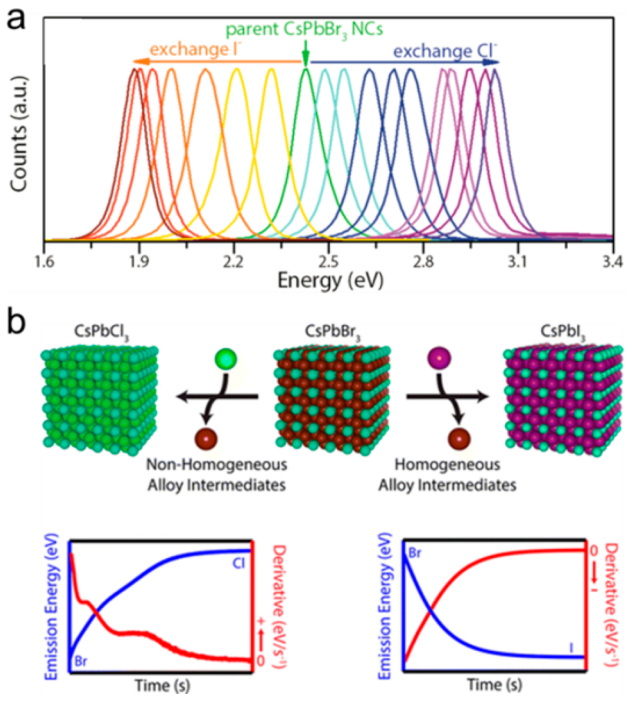

Figure 35. Anion-exchange reactions in halide perovskite NCs. (a) Fast anion exchange on $CsPbBr_3$ NCs leads to mixed halide NCs and then either to pure $CsPbCl_3$ or $CsPbI_3$ NCs. Hence, starting from a single sample of NCs emitting in the green region of the spectrum, NCs emitting in any region of the visible spectrum can be prepared. Reproduced from ref 419. Copyright 2015 American Chemical Society. (b) Anion exchange with iodine in $CsPbBr_3$ NCs is surface-reaction limited: once the I^- ions enter the NCs, all anionic sites inside the NC can be equally exchanged. Partially exchanged NCs have a homogeneous alloy phase, as evident also from the optical spectra. Cl^- ions instead have limited mobility in the NCs, so that exchange proceeds through intermediate stages in which the NCs have regions of chloride-rich or iodide-rich composition. Consequently, variations in the optical absorption and emission spectra are less smooth than in the iodide-exchange case. Reproduced from ref 421. Copyright 2016 American Chemical Society.

DOI: 10.1021/acs.chemrev.8b00158
Chem. Rev. 2018, 118, 7804−7864

exchange with Cl^- ions is slower. This is explained considering that Cl^- ions form stronger bonds than those of Br^- ions with Pb^{2+}; therefore, they are slow diffusers. Also, partial exchange with Cl^- ions produces regions of different halide compositions within an individual NC. Partial anion exchange on halide perovskite nanowires, through a lithographic approach, has recently been shown to deliver individual nanowires with elaborate patterns of segments having different halide compositions, hence different emission colors.[422] These transformations in nanowires are exemplary as they demonstrate that anion diffusion and exchange in the perovskite lattice, at least in the case of nanowires, is apparently anisotropic: the halide ions do not seem to be able to diffuse from the unmasked regions to the masked regions of the wire and replace the halide ions present in the latter regions.

5.2.2. Improved Stability and Optical Properties in Halide-Rich Perovskite NCs. Various recent works have investigated how the growth conditions, especially if these are halide rich or halide poor, can impact on the overall optical properties of the resulting perovskite bulk crystals and NCs. For instance, Kang et al. calculated that in the case of $CsPbBr_3$ moderate or Br-poor conditions can reduce the density of defects in this material with beneficial effects for the optical properties.[423] On the other hand, various experimental works on perovskite NCs have shown that halide-rich conditions lead to NCs that are more stable and of higher optical quality. A recent report from Jeong's group describes an effective passivation strategy of $CsPbX_3$ NCs by introducing metal halides on the NC surfaces through an in situ synthesis.[424] The authors used metal bromides (e.g., $ZnBr_2$, $InBr_3$, $CuBr_2$, etc.) or metal iodides (e.g., ZnI_2) as an additional source of halide ions in the synthesis of $CsPbBr_3$ and $CsPbI_3$ NCs. These salts were introduced in the reaction mixture during the standard NC synthesis procedure, based on the report by Protesescu et al.[425] The improved structural stability of the resulting NCs (which translated into stable physicochemical properties in ambient conditions) was ascribed to a halide-rich (actually, lead-halide-rich) surface, as revealed by XPS analysis. Also, perovskite NCs prepared according to the standard synthesis of Protesescu et al. had a propensity to undergo lateral fusion upon aging, which was prevented by such halide passivation. This translated into an increased retention of the PL quantum yield of the halide-passivated NCs. Similar to their earlier work on PbSe NCs described above,[69] the authors attributed this improved stability to the formation of a lead bromide adlayer on the surfaces of the NCs and/or native lead bromide surface termination that was facilitated by the presence of species like $ZnBr_2$ which altered growth conditions. Later, Di Stasio et al. used a similar passivation strategy, albeit postsynthetic in nature, using lead bromide treatment on $CsPbBr_3$ NC solid state films to obtain near-unity PLQY.[426] Another possible reason for the improvement in PLQY and stability in halide-rich perovskites is that they should have a low concentration of halide vacancies. Depending on the type of materials, these vacancies should form trap states that are shallow or deeper. For example, in cubic $MAPbX_3$, iodine vacancies are shallower than bromine and chlorine ones.[427] In any case, such trap states would cause a decrease in the radiative recombination efficiency.

Another synthetic route by which it is possible to tune the composition of the $CsPbX_3$ NCs is the so-called "three precursors" approach. It consists in the dissolution of Cs^+ and Pb^{2+} cations in fatty acids, after which an alkylammonium halide salt is introduced.[428] Li et al. used this procedure to prepare $CsPBX_3$ NCs for use in lighting and display applications.[429] Working under Br-rich conditions, they found (by XPS analysis) that Br-rich surfaces (with Br:Pb ratios around 3.6−3.7:1, that is, higher than the 3:1 stoichiometric ratio) led to higher PLQYs. This was explained as due to a surface passivation of the $CsPbBr_3$ NCs by a $PbBr_x$ shell characterized by a higher band gap, similar to the traditional CdSe/ZnS core/shell NC case.

Following a similar goal of controlling the surface composition, Imran et al. devised a new synthesis approach based on benzoyl halides as halide precursors.[430] These are injected into a solution of metal cations and ligands (oleylamine and oleic acid). Benzoyl halides are highly reactive chemicals, and their introduction in the reaction environment immediately starts the nucleation and the growth of metal halide NCs. With this method either all-inorganic or organic−inorganic, phase-pure $APbX_3$ (A = Cs, MA or FA and X = Cl, Br or I) NCs with control over the size distribution could be grown. By dosing the amount of benzoyl halides added (hence the concentration of halide ions) it was possible to synthesize NCs with a surface rich in halide ions, which again translated into higher optical properties, phase stability, and also higher phase purity compared to the more standard synthesis approached to perovskite NCs. On a broader perspective, much work in underway in various groups to understand the type of surface termination and ligand passivation of halide perovskite NCs depending on the synthesis conditions and how this influences the optical quality and overall stability of the NCs.[431]

5.2.3. Visible-Light-Induced Anion Phase Segregation in Mixed-Halide Perovskites. This effect has been systematically observed and discussed extensively in films of hybrid methylammonium halide perovskites with mixed Br/I composition ($MAPb(I_{1-x}Br_x)_3$) and consists in the segregation, driven by light, of iodide ions in low-band-gap domains that are iodide rich and high-band-gap domains that are bromide rich, an effect that is detrimental for solar cells.[432−434] This is again a consequence of the high ionic mobility in these materials. Mixed-halide perovskite NCs can also be prepared routinely by direct synthesis or by postsynthesis anions exchange, as discussed previously. It is not clear, to date, how light-induced anion segregation operates in the corresponding mixed-halide NCs. Lignos et al. synthesized formamidinium lead halide perovskite NCs using a microfluidic approach and found that $FAPb(Cl_{1-x}Br_x)_3$ NCs with a chloride content over 40% were unstable and rapidly decomposed into nonemitting $FAPbCl_3$ NCs and Br-rich $FAPb(Cl/Br)_3$ NCs.[435] While it was not clarified by the authors whether this was a direct consequence of irradiation by visible light, the observed effect was most likely recorded under irradiation conditions.[435]

6. OUTLOOK

In this review, we have given an account of the many roles played by halide ions in the synthesis and postsynthesis processing of NCs. As synthesis methods of nanoscale materials develop further and their implementation in devices becomes more standardized, some important developments are foreseen. First, a more detailed understanding of the interaction of halide ions with the surface of NCs is required. Halides hardly interact with the surface as naked ions but rather in synergy with the ligand molecules already present on the surface and/or with other molecules from the growth medium. Understanding the mechanisms of these interactions and their influence on surface stability and electronic properties of the particles will require extensive experimental investigations and computational

DOI: 10.1021/acs.chemrev.8b00158
Chem. Rev. 2018, 118, 7804−7864

modeling. Perhaps one can say that this type of investigation has reached maturity for some classes of materials, mainly the noble metals, simply because they have been studied for many years. In comparison, semiconductor NCs remain much less explored. Given the dramatic effects that even trace amounts of halide species can have not only on the synthesis of semiconductor NCs but also on their optoelectronic and electrical properties, many efforts need to be devoted in this direction. This will be especially true in the case of two-dimensional materials, which are so either because of their layered structure or simply because they can prepared in nanosheet or nanoplatelet shapes. A remarkable example was given in this review for the case of PbSe nanosheets. Overall, however, it remains to be seen whether over time the community will be able to elaborate a comprehensive and predictive scheme of the role of various chemical species or, more broadly speaking, of the reactions conditions in the kinetics and thermodynamics of growth of nanomaterials. To date, achieving a specific size and shape for a given namomaterial is still rather an art than a consolidated science, and models for size and shape evolution are still being intensively developed.[436]

Halides are an important constituent of halide perovskites, which have come under the spotlight recently as promising materials in photovoltaics and light-emitting devices, as discussed in the previous section. Such surge of interest in halide perovskites has sparked research in studying phenomena such as halide ion diffusion and exchange and their role in the optoelectronic properties and stability of this important class of compounds. Reports on perovskite NCs and their postsynthesis transformations have followed suit. Both fundamental and practical problems arise when interfacing halide perovskites (both as thin films of micrometer size crystals or NCs and as bulk single crystals) with other materials in devices: for example, one needs to understand the electronic structure and alignment of levels at such interfaces, which calls for a fine study of the structural and compositional nature of these interfaces. Metal oxides and inorganic semiconductors have rather rigid lattices, whereas halide perovskites, especially those incorporating alkylammonium ions, have much softer lattices, characterized by intense vibrational dynamics. This raises a question on whether there can be a stable epitaxial interface between a soft and a rigid lattice, which boils down to how such interface can be realized, and this is where the investigation of the interaction of halide ions with the surfaces of traditional inorganic materials kicks in again. Halide perovskites with different halide compositions have markedly different stabilities in terms of both structure and reactivity toward various external agents, and halide ion segregation can occur under various circumstances. As we speak, the reasons underlying these phenomena are not sorted out entirely. Nevertheless, efforts on interfacing halide perovskite NCs with different inorganic materials are proceeding at a sustained pace.[437,438]

An extreme case of nanomaterials grown in a halide-rich environment is represented by the synthesis approaches using salt melts as media. For example, Lei et al. in 2011 synthesized boron carbide nanostructures in a LiCl/KCl salt melt. This type of approach can be considered "green", and the materials that are prepared are soluble in water.[439] Also, because high temperatures can be reached in salt melts, one can envisage the synthesis and manipulations of entire classes of materials that now cannot be fabricated by solution methods given the temperature limitation of traditional chemicals used in colloidal chemistry. Another fascinating direction in the use of mixtures of molten salts characterized by low boiling points resides in the postsynthesis processing of NCs.[440] Here too, the reported salt melts are essentially metal halides. In addition, to provide a stable medium for a wide variety of nanocrystalline materials, these mixtures have been shown to be an optimal environment for curing structural defects in classes semiconductor NCs (for example, the III−V semiconductors) that would otherwise require temperatures that are too high for most organic solvents and surfactants.[441] Preliminary computational studies have shown that the solvent ions bound to the surface of the NCs give rise to oscillations in the charge density in the region of solvent surrounding the particles, and this somehow stabilizes the NCs and avoids inter-NC aggregation.[440] One can imagine that this field will expand further by the identification of reactant species that elicit various types of postsynthesis transformations in NCs.

Clearly, the use of salt melts calls for a completely new set of studies aiming at identifying new precursors species and their interactions in environment so rich in halide ions. All of these new types of NCs will have their surface passivated with halide ions, and this in turn will stimulate research in how such type of passivation will influence the stability and the electronic behavior of the NCs once removed from the molten salt medium and transferred into another environment. We have already seen that for NCs made of the archetypal type of covalent lattice, namely, silicon, halide passivation brings about severe changes in stability and electronic properties. A similar pattern should be expected for NCs of other strongly covalent materials.

Another interesting direction in the NC community is represented by the encapsulation of emitting semiconductor NCs in an alkali halide matrix to provide improved stability from exposure to heat, light, and moisture. Recent works include the synthesis of NaCl-protected CdTe and CdHgTe NCs emitting in the near-infrared.[442,443] This approach has been extensively tested on halide perovskite NCs, for instance, by encapsulating them in a potassium halide matrix or even in a matrix made of Cs_4PbX_6.[444,445] Noteworthy in this respect is the work on semiconductor quantum dots (essentially PbS) embedded in a bulk halide perovskite matrix, a film which was characterized by excellent optoelectronic properties.[446] This was traced back to the efficient conversion of carriers generated in the perovskite matrix into an exciton localized in the PbS NCs. This aspect brings us back to the open questions related to interfacing of halide perovskites and other inorganic materials mentioned earlier. In principle, different types of halide-containing shells or matrixes embedding inorganic NCs can be used to modulate the dielectric constant of the medium surrounding the NCs, providing an additional tool to tune their optical properties. This field of research is at its beginning, and we foresee many interesting developments in the coming years.

AUTHOR INFORMATION

Corresponding Authors

*E-mail: sandeep.ghosh@utexas.edu.
*E-mail: liberato.manna@iit.it.

ORCID

Sandeep Ghosh: 0000-0002-1149-9199
Liberato Manna: 0000-0003-4386-7985

Notes

The authors declare no competing financial interest.

DOI: 10.1021/acs.chemrev.8b00158
Chem. Rev. 2018, 118, 7804−7864

Biographies

Sandeep Ghosh is a postdoctoral researcher in Delia Milliron's group in the McKetta Department of Chemical Engineering in the University of Texas (UT) at Austin, TX, since February 2017. Prior to joining UT, he was a postdoctoral researcher in the Istituto Italiano di Tecnologia Genoa, Italy, from 2012 to 2016 under the mentorship of Liberato Manna, where he researched colloidal inorganic nanocrystals and their growth, transformation, and surface characteristics. He received his B.Sc. degree (2004) in Chemistry from Jadavpur University, Kolkata, and his M.S. (2007) and Ph.D. (2011) degrees in Chemistry from the Indian Institute of Science (IISc), Bangalore, India. A one year internship stint in 2009 with Izumi Ichinose in the National Institute for Materials Science (NIMS), Tsukuba, Japan, comprises part of his Ph.D. studies, where his research was focused on ultrathin polymeric membranes for water filtration. His research interests include exploring colloidal semiconductor nanocrystals with regard to the correlation between their internal structure and their optoelectronic properties, with the goal of tweaking the underlying chemistry to arrive at smart functional nanomaterials.

Liberato Manna received his Ph.D. degree in Chemistry in 2001 from the University of Bari (Italy) and worked at UC Berkeley (USA) as a Visiting Student and subsequently at the Lawrence Berkeley Lab (USA) as a postdoctoral fellow until 2003. He was then Scientist at the National Nanotechnology Lab in Lecce (Italy), and he moved to the Istituto Italiano di Tecnologia (IIT), Genova (Italy), in 2009 as Director of the Nanochemistry Department. He has also been part-time professor at TU Delft (The Netherlands) and at the University of Genova (Italy). Currently, he is also Deputy Director of IIT for the Materials and Nanotechnology programs. His research interests include the synthesis and assembly of colloidal nanocrystals, the study of structural, chemical, and surface transformations in nanoscale materials, and their applications in energy, photonics, and electronics.

ACKNOWLEDGMENTS

The research leading to these results has received funding from the seventh European Community Framework Programme under Grant Agreement No. 614897 (ERC Consolidator Grant "TRANS-NANO") and framework programme for research and Innovation Horizon 2020 (2014−2020) under the Marie Skłodowska-Curie Grant Agreement COMPASS No. 691185. The authors gratefully acknowledge critical reading of the manuscript by Brian A. Korgel (UT Austin).

REFERENCES

(1) Kovalenko, M. V.; Manna, L.; Cabot, A.; Hens, Z.; Talapin, D. V.; Kagan, C. R.; Klimov, V. I.; Rogach, A. L.; Reiss, P.; Milliron, D. J.; Guyot-Sionnnest, P.; Konstantatos, G.; Parak, W. J.; Hyeon, T.; Korgel, B. A.; Murray, C. B.; Heiss, W. Prospects of Nanoscience with Nanocrystals. *ACS Nano* **2015**, *9*, 1012−1057.

(2) Murray, C. B.; Norris, D. J.; Bawendi, M. G. Synthesis and characterization of nearly monodisperse CdE (E = sulfur, selenium, tellurium) semiconductor nanocrystallites. *J. Am. Chem. Soc.* **1993**, *115*, 8706−8715.

(3) Han, S.-K.; Gu, C.; Zhao, S.; Xu, S.; Gong, M.; Li, Z.; Yu, S.-H. Precursor Triggering Synthesis of Self-Coupled Sulfide Polymorphs with Enhanced Photoelectrochemical Properties. *J. Am. Chem. Soc.* **2016**, *138*, 12913−12919.

(4) Buck, M. R.; Bondi, J. F.; Schaak, R. E. A total-synthesis framework for the construction of high-order colloidal hybrid nanoparticles. *Nat. Chem.* **2012**, *4*, 37−44.

(5) Deka, S.; Miszta, K.; Dorfs, D.; Genovese, A.; Bertoni, G.; Manna, L. Octapod-Shaped Colloidal Nanocrystals of Cadmium Chalcogenides via "One-Pot" Cation Exchange and Seeded Growth. *Nano Lett.* **2010**, *10*, 3770−3776.

(6) Cushing, B. L.; Kolesnichenko, V. L.; O'Connor, C. J. Recent Advances in the Liquid-Phase Syntheses of Inorganic Nanoparticles. *Chem. Rev.* **2004**, *104*, 3893−3946.

(7) Tang, J.; Kemp, K. W.; Hoogland, S.; Jeong, K. S.; Liu, H.; Levina, L.; Furukawa, M.; Wang, X.; Debnath, R.; Cha, D.; Chou, K. W.; Fischer, A.; Amassian, A.; Asbury, J. B.; Sargent, E. H. Colloidal-quantum-dot photovoltaics using atomic-ligand passivation. *Nat. Mater.* **2011**, *10*, 765−771.

(8) De Roo, J.; Van den Broeck, F.; De Keukeleere, K.; Martins, J. C.; Van Driessche, I.; Hens, Z. Unravelling the Surface Chemistry of Metal Oxide Nanocrystals, the Role of Acids and Bases. *J. Am. Chem. Soc.* **2014**, *136*, 9650−9657.

(9) Kim, K.; Yoo, D.; Choi, H.; Tamang, S.; Ko, J.-H.; Kim, S.; Kim, Y.-H.; Jeong, S. Halide−Amine Co-Passivated Indium Phosphide Colloidal Quantum Dots in Tetrahedral Shape. *Angew. Chem.* **2016**, *128*, 3778−3782.

(10) Smith, D. K.; Miller, N. R.; Korgel, B. A. Iodide in CTAB Prevents Gold Nanorod Formation. *Langmuir* **2009**, *25*, 9518−9524.

(11) Kim, M. R.; Miszta, K.; Povia, M.; Brescia, R.; Christodoulou, S.; Prato, M.; Marras, S.; Manna, L. Influence of Chloride Ions on the Synthesis of Colloidal Branched CdSe/CdS Nanocrystals by Seeded Growth. *ACS Nano* **2012**, *6*, 11088−11096.

(12) Juarez, B. H. The Role of Halogens in the Synthesis of Semiconductor Nanocrystals. *Z. Phys. Chem.* **2015**, *229*, 119.

(13) Lohse, S. E.; Burrows, N. D.; Scarabelli, L.; Liz-Marzán, L. M.; Murphy, C. J. Anisotropic Noble Metal Nanocrystal Growth: The Role of Halides. *Chem. Mater.* **2014**, *26*, 34−43.

(14) Andersen, T. N.; Bockris, J. O. M. Forces involved in the "specific" adsorption of ions on metals from aqueous solution. *Electrochim. Acta* **1964**, *9*, 347−371.

(15) Habib, M. A.; Bockris, J. O. M. Specific Adsorption of Ions. In *Comprehensive Treatise of Electrochemistry: The Double Layer*, Bockris, J. O. M., Conway, B. E., Yeager, E., Eds.; Springer US: Boston, MA, 1980; pp 135−219.

(16) Magnussen, O. M.; Ocko, B. M.; Wang, J. X.; Adzic, R. R. In-Situ X-ray Diffraction and STM Studies of Bromide Adsorption on Au(111) Electrodes. *J. Phys. Chem.* **1996**, *100*, 5500−5508.

(17) Magnussen, O. M. Ordered Anion Adlayers on Metal Electrode Surfaces. *Chem. Rev.* **2002**, *102*, 679−726.

(18) Magnussen, O. M.; Ocko, B. M.; Adzic, R. R.; Wang, J. X. X-ray diffraction studies of ordered chloride and bromide monolayers at the Au(111)-solution interface. *Phys. Rev. B: Condens. Matter Mater. Phys.* **1995**, *51*, 5510−5513.

(19) Despić, A. R. Deposition and Dissolution of Metals and Alloys. Part B: Mechanisms, Kinetics, Texture, and Morphology. In *Comprehensive Treatise of Electrochemistry: Vol. 7 Kinetics and Mechanisms of Electrode Processes*, Conway, B. E., Bockris, J. O. M., Yeager, E., Khan, S. U. M., White, R. E., Eds.; Springer US: Boston, MA, 1983; pp 451−528.

(20) Schimpf, J. A.; McBride, J. R.; Soriaga, M. P. Adsorbate-catalyzed layer-by-layer metal dissolution in halide-free solutions: Pd(111) ($\sqrt{3}\times\sqrt{3}$)R30°-I. *J. Phys. Chem.* **1993**, *97*, 10518−10520.

(21) Adžić, R. R.; Wang, J. X. Structure and inhibition effects of anion adlayers during the course of O_2 reduction. *Electrochim. Acta* **2000**, *45*, 4203−4210.

(22) Marković, N. M.; Gasteiger, H. A.; Grgur, B. N.; Ross, P. N. Oxygen reduction reaction on Pt(111): effects of bromide. *J. Electroanal. Chem.* **1999**, *467*, 157−163.

(23) Ruda, H. E. Reactions on Semiconductor Surfaces. *Science* **1999**, *283*, 646−647.

(24) Seker, F.; Meeker, K.; Kuech, T. F.; Ellis, A. B. Surface Chemistry of Prototypical Bulk II−VI and III−V Semiconductors and Implications for Chemical Sensing. *Chem. Rev.* **2000**, *100*, 2505−2536.

(25) Simpson, W. C.; Yarmoff, J. A. Fundamental Studies of Halogen Reactions With III-V Semiconductor Surfaces. *Annu. Rev. Phys. Chem.* **1996**, *47*, 527−554.

DOI: 10.1021/acs.chemrev.8b00158
Chem. Rev. 2018, 118, 7804−7864

(26) Strehlow, W. H. Chemical Polishing of II-VI Compounds. *J. Appl. Phys.* **1969**, *40*, 2928−2932.
(27) Hodes, G.; Manassen, J.; Cahen, D. Effect of Surface Etching and Morphology on the Stability of CdSe/S_x^{2-} Photoelectrochemical Cells. *J. Electrochem. Soc.* **1981**, *128*, 2325−2330.
(28) Hickman, J. J.; Wrighton, M. S. Face-specific interactions of anionic sulfur donors with oriented crystals of (0001) CdX (X = selenium, sulfur) and correlation with electrochemical properties. *J. Am. Chem. Soc.* **1991**, *113*, 4440−4448.
(29) Komisarchik, M. S.; Prokator, L. M.; Orlov, Y. F. Mechanism of the etching of Cadmium Selenide in an alcoholic solution of bromine. *Inorg. Mater.* **1984**, *20*, 16−19.
(30) Liu, Y.; Komrowski, A. J.; Kummel, A. C. Site-Selective Reaction of Br_2 with Second Layer Ga Atoms on the As-rich GaAs(001)-2 × 4 Surface. *Phys. Rev. Lett.* **1998**, *81*, 413−416.
(31) Srivastava, G. P. Theory of semiconductor surface reconstruction. *Rep. Prog. Phys.* **1997**, *60*, 561−613.
(32) Van Vechten, J. A. A simple man's view of the passivation of semiconductors. *Corros. Sci.* **1990**, *31*, 39−52.
(33) Boles, M. A.; Ling, D.; Hyeon, T.; Talapin, D. V. The surface science of nanocrystals. *Nat. Mater.* **2016**, *15*, 141−153.
(34) McLean, J. G.; Kruse, P.; Guo-Ping, J.; Ruda, H. E.; Kummel, A. C. Anomalous Mobility of Strongly Bound Surface Species: Cl on GaAs(001)-c(8 × 2). *Phys. Rev. Lett.* **2000**, *85*, 1488−1491.
(35) Jensen, J. A.; Yan, C.; Kummel, A. C. Direct Chemisorption Site Selectivity for Molecular Halogens on the Si(111)- (7 × 7) Surface. *Phys. Rev. Lett.* **1996**, *76*, 1388−1391.
(36) Wang, W. K.; Simpson, W. C.; Yarmoff, J. A. Passivation versus Etching: Adsorption of I_2 on InAs(001). *Phys. Rev. Lett.* **1998**, *81*, 1465−1468.
(37) Pearson, R. G. Hard and soft acids and bases, HSAB, part 1: Fundamental principles. *J. Chem. Educ.* **1968**, *45*, 581−587.
(38) Pearson, R. G. Hard and soft acids and bases, HSAB, part II: Underlying theories. *J. Chem. Educ.* **1968**, *45*, 643−648.
(39) Owen, J. The coordination chemistry of nanocrystal surfaces. *Science* **2015**, *347*, 615−616.
(40) Mourdikoudis, S.; Liz-Marzán, L. M. Oleylamine in Nanoparticle Synthesis. *Chem. Mater.* **2013**, *25*, 1465−1476.
(41) LaMer, V. K.; Dinegar, R. H. Theory, Production and Mechanism of Formation of Monodispersed Hydrosols. *J. Am. Chem. Soc.* **1950**, *72*, 4847−4854.
(42) Ratke, L.; Voorhees, P. W. *Growth and Coarsening: Ostwald Ripening in Material Processing*; Springer, 2002.
(43) Yin, Y.; Alivisatos, A. P. Colloidal nanocrystal synthesis and the organic-inorganic interface. *Nature* **2005**, *437*, 664−670.
(44) Xia, Y.; Xia, X.; Peng, H.-C. Shape-Controlled Synthesis of Colloidal Metal Nanocrystals: Thermodynamic versus Kinetic Products. *J. Am. Chem. Soc.* **2015**, *137*, 7947−7966.
(45) Agrawal, A.; Cho, S. H.; Zandi, O.; Ghosh, S.; Johns, R. W.; Milliron, D. J. Localized Surface Plasmon Resonance in Semiconductor Nanocrystals. *Chem. Rev.* **2018**, *118*, 3121−3207.
(46) Manna, L.; Wang, L. W.; Cingolani, R.; Alivisatos, A. P. First-principles modeling of unpassivated and surfactant-passivated bulk facets of wurtzite CdSe: a model system for studying the anisotropic growth of CdSe nanocrystals. *J. Phys. Chem. B* **2005**, *109*, 6183−6192.
(47) Wang, F.; Tang, R.; Buhro, W. E. The Trouble with TOPO; Identification of Adventitious Impurities Beneficial to the Growth of Cadmium Selenide Quantum Dots, Rods, and Wires. *Nano Lett.* **2008**, *8*, 3521−3524.
(48) Wang, F.; Tang, R.; Kao, J. L. F.; Dingman, S. D.; Buhro, W. E. Spectroscopic Identification of Tri-n-octylphosphine Oxide (TOPO) Impurities and Elucidation of Their Roles in Cadmium Selenide Quantum-Wire Growth. *J. Am. Chem. Soc.* **2009**, *131*, 4983−4994.
(49) Wolcott, A.; Fitzmorris, R. C.; Muzaffery, O.; Zhang, J. Z. CdSe Quantum Rod Formation Aided By In Situ TOPO Oxidation. *Chem. Mater.* **2010**, *22*, 2814−2821.
(50) Steckel, J. S.; Yen, B. K. H.; Oertel, D. C.; Bawendi, M. G. On the Mechanism of Lead Chalcogenide Nanocrystal Formation. *J. Am. Chem. Soc.* **2006**, *128*, 13032−13033.
(51) Houtepen, A. J.; Koole, R.; Vanmaekelbergh, D.; Meeldijk, J.; Hickey, S. G. The Hidden Role of Acetate in the PbSe Nanocrystal Synthesis. *J. Am. Chem. Soc.* **2006**, *128*, 6792−6793.
(52) Franke, D.; Harris, D. K.; Chen, O.; Bruns, O. T.; Carr, J. A.; Wilson, M. W. B.; Bawendi, M. G. Continuous injection synthesis of indium arsenide quantum dots emissive in the short-wavelength infrared. *Nat. Commun.* **2016**, *7*, 12749.
(53) Xie, R.; Rutherford, M.; Peng, X. Formation of High-Quality I−III−VI Semiconductor Nanocrystals by Tuning Relative Reactivity of Cationic Precursors. *J. Am. Chem. Soc.* **2009**, *131*, 5691−5697.
(54) Zhong, H.; Lo, S. S.; Mirkovic, T.; Li, Y.; Ding, Y.; Li, Y.; Scholes, G. D. Noninjection Gram-Scale Synthesis of Monodisperse Pyramidal $CuInS_2$ Nanocrystals and Their Size-Dependent Properties. *ACS Nano* **2010**, *4*, 5253−5262.
(55) Ahmadi, M.; Pramana, S. S.; Xi, L.; Boothroyd, C.; Lam, Y. M.; Mhaisalkar, S. Evolution Pathway of CIGSe Nanocrystals for Solar Cell Applications. *J. Phys. Chem. C* **2012**, *116*, 8202−8209.
(56) Ghosh, S.; Avellini, T.; Petrelli, A.; Kriegel, I.; Gaspari, R.; Almeida, G.; Bertoni, G.; Cavalli, A.; Scotognella, F.; Pellegrino, T.; Manna, L. Colloidal $CuFeS_2$ Nanocrystals: Intermediate Fe d-Band Leads to High Photothermal Conversion Efficiency. *Chem. Mater.* **2016**, *28*, 4848−4858.
(57) Lim, J.; Bae, W. K.; Park, K. U.; zur Borg, L.; Zentel, R.; Lee, S.; Char, K. Controlled Synthesis of CdSe Tetrapods with High Morphological Uniformity by the Persistent Kinetic Growth and the Halide-Mediated Phase Transformation. *Chem. Mater.* **2013**, *25*, 1443−1449.
(58) Hu, L.; Kim, H. S.; Lee, J.-Y.; Peumans, P.; Cui, Y. Scalable Coating and Properties of Transparent, Flexible, Silver Nanowire Electrodes. *ACS Nano* **2010**, *4*, 2955−2963.
(59) Ghosh, S.; Gaspari, R.; Bertoni, G.; Spadaro, M. C.; Prato, M.; Turner, S.; Cavalli, A.; Manna, L.; Brescia, R. Pyramid-Shaped Wurtzite CdSe Nanocrystals with Inverted Polarity. *ACS Nano* **2015**, *9*, 8537−8546.
(60) Rodríguez-Fernández, J.; Pérez-Juste, J.; Mulvaney, P.; Liz-Marzán, L. M. Spatially-Directed Oxidation of Gold Nanoparticles by Au(III)−CTAB Complexes. *J. Phys. Chem. B* **2005**, *109*, 14257−14261.
(61) Schliehe, C.; Juarez, B. H.; Pelletier, M.; Jander, S.; Greshnykh, D.; Nagel, M.; Meyer, A.; Foerster, S.; Kornowski, A.; Klinke, C.; Weller, H. Ultrathin PbS sheets by two-dimensional oriented attachment. *Science* **2010**, *329*, 550−553.
(62) Wiley, B.; Herricks, T.; Sun, Y.; Xia, Y. Polyol Synthesis of Silver Nanoparticles: Use of Chloride and Oxygen to Promote the Formation of Single-Crystal, Truncated Cubes and Tetrahedrons. *Nano Lett.* **2004**, *4*, 1733−1739.
(63) Lim, B.; Jiang, M.; Tao, J.; Camargo, P. H. C.; Zhu, Y.; Xia, Y. Shape-Controlled Synthesis of Pd Nanocrystals in Aqueous Solutions. *Adv. Funct. Mater.* **2009**, *19*, 189−200.
(64) Green, M. L. H. A new approach to the formal classification of covalent compounds of the elements. *J. Organomet. Chem.* **1995**, *500*, 127−148.
(65) Green, M. L. H.; Parkin, G. Application of the Covalent Bond Classification Method for the Teaching of Inorganic Chemistry. *J. Chem. Educ.* **2014**, *91*, 807−816.
(66) Norman, Z. M.; Anderson, N. C.; Owen, J. S. Electrical Transport and Grain Growth in Solution-Cast, Chloride-Terminated Cadmium Selenide Nanocrystal Thin Films. *ACS Nano* **2014**, *8*, 7513−7521.
(67) Ip, A. H.; Thon, S. M.; Hoogland, S.; Voznyy, O.; Zhitomirsky, D.; Debnath, R.; Levina, L.; Rollny, L. R.; Carey, G. H.; Fischer, A.; Kemp, K. W.; Kramer, I. J.; Ning, Z.; Labelle, A. J.; Chou, K. W.; Amassian, A.; Sargent, E. H. Hybrid passivated colloidal quantum dot solids. *Nat. Nanotechnol.* **2012**, *7*, 577−582.
(68) Greaney, M. J.; Couderc, E.; Zhao, J.; Nail, B. A.; Mecklenburg, M.; Thornbury, W.; Osterloh, F. E.; Bradforth, S. E.; Brutchey, R. L. Controlling the Trap State Landscape of Colloidal CdSe Nanocrystals with Cadmium Halide Ligands. *Chem. Mater.* **2015**, *27*, 744−756.
(69) Woo, J. Y.; Ko, J. H.; Song, J. H.; Kim, K.; Choi, H.; Kim, Y. H.; Lee, D. C.; Jeong, S. Ultrastable PbSe nanocrystal quantum dots via in

DOI: 10.1021/acs.chemrev.8b00158
Chem. Rev. 2018, 118, 7804−7864

situ formation of atomically thin halide adlayers on PbSe(100). *J. Am. Chem. Soc.* **2014**, *136*, 8883−8886.
(70) Brown, P. R.; Kim, D.; Lunt, R. R.; Zhao, N.; Bawendi, M. G.; Grossman, J. C.; Bulović, V. Energy Level Modification in Lead Sulfide Quantum Dot Thin Films through Ligand Exchange. *ACS Nano* **2014**, *8*, 5863−5872.
(71) Zhang, H.; Jang, J.; Liu, W.; Talapin, D. V. Colloidal Nanocrystals with Inorganic Halide, Pseudohalide, and Halometallate Ligands. *ACS Nano* **2014**, *8*, 7359−7369.
(72) Zhang, J.; Gao, J.; Church, C. P.; Miller, E. M.; Luther, J. M.; Klimov, V. I.; Beard, M. C. PbSe quantum dot solar cells with more than 6% efficiency fabricated in ambient atmosphere. *Nano Lett.* **2014**, *14*, 6010−6015.
(73) Wheeler, L. M.; Neale, N. R.; Chen, T.; Kortshagen, U. R. Hypervalent surface interactions for colloidal stability and doping of silicon nanocrystals. *Nat. Commun.* **2013**, *4*, 2197.
(74) Owen, J. S.; Brus, L. E. Chemical Synthesis and Luminescence Applications of Colloidal Semiconductor Quantum Dots. *J. Am. Chem. Soc.* **2017**, *139*, 10939−10943.
(75) Akkerman, Q. A.; Raino, G.; Kovalenko, M. V.; Manna, L. Genesis, challenges and opportunities for colloidal lead halide perovskite nanocrystals. *Nat. Mater.* **2018**, *17*, 394−405.
(76) Buin, A.; Comin, R.; Xu, J.; Ip, A. H.; Sargent, E. H. Halide-Dependent Electronic Structure of Organolead Perovskite Materials. *Chem. Mater.* **2015**, *27*, 4405−4412.
(77) Ravi, V. K.; Markad, G. B.; Nag, A. Band Edge Energies and Excitonic Transition Probabilities of Colloidal $CsPbX_3$ (X = Cl, Br, I) Perovskite Nanocrystals. *ACS Energy Lett.* **2016**, *1*, 665−671.
(78) Manser, J. S.; Christians, J. A.; Kamat, P. V. Intriguing Optoelectronic Properties of Metal Halide Perovskites. *Chem. Rev.* **2016**, *116*, 12956−13008.
(79) Abeyweera, S. C.; Rasamani, K. D.; Sun, Y. Ternary Silver Halide Nanocrystals. *Acc. Chem. Res.* **2017**, *50*, 1754−1761.
(80) Chen, M.; Wu, B.; Yang, J.; Zheng, N. Small Adsorbate-Assisted Shape Control of Pd and Pt Nanocrystals. *Adv. Mater.* **2012**, *24*, 862−879.
(81) Sau, T. K.; Rogach, A. L.; Jäckel, F.; Klar, T. A.; Feldmann, J. Properties and Applications of Colloidal Nonspherical Noble Metal Nanoparticles. *Adv. Mater.* **2010**, *22*, 1805−1825.
(82) Zhao, P.; Li, N.; Astruc, D. State of the art in gold nanoparticle synthesis. *Coord. Chem. Rev.* **2013**, *257*, 638−665.
(83) Boisselier, E.; Astruc, D. Gold nanoparticles in nanomedicine: preparations, imaging, diagnostics, therapies and toxicity. *Chem. Soc. Rev.* **2009**, *38*, 1759−1782.
(84) Saha, K.; Agasti, S. S.; Kim, C.; Li, X.; Rotello, V. M. Gold Nanoparticles in Chemical and Biological Sensing. *Chem. Rev.* **2012**, *112*, 2739−2779.
(85) Daniel, M.-C.; Astruc, D. Gold Nanoparticles: Assembly, Supramolecular Chemistry, Quantum-Size-Related Properties, and Applications toward Biology, Catalysis, and Nanotechnology. *Chem. Rev.* **2004**, *104*, 293−346.
(86) Linic, S.; Christopher, P.; Ingram, D. B. Plasmonic-metal nanostructures for efficient conversion of solar to chemical energy. *Nat. Mater.* **2011**, *10*, 911.
(87) Shankar, S. S.; Bhargava, S.; Sastry, M. Synthesis of Gold Nanospheres and Nanotriangles by the Turkevich Approach. *J. Nanosci. Nanotechnol.* **2005**, *5*, 1721−1727.
(88) Rai, A.; Singh, A.; Ahmad, A.; Sastry, M. Role of Halide Ions and Temperature on the Morphology of Biologically Synthesized Gold Nanotriangles. *Langmuir* **2006**, *22*, 736−741.
(89) Shankar, S. S.; Rai, A.; Ankamwar, B.; Singh, A.; Ahmad, A.; Sastry, M. Biological synthesis of triangular gold nanoprisms. *Nat. Mater.* **2004**, *3*, 482−488.
(90) Jana, N. R.; Gearheart, L.; Murphy, C. J. Seed-Mediated Growth Approach for Shape-Controlled Synthesis of Spheroidal and Rod-like Gold Nanoparticles Using a Surfactant Template. *Adv. Mater.* **2001**, *13*, 1389−1393.
(91) Nikoobakht, B.; El-Sayed, M. A. Preparation and Growth Mechanism of Gold Nanorods (NRs) Using Seed-Mediated Growth Method. *Chem. Mater.* **2003**, *15*, 1957−1962.
(92) Sau, T. K.; Murphy, C. J. Room Temperature, High-Yield Synthesis of Multiple Shapes of Gold Nanoparticles in Aqueous Solution. *J. Am. Chem. Soc.* **2004**, *126*, 8648−8649.
(93) Brown, K. R.; Walter, D. G.; Natan, M. J. Seeding of Colloidal Au Nanoparticle Solutions. 2. Improved Control of Particle Size and Shape. *Chem. Mater.* **2000**, *12*, 306−313.
(94) Vigderman, L.; Zubarev, E. R. High-Yield Synthesis of Gold Nanorods with Longitudinal SPR Peak Greater than 1200 nm Using Hydroquinone as a Reducing Agent. *Chem. Mater.* **2013**, *25*, 1450−1457.
(95) Smith, D. K.; Korgel, B. A. The Importance of the CTAB Surfactant on the Colloidal Seed-Mediated Synthesis of Gold Nanorods. *Langmuir* **2008**, *24*, 644−649.
(96) Ha, T. H.; Koo, H.-J.; Chung, B. H. Shape-Controlled Syntheses of Gold Nanoprisms and Nanorods Influenced by Specific Adsorption of Halide Ions. *J. Phys. Chem. C* **2007**, *111*, 1123−1130.
(97) Wang, Z. L.; Mohamed, M. B.; Link, S.; El-Sayed, M. A. Crystallographic facets and shapes of gold nanorods of different aspect ratios. *Surf. Sci.* **1999**, *440*, L809−L814.
(98) Grzelczak, M.; Sánchez-Iglesias, A.; Rodríguez-González, B.; Alvarez-Puebla, R.; Pérez-Juste, J.; Liz-Marzán, L. M. Influence of Iodide Ions on the Growth of Gold Nanorods: Tuning Tip Curvature and Surface Plasmon Resonance. *Adv. Funct. Mater.* **2008**, *18*, 3780−3786.
(99) Magid, L. J.; Han, Z.; Warr, G. G.; Cassidy, M. A.; Butler, P. D.; Hamilton, W. A. Effect of Counterion Competition on Micellar Growth Horizons for Cetyltrimethylammonium Micellar Surfaces: Electrostatics and Specific Binding. *J. Phys. Chem. B* **1997**, *101*, 7919−7927.
(100) Velegol, S. B.; Fleming, B. D.; Biggs, S.; Wanless, E. J.; Tilton, R. D. Counterion Effects on Hexadecyltrimethylammonium Surfactant Adsorption and Self-Assembly on Silica. *Langmuir* **2000**, *16*, 2548−2556.
(101) Kawasaki, H.; Nishimura, K.; Arakawa, R. Influence of the Counterions of Cetyltrimetylammonium Salts on the Surfactant Adsorption onto Gold Surfaces and the Formation of Gold Nanoparticles. *J. Phys. Chem. C* **2007**, *111*, 2683−2690.
(102) Fan, X.; Guo, Z. R.; Hong, J. M.; Zhang, Y.; Zhang, J. N.; Gu, N. Size-controlled growth of colloidal gold nanoplates and their high-purity acquisition. *Nanotechnology* **2010**, *21*, 105602.
(103) Liu; Guyot-Sionnest, P. Mechanism of Silver(I)-Assisted Growth of Gold Nanorods and Bipyramids. *J. Phys. Chem. B* **2005**, *109*, 22192−22200.
(104) Hubert, F.; Testard, F.; Spalla, O. Cetyltrimethylammonium Bromide Silver Bromide Complex as the Capping Agent of Gold Nanorods. *Langmuir* **2008**, *24*, 9219−9222.
(105) Millstone, J. E.; Wei, W.; Jones, M. R.; Yoo, H.; Mirkin, C. A. Iodide Ions Control Seed-Mediated Growth of Anisotropic Gold Nanoparticles. *Nano Lett.* **2008**, *8*, 2526−2529.
(106) Rayavarapu, R. G.; Ungureanu, C.; Krystek, P.; van Leeuwen, T. G.; Manohar, S. Iodide Impurities in Hexadecyltrimethylammonium Bromide (CTAB) Products: Lot−Lot Variations and Influence on Gold Nanorod Synthesis. *Langmuir* **2010**, *26*, 5050−5055.
(107) Zhang, J.; Langille, M. R.; Personick, M. L.; Zhang, K.; Li, S.; Mirkin, C. A. Concave Cubic Gold Nanocrystals with High-Index Facets. *J. Am. Chem. Soc.* **2010**, *132*, 14012−14014.
(108) Ming, T.; Feng, W.; Tang, Q.; Wang, F.; Sun, L.; Wang, J.; Yan, C. Growth of Tetrahexahedral Gold Nanocrystals with High-Index Facets. *J. Am. Chem. Soc.* **2009**, *131*, 16350−16351.
(109) Chung, P.-J.; Lyu, L.-M.; Huang, M. H. Seed-Mediated and Iodide-Assisted Synthesis of Gold Nanocrystals with Systematic Shape Evolution from Rhombic Dodecahedral to Octahedral Structures. *Chem. - Eur. J.* **2011**, *17*, 9746−9752.
(110) Garg, N.; Scholl, C.; Mohanty, A.; Jin, R. The Role of Bromide Ions in Seeding Growth of Au Nanorods. *Langmuir* **2010**, *26*, 10271−10276.

DOI: 10.1021/acs.chemrev.8b00158
Chem. Rev. 2018, 118, 7804−7864

(111) Wu, H.-L.; Kuo, C.-H.; Huang, M. H. Seed-Mediated Synthesis of Gold Nanocrystals with Systematic Shape Evolution from Cubic to Trisoctahedral and Rhombic Dodecahedral Structures. *Langmuir* **2010**, *26*, 12307−12313.
(112) Bullen, C.; Zijlstra, P.; Bakker, E.; Gu, M.; Raston, C. Chemical Kinetics of Gold Nanorod Growth in Aqueous CTAB Solutions. *Cryst. Growth Des.* **2011**, *11*, 3375−3380.
(113) Si, S.; Leduc, C.; Delville, M.-H.; Lounis, B. Short Gold Nanorod Growth Revisited: The Critical Role of the Bromide Counterion. *ChemPhysChem* **2012**, *13*, 193−202.
(114) Jiao, Z.; Xia, H.; Tao, X. Modulation of Localized Surface Plasmon Resonance of Nanostructured Gold Crystals by Tuning Their Tip Curvature with Assistance of Iodide and Silver(I) Ions. *J. Phys. Chem. C* **2011**, *115*, 7887−7895.
(115) Langille, M. R.; Personick, M. L.; Zhang, J.; Mirkin, C. A. Defining Rules for the Shape Evolution of Gold Nanoparticles. *J. Am. Chem. Soc.* **2012**, *134*, 14542−14554.
(116) DuChene, J. S.; Niu, W.; Abendroth, J. M.; Sun, Q.; Zhao, W.; Huo, F.; Wei, W. D. Halide Anions as Shape-Directing Agents for Obtaining High-Quality Anisotropic Gold Nanostructures. *Chem. Mater.* **2013**, *25*, 1392−1399.
(117) Chen, L.; Ji, F.; Xu, Y.; He, L.; Mi, Y.; Bao, F.; Sun, B.; Zhang, X.; Zhang, Q. High-yield seedless synthesis of triangular gold nanoplates through oxidative etching. *Nano Lett.* **2014**, *14*, 7201−7206.
(118) Ye, X.; Gao, Y.; Chen, J.; Reifsnyder, D. C.; Zheng, C.; Murray, C. B. Seeded Growth of Monodisperse Gold Nanorods Using Bromide-Free Surfactant Mixtures. *Nano Lett.* **2013**, *13*, 2163−2171.
(119) Meena, S. K.; Sulpizi, M. Understanding the microscopic origin of gold nanoparticle anisotropic growth from molecular dynamics simulations. *Langmuir* **2013**, *29*, 14954−14961.
(120) Meena, S. K.; Celiksoy, S.; Schafer, P.; Henkel, A.; Sonnichsen, C.; Sulpizi, M. The role of halide ions in the anisotropic growth of gold nanoparticles: a microscopic, atomistic perspective. *Phys. Chem. Chem. Phys.* **2016**, *18*, 13246−13254.
(121) Almora-Barrios, N.; Novell-Leruth, G.; Whiting, P.; Liz-Marzan, L. M.; Lopez, N. Theoretical description of the role of halides, silver, and surfactants on the structure of gold nanorods. *Nano Lett.* **2014**, *14*, 871−875.
(122) Murphy, C. J.; Sau, T. K.; Gole, A. M.; Orendorff, C. J.; Gao, J.; Gou, L.; Hunyadi, S. E.; Li, T. Anisotropic Metal Nanoparticles: Synthesis, Assembly, and Optical Applications. *J. Phys. Chem. B* **2005**, *109*, 13857−13870.
(123) Pal, T.; Jana, N. R.; Sau, T. K. Nucleophile induced dissolution of gold. *Corros. Sci.* **1997**, *39*, 981−986.
(124) Cheng, W.; Dong, S.; Wang, E. Iodine-Induced Gold-Nanoparticle Fusion/Fragmentation/Aggregation and Iodine-Linked Nanostructured Assemblies on a Glass Substrate. *Angew. Chem., Int. Ed.* **2003**, *42*, 449−452.
(125) Singh, S.; Pasricha, R.; Bhatta, U. M.; Satyam, P. V.; Sastry, M.; Prasad, B. L. V. Effect of halogen addition to monolayer protected gold nanoparticles. *J. Mater. Chem.* **2007**, *17*, 1614−1619.
(126) Kanehara, M.; Sakurai, J.-i.; Sugimura, H.; Teranishi, T. Room-Temperature Size Evolution of Thiol-Protected Gold Nanoparticles Assisted by Proton Acids and Halogen Anions. *J. Am. Chem. Soc.* **2009**, *131*, 1630−1631.
(127) Tsung, C.-K.; Kou, X.; Shi, Q.; Zhang, J.; Yeung, M. H.; Wang, J.; Stucky, G. D. Selective Shortening of Single-Crystalline Gold Nanorods by Mild Oxidation. *J. Am. Chem. Soc.* **2006**, *128*, 5352−5353.
(128) Zhu, Q.; Wu, J.; Zhao, J.; Ni, W. Role of Bromide in Hydrogen Peroxide Oxidation of CTAB-Stabilized Gold Nanorods in Aqueous Solutions. *Langmuir* **2015**, *31*, 4072−4077.
(129) Wang, J.; Li, Y. F.; Huang, C. Z. Identification of Iodine-Induced Morphological Transformation of Gold Nanorods. *J. Phys. Chem. C* **2008**, *112*, 11691−11695.
(130) Figuerola, A.; Franchini, I. R.; Fiore, A.; Mastria, R.; Falqui, A.; Bertoni, G.; Bals, S.; Van Tendeloo, G.; Kudera, S.; Cingolani, R.; Manna, L. End-to-End Assembly of Shape-Controlled Nanocrystals via a Nanowelding Approach Mediated by Gold Domains. *Adv. Mater.* **2009**, *21*, 550−554.
(131) Guo, Z.; Zhang, Y.; Xu, A.; Wang, M.; Huang, L.; Xu, K.; Gu, N. Layered Assemblies of Single Crystal Gold Nanoplates: Direct Room Temperature Synthesis and Mechanistic Study. *J. Phys. Chem. C* **2008**, *112*, 12638−12645.
(132) Soejima, T.; Kimizuka, N. One-Pot Room-Temperature Synthesis of Single-Crystalline Gold Nanocorolla in Water. *J. Am. Chem. Soc.* **2009**, *131*, 14407−14412.
(133) Dasog, M.; Scott, R. W. J. Understanding the Oxidative Stability of Gold Monolayer-Protected Clusters in the Presence of Halide Ions under Ambient Conditions. *Langmuir* **2007**, *23*, 3381−3387.
(134) George, C.; Dorfs, D.; Bertoni, G.; Falqui, A.; Genovese, A.; Pellegrino, T.; Roig, A.; Quarta, A.; Comparelli, R.; Curri, M. L.; Cingolani, R.; Manna, L. A Cast-Mold Approach to Iron Oxide and Pt/Iron Oxide Nanocontainers and Nanoparticles with a Reactive Concave Surface. *J. Am. Chem. Soc.* **2011**, *133*, 2205−2217.
(135) Liu, Y.; Liu, L.; Guo, R. Br^--Induced Facile Fabrication of Spongelike Gold/Amino Acid Nanocomposites and Their Applications in Surface-Enhanced Raman Scattering. *Langmuir* **2010**, *26*, 13479−13485.
(136) Zhang, Z.; Li, H.; Zhang, F.; Wu, Y.; Guo, Z.; Zhou, L.; Li, J. Investigation of Halide-Induced Aggregation of Au Nanoparticles into Spongelike Gold. *Langmuir* **2014**, *30*, 2648−2659.
(137) Stein, B.; Zopes, D.; Schmudde, M.; Schneider, R.; Mohsen, A.; Goroncy, C.; Mathur, S.; Graf, C. Kinetics of aggregation and growth processes of PEG-stabilised mono- and multivalent gold nanoparticles in highly concentrated halide solutions. *Faraday Discuss.* **2015**, *181*, 85−102.
(138) Weng, G.; Dong, X.; Li, J.; Zhao, J. Halide ions can trigger the oxidative etching of gold nanorods with the iodide ions being the most efficient. *J. Mater. Sci.* **2016**, *51*, 7678−7690.
(139) Yu, Y.; Goodfellow, B. W.; Rasch, M. R.; Bosoy, C.; Smilgies, D.-M.; Korgel, B. A. Role of Halides in the Ordered Structure Transitions of Heated Gold Nanocrystal Superlattices. *Langmuir* **2015**, *31*, 6924−6932.
(140) Zhang, Z.; Chen, Z.; Cheng, F.; Zhang, Y.; Chen, L. Iodine-mediated etching of gold nanorods for plasmonic sensing of dissolved oxygen and salt iodine. *Analyst* **2016**, *141*, 2955−2961.
(141) Desmonda, C.; Kar, S.; Tai, Y. Formation of gold nanostructures on copier paper surface for cost effective SERS active substrate − Effect of halide additives. *Appl. Surf. Sci.* **2016**, *367*, 362−369.
(142) Saa, L.; Coronado-Puchau, M.; Pavlov, V.; Liz-Marzan, L. M. Enzymatic etching of gold nanorods by horseradish peroxidase and application to blood glucose detection. *Nanoscale* **2014**, *6*, 7405−7409.
(143) Tsuji, M.; Nishio, M.; Jiang, P.; Miyamae, N.; Lim, S.; Matsumoto, K.; Ueyama, D.; Tang, X.-L. Role of chloride ions in the formation of Au@Ag core−shell nanocrystal structures by using a microwave−polyol method. *Colloids Surf., A* **2008**, *317*, 247−255.
(144) Hong, S.; Choi, Y.; Park, S. Shape Control of Ag Shell Growth on Au Nanodisks. *Chem. Mater.* **2011**, *23*, 5375−5378.
(145) Gómez-Graña, S.; Goris, B.; Altantzis, T.; Fernández-López, C.; Carbó-Argibay, E.; Guerrero-Martínez, A.; Almora-Barrios, N.; López, N.; Pastoriza-Santos, I.; Pérez-Juste, J.; Bals, S.; Van Tendeloo, G.; Liz-Marzán, L. M. Au@Ag Nanoparticles: Halides Stabilize {100} Facets. *J. Phys. Chem. Lett.* **2013**, *4*, 2209−2216.
(146) Park, K.; Drummy, L. F.; Vaia, R. A. Ag shell morphology on Au nanorod core: role of Ag precursor complex. *J. Mater. Chem.* **2011**, *21*, 15608−15618.
(147) Ahn, J.; Wang, D.; Ding, Y.; Zhang, J.; Qin, D. Site-Selective Carving and Co-Deposition: Transformation of Ag Nanocubes into Concave Nanocrystals Encased by Au−Ag Alloy Frames. *ACS Nano* **2018**, *12*, 298−307.
(148) Lee, Y. W.; Kim, M.; Kim, Z. H.; Han, S. W. One-Step Synthesis of Au@Pd Core−Shell Nanooctahedron. *J. Am. Chem. Soc.* **2009**, *131*, 17036−17037.
(149) Lu, C.-L.; Prasad, K. S.; Wu, H.-L.; Ho, J.-a. A.; Huang, M. H. Au Nanocube-Directed Fabrication of Au−Pd Core−Shell Nanocrystals with Tetrahexahedral, Concave Octahedral, and Octahedral Structures

DOI: 10.1021/acs.chemrev.8b00158
Chem. Rev. 2018, 118, 7804−7864

and Their Electrocatalytic Activity. *J. Am. Chem. Soc.* **2010**, *132*, 14546−14553.
(150) Annan, W.; Qing, P.; Yadong, L. Rod-Shaped Au−Pd Core−Shell Nanostructures. *Chem. Mater.* **2011**, *23*, 3217−3222.
(151) Xu, L.; Wang, K.; Jiang, B.; Chen, W.; Liu, F.; Hao, H.; Zou, C.; Yang, Y.; Huang, S. Competitive Effect in The Growth of Pd−Au−Pd Segmental Nanorods. *Chem. Mater.* **2016**, *28*, 7394−7403.
(152) Rodal-Cedeira, S.; Montes-García, V.; Polavarapu, L.; Solís, D. M.; Heidari, H.; La Porta, A.; Angiola, M.; Martucci, A.; Taboada, J. M.; Obelleiro, F.; Bals, S.; Pérez-Juste, J.; Pastoriza-Santos, I. Plasmonic Au@Pd Nanorods with Boosted Refractive Index Susceptibility and SERS Efficiency: A Multifunctional Platform for Hydrogen Sensing and Monitoring of Catalytic Reactions. *Chem. Mater.* **2016**, *28*, 9169−9180.
(153) Guo, J.; Zhang, Y.; Shi, L.; Zhu, Y.; Mideksa, M. F.; Hou, K.; Zhao, W.; Wang, D.; Zhao, M.; Zhang, X.; Lv, J.; Zhang, J.; Wang, X.; Tang, Z. Boosting Hot Electrons in Hetero-superstructures for Plasmon-Enhanced Catalysis. *J. Am. Chem. Soc.* **2017**, *139*, 17964−17972.
(154) Ng, K. C.; Lin, F.-C.; Yang, P.-W.; Chuang, Y.-C.; Chang, C.-K.; Yeh, A.-H.; Kuo, C.-S.; Kao, C.-R.; Liu, C.-C.; Jeng, U. S.; Huang, J.-S.; Kuo, C.-H. Fabrication of Bimetallic Au−Pd−Au Nanobricks as an Archetype of Robust Nanoplasmonic Sensors. *Chem. Mater.* **2018**, *30*, 204−213.
(155) Hsu, S.-C.; Chuang, Y.-C.; Sneed, B. T.; Cullen, D. A.; Chiu, T.-W.; Kuo, C.-H. Turning the Halide Switch in the Synthesis of Au−Pd Alloy and Core−Shell Nanoicosahedra with Terraced Shells: Performance in Electrochemical and Plasmon-Enhanced Catalysis. *Nano Lett.* **2016**, *16*, 5514−5520.
(156) Im, S. H.; Lee, Y. T.; Wiley, B.; Xia, Y. Large-Scale Synthesis of Silver Nanocubes: The Role of HCl in Promoting Cube Perfection and Monodispersity. *Angew. Chem., Int. Ed.* **2005**, *44*, 2154−2157.
(157) Wiley, B. J.; Xiong, Y.; Li, Z.-Y.; Yin, Y.; Xia, Y. Right Bipyramids of Silver: A New Shape Derived from Single Twinned Seeds. *Nano Lett.* **2006**, *6*, 765−768.
(158) Wiley, B. J.; Chen, Y.; McLellan, J. M.; Xiong, Y.; Li, Z.-Y.; Ginger, D.; Xia, Y. Synthesis and Optical Properties of Silver Nanobars and Nanorice. *Nano Lett.* **2007**, *7*, 1032−1036.
(159) Zhang, Q.; Moran, C. H.; Xia, X.; Rycenga, M.; Li, N.; Xia, Y. Synthesis of Ag Nanobars in the Presence of Single-Crystal Seeds and a Bromide Compound, and Their Surface-Enhanced Raman Scattering (SERS) Properties. *Langmuir* **2012**, *28*, 9047−9054.
(160) da Silva, R. R.; Yang, M.; Choi, S.-I.; Chi, M.; Luo, M.; Zhang, C.; Li, Z.-Y.; Camargo, P. H. C.; Ribeiro, S. J. L.; Xia, Y. Facile Synthesis of Sub-20 nm Silver Nanowires through a Bromide-Mediated Polyol Method. *ACS Nano* **2016**, *10*, 7892−7900.
(161) Ajayan, P. M.; Marks, L. D. Quasimelting and phases of small particles. *Phys. Rev. Lett.* **1988**, *60*, 585−587.
(162) Marks, L. D. Experimental studies of small particle structures. *Rep. Prog. Phys.* **1994**, *57*, 603−649.
(163) Schuette, W. M.; Buhro, W. E. Silver Chloride as a Heterogeneous Nucleant for the Growth of Silver Nanowires. *ACS Nano* **2013**, *7*, 3844−3853.
(164) Zhou, S.; Li, J.; Gilroy, K. D.; Tao, J.; Zhu, C.; Yang, X.; Sun, X.; Xia, Y. Facile Synthesis of Silver Nanocubes with Sharp Corners and Edges in an Aqueous Solution. *ACS Nano* **2016**, *10*, 9861−9870.
(165) Chang, S.; Chen, K.; Hua, Q.; Ma, Y.; Huang, W. Evidence for the Growth Mechanisms of Silver Nanocubes and Nanowires. *J. Phys. Chem. C* **2011**, *115*, 7979−7986.
(166) Li, B.; Long, R.; Zhong, X.; Bai, Y.; Zhu, Z.; Zhang, X.; Zhi, M.; He, J.; Wang, C.; Li, Z.-Y.; Xiong, Y. Investigation of Size-Dependent Plasmonic and Catalytic Properties of Metallic Nanocrystals Enabled by Size Control with HCl Oxidative Etching. *Small* **2012**, *8*, 1710−1716.
(167) Hecht, D. S.; Hu, L.; Irvin, G. Emerging Transparent Electrodes Based on Thin Films of Carbon Nanotubes, Graphene, and Metallic Nanostructures. *Adv. Mater.* **2011**, *23*, 1482−1513.
(168) Lee, E.-J.; Chang, M.-H.; Kim, Y.-S.; Kim, J.-Y. High-pressure polyol synthesis of ultrathin silver nanowires: Electrical and optical properties. *APL Mater.* **2013**, *1*, 042118.
(169) Li, B.; Ye, S.; Stewart, I. E.; Alvarez, S.; Wiley, B. J. Synthesis and Purification of Silver Nanowires To Make Conducting Films with a Transmittance of 99%. *Nano Lett.* **2015**, *15*, 6722−6726.
(170) Gou, L.; Chipara, M.; Zaleski, J. M. Convenient, Rapid Synthesis of Ag Nanowires. *Chem. Mater.* **2007**, *19*, 1755−1760.
(171) Foresti, M. L.; Innocenti, M.; Kobayashi, H.; Pezzatini, G.; Guidelli, R. Bromide electrosorption on the low-index faces of silver. *J. Chem. Soc., Faraday Trans.* **1996**, *92*, 3747−3756.
(172) Liu, S.; Yue, J.; Gedanken, A. Synthesis of Long Silver Nanowires from AgBr Nanocrystals. *Adv. Mater.* **2001**, *13*, 656−658.
(173) Kim, M. H.; Kwak, S. K.; Im, S. H.; Lee, J.-B.; Choi, K.-Y.; Byun, D.-J. Maneuvering the growth of silver nanoplates: use of halide ions to promote vertical growth. *J. Mater. Chem. C* **2014**, *2*, 6165−6170.
(174) Zhang, J.; Liu, J.; Xie, Z.-X.; Qin, D. $HAuCl_4$: A Dual Agent for Studying the Chloride-Assisted Vertical Growth of Citrate-Free Ag Nanoplates with Au Serving as a Marker. *Langmuir* **2014**, *30*, 15520−15530.
(175) Tsuji, M.; Matsumoto, K.; Jiang, P.; Matsuo, R.; Tang, X.-L.; Kamarudin, K. S. N. Roles of Pt seeds and chloride anions in the preparation of silver nanorods and nanowires by microwave-polyol method. *Colloids Surf., A* **2008**, *316*, 266−277.
(176) Tang, X.; Tsuji, M.; Jiang, P.; Nishio, M.; Jang, S.-M.; Yoon, S.-H. Rapid and high-yield synthesis of silver nanowires using air-assisted polyol method with chloride ions. *Colloids Surf., A* **2009**, *338*, 33−39.
(177) Coskun, S.; Aksoy, B.; Unalan, H. E. Polyol Synthesis of Silver Nanowires: An Extensive Parametric Study. *Cryst. Growth Des.* **2011**, *11*, 4963−4969.
(178) Chang, Y.-H.; Lu, Y.-C.; Chou, K.-S. Diameter Control of Silver Nanowires by Chloride Ions and Its Application as Transparent Conductive Coating. *Chem. Lett.* **2011**, *40*, 1352−1353.
(179) Zhan, K.; Su, R.; Bai, S.; Yu, Z.; Cheng, N.; Wang, C.; Xu, S.; Liu, W.; Guo, S.; Zhao, X.-Z. One-pot stirring-free synthesis of silver nanowires with tunable lengths and diameters via a Fe^{3+} & Cl^- co-mediated polyol method and their application as transparent conductive films. *Nanoscale* **2016**, *8*, 18121−18133.
(180) An, J.; Tang, B.; Zheng, X.; Zhou, J.; Dong, F.; Xu, S.; Wang, Y.; Zhao, B.; Xu, W. Sculpturing Effect of Chloride Ions in Shape Transformation from Triangular to Discal Silver Nanoplates. *J. Phys. Chem. C* **2008**, *112*, 15176−15182.
(181) Wang, Z. L. Transmission Electron Microscopy of Shape-Controlled Nanocrystals and Their Assemblies. *J. Phys. Chem. B* **2000**, *104*, 1153−1175.
(182) Tang, B.; Xu, S.; An, J.; Zhao, B.; Xu, W.; Lombardi, J. R. Kinetic effects of halide ions on the morphological evolution of silver nanoplates. *Phys. Chem. Chem. Phys.* **2009**, *11*, 10286−10292.
(183) Jiang, X. C.; Yu, A. B. Silver Nanoplates: A Highly Sensitive Material toward Inorganic Anions. *Langmuir* **2008**, *24*, 4300−4309.
(184) Cathcart, N.; Frank, A. J.; Kitaev, V. Silver nanoparticles with planar twinned defects: effect of halides for precise tuning of plasmon resonance maxima from 400 to > 900 nm. *Chem. Commun.* **2009**, 7170−7172.
(185) Linnert, T.; Mulvaney, P.; Henglein, A. Surface chemistry of colloidal silver: surface plasmon damping by chemisorbed iodide, hydrosulfide (SH^-), and phenylthiolate. *J. Phys. Chem.* **1993**, *97*, 679−682.
(186) Xiong, Y.; Chen, J.; Wiley, B.; Xia, Y.; Aloni, S.; Yin, Y. Understanding the Role of Oxidative Etching in the Polyol Synthesis of Pd Nanoparticles with Uniform Shape and Size. *J. Am. Chem. Soc.* **2005**, *127*, 7332−7333.
(187) Xiong, Y.; McLellan, J. M.; Chen, J.; Yin, Y.; Li, Z.-Y.; Xia, Y. Kinetically Controlled Synthesis of Triangular and Hexagonal Nanoplates of Palladium and Their SPR/SERS Properties. *J. Am. Chem. Soc.* **2005**, *127*, 17118−17127.
(188) Xiong, Y.; Cai, H.; Wiley, B. J.; Wang, J.; Kim, M. J.; Xia, Y. Synthesis and Mechanistic Study of Palladium Nanobars and Nanorods. *J. Am. Chem. Soc.* **2007**, *129*, 3665−3675.
(189) Peng, H.-C.; Xie, S.; Park, J.; Xia, X.; Xia, Y. Quantitative Analysis of the Coverage Density of Br^- Ions on Pd{100} Facets and Its

DOI: 10.1021/acs.chemrev.8b00158
Chem. Rev. 2018, 118, 7804−7864

Role in Controlling the Shape of Pd Nanocrystals. *J. Am. Chem. Soc.* **2013**, *135*, 3780−3783.
(190) Liu, M.; Zheng, Y.; Zhang, L.; Guo, L.; Xia, Y. Transformation of Pd Nanocubes into Octahedra with Controlled Sizes by Maneuvering the Rates of Etching and Regrowth. *J. Am. Chem. Soc.* **2013**, *135*, 11752−11755.
(191) Xia, X.; Choi, S.-I.; Herron, J. A.; Lu, N.; Scaranto, J.; Peng, H.-C.; Wang, J.; Mavrikakis, M.; Kim, M. J.; Xia, Y. Facile Synthesis of Palladium Right Bipyramids and Their Use as Seeds for Overgrowth and as Catalysts for Formic Acid Oxidation. *J. Am. Chem. Soc.* **2013**, *135*, 15706−15709.
(192) Niu, W.; Zhang, L.; Xu, G. Shape-Controlled Synthesis of Single-Crystalline Palladium Nanocrystals. *ACS Nano* **2010**, *4*, 1987−1996.
(193) Xiong, Y.; Wiley, B.; Chen, J.; Li, Z.-Y.; Yin, Y.; Xia, Y. Corrosion-Based Synthesis of Single-Crystal Pd Nanoboxes and Nanocages and Their Surface Plasmon Properties. *Angew. Chem., Int. Ed.* **2005**, *44*, 7913−7917.
(194) Carrasquillo, A.; Jeng, J.-J.; Barriga, R. J.; Temesghen, W. F.; Soriaga, M. P. Electrode-surface coordination chemistry: ligand substitution and competitive coordination of halides at well-defined Pd(100) and Pd(111) single crystals. *Inorg. Chim. Acta* **1997**, *255*, 249−254.
(195) Huang, X.; Zhang, H.; Guo, C.; Zhou, Z.; Zheng, N. Simplifying the Creation of Hollow Metallic Nanostructures: One-Pot Synthesis of Hollow Palladium/Platinum Single-Crystalline Nanocubes. *Angew. Chem., Int. Ed.* **2009**, *48*, 4808−4812.
(196) Yoo, S.-H.; Lee, J.-H.; Delley, B.; Soon, A. Why does bromine square palladium off? An ab initio study of brominated palladium and its nanomorphology. *Phys. Chem. Chem. Phys.* **2014**, *16*, 18570−18577.
(197) Ruditskiy, A.; Vara, M.; Huang, H.; Xia, Y. Oxidative Etching of Pd Decahedral Nanocrystals with a Penta-twinned Structure and Its Impact on Their Growth Behavior. *Chem. Mater.* **2017**, *29*, 5394−5400.
(198) Huang, X.; Zheng, N. One-Pot, High-Yield Synthesis of 5-Fold Twinned Pd Nanowires and Nanorods. *J. Am. Chem. Soc.* **2009**, *131*, 4602−4603.
(199) Wang, C.; Wang, L.; Long, R.; Ma, L.; Wang, L.; Li, Z.; Xiong, Y. Anisotropic growth of palladium twinned nanostructures controlled by kinetics and their unusual activities in galvanic replacement. *J. Mater. Chem.* **2012**, *22*, 8195−8198.
(200) Liu, S.-Y.; Shen, Y.-T.; Chiu, C.-Y.; Rej, S.; Lin, P.-H.; Tsao, Y.-C.; Huang, M. H. Direct Synthesis of Palladium Nanocrystals in Aqueous Solution with Systematic Shape Evolution. *Langmuir* **2015**, *31*, 6538−6545.
(201) Lu, N.; Chen, W.; Fang, G.; Chen, B.; Yang, K.; Yang, Y.; Wang, Z.; Huang, S.; Li, Y. 5-fold Twinned Nanowires and Single Twinned Right Bipyramids of Pd: Utilizing Small Organic Molecules To Tune the Etching Degree of O_2/Halides. *Chem. Mater.* **2014**, *26*, 2453−2459.
(202) Zhang, J.; Feng, C.; Deng, Y.; Liu, L.; Wu, Y.; Shen, B.; Zhong, C.; Hu, W. Shape-Controlled Synthesis of Palladium Single-Crystalline Nanoparticles: The Effect of HCl Oxidative Etching and Facet-Dependent Catalytic Properties. *Chem. Mater.* **2014**, *26*, 1213−1218.
(203) Nalajala, N.; Chakraborty, A.; Bera, B.; Neergat, M. Chloride (Cl^-) ion-mediated shape control of palladium nanoparticles. *Nanotechnology* **2016**, *27*, 065603.
(204) Navas, M. P.; Soni, R. K. Bromide (Br^-) ion-mediated synthesis of anisotropic palladium nanocrystals by laser ablation. *Appl. Surf. Sci.* **2016**, *390*, 718−727.
(205) Xiong, Y.; Cai, H.; Yin, Y.; Xia, Y. Synthesis and characterization of fivefold twinned nanorods and right bipyramids of palladium. *Chem. Phys. Lett.* **2007**, *440*, 273−278.
(206) Lim, B.; Kobayashi, H.; Camargo, P. H. C.; Allard, L. F.; Liu, J.; Xia, Y. New insights into the growth mechanism and surface structure of palladium nanocrystals. *Nano Res.* **2010**, *3*, 180−188.
(207) Jin, M.; Liu, H.; Zhang, H.; Xie, Z.; Liu, J.; Xia, Y. Synthesis of Pd nanocrystals enclosed by {100} facets and with sizes < 10 nm for application in CO oxidation. *Nano Res.* **2011**, *4*, 83−91.
(208) Jin, M.; Zhang, H.; Xie, Z.; Xia, Y. Palladium Concave Nanocubes with High-Index Facets and Their Enhanced Catalytic Properties. *Angew. Chem., Int. Ed.* **2011**, *50*, 7850−7854.
(209) Zhang, H.; Jin, M.; Xiong, Y.; Lim, B.; Xia, Y. Shape-Controlled Synthesis of Pd Nanocrystals and Their Catalytic Applications. *Acc. Chem. Res.* **2013**, *46*, 1783−1794.
(210) Peng, H.-C.; Li, Z.; Aldahondo, G.; Huang, H.; Xia, Y. Seed-Mediated Synthesis of Pd Nanocrystals: The Effect of Surface Capping on the Heterogeneous Nucleation and Growth. *J. Phys. Chem. C* **2016**, *120*, 11754−11761.
(211) Yin, A.-X.; Min, X.-Q.; Zhang, Y.-W.; Yan, C.-H. Shape-Selective Synthesis and Facet-Dependent Enhanced Electrocatalytic Activity and Durability of Monodisperse Sub-10 nm Pt−Pd Tetrahedrons and Cubes. *J. Am. Chem. Soc.* **2011**, *133*, 3816−3819.
(212) Zhang, H.; Jin, M.; Wang, J.; Li, W.; Camargo, P. H. C.; Kim, M. J.; Yang, D.; Xie, Z.; Xia, Y. Synthesis of Pd−Pt Bimetallic Nanocrystals with a Concave Structure through a Bromide-Induced Galvanic Replacement Reaction. *J. Am. Chem. Soc.* **2011**, *133*, 6078−6089.
(213) Xie, S.; Lu, N.; Xie, Z.; Wang, J.; Kim, M. J.; Xia, Y. Synthesis of Pd-Rh Core−Frame Concave Nanocubes and Their Conversion to Rh Cubic Nanoframes by Selective Etching of the Pd Cores. *Angew. Chem., Int. Ed.* **2012**, *51*, 10266−10270.
(214) Huang, X.; Li, Y.; Li, Y.; Zhou, H.; Duan, X.; Huang, Y. Synthesis of PtPd Bimetal Nanocrystals with Controllable Shape, Composition, and Their Tunable Catalytic Properties. *Nano Lett.* **2012**, *12*, 4265−4270.
(215) Li, H.-H.; Ma, S.-Y.; Fu, Q.-Q.; Liu, X.-J.; Wu, L.; Yu, S.-H. Scalable Bromide-Triggered Synthesis of Pd@Pt Core−Shell Ultrathin Nanowires with Enhanced Electrocatalytic Performance toward Oxygen Reduction Reaction. *J. Am. Chem. Soc.* **2015**, *137*, 7862−7868.
(216) Zhang, J.; Wan, L.; Liu, L.; Deng, Y.; Zhong, C.; Hu, W. PdPt bimetallic nanoparticles enabled by shape control with halide ions and their enhanced catalytic activities. *Nanoscale* **2016**, *8*, 3962−3972.
(217) Zhou, M.; Wang, H.; Vara, M.; Hood, Z. D.; Luo, M.; Yang, T. H.; Bao, S.; Chi, M.; Xiao, P.; Zhang, Y.; Xia, Y. Quantitative Analysis of the Reduction Kinetics Responsible for the One-Pot Synthesis of Pd-Pt Bimetallic Nanocrystals with Different Structures. *J. Am. Chem. Soc.* **2016**, *138*, 12263−12270.
(218) Zhang, L.; Choi, S.-I.; Tao, J.; Peng, H.-C.; Xie, S.; Zhu, Y.; Xie, Z.; Xia, Y. Pd−Cu Bimetallic Tripods: A Mechanistic Understanding of the Synthesis and Their Enhanced Electrocatalytic Activity for Formic Acid Oxidation. *Adv. Funct. Mater.* **2014**, *24*, 7520−7529.
(219) Luo, Z.; Ibáñez, M.; Antolín, A. M.; Genç, A.; Shavel, A.; Contreras, S.; Medina, F.; Arbiol, J.; Cabot, A. Size and Aspect Ratio Control of Pd_2Sn Nanorods and Their Water Denitration Properties. *Langmuir* **2015**, *31*, 3952−3957.
(220) Filankembo, A.; Giorgio, S.; Lisiecki, I.; Pileni, M. P. Is the Anion the Major Parameter in the Shape Control of Nanocrystals? *J. Phys. Chem. B* **2003**, *107*, 7492−7500.
(221) Kitchens, C. L.; McLeod, M. C.; Roberts, C. B. Chloride Ion Effects on Synthesis and Directed Assembly of Copper Nanoparticles in Liquid and Compressed Alkane Microemulsions. *Langmuir* **2005**, *21*, 5166−5173.
(222) Huang, C.-C.; Hwu, J. R.; Su, W.-C.; Shieh, D.-B.; Tzeng, Y.; Yeh, C.-S. Surfactant-Assisted Hollowing of Cu Nanoparticles Involving Halide-Induced Corrosion−Oxidation Processes. *Chem. - Eur. J.* **2006**, *12*, 3805−3810.
(223) Venkatasubramanian, R.; He, J.; Johnson, M. W.; Stern, I.; Kim, D. H.; Pesika, N. S. Additive-Mediated Electrochemical Synthesis of Platelike Copper Crystals for Methanol Electrooxidation. *Langmuir* **2013**, *29*, 13135−13139.
(224) Zhang, Y.; Grass, M. E.; Kuhn, J. N.; Tao, F.; Habas, S. E.; Huang, W.; Yang, P.; Somorjai, G. A. Highly Selective Synthesis of Catalytically Active Monodisperse Rhodium Nanocubes. *J. Am. Chem. Soc.* **2008**, *130*, 5868−5869.
(225) Yuan, Q.; Zhou, Z.; Zhuang, J.; Wang, X. Tunable Aqueous Phase Synthesis and Shape-Dependent Electrochemical Properties of Rhodium Nanostructures. *Inorg. Chem.* **2010**, *49*, 5515−5521.

DOI: 10.1021/acs.chemrev.8b00158
Chem. Rev. 2018, 118, 7804−7864

(226) Bi, Y.; Lu, G. Iodide ions control galvanic replacement growth of uniform rhodiumnanotubes at room temperature. *Chem. Commun.* **2008**, 6402−6404.
(227) Sneed, B. T.; Kuo, C.-H.; Brodsky, C. N.; Tsung, C.-K. Iodide-Mediated Control of Rhodium Epitaxial Growth on Well-Defined Noble Metal Nanocrystals: Synthesis, Characterization, and Structure-Dependent Catalytic Properties. *J. Am. Chem. Soc.* **2012**, *134*, 18417−18426.
(228) Yamada, M.; Kon, S.; Miyake, M. Synthesis and Size Control of Pt Nanocubes with High Selectivity Using the Additive Effect of NaI. *Chem. Lett.* **2005**, *34*, 1050−1051.
(229) Yu, T.; Kim, D. Y.; Zhang, H.; Xia, Y. Platinum Concave Nanocubes with High-Index Facets and Their Enhanced Activity for Oxygen Reduction Reaction. *Angew. Chem.* **2011**, *123*, 2825−2829.
(230) Cai, Y.; Ma, C.; Zhu, Y.; Wang, J. X.; Adzic, R. R. Low-Coordination Sites in Oxygen-Reduction Electrocatalysis: Their Roles and Methods for Removal. *Langmuir* **2011**, *27*, 8540−8547.
(231) Yin, J.; Wang, J.; Li, M.; Jin, C.; Zhang, T. Iodine Ions Mediated Formation of Monomorphic Single-Crystalline Platinum Nanoflowers. *Chem. Mater.* **2012**, *24*, 2645−2654.
(232) Michel, J. A.; Morris Iii, W. H.; Lukehart, C. M. Synthesis of shaped Pt nanoparticles using common anions or small molecules as shape-directing agents: observation of a strong halide or pseudo-halide effect. *J. Mater. Chem. A* **2015**, *3*, 2012−2018.
(233) Martínez-Rodríguez, R. A.; Vidal-Iglesias, F. J.; Solla-Gullón, J.; Cabrera, C. R.; Feliu, J. M. Synthesis of Pt Nanoparticles in Water-in-Oil Microemulsion: Effect of HCl on Their Surface Structure. *J. Am. Chem. Soc.* **2014**, *136*, 1280−1283.
(234) Fan, N.; Yang, Y.; Wang, W.; Zhang, L.; Chen, W.; Zou, C.; Huang, S. Selective Etching Induces Selective Growth and Controlled Formation of Various Platinum Nanostructures by Modifying Seed Surface Free Energy. *ACS Nano* **2012**, *6*, 4072−4082.
(235) Hwang, E.-T.; Lee, Y.-W.; Park, H.-C.; Kwak, D.-H.; Kim, D.-M.; Kim, S.-J.; Kim, M.-C.; Lee, J.-Y.; Lee, S.; Park, K.-W. Synthesis of Pt-Rich@Pt-Ni alloy core-shell nanoparticles using halides. *RSC Adv.* **2015**, *5*, 8301−8306.
(236) Choi, J.; Lee, Y.; Kim, J.; Lee, H. Enhancing stability of octahedral PtNi nanoparticles for oxygen reduction reaction by halide treatment. *J. Power Sources* **2016**, *307*, 883−890.
(237) Huang, L.; Zhang, X.; Han, Y.; Wang, Q.; Fang, Y.; Dong, S. High-Index Facets Bounded Platinum-Lead Concave Nanocubes with Enhanced Electrocatalytic Properties. *Chem. Mater.* **2017**, *29*, 4557−4562.
(238) Lacroix, L.-M.; Frey Huls, N.; Ho, D.; Sun, X.; Cheng, K.; Sun, S. Stable Single-Crystalline Body Centered Cubic Fe Nanoparticles. *Nano Lett.* **2011**, *11*, 1641−1645.
(239) Zhang, S.; Jiang, G.; Filsinger, G. T.; Wu, L.; Zhu, H.; Lee, J.; Wu, Z.; Sun, S. Halide ion-mediated growth of single crystalline Fe nanoparticles. *Nanoscale* **2014**, *6*, 4852−4856.
(240) Yang, C.; Zhao, H.; Hou, Y.; Ma, D. Fe_5C_2 Nanoparticles: A Facile Bromide-Induced Synthesis and as an Active Phase for Fischer−Tropsch Synthesis. *J. Am. Chem. Soc.* **2012**, *134*, 15814−15821.
(241) Gao, J.; Wang, X.; Pan, X.; Ren, X.; Han, Y.; Yang, X.; Yang, H. Facile synthesis of nanocrystalline Fe/Fe_3C induced by bromide. *J. Mater. Sci.: Mater. Electron.* **2016**, *27*, 64−69.
(242) Yang, Z.; Zhao, T.; Huang, X.; Chu, X.; Tang, T.; Ju, Y.; Wang, Q.; Hou, Y.; Gao, S. Modulating the phases of iron carbide nanoparticles: from a perspective of interfering with the carbon penetration of Fe@Fe_3O_4 by selectively adsorbed halide ions. *Chem. Sci.* **2017**, *8*, 473−481.
(243) Palencia, C.; Lauwaet, K.; de la Cueva, L.; Acebron, M.; Conde, J. J.; Meyns, M.; Klinke, C.; Gallego, J. M.; Otero, R.; Juarez, B. H. Cl-capped CdSe nanocrystals via in situ generation of chloride anions. *Nanoscale* **2014**, *6*, 6812−6818.
(244) Meyns, M.; Iacono, F.; Palencia, C.; Geweke, J.; Coderch, M. D.; Fittschen, U. E. A.; Gallego, J. M.; Otero, R.; Juárez, B. H.; Klinke, C. Shape Evolution of CdSe Nanoparticles Controlled by Halogen Compounds. *Chem. Mater.* **2014**, *26*, 1813−1821.
(245) de la Cueva, L.; Lauwaet, K.; Otero, R.; Gallego, J. M.; Alonso, C.; Juarez, B. H. Effect of Chloride Ligands on CdSe Nanocrystals by Cyclic Voltammetry and X-ray Photoelectron Spectroscopy. *J. Phys. Chem. C* **2014**, *118*, 4998−5004.
(246) Saruyama, M.; Kanehara, M.; Teranishi, T. Drastic Structural Transformation of Cadmium Chalcogenide Nanoparticles Using Chloride Ions and Surfactants. *J. Am. Chem. Soc.* **2010**, *132*, 3280−3282.
(247) Zou, Y.; Li, D.; Yang, D. Shape and phase control of CdS nanocrystals using cationic surfactant in noninjection synthesis. *Nanoscale Res. Lett.* **2011**, *6*, 374.
(248) Hinrichs, D.; Galchenko, M.; Kodanek, T.; Naskar, S.; Bigall, N. C.; Dorfs, D. Chloride Ion Mediated Synthesis of Metal/Semiconductor Hybrid Nanocrystals. *Small* **2016**, *12*, 2588−94.
(249) Bertoni, G.; Grillo, V.; Brescia, R.; Ke, X.; Bals, S.; Catellani, A.; Li, H.; Manna, L. Direct Determination of Polarity, Faceting, and Core Location in Colloidal Core/Shell Wurtzite Semiconductor Nanocrystals. *ACS Nano* **2012**, *6*, 6453−6461.
(250) de la Cueva, L.; Meyns, M.; Bastús, N. G.; Rodríguez-Fernández, J.; Otero, R.; Gallego, J. M.; Alonso, C.; Klinke, C.; Juárez, B. H. Shell or Dots − Precursor Controlled Morphology of Au−Se Deposits on CdSe Nanoparticles. *Chem. Mater.* **2016**, *28*, 2704−2714.
(251) Iacono, F.; Palencia, C.; de la Cueva, L.; Meyns, M.; Terracciano, L.; Vollmer, A.; de la Mata, M. J.; Klinke, C.; Gallego, J. M.; Juarez, B. H.; Otero, R. Interfacing Quantum Dots and Graphitic Surfaces with Chlorine Atomic Ligands. *ACS Nano* **2013**, *7*, 2559−2565.
(252) Lim, S. J.; Kim, W.; Jung, S.; Seo, J.; Shin, S. K. Anisotropic Etching of Semiconductor Nanocrystals. *Chem. Mater.* **2011**, *23*, 5029−5036.
(253) Lim, S. J.; Kim, W.; Shin, S. K. Surface-Dependent, Ligand-Mediated Photochemical Etching of CdSe Nanoplatelets. *J. Am. Chem. Soc.* **2012**, *134*, 7576−7579.
(254) Kim, D.; Kim, W. D.; Kang, M. S.; Kim, S.-H.; Lee, D. C. Self-Organization of Nanorods into Ultra-Long Range Two-Dimensional Monolayer End-to-End Network. *Nano Lett.* **2015**, *15*, 714−720.
(255) Gerdes, F.; Navio, C.; Juarez, B. H.; Klinke, C. Size, Shape, and Phase Control in Ultrathin CdSe Nanosheets. *Nano Lett.* **2017**, *17*, 4165−4171.
(256) Qu, L.; Peng, Z. A.; Peng, X. Alternative Routes toward High Quality CdSe Nanocrystals. *Nano Lett.* **2001**, *1*, 333−337.
(257) Lazell, M.; O'Brien, P. Synthesis of CdS nanocrystals using cadmium dichloride and trioctylphosphine sulfide. *J. Mater. Chem.* **1999**, *9*, 1381−1382.
(258) Pawar, A. S.; Masikane, S. C.; Mlowe, S.; Garje, S. S.; Revaprasadu, N. Preparation of CdS Nanoparticles from Thiosemicarbazone Complexes: Morphological Influence of Chlorido and Iodido Ligands. *Eur. J. Inorg. Chem.* **2016**, *2016*, 366−372.
(259) McCandless, B. E.; Moulton, L. V.; Birkmire, R. W. Recrystallization and sulfur diffusion in $CdCl_2$-treated CdTe/CdS thin films. *Prog. Photovoltaics* **1997**, *5*, 249−260.
(260) Major, J. D.; Al Turkestani, M.; Bowen, L.; Brossard, M.; Li, C.; Lagoudakis, P.; Pennycook, S. J.; Phillips, L. J.; Treharne, R. E.; Durose, K. In-depth analysis of chloride treatments for thin-film CdTe solar cells. *Nat. Commun.* **2016**, *7*, 13231.
(261) Rose, D. H.; Hasoon, F. S.; Dhere, R. G.; Albin, D. S.; Ribelin, R. M.; Li, X. S.; Mahathongdy, Y.; Gessert, T. A.; Sheldon, P. Fabrication procedures and process sensitivities for CdS/CdTe solar cells. *Prog. Photovoltaics* **1999**, *7*, 331−340.
(262) Gur, I.; Fromer, N. A.; Geier, M. L.; Alivisatos, A. P. Air-Stable All-Inorganic Nanocrystal Solar Cells Processed from Solution. *Science* **2005**, *310*, 462−465.
(263) MacDonald, B. I.; Martucci, A.; Rubanov, S.; Watkins, S. E.; Mulvaney, P.; Jasieniak, J. J. Layer-by-Layer Assembly of Sintered $CdSe_xTe_{1-x}$ Nanocrystal Solar Cells. *ACS Nano* **2012**, *6*, 5995−6004.
(264) Jasieniak, J.; MacDonald, B. I.; Watkins, S. E.; Mulvaney, P. Solution-Processed Sintered Nanocrystal Solar Cells via Layer-by-Layer Assembly. *Nano Lett.* **2011**, *11*, 2856−2864.

DOI: 10.1021/acs.chemrev.8b00158
Chem. Rev. 2018, 118, 7804−7864

(265) Owen, J. S.; Park, J.; Trudeau, P.-E.; Alivisatos, A. P. Reaction Chemistry and Ligand Exchange at Cadmium−Selenide Nanocrystal Surfaces. *J. Am. Chem. Soc.* **2008**, *130*, 12279−12281.
(266) Anderson, N. C.; Owen, J. S. Soluble, Chloride-Terminated CdSe Nanocrystals: Ligand Exchange Monitored by ^{1}H and ^{31}P NMR Spectroscopy. *Chem. Mater.* **2013**, *25*, 69−76.
(267) Zanella, M.; Maserati, L.; Pernia Leal, M.; Prato, M.; Lavieville, R.; Povia, M.; Krahne, R.; Manna, L. Atomic Ligand Passivation of Colloidal Nanocrystal Films via their Reaction with Propyltrichlorosilane. *Chem. Mater.* **2013**, *25*, 1423−1429.
(268) Li, X.; Zhao, Y.-B.; Fan, F.; Levina, L.; Liu, M.; Quintero-Bermudez, R.; Gong, X.; Quan, L. N.; Fan, J.; Yang, Z.; Hoogland, S.; Voznyy, O.; Lu, Z.-H.; Sargent, E. H. Bright colloidal quantum dot light-emitting diodes enabled by efficient chlorination. *Nat. Photonics* **2018**, *12*, 159−164.
(269) Niu, G.; Wang, L.; Gao, R.; Li, W.; Guo, X.; Dong, H.; Qiu, Y. Inorganic halogen ligands in quantum dots: I^-, Br^-, Cl^- and film fabrication through electrophoretic deposition. *Phys. Chem. Chem. Phys.* **2013**, *15*, 19595−19600.
(270) Zhang, H.; Kurley, J. M.; Russell, J. C.; Jang, J.; Talapin, D. V. Solution-Processed, Ultrathin Solar Cells from $CdCl_3^-$-Capped CdTe Nanocrystals: The Multiple Roles of $CdCl_3^-$ Ligands. *J. Am. Chem. Soc.* **2016**, *138*, 7464−7467.
(271) Kim, W. D.; Kim, J.-H.; Lee, S.; Lee, S.; Woo, J. Y.; Lee, K.; Chae, W.-S.; Jeong, S.; Bae, W. K.; McGuire, J. A.; Moon, J. H.; Jeong, M. S.; Lee, D. C. Role of Surface States in Photocatalysis: Study of Chlorine-Passivated CdSe Nanocrystals for Photocatalytic Hydrogen Generation. *Chem. Mater.* **2016**, *28*, 962−968.
(272) Wang, Y.; Zhang, Y.; Zhang, W. First-principles study of the halide-passivation effects on the electronic structures of CdSe quantum dots. *RSC Adv.* **2014**, *4*, 19302−19309.
(273) Page, R. C.; Espinobarro-Velazquez, D.; Leontiadou, M. A.; Smith, C.; Lewis, E. A.; Haigh, S. J.; Li, C.; Radtke, H.; Pengpad, A.; Bondino, F.; Magnano, E.; Pis, I.; Flavell, W. R.; O'Brien, P.; Binks, D. J. Near-Unity Quantum Yields from Chloride Treated CdTe Colloidal Quantum Dots. *Small* **2015**, *11*, 1548−1554.
(274) Cademartiri, L.; Bertolotti, J.; Sapienza, R.; Wiersma, D. S.; von Freymann, G.; Ozin, G. A. Multigram Scale, Solventless, and Diffusion-Controlled Route to Highly Monodisperse PbS Nanocrystals. *J. Phys. Chem. B* **2006**, *110*, 671−673.
(275) Zhang, J.; Gao, J.; Miller, E. M.; Luther, J. M.; Beard, M. C. Diffusion-controlled synthesis of PbS and PbSe quantum dots with in situ halide passivation for quantum dot solar cells. *ACS Nano* **2014**, *8*, 614−622.
(276) Zhang, Z.; Liu, C.; Zhao, X. Utilizing Sn Precursor To Promote the Nucleation of PbSe Quantum Dots with in Situ Halide Passivation. *J. Phys. Chem. C* **2015**, *119*, 5626−5632.
(277) Reilly, N.; Wehrung, M.; O'Dell, R. A.; Sun, L. Ultrasmall colloidal PbS quantum dots. *Mater. Chem. Phys.* **2014**, *147*, 1−4.
(278) Kandel, S. R.; Chiluwal, S.; Jiang, Z.; Tang, Y.; Roland, P. J.; Subedi, K.; Dimick, D. M.; Moroz, P.; Zamkov, M.; Ellingson, R.; Hu, J.; Voevodin, A. A.; Sun, L. One-dimensional growth of colloidal PbSe nanorods in chloroalkanes. *Phys. Status Solidi RRL* **2016**, *10*, 833−837.
(279) Bhandari, G. B.; Subedi, K.; He, Y.; Jiang, Z.; Leopold, M.; Reilly, N.; Lu, H. P.; Zayak, A. T.; Sun, L. Thickness-Controlled Synthesis of Colloidal PbS Nanosheets and Their Thickness-Dependent Energy Gaps. *Chem. Mater.* **2014**, *26*, 5433−5436.
(280) Bae, W. K.; Joo, J.; Padilha, L. A.; Won, J.; Lee, D. C.; Lin, Q.; Koh, W. K.; Luo, H.; Klimov, V. I.; Pietryga, J. M. Highly effective surface passivation of PbSe quantum dots through reaction with molecular chlorine. *J. Am. Chem. Soc.* **2012**, *134*, 20160−20168.
(281) Koh, W.-k.; Dandu, N. K.; Fidler, A. F.; Klimov, V. I.; Pietryga, J. M.; Kilina, S. V. Thickness-Controlled Quasi-Two-Dimensional Colloidal PbSe Nanoplatelets. *J. Am. Chem. Soc.* **2017**, *139*, 2152−2155.
(282) Sykora, M.; Koposov, A. Y.; McGuire, J. A.; Schulze, R. K.; Tretiak, O.; Pietryga, J. M.; Klimov, V. I. Effect of Air Exposure on Surface Properties, Electronic Structure, and Carrier Relaxation in PbSe Nanocrystals. *ACS Nano* **2010**, *4*, 2021−2034.
(283) Choi, H.; Ko, J. H.; Kim, Y. H.; Jeong, S. Steric-hindrance-driven shape transition in PbS quantum dots: understanding size-dependent stability. *J. Am. Chem. Soc.* **2013**, *135*, 5278−81.
(284) Lu, H.; Joy, J.; Gaspar, R. L.; Bradforth, S. E.; Brutchey, R. L. Iodide-Passivated Colloidal PbS Nanocrystals Leading to Highly Efficient Polymer:Nanocrystal Hybrid Solar Cells. *Chem. Mater.* **2016**, *28*, 1897−1906.
(285) Sayevich, V.; Gaponik, N.; Plötner, M.; Kruszynska, M.; Gemming, T.; Dzhagan, V. M.; Akhavan, S.; Zahn, D. R. T.; Demir, H. V.; Eychmüller, A. Stable Dispersion of Iodide-Capped PbSe Quantum Dots for High-Performance Low-Temperature Processed Electronics and Optoelectronics. *Chem. Mater.* **2015**, *27*, 4328−4337.
(286) Kim, S.; Noh, J.; Choi, H.; Ha, H.; Song, J. H.; Shim, H. C.; Jang, J.; Beard, M. C.; Jeong, S. One-Step Deposition of Photovoltaic Layers Using Iodide Terminated PbS Quantum Dots. *J. Phys. Chem. Lett.* **2014**, *5*, 4002−4007.
(287) Ning, Z.; Ren, Y.; Hoogland, S.; Voznyy, O.; Levina, L.; Stadler, P.; Lan, X.; Zhitomirsky, D.; Sargent, E. H. All-inorganic colloidal quantum dot photovoltaics employing solution-phase halide passivation. *Adv. Mater.* **2012**, *24*, 6295−6299.
(288) Zhitomirsky, D.; Furukawa, M.; Tang, J.; Stadler, P.; Hoogland, S.; Voznyy, O.; Liu, H.; Sargent, E. H. N-type colloidal-quantum-dot solids for photovoltaics. *Adv. Mater.* **2012**, *24*, 6181−6185.
(289) Voznyy, O.; Zhitomirsky, D.; Stadler, P.; Ning, Z.; Hoogland, S.; Sargent, E. H. A Charge-Orbital Balance Picture of Doping in Colloidal Quantum Dot Solids. *ACS Nano* **2012**, *6*, 8448−8455.
(290) Zhang, Z.; Yang, J.; Wen, X.; Yuan, L.; Shrestha, S.; Stride, J. A.; Conibeer, G. J.; Patterson, R. J.; Huang, S. Effect of Halide Treatments on PbSe Quantum Dot Thin Films: Stability, Hot Carrier Lifetime, and Application to Photovoltaics. *J. Phys. Chem. C* **2015**, *119*, 24149−24155.
(291) Ning, Z.; Voznyy, O.; Pan, J.; Hoogland, S.; Adinolfi, V.; Xu, J.; Li, M.; Kirmani, A. R.; Sun, J.-P.; Minor, J.; Kemp, K. W.; Dong, H.; Rollny, L.; Labelle, A.; Carey, G.; Sutherland, B.; Hill, I.; Amassian, A.; Liu, H.; Tang, J.; Bakr, O. M.; Sargent, E. H. Air-stable n-type colloidal quantum dot solids. *Nat. Mater.* **2014**, *13*, 822−828.
(292) Zhang, H.; Yang, J.; Chen, J. R.; Engstrom, J. R.; Hanrath, T.; Wise, F. W. Tuning of Coupling and Surface Quality of PbS Nanocrystals via a Combined Ammonium Sulfide and Iodine Treatment. *J. Phys. Chem. Lett.* **2016**, *7*, 642−646.
(293) Chuang, C.-H. M.; Brown, P. R.; Bulović, V.; Bawendi, M. G. Improved performance and stability in quantum dot solar cells through band alignment engineering. *Nat. Mater.* **2014**, *13*, 796−801.
(294) Yazdani, N.; Bozyigit, D.; Vuttivorakulchai, K.; Luisier, M.; Infante, I.; Wood, V. Tuning Electron-Phonon Interactions in Nanocrystals through Surface Termination. *Nano Lett.* **2018**, *18*, 2233−2242.
(295) Zhitomirsky, D.; Voznyy, O.; Levina, L.; Hoogland, S.; Kemp, K. W.; Ip, A. H.; Thon, S. M.; Sargent, E. H. Engineering colloidal quantum dot solids within and beyond the mobility-invariant regime. *Nat. Commun.* **2014**, *5*, 4803.
(296) Ibáñez, M.; Korkosz, R. J.; Luo, Z.; Riba, P.; Cadavid, D.; Ortega, S.; Cabot, A.; Kanatzidis, M. G. Electron Doping in Bottom-Up Engineered Thermoelectric Nanomaterials through HCl-Mediated Ligand Displacement. *J. Am. Chem. Soc.* **2015**, *137*, 4046−4049.
(297) Balazs, D. M.; Dirin, D. N.; Fang, H.-H.; Protesescu, L.; ten Brink, G. H.; Kooi, B. J.; Kovalenko, M. V.; Loi, M. A. Counterion-Mediated Ligand Exchange for PbS Colloidal Quantum Dot Superlattices. *ACS Nano* **2015**, *9*, 11951−11959.
(298) Azmi, R.; Sinaga, S.; Aqoma, H.; Seo, G.; Ahn, T. K.; Park, M.; Ju, S.-Y.; Lee, J.-W.; Kim, T.-W.; Oh, S.-H.; Jang, S.-Y. Highly efficient air-stable colloidal quantum dot solar cells by improved surface trap passivation. *Nano Energy* **2017**, *39*, 86−94.
(299) Katsiev, K.; Ip, A. H.; Fischer, A.; Tanabe, I.; Zhang, X.; Kirmani, A. R.; Voznyy, O.; Rollny, L. R.; Chou, K. W.; Thon, S. M.; Carey, G. H.; Cui, X.; Amassian, A.; Dowben, P.; Sargent, E. H.; Bakr, O. M. The Complete In-Gap Electronic Structure of Colloidal Quantum Dot Solids and Its Correlation with Electronic Transport and Photovoltaic Performance. *Adv. Mater.* **2014**, *26*, 937−942.

DOI: 10.1021/acs.chemrev.8b00158
Chem. Rev. 2018, 118, 7804−7864

(300) Marshall, A. R.; Young, M. R.; Nozik, A. J.; Beard, M. C.; Luther, J. M. Exploration of Metal Chloride Uptake for Improved Performance Characteristics of PbSe Quantum Dot Solar Cells. *J. Phys. Chem. Lett.* **2015**, *6*, 2892−2899.
(301) Crisp, R. W.; Kroupa, D. M.; Marshall, A. R.; Miller, E. M.; Zhang, J.; Beard, M. C.; Luther, J. M. Metal Halide Solid-State Surface Treatment for High Efficiency PbS and PbSe QD Solar Cells. *Sci. Rep.* **2015**, *5*, 9945.
(302) Bohm, M. L.; Jellicoe, T. C.; Rivett, J. P.; Sadhanala, A.; Davis, N. J.; Morgenstern, F. S.; Godel, K. C.; Govindasamy, J.; Benson, C. G.; Greenham, N. C.; Ehrler, B. Size and Energy Level Tuning of Quantum Dot Solids via a Hybrid Ligand Complex. *J. Phys. Chem. Lett.* **2015**, *6*, 3510−3514.
(303) Wu, W.-Y.; Chakrabortty, S.; Chang, C. K. L.; Guchhait, A.; Lin, M.; Chan, Y. Promoting 2D Growth in Colloidal Transition Metal Sulfide Semiconductor Nanostructures via Halide Ions. *Chem. Mater.* **2014**, *26*, 6120−6126.
(304) van der Stam, W.; Akkerman, Q. A.; Ke, X.; van Huis, M. A.; Bals, S.; de Mello Donega, C. Solution-Processable Ultrathin Size- and Shape-Controlled Colloidal $Cu_{2-x}S$ Nanosheets. *Chem. Mater.* **2015**, *27*, 283−291.
(305) Nørby, P.; Johnsen, S.; Iversen, B. B. In Situ X-ray Diffraction Study of the Formation, Growth, and Phase Transition of Colloidal $Cu_{2-x}S$ Nanocrystals. *ACS Nano* **2014**, *8*, 4295−4303.
(306) van der Stam, W.; Rabouw, F. T.; Geuchies, J. J.; Berends, A. C.; Hinterding, S. O. M.; Geitenbeek, R. G.; van der Lit, J.; Prévost, S.; Petukhov, A. V.; de Mello Donegá, C. In-situ Probing of Stack-Templated Growth of Ultrathin $Cu_{2-x}S$ Nanosheets. *Chem. Mater.* **2016**, *28*, 6381−6389.
(307) Espinet, P.; Lequerica, M. C.; Martín-Alvarez, J. M. Synthesis, Structural Characterization and Mesogenic Behavior of Copper(I) n-Alkylthiolates. *Chem. - Eur. J.* **1999**, *5*, 1982−1986.
(308) Bryks, W.; Lupi, E.; Ngo, C.; Tao, A. R. Digenite Nanosheets Synthesized by Thermolysis of Layered Copper-Alkanethiolate Frameworks. *J. Am. Chem. Soc.* **2016**, *138*, 13717−13725.
(309) Hsu, S.-W.; Ngo, C.; Bryks, W.; Tao, A. R. Shape Focusing During the Anisotropic Growth of CuS Triangular Nanoprisms. *Chem. Mater.* **2015**, *27*, 4957−4963.
(310) Liu, J.; Tian, Y.; Wu, Z.; Ai, L.; Liu, Y.; Cui, J.; Yu, W.; Zhang, H.; Yang, B. Analogous self-assembly and crystallization: a chloride-directed orientated self-assembly of Cu nanoclusters and subsequent growth of $Cu_{2-x}S$ nanocrystals. *Nanoscale* **2017**, *9*, 10335−10343.
(311) Zhai, Y.; Shim, M. Effects of Copper Precursor Reactivity on the Shape and Phase of Copper Sulfide Nanocrystals. *Chem. Mater.* **2017**, *29*, 2390.
(312) Lee, J.; Yang, J. H.; Park, C.; Kim, J. H.; Kang, M. S. Electronic Properties of $Cu_{2-x}Se$ Nanocrystal Thin Films Treated with Short Ligand (S^{2-}, SCN^{-}, and Cl^{-}) Solutions. *J. Phys. Chem. C* **2016**, *120*, 14899.
(313) Corriu, R. J. P. Hypervalent species of silicon: structure and reactivity. *J. Organomet. Chem.* **1990**, *400*, 81−106.
(314) Kortshagen, U. R.; Sankaran, R. M.; Pereira, R. N.; Girshick, S. L.; Wu, J. J.; Aydil, E. S. Nonthermal Plasma Synthesis of Nanocrystals: Fundamental Principles, Materials, and Applications. *Chem. Rev.* **2016**, *116*, 11061−11127.
(315) Martínez, A.; Alonso, J. C.; Sansores, L. E.; Salcedo, R. Electronic Structure of Silicon Nanocrystals Passivated with Nitrogen and Chlorine. *J. Phys. Chem. C* **2010**, *114*, 12427−12431.
(316) Holman, Z. C.; Kortshagen, U. R. Nanocrystal Inks without Ligands: Stable Colloids of Bare Germanium Nanocrystals. *Nano Lett.* **2011**, *11*, 2133−2136.
(317) Baldwin, R. K.; Pettigrew, K. A.; Ratai, E.; Augustine, M. P.; Kauzlarich, S. M. Solution reduction synthesis of surface stabilized silicon nanoparticles. *Chem. Commun.* **2002**, 1822−1823.
(318) Dasog, M.; De los Reyes, G. B.; Titova, L. V.; Hegmann, F. A.; Veinot, J. G. C. Size vs Surface: Tuning the Photoluminescence of Freestanding Silicon Nanocrystals Across the Visible Spectrum via Surface Groups. *ACS Nano* **2014**, *8*, 9636−9648.
(319) Islam, M. A.; Purkait, T. K.; Veinot, J. G. C. Chloride Surface Terminated Silicon Nanocrystal Mediated Synthesis of Poly(3-hexylthiophene). *J. Am. Chem. Soc.* **2014**, *136*, 15130−15133.
(320) Dasog, M.; Bader, K.; Veinot, J. G. C. Influence of Halides on the Optical Properties of Silicon Quantum Dots. *Chem. Mater.* **2015**, *27*, 1153−1156.
(321) Park, J.; An, K.; Hwang, Y.; Park, J.-G.; Noh, H.-J.; Kim, J.-Y.; Park, J.-H.; Hwang, N.-M.; Hyeon, T. Ultra-large-scale syntheses of monodisperse nanocrystals. *Nat. Mater.* **2004**, *3*, 891−895.
(322) Kwon, S. G.; Piao, Y.; Park, J.; Angappane, S.; Jo, Y.; Hwang, N.-M.; Park, J.-G.; Hyeon, T. Kinetics of Monodisperse Iron Oxide Nanocrystal Formation by "Heating-Up" Process. *J. Am. Chem. Soc.* **2007**, *129*, 12571−12584.
(323) Chen, X.; Mao, S. S. Titanium Dioxide Nanomaterials: Synthesis, Properties, Modifications, and Applications. *Chem. Rev.* **2007**, *107*, 2891−2959.
(324) Fujishima, A.; Zhang, X.; Tryk, D. A. TiO_2 photocatalysis and related surface phenomena. *Surf. Sci. Rep.* **2008**, *63*, 515−582.
(325) Diebold, U. The surface science of titanium dioxide. *Surf. Sci. Rep.* **2003**, *48*, 53−229.
(326) Linsebigler, A. L.; Lu, G.; Yates, J. T. Photocatalysis on TiO_2 Surfaces: Principles, Mechanisms, and Selected Results. *Chem. Rev.* **1995**, *95*, 735−758.
(327) Kandiel, T. A.; Feldhoff, A.; Robben, L.; Dillert, R.; Bahnemann, D. W. Tailored Titanium Dioxide Nanomaterials: Anatase Nanoparticles and Brookite Nanorods as Highly Active Photocatalysts. *Chem. Mater.* **2010**, *22*, 2050−2060.
(328) Diebold, U.; Hebenstreit, W.; Leonardelli, G.; Schmid, M.; Varga, P. High Transient Mobility of Chlorine on TiO_2(110): Evidence for "Cannon-Ball" Trajectories of Hot Adsorbates. *Phys. Rev. Lett.* **1998**, *81*, 405−408.
(329) Vogtenhuber, D.; Podloucky, R.; Redinger, J.; Hebenstreit, E. L. D.; Hebenstreit, W.; Diebold, U. Ab initio and experimental studies of chlorine adsorption on the rutile TiO_2 (110) surface. *Phys. Rev. B: Condens. Matter Mater. Phys.* **2002**, *65*, 125411.
(330) Hebenstreit, E. L. D.; Hebenstreit, W.; Geisler, H.; Ventrice, C. A.; Hite, D. A.; Sprunger, P. T.; Diebold, U. The adsorption of chlorine on TiO_2(110) studied with scanning tunneling microscopy and photoemission spectroscopy. *Surf. Sci.* **2002**, *505*, 336−348.
(331) Yang, H. G.; Sun, C. H.; Qiao, S. Z.; Zou, J.; Liu, G.; Smith, S. C.; Cheng, H. M.; Lu, G. Q. Anatase TiO_2 single crystals with a large percentage of reactive facets. *Nature* **2008**, *453*, 638.
(332) Lazzeri, M.; Vittadini, A.; Selloni, A. Structure and energetics of stoichiometric TiO_2 anatase surfaces. *Phys. Rev. B: Condens. Matter Mater. Phys.* **2001**, *63*, 155409.
(333) Yang, H. G.; Liu, G.; Qiao, S. Z.; Sun, C. H.; Jin, Y. G.; Smith, S. C.; Zou, J.; Cheng, H. M.; Lu, G. Q. Solvothermal Synthesis and Photoreactivity of Anatase TiO_2 Nanosheets with Dominant {001} Facets. *J. Am. Chem. Soc.* **2009**, *131*, 4078−4083.
(334) Alivov, Y.; Fan, Z. Y. A Method for Fabrication of Pyramid-Shaped TiO_2 Nanoparticles with a High {001} Facet Percentage. *J. Phys. Chem. C* **2009**, *113*, 12954−12957.
(335) Zhang, D.; Li, G.; Yang, X.; Yu, J. C. A micrometer-size TiO_2 single-crystal photocatalyst with remarkable 80% level of reactive facets. *Chem. Commun.* **2009**, 4381−4383.
(336) Zhao, X.; Jin, W.; Cai, J.; Ye, J.; Li, Z.; Ma, Y.; Xie, J.; Qi, L. Shape- and Size-Controlled Synthesis of Uniform Anatase TiO_2 Nanocuboids Enclosed by Active {100} and {001} Facets. *Adv. Funct. Mater.* **2011**, *21*, 3554−3563.
(337) Zhang, D.; Li, G.; Wang, H.; Chan, K. M.; Yu, J. C. Biocompatible Anatase Single-Crystal Photocatalysts with Tunable Percentage of Reactive Facets. *Cryst. Growth Des.* **2010**, *10*, 1130−1137.
(338) Yu, J.; Xiang, Q.; Ran, J.; Mann, S. One-step hydrothermal fabrication and photocatalytic activity of surface-fluorinated TiO_2 hollow microspheres and tabular anatase single micro-crystals with high-energy facets. *CrystEngComm* **2010**, *12*, 872−879.

DOI: 10.1021/acs.chemrev.8b00158
Chem. Rev. 2018, 118, 7804−7864

(339) Chen, C.; Hu, R.; Mai, K.; Ren, Z.; Wang, H.; Qian, G.; Wang, Z. Shape Evolution of Highly Crystalline Anatase TiO_2 Nanobipyramids. *Cryst. Growth Des.* **2011**, *11*, 5221−5226.
(340) Trentler, T. J.; Denler, T. E.; Bertone, J. F.; Agrawal, A.; Colvin, V. L. Synthesis of TiO_2 Nanocrystals by Nonhydrolytic Solution-Based Reactions. *J. Am. Chem. Soc.* **1999**, *121*, 1613−1614.
(341) Ichimura, A. S.; Mack, B. M.; Usmani, S. M.; Mars, D. G. Direct Synthesis of Anatase Films with ∼ 100% (001) Facets and [001] Preferred Orientation. *Chem. Mater.* **2012**, *24*, 2324−2329.
(342) Menzel, R.; Duerrbeck, A.; Liberti, E.; Yau, H. C.; McComb, D.; Shaffer, M. S. P. Determining the Morphology and Photocatalytic Activity of Two-Dimensional Anatase Nanoplatelets Using Reagent Stoichiometry. *Chem. Mater.* **2013**, *25*, 2137−2145.
(343) Wang, X.; He, H.; Chen, Y.; Zhao, J.; Zhang, X. Anatase TiO_2 hollow microspheres with exposed {001} facets: Facile synthesis and enhanced photocatalysis. *Appl. Surf. Sci.* **2012**, *258*, 5863−5868.
(344) Liu, N.; Zhao, Y.; Wang, X.; Peng, H.; Li, G. Facile synthesis and enhanced photocatalytic properties of truncated bipyramid-shaped anatase TiO_2 nanocrystals. *Mater. Lett.* **2013**, *102*−*103*, 53−55.
(345) Zhao, Y.; Zhang, Y.; Liu, H.; Ji, H.; Ma, W.; Chen, C.; Zhu, H.; Zhao, J. Control of Exposed Facet and Morphology of Anatase Crystals through TiO_xF_y Precursor Synthesis and Impact of the Facet on Crystal Phase Transition. *Chem. Mater.* **2014**, *26*, 1014−1018.
(346) Selloni, A. Anatase shows its reactive side. *Nat. Mater.* **2008**, *7*, 613.
(347) Liu, S.; Yu, J.; Jaroniec, M. Anatase TiO_2 with Dominant High-Energy {001} Facets: Synthesis, Properties, and Applications. *Chem. Mater.* **2011**, *23*, 4085−4093.
(348) Han, X.; Kuang, Q.; Jin, M.; Xie, Z.; Zheng, L. Synthesis of Titania Nanosheets with a High Percentage of Exposed (001) Facets and Related Photocatalytic Properties. *J. Am. Chem. Soc.* **2009**, *131*, 3152−3153.
(349) Wen, C. Z.; Zhou, J. Z.; Jiang, H. B.; Hu, Q. H.; Qiao, S. Z.; Yang, H. G. Synthesis of micro-sized titanium dioxide nanosheets wholly exposed with high-energy {001} and {100} facets. *Chem. Commun.* **2011**, *47*, 4400−4402.
(350) Sun, C.; Selloni, A.; Du, A.; Smith, S. C. Interaction of Water with the Fluorine-Covered Anatase TiO_2 (001) Surface. *J. Phys. Chem. C* **2011**, *115*, 17092−17096.
(351) Zhang, H.; Wang, Y.; Liu, P.; Han, Y.; Yao, X.; Zou, J.; Cheng, H.; Zhao, H. Anatase TiO_2 Crystal Facet Growth: Mechanistic Role of Hydrofluoric Acid and Photoelectrocatalytic Activity. *ACS Appl. Mater. Interfaces* **2011**, *3*, 2472−2478.
(352) Zhang, Q.; Gao, L. Preparation of Oxide Nanocrystals with Tunable Morphologies by the Moderate Hydrothermal Method: Insights from Rutile TiO_2. *Langmuir* **2003**, *19*, 967−971.
(353) Gordon, T. R.; Cargnello, M.; Paik, T.; Mangolini, F.; Weber, R. T.; Fornasiero, P.; Murray, C. B. Nonaqueous Synthesis of TiO_2 Nanocrystals Using TiF_4 to Engineer Morphology, Oxygen Vacancy Concentration, and Photocatalytic Activity. *J. Am. Chem. Soc.* **2012**, *134*, 6751−6761.
(354) Wang, C. M.; Mallouk, T. E. Wide-range tuning of the titanium dioxide flat-band potential by adsorption of fluoride and hydrofluoric acid. *J. Phys. Chem.* **1990**, *94*, 4276−4280.
(355) Hattori, A.; Yamamoto, M.; Tada, H.; Ito, S. A Promoting Effect of NH_4F Addition on the Photocatalytic Activity of Sol-Gel TiO_2 Films. *Chem. Lett.* **1998**, *27*, 707−708.
(356) Hattori, A.; Shimoda, K.; Tada, H.; Ito, S. Photoreactivity of Sol−Gel TiO_2 Films Formed on Soda-Lime Glass Substrates: Effect of SiO_2 Underlayer Containing Fluorine. *Langmuir* **1999**, *15*, 5422−5425.
(357) Yu, J. C.; Yu; Ho; Jiang; Zhang. Effects of F- Doping on the Photocatalytic Activity and Microstructures of Nanocrystalline TiO_2 Powders. *Chem. Mater.* **2002**, *14*, 3808−3816.
(358) Luo, H.; Takata, T.; Lee, Y.; Zhao, J.; Domen, K.; Yan. Photocatalytic Activity Enhancing for Titanium Dioxide by Co doping with Bromine and Chlorine. *Chem. Mater.* **2004**, *16*, 846−849.
(359) Li, D.; Haneda, H.; Labhsetwar, N. K.; Hishita, S.; Ohashi, N. Visible-light-driven photocatalysis on fluorine-doped TiO_2 powders by the creation of surface oxygen vacancies. *Chem. Phys. Lett.* **2005**, *401*, 579−584.
(360) Yamaki, T.; Umebayashi, T.; Sumita, T.; Yamamoto, S.; Maekawa, M.; Kawasuso, A.; Itoh, H. Fluorine-doping in titanium dioxide by ion implantation technique. *Nucl. Instrum. Methods Phys. Res., Sect. B* **2003**, *206*, 254−258.
(361) Czoska, A. M.; Livraghi, S.; Chiesa, M.; Giamello, E.; Agnoli, S.; Granozzi, G.; Finazzi, E.; Valentin, C. D.; Pacchioni, G. The Nature of Defects in Fluorine-Doped TiO_2. *J. Phys. Chem. C* **2008**, *112*, 8951−8956.
(362) Li, J.; Liu, C.; Ye, Y.; Zhu, J.; Wang, S.; Guo, J.; Sham, T.-K. Tracking the Local Effect of Fluorine Self-Doping in Anodic TiO_2 Nanotubes. *J. Phys. Chem. C* **2016**, *120*, 4623−4628.
(363) Seo, H.; Baker, L. R.; Hervier, A.; Kim, J.; Whitten, J. L.; Somorjai, G. A. Generation of Highly n-Type Titanium Oxide Using Plasma Fluorine Insertion. *Nano Lett.* **2011**, *11*, 751−756.
(364) Rex, R. E.; Knorr, F. J.; McHale, J. L. Imaging Luminescent Traps on Single Anatase TiO_2 Crystals: The Influence of Surface Capping on Photoluminescence and Charge Transport. *J. Phys. Chem. C* **2015**, *119*, 26212−26218.
(365) Ma, X.; Dai, Y.; Wei, W.; Huang, B.; Whangbo, M.-H. Insights into How Fluorine-Adsorption and n-Type Doping Affect the Relative Stability of the (001) and (101) Surfaces of TiO_2: Enhancing the Exposure of More Active but Thermodynamically Less Stable (001). *J. Phys. Chem. Lett.* **2015**, *6*, 1876−1882.
(366) Papari, G. P.; Silvestri, B.; Vitiello, G.; De Stefano, L.; Rea, I.; Luciani, G.; Aronne, A.; Andreone, A. Morphological, Structural, and Charge Transfer Properties of F-Doped ZnO: A Spectroscopic Investigation. *J. Phys. Chem. C* **2017**, *121*, 16012−16020.
(367) Cui, J. B.; Soo, Y. C.; Chen, T. P.; Gibson, U. J. Low-Temperature Growth and Characterization of Cl-Doped ZnO Nanowire Arrays. *J. Phys. Chem. C* **2008**, *112*, 4475−4479.
(368) Wang, F.; Seo, J.-H.; Li, Z.; Kvit, A. V.; Ma, Z.; Wang, X. Cl-Doped ZnO Nanowires with Metallic Conductivity and Their Application for High-Performance Photoelectrochemical Electrodes. *ACS Appl. Mater. Interfaces* **2014**, *6*, 1288−1293.
(369) Tena-Zaera, R.; Elias, J.; Lévy-Clément, C.; Bekeny, C.; Voss, T.; Mora-Seró, I.; Bisquert, J. Influence of the Potassium Chloride Concentration on the Physical Properties of Electrodeposited ZnO Nanowire Arrays. *J. Phys. Chem. C* **2008**, *112*, 16318−16323.
(370) Elias, J.; Tena-Zaera, R.; Lévy-Clément, C. Effect of the Chemical Nature of the Anions on the Electrodeposition of ZnO Nanowire Arrays. *J. Phys. Chem. C* **2008**, *112*, 5736−5741.
(371) Xu, H. Y.; Liu, Y. C.; Mu, R.; Shao, C. L.; Lu, Y. M.; Shen, D. Z.; Fan, X. W. F-doping effects on electrical and optical properties of ZnO nanocrystalline films. *Appl. Phys. Lett.* **2005**, *86*, 123107.
(372) Gao, X.; Li, X.; Gao, W.; Qiu, J.; Gan, X.; Wang, C.; Leng, X. Nanocrystalline/nanoporous ZnO spheres, hexapods and disks transformed from zinc fluorohydroxide, their self-assembly and patterned growth. *CrystEngComm* **2011**, *13*, 4741−4747.
(373) Zhang, J.; Liu, T.; Zhang, Y.; Zeng, W.; Pan, F.; Peng, X. Hydrothermal synthesis and growth mechanisms of different ZnO nanostructures and their gas-sensing properties. *J. Mater. Sci.: Mater. Electron.* **2015**, *26*, 1347−1353.
(374) Lee, H. B.; Ginting, R. T.; Tan, S. T.; Tan, C. H.; Alshanableh, A.; Oleiwi, H. F.; Yap, C. C.; Jumali, M. H. H.; Yahaya, M. Controlled Defects of Fluorine-incorporated ZnO Nanorods for Photovoltaic Enhancement. *Sci. Rep.* **2016**, *6*, 32645.
(375) Wang, H.; Rogach, A. L. Hierarchical SnO_2 Nanostructures: Recent Advances in Design, Synthesis, and Applications. *Chem. Mater.* **2014**, *26*, 123−133.
(376) Han, X.; Jin, M.; Xie, S.; Kuang, Q.; Jiang, Z.; Jiang, Y.; Xie, Z.; Zheng, L. Synthesis of Tin Dioxide Octahedral Nanoparticles with Exposed High-Energy {221} Facets and Enhanced Gas-Sensing Properties. *Angew. Chem., Int. Ed.* **2009**, *48*, 9180−9183.
(377) Wang, H.; Fu, F.; Zhang, F.; Wang, H.-E.; Kershaw, S. V.; Xu, J.; Sun, S.-G.; Rogach, A. L. Hydrothermal synthesis of hierarchical SnO_2 microspheres for gas sensing and lithium-ion batteries applications:

DOI: 10.1021/acs.chemrev.8b00158
Chem. Rev. 2018, 118, 7804−7864

Fluoride-mediated formation of solid and hollow structures. *J. Mater. Chem.* **2012**, *22*, 2140−2148.
(378) Xu, Z.; Shen, C.; Tian, Y.; Shi, X.; Gao, H. J. Organic phase synthesis of monodisperse iron oxide nanocrystals using iron chloride as precursor. *Nanoscale* **2010**, *2*, 1027−1032.
(379) Ma, R.; Wang, M.; Dam, D. T.; Dong, Y.; Chen, Y.; Moon, S. K.; Yoon, Y.-J.; Lee, J.-M. Halide-Ion-Assisted Synthesis of Different α-Fe_2O_3 Hollow Structures and Their Lithium-Ion Storage Properties. *ChemPlusChem* **2015**, *80*, 522−528.
(380) Guardia, P.; Nitti, S.; Materia, M. E.; Pugliese, G.; Yaacoub, N.; Greneche, J. M.; Lefevre, C.; Manna, L.; Pellegrino, T. Gold-iron oxide dimers for magnetic hyperthermia: the key role of chloride ions in the synthesis to boost the heating efficiency. *J. Mater. Chem. B* **2017**, *5*, 4587−4594.
(381) Selishcheva, E.; Parisi, J.; Kolny-Olesiak, J. Copper-assisted shape control in colloidal synthesis of indium oxide nanoparticles. *J. Nanopart. Res.* **2012**, *14*, 711.
(382) Wang, T.; Radovanovic, P. V. Free Electron Concentration in Colloidal Indium Tin Oxide Nanocrystals Determined by Their Size and Structure. *J. Phys. Chem. C* **2011**, *115*, 406−413.
(383) Agrawal, A.; Singh, A.; Yazdi, S.; Singh, A.; Ong, G. K.; Bustillo, K.; Johns, R. W.; Ringe, E.; Milliron, D. J. Resonant Coupling between Molecular Vibrations and Localized Surface Plasmon Resonance of Faceted Metal Oxide Nanocrystals. *Nano Lett.* **2017**, *17*, 2611−2620.
(384) Kim, M. H.; Lim, B.; Lee, E. P.; Xia, Y. Polyol synthesis of Cu_2O nanoparticles: use of chloride to promote the formation of a cubic morphology. *J. Mater. Chem.* **2008**, *18*, 4069−4073.
(385) Wang, Q.; kuang, Q.; Wang, K.; Wang, X.; Xie, Z. A surfactant free synthesis and formation mechanism of hollow Cu_2O nanocubes using Cl^- ions as the morphology regulator. *RSC Adv.* **2015**, *5*, 61421−61425.
(386) Niederberger, M.; Garnweitner, G.; Pinna, N.; Antonietti, M. Nonaqueous and Halide-Free Route to Crystalline $BaTiO_3$, $SrTiO_3$, and $(Ba,Sr)TiO_3$ Nanoparticles via a Mechanism Involving C−C Bond Formation. *J. Am. Chem. Soc.* **2004**, *126*, 9120−9126.
(387) Pinna, N.; Garnweitner, G.; Antonietti, M.; Niederberger, M. A General Nonaqueous Route to Binary Metal Oxide Nanocrystals Involving a C−C Bond Cleavage. *J. Am. Chem. Soc.* **2005**, *127*, 5608−5612.
(388) Behar, D.; Rabani, J. Laser Photolysis of TiO_2 Layers in the Presence of Aqueous Iodide. *J. Phys. Chem. B* **2001**, *105*, 6324−6329.
(389) Zang, L.; Qu, P.; Zhao, J.; Shen, T.; Hidaka, H. Photocatalytic bleaching of p-nitrosodimethylaniline in TiO_2 aqueous suspensions: A kinetic treatment involving some primary events photoinduced on the particle surface. *J. Mol. Catal. A: Chem.* **1997**, *120*, 235−245.
(390) Rodríguez, E. M.; Márquez, G.; Tena, M.; Álvarez, P. M.; Beltrán, F. J. Determination of main species involved in the first steps of TiO_2 photocatalytic degradation of organics with the use of scavengers: The case of ofloxacin. *Appl. Catal., B* **2015**, *178*, 44−53.
(391) Kim, Y. I.; Salim, S.; Huq, M. J.; Mallouk, T. E. Visible-light photolysis of hydrogen iodide using sensitized layered semiconductor particles. *J. Am. Chem. Soc.* **1991**, *113*, 9561−9563.
(392) Ayed, C.; Huang, W.; Li, R.; da Silva, L. C.; Wang, D.; Suraeva, O.; Najjar, W.; Zhang, K. A. I. Conjugated Microporous Polymers with Immobilized TiO_2 Nanoparticles for Enhanced Visible Light Photocatalysis. *Part. Part. Syst. Char.* **2018**, *35*, 1700234.
(393) Wang, B.; Li, C.; Cui, H.; Zhang, J.; Zhai, J.; Li, Q. Shifting mechanisms in the initial stage of dye photodegradation by hollow TiO_2 nanospheres. *J. Mater. Sci.* **2014**, *49*, 1336−1344.
(394) Tian, L.; Ye, L.; Liu, J.; Zan, L. Solvothermal synthesis of CNTs−WO_3 hybrid nanostructures with high photocatalytic activity under visible light. *Catal. Commun.* **2012**, *17*, 99−103.
(395) Carroll, B. H.; Higgins, G. C.; James, T. H. *Introduction to photographic theory: the silver halide process*; J. Wiley, 1980.
(396) Tani, T. *Silver Nanoparticles: From Silver Halide Photography to Plasmonics*; Oxford University Press, 2015.
(397) Xie, Q.; Xu, Z.; Hu, B.; He, X.; Zhu, L. Preparation of a novel silk microfiber covered by AgCl nanoparticles with antimicrobial activity. *Microsc. Res. Tech.* **2017**, *80*, 272−279.
(398) Wang, H.; Lang, X.; Gao, J.; Liu, W.; Wu, D.; Wu, Y.; Guo, L.; Li, J. Polyhedral AgBr Microcrystals with an Increased Percentage of Exposed {111} Facets as a Highly Efficient Visible-Light Photocatalyst. *Chem. - Eur. J.* **2012**, *18*, 4620−4626.
(399) Heise, H. M.; Delbeck, S.; Küpper, L. In *Molecular and Laser Spectroscopy*; Gupta, V. P., Ed.; Elsevier, 2018; Chapter 3 (Recent Advances in Sensor Developments Based on Silver Halide Fibers for Mid-Infrared Spectrometric Analysis), pp 39−63.
(400) Keller, K.; Kampfer, H.; Matejec, R.; Lapp, O.; Krafft, W.; Frenken, H.; Lührig, H.; Scheerer, R.; Heilmann, M.; Meckl, H.; Bergthaller, P.; Hübner, D.; Wolff, E.; Morcher, B.; Zahn, W.; Buschmann, H.; Blank, R.; Tromnau, R.; Plamper, J.; Seiler, A.; Nieswandt, K.; Boie, I.; Moisar, E.; Winiker, R.; Schellenberg, M.; Ketellapper, L. Photography. In *Ullmann's Encyclopedia of Industrial Chemistry*; Wiley-VCH Verlag GmbH & Co. KGaA, 2000.
(401) Xu, S.; Li, Y. Different morphology at different reactant molar ratios: synthesis of silver halide low-dimensional nanomaterials in microemulsions. *J. Mater. Chem.* **2003**, *13*, 163−165.
(402) Pillai, V.; Kumar, P.; Hou, M. J.; Ayyub, P.; Shah, D. O. Preparation of nanoparticles of silver halides, superconductors and magnetic materials using water-in-oil microemulsions as nano-reactors. *Adv. Colloid Interface Sci.* **1995**, *55*, 241−269.
(403) Gupta, V. K. N.; Mehra, A.; Thaokar, R. Worm-like micelles as templates: Formation of anisotropic silver halide nanoparticles. *Colloids Surf., A* **2012**, *393*, 73−80.
(404) Shukla, D.; Joshi, A. A.; Mehra, A. Modeling of Formation of Nanoparticles in Reverse Micellar Systems: Ostwald Ripening of Silver Halide Particles. *Langmuir* **2009**, *25*, 3786−3793.
(405) Nikolenko, D. Y.; Brichkin, S. B.; Razumov, V. F. Synthesis of mixed silver halide nanocrystals in reversed micelles. *High Energy Chem.* **2008**, *42*, 305−310.
(406) Yin, B.; Huang, X.; Mishra, R.; Sadtler, B. Compositionally Induced Twin Defects Control the Shape of Ternary Silver Halide Nanocrystals. *Chem. Mater.* **2017**, *29*, 1014−1021.
(407) He, X.; Qiu, Y.; Yang, S. Fully-Inorganic Trihalide Perovskite Nanocrystals: A New Research Frontier of Optoelectronic Materials. *Adv. Mater.* **2017**, *29*, 1700775.
(408) Correa-Baena, J.-P.; Abate, A.; Saliba, M.; Tress, W.; Jesper Jacobsson, T.; Gratzel, M.; Hagfeldt, A. The rapid evolution of highly efficient perovskite solar cells. *Energy Environ. Sci.* **2017**, *10*, 710−727.
(409) Seth, S.; Samanta, A. Photoluminescence of Zero-Dimensional Perovskites and Perovskite-Related Materials. *J. Phys. Chem. Lett.* **2018**, *9*, 176−183.
(410) Fujito, H.; Kunioku, H.; Kato, D.; Suzuki, H.; Higashi, M.; Kageyama, H.; Abe, R. Layered Perovskite Oxychloride Bi_4NbO_8Cl: A Stable Visible Light Responsive Photocatalyst for Water Splitting. *J. Am. Chem. Soc.* **2016**, *138*, 2082−2085.
(411) Xiao, J.-R.; Yang, S.-H.; Feng, F.; Xue, H.-G.; Guo, S.-P. A review of the structural chemistry and physical properties of metal chalcogenide halides. *Coord. Chem. Rev.* **2017**, *347*, 23−47.
(412) Huang, H.; Polavarapu, L.; Sichert, J. A.; Susha, A. S.; Urban, A. S.; Rogach, A. L. Colloidal lead halide perovskite nanocrystals: synthesis, optical properties and applications. *NPG Asia Mater.* **2016**, *8*, e328.
(413) Tan, H.; Jain, A.; Voznyy, O.; Lan, X.; García de Arquer, F. P.; Fan, J. Z.; Quintero-Bermudez, R.; Yuan, M.; Zhang, B.; Zhao, Y.; Fan, F.; Li, P.; Quan, L. N.; Zhao, Y.; Lu, Z.-H.; Yang, Z.; Hoogland, S.; Sargent, E. H. Efficient and stable solution-processed planar perovskite solar cells via contact passivation. *Science* **2017**, *355*, 722−726.
(414) Swarnkar, A.; Ravi, V. K.; Nag, A. Beyond Colloidal Cesium Lead Halide Perovskite Nanocrystals: Analogous Metal Halides and Doping. *ACS Energy Lett.* **2017**, *2*, 1089−1098.
(415) Green, M. A.; Jiang, Y.; Soufiani, A. M.; Ho-Baillie, A. Optical Properties of Photovoltaic Organic−Inorganic Lead Halide Perovskites. *J. Phys. Chem. Lett.* **2015**, *6*, 4774−4785.
(416) Yang, T.-Y.; Gregori, G.; Pellet, N.; Grätzel, M.; Maier, J. The Significance of Ion Conduction in a Hybrid Organic−Inorganic Lead-Iodide-Based Perovskite Photosensitizer. *Angew. Chem., Int. Ed.* **2015**, *54*, 7905−7910.

DOI: 10.1021/acs.chemrev.8b00158
Chem. Rev. 2018, 118, 7804−7864

(417) Li, G.; Ho, J. Y.-L.; Wong, M.; Kwok, H. S. Reversible Anion Exchange Reaction in Solid Halide Perovskites and Its Implication in Photovoltaics. *J. Phys. Chem. C* **2015**, *119*, 26883−26888.
(418) Jang, D. M.; Park, K.; Kim, D. H.; Park, J.; Shojaei, F.; Kang, H. S.; Ahn, J.-P.; Lee, J. W.; Song, J. K. Reversible Halide Exchange Reaction of Organometal Trihalide Perovskite Colloidal Nanocrystals for Full-Range Band Gap Tuning. *Nano Lett.* **2015**, *15*, 5191−5199.
(419) Akkerman, Q. A.; D'Innocenzo, V.; Accornero, S.; Scarpellini, A.; Petrozza, A.; Prato, M.; Manna, L. Tuning the Optical Properties of Cesium Lead Halide Perovskite Nanocrystals by Anion Exchange Reactions. *J. Am. Chem. Soc.* **2015**, *137*, 10276−10281.
(420) Solis-Ibarra, D.; Smith, I. C.; Karunadasa, H. I. Post-synthetic halide conversion and selective halogen capture in hybrid perovskites. *Chem. Sci.* **2015**, *6*, 4054−4059.
(421) Koscher, B. A.; Bronstein, N. D.; Olshansky, J. H.; Bekenstein, Y.; Alivisatos, A. P. Surface- vs Diffusion-Limited Mechanisms of Anion Exchange in $CsPbBr_3$ Nanocrystal Cubes Revealed through Kinetic Studies. *J. Am. Chem. Soc.* **2016**, *138*, 12065−12068.
(422) Dou, L.; Lai, M.; Kley, C. S.; Yang, Y.; Bischak, C. G.; Zhang, D.; Eaton, S. W.; Ginsberg, N. S.; Yang, P. Spatially resolved multicolor $CsPbX_3$ nanowire heterojunctions via anion exchange. *Proc. Natl. Acad. Sci. U. S. A.* **2017**, *114*, 7216−7221.
(423) Kang, J.; Wang, L.-W. High Defect Tolerance in Lead Halide Perovskite $CsPbBr_3$. *J. Phys. Chem. Lett.* **2017**, *8*, 489−493.
(424) Woo, J. Y.; Kim, Y.; Bae, J.; Kim, T. G.; Kim, J. W.; Lee, D. C.; Jeong, S. Highly Stable Cesium Lead Halide Perovskite Nanocrystals through in Situ Lead Halide Inorganic Passivation. *Chem. Mater.* **2017**, *29*, 7088−7092.
(425) Protesescu, L.; Yakunin, S.; Bodnarchuk, M. I.; Krieg, F.; Caputo, R.; Hendon, C. H.; Yang, R. X.; Walsh, A.; Kovalenko, M. V. Nanocrystals of Cesium Lead Halide Perovskites ($CsPbX_3$, X = Cl, Br, and I): Novel Optoelectronic Materials Showing Bright Emission with Wide Color Gamut. *Nano Lett.* **2015**, *15*, 3692−3696.
(426) Di Stasio, F.; Christodoulou, S.; Huo, N.; Konstantatos, G. Near-Unity Photoluminescence Quantum Yield in $CsPbBr_3$ Nanocrystal Solid-State Films via Postsynthesis Treatment with Lead Bromide. *Chem. Mater.* **2017**, *29*, 7663−7667.
(427) Motti, S. G.; Gandini, M.; Barker, A. J.; Ball, J. M.; Srimath Kandada, A. R.; Petrozza, A. Photoinduced Emissive Trap States in Lead Halide Perovskite Semiconductors. *ACS Energy Lett.* **2016**, *1*, 726−730.
(428) Wei, S.; Yang, Y.; Kang, X.; Wang, L.; Huang, L.; Pan, D. Room-temperature and gram-scale synthesis of $CsPbX_3$ (X = Cl, Br, I) perovskite nanocrystals with 50−85% photoluminescence quantum yields. *Chem. Commun.* **2016**, *52*, 7265−7268.
(429) Li, X.; Wu, Y.; Zhang, S.; Cai, B.; Gu, Y.; Song, J.; Zeng, H. $CsPbX_3$ Quantum Dots for Lighting and Displays: Room-Temperature Synthesis, Photoluminescence Superiorities, Underlying Origins and White Light-Emitting Diodes. *Adv. Funct. Mater.* **2016**, *26*, 2435−2445.
(430) Imran, M.; Caligiuri, V.; Wang, M.; Goldoni, L.; Prato, M.; Krahne, R.; De Trizio, L.; Manna, L. Benzoyl Halides as Alternative Precursors for the Colloidal Synthesis of Lead-Based Halide Perovskite Nanocrystals. *J. Am. Chem. Soc.* **2018**, *140*, 2656−2664.
(431) Yang, D.; Li, X.; Zeng, H. Surface Chemistry of All Inorganic Halide Perovskite Nanocrystals: Passivation Mechanism and Stability. *Adv. Mater. Interfaces* **2018**, *5*, 1701662.
(432) Yoon, S. J.; Draguta, S.; Manser, J. S.; Sharia, O.; Schneider, W. F.; Kuno, M.; Kamat, P. V. Tracking Iodide and Bromide Ion Segregation in Mixed Halide Lead Perovskites during Photoirradiation. *ACS Energy Lett.* **2016**, *1*, 290−296.
(433) Brennan, M. C.; Draguta, S.; Kamat, P. V.; Kuno, M. Light-Induced Anion Phase Segregation in Mixed Halide Perovskites. *ACS Energy Lett.* **2018**, *3*, 204−213.
(434) Samu, G. F.; Janáky, C.; Kamat, P. V. A Victim of Halide Ion Segregation. How Light Soaking Affects Solar Cell Performance of Mixed Halide Lead Perovskites. *ACS Energy Lett.* **2017**, *2*, 1860−1861.
(435) Lignos, I.; Protesescu, L.; Emiroglu, D. B.; Maceiczyk, R.; Schneider, S.; Kovalenko, M. V.; deMello, A. J. Unveiling the Shape Evolution and Halide-Ion-Segregation in Blue-Emitting Formamidinium Lead Halide Perovskite Nanocrystals Using an Automated Microfluidic Platform. *Nano Lett.* **2018**, *18*, 1246−1252.
(436) Riedinger, A.; Ott, F. D.; Mule, A.; Mazzotti, S.; Knusel, P. N.; Kress, S. J. P.; Prins, F.; Erwin, S. C.; Norris, D. J. An intrinsic growth instability in isotropic materials leads to quasi-two-dimensional nanoplatelets. *Nat. Mater.* **2017**, *16*, 743−748.
(437) Loiudice, A.; Saris, S.; Oveisi, E.; Alexander, D. T. L.; Buonsanti, R. $CsPbBr_3$ QD/AlOx Inorganic Nanocomposites with Exceptional Stability in Water, Light, and Heat. *Angew. Chem., Int. Ed.* **2017**, *56*, 10696−10701.
(438) Li, Z.; Kong, L.; Huang, S.; Li, L. Highly Luminescent and Ultrastable $CsPbBr_3$ Perovskite Quantum Dots Incorporated into a Silica/Alumina Monolith. *Angew. Chem.* **2017**, *129*, 8246−8250.
(439) Lei, W.; Portehault, D.; Dimova, R.; Antonietti, M. Boron Carbon Nitride Nanostructures from Salt Melts: Tunable Water-Soluble Phosphors. *J. Am. Chem. Soc.* **2011**, *133*, 7121−7127.
(440) Zhang, H.; Dasbiswas, K.; Ludwig, N. B.; Han, G.; Lee, B.; Vaikuntanathan, S.; Talapin, D. V. Stable colloids in molten inorganic salts. *Nature* **2017**, *542*, 328−331.
(441) Srivastava, V.; Liu, W.; Janke, E. M.; Kamysbayev, V.; Filatov, A. S.; Sun, C.-J.; Lee, B.; Rajh, T.; Schaller, R. D.; Talapin, D. V. Understanding and Curing Structural Defects in Colloidal GaAs Nanocrystals. *Nano Lett.* **2017**, *17*, 2094−2101.
(442) Kalytchuk, S.; Zhovtiuk, O.; Rogach, A. L. Sodium chloride protected CdTe quantum dot based solid-state luminophores with high color quality and fluorescence efficiency. *Appl. Phys. Lett.* **2013**, *103*, 103105.
(443) Kalytchuk, S.; Adam, M.; Tomanec, O.; Zbořil, R.; Gaponik, N.; Rogach, A. L. Sodium Chloride Protected CdHgTe Quantum Dot Based Solid-State Near-Infrared Luminophore for Light-Emitting Devices and Luminescence Thermometry. *ACS Photonics* **2017**, *4*, 1459−1465.
(444) Guhrenz, C.; Benad, A.; Ziegler, C.; Haubold, D.; Gaponik, N.; Eychmüller, A. Solid-State Anion Exchange Reactions for Color Tuning of $CsPbX_3$ Perovskite Nanocrystals. *Chem. Mater.* **2016**, *28*, 9033−9040.
(445) Quan, L. N.; Quintero-Bermudez, R.; Voznyy, O.; Walters, G.; Jain, A.; Fan, J. Z.; Zheng, X.; Yang, Z.; Sargent, E. H. Highly Emissive Green Perovskite Nanocrystals in a Solid State Crystalline Matrix. *Adv. Mater.* **2017**, *29*, 1605945.
(446) Ning, Z.; Gong, X.; Comin, R.; Walters, G.; Fan, F.; Voznyy, O.; Yassitepe, E.; Buin, A.; Hoogland, S.; Sargent, E. H. Quantum-dot-in-perovskite solids. *Nature* **2015**, *523*, 324.

DOI: 10.1021/acs.chemrev.8b00158
Chem. Rev. 2018, 118, 7804−7864